The Mechanical Behaviour and Critical State of Glacial Sediments

By

Fatin N. Altuhafi

A dissertation submitted to University College London in accordance with the requirements of the degree of Doctor of Philosophy

Department of Civil and Environmental Engineering
University College London

May 2007

ProQuest LLC
789 East Eisenhower Parkway
P.O. Box 1346
Ann Arbor, MI 48106-1346

Declaration

I, Fatin N. Altuhafi, confirm that the work presented in this dissertation is my own. Where information has been derived from other sources, I confirm that this has been indicated in the dissertation.

The dissertation has not been presented at any other University for examination either in the United Kingdom or overseas.

May 2007

Acknowledgements

This Ph.D. thesis is the outcome of four years of hard but stimulating research work. It would never have been possible for me to finish this work, if it had not been for the support from many people. Unfortunately I will not be able to mention all of them individually but I would like to thank some in particular.

Firstly, I would like to express my gratitude to my supervisors; Dr. Beatrice Baudet and Prof. Peter Sammonds, without their never-ending encouragement, support and guidance, this work would have never been presented.

The first few, but important steps of this research were done by the help of Dr. Catherine Stafford, who also was a member of the Icelandic research expedition, when the samples used in this study were collected. I also would like to express my deep gratitude to the technical staff in the Earth Science laboratory, in particular to Neil Hughes for his never ending help and support, without which this research would never be finalised.

The ring shear tests were performed at the Soil Mechanics laboratory at the Imperial College, in collaboration with Dr. Matthew Coop, for whom I owe to most of the valuable advice and guidance all through the research work.

I would also like to express my sincere gratitude to Dr. Pedro Ferreira for his continuous valuable help and advice in most of laboratory work, and for being there for me to solve difficult problems.

My thanks are also directed to Steve Boon, John Bowles, James Davy and Dr. David Dobson from the Earth Sciences for their valuable help.

The research was made possible through funding from CARA (Council for Assisting Refugee Academics) in the first year. The Second and the third

year of the research were funded by a Civil Engineering departmental EPSRC studentship.

Finally, I am very grateful to my family for their ever-present support and love. For my dear husband Aboudi, for his patience, encouragement and never ending support. My thanks also go for my sister Rasha, for being there for me all through the hard times, and not to forget my children Dania and Yousif, for putting up with ever-very-busy mad mum.

The Mechanical Behaviour and Critical State of Glacial Sediments

Abstract:

This research contributes to the debate on glacier dynamics, which have a significant effect on global climate change and sea-level changes. Glacier advances and retreats have great effects which can be viewed not only from their influence upon human and habitats within their immediate locality but their much more pervasive influence on all global habitats due to the effect of modern ice masses on global climate and sea-level.

One of the most fundamental characteristics of glaciers and ice sheets is their ability to move. In the early models adopted to simulate glacier flow, glaciers were thought to rest on clean bedrock. However, borehole studies in different glacial areas revealed the presence of a bed of deformable sediment underneath some glaciers. Although the old common model assumed that glacier movement is generated by sliding processes, recent research proved that a high percentage of glacier movement is attributed to the shearing process of the saturated bed sediment.

In the glacial environment, sediment production, deformation and deposition cannot be separated conceptually. Sediments produced by the direct erosion of lithified material by glacier ice typically contain particles spanning a large size distribution. Frequent interaction, between particles and between particles and the rigid bed, results in their substantial modification during transport. Inter-particle stresses are often high enough to cause fracture and abrasion of particles. The grain size distribution of sediments is a fundamental control on sediment deformation properties. The evolution of particle size distribution of glacial sediment, due to glacier movement, would result in an increase in the fine modes of their particles with the increase of transport distance, but there appears to be a lower size limit beyond which no further particle crushing occurrs, regardless of transport distance. This

complies with those findings which studied breakage potentials of some granular soils.

Tests carried out on samples of a glacial sediment which were collected from Langjökull- Iceland, indicated that this sediment had been subjected to pervasive deformation underneath glaciers, which involved sediment particle breakage, resulting in this sediment reaching a terminal grading state such that no further significant particle breakage could be achieved under any further pressure or strains. The sediment behaviour accordingly was completely different to that expected for granular soils which follow a Critical State (CS) framework. The sediment exhibited a stiff behaviour represented by the lack of a clear yielding point in its compression curves, and no unique Normal Compression Line was observed, indicating that a transitional behaviour can be obtained from this sediment which has reached its terminal grading. On the other hand, a differently graded sample from the same sediment exhibited a behaviour similar to granular soils which deform following a CS framework, in which a clear yielding point, which is associated with particle breakage, and a tendency to form a unique Normal Compression Line is observed, an implication that the grading of the sediment is a key factor in defining the mechanical behaviour of the sediment.

The research also addresses the rheology of glacial sediment deformation by investigating the influence of strain rate on its mechanical behaviour, and comparing the results obtained from Langjökull sediment with existing data of tests which were carried out on another glacial sediment which was collected from Ice Stream B- West Antarctica.

Table of Contents

Declaration i

Acknowledgments ii

Abstract iv

Table of Contents vi

List of Figures xi

List of Tables xvii

Notations xviii

Chapter One Introduction 1

1.1 Introduction 1

1.2 The subglacial environment 5

1.2.1 Cold bed glaciers and temperate ice bed conditions 6

1.2.2 Origin of glacial sediments 8

1.3 Geotechnical theoretical aspects 10

1.3.1 Stresses in soils 10

1.3.2 Mohr-Coulomb failure theory 11

1.3.3 Critical State framework 12

1.4 Research aims and objectives 15

1.5 Methodology 16

1.6 Structure of the thesis 17

Chapter Two Literature Review 22

2.1 Introduction 22

2.2 Subglacial stresses and subglacial deformations 23

2.2.1 Pore water pressure underneath glacier 24

2.2.2 Bed coupling/decoupling and glacier movement 25

2.3 Behaviour of granular sediments within the Critical State framework 26

2.3.1 Stress-dilatancy of granular material 27

2.3.2 State boundary surfaces 29

2.4 The effect of the presence of fines on the mechanical behaviour of sediments 30

2.5 Transitional behaviour of sediments 34
2.6 Particle breakage in subglacial sediments 35
2.6.1 Particle breakage as a geotechnical concept 38
2.6.2 Particles breakage development during compression and shearing 39
2.6.3 Critical or terminal grading of the sediments 40
2.6.4 Geomaterial with changing grading 42
2.7 Time dependent behaviour of sediments-shearing rate effect on the sediment shearing behaviour 44
2.7.1 The Isotach behaviour 45
2.7.2 TESRA behaviour (Temporary Effect of Strain Rate) 46
2.8 Shearing rate in subglacial environment 48
2.8.1 Boulton and Hindmarsh experiment under Bréiðamerkurjökull 49
2.8.2 Contradicting studies 51

Chapter Three The Research Sediment-Langjökull sediment 83
3.1 Langjökull Glacier – Iceland 83
3.2 Sampling and sample storage 84
3.3 General description of the sediment 85
3.4 Particles size distribution and specific gravity 86
3.5 Mineralogy 87

Chapter Four Testing apparatus and testing procedures 100
4.1 Introduction 100
4.2 Modified oedometer cell for one-dimensional compression 101
4.3 The use of triaxial cell to investigate the compression and shearing behaviour of the sediment 102
4.3.1 Standard triaxial cell 102
4.3.2 High pressure triaxial cell 103
4.3.3 Fully computer controlled triaxial cell 106
4.3.4 Small strain local instrumentation 108
4.3.5 Calibration of instrumentation 109
4.3.6 Sample preparation for triaxial cell tests 110

4.3.7 Triaxial tests testing procedure 113
4.3.7.1 Testing procedure by standard and high pressure triaxial cell 113
4.3.7.2 Testing procedure by fully computer controlled triaxial cell 116
4.4 Ring shear apparatus 117
4.4.1 Testing procedure in the Bishop's ring shear apparatus 119
4.5 High pressure permeameter 120
4.5.1 Test procedure in the permeameter 122
4.6 Additional Tests 123
4.6.1 Specific gravity (particle density) test 123
4.6.2 Particle size distribution of Langjökull sediment 124
4.6.2.1 Sieve analysis 124
4.6.2.2 Sedimentation test 125
4.6.3 Scanning electron microscopy sample preparation 125
4.6.4 X-ray diffractometer 126

Chapter Five The mechanical behaviour of Langjökull glacial sediment 142
5.1 Introduction 142
5.2 Tests on Langjökull sediment 143
5.3 Compression tests on Langjökull sediment 143
5.3.1 Isotropic compression tests by the means of the high pressure triaxial cell 144
5.3.2 Isotropic compression tests by the permeameter 145
5.3.3 One-dimensional compression tests 145
5.4 Shearing tests by triaxial cells apparatus 146
5.5 Ring shear shearing tests 150
5.6 Effect of shearing rate on the sediment's behaviour 151

Chapter Six Particle breakage in Langjökull sediment 157
6.1 Introduction 157
6.2 Particle breakage of Langjökull sediment induced by pure isotropic compression 158
6.3 Particle breakage of Langjökull sediment induced by shearing 160
6.4 Effect of sediment grading on its breakage potential 161

6.5 effect of sediment grading on compression behaviour 164

Chapter Seven Sediment behaviour during shearing 191
7.1 Introduction 191
7.2 Stress-Strain behaviour during shearing 192
7.2.1 Drained triaxial compression tests 192
7.2.2 Undrained triaxial compression tests 194
7.3 Critical State Line in the p'-q' plane and stress paths during undrained shearing 196
7.4 Critical state Line in the v-lnp' plane 197
7.4.1 Behaviour of samples during drained shearing tests 198
7.4.2 Stress-dilatancy during drained shearing 200
7.4.3 Shearing modulus and Young modulus 202
7.5 Normalisation of stress paths-boundary surfaces hypothesis 203
7.6 Residual strength of the Langjökull sediment 205
7.7 The uniqueness of the Critical State Line of the Langjökull sediment 205

Chapter Eight Viscous behaviour of subglacial sediments 224
8.1 introduction 224
8.2 Strain rate effect on shearing behaviour of the Langjökull sediment 225
8.2.1 Shearing rate effect on Langjökull sediment shearing behaviour in triaxial cell 226
8.2.2 Strain rate effect on the residual strength of Langjökull sediment 228
8.3 Existing data (Results from Ice stream B-Antarctica) new analysis 229
8.4 Viscous behaviour of subglacial sediment 232

Chapter Nine Conclusions and recommendations for further studies 247
9.1 Summary and conclusions 247
9.1.1 The Langjökull glacial sediment 248
9.1.2 The effect of subglacial deformations on the sediment particle size distribution evolution 248
9.1.3 The sediment behaviour within the Critical State framework 250

9.1.4 The viscous behaviour of the sediment and the effect of strain rate on the sediment behaviour 251
9.2 Recommendations for further studies 253

References 255
Appendix 1 264
Appendix 2 265

List of figures

1-1 Ice flow on different bed conditions. 19

1-2 Mohr circle and stress conditions at failure. 19

1-3 Normal and Critical State Lines in the v-ln p' plane, schematic diagram. 20

1-4 Critical State Line in the mean effective stress- deviator stress plane, schematic diagram. 20

1-5 The boundary surfaces in the q';p':v space. 21

1-6 Stress paths for drained tests on clay samples. 21

2-1 Sketch of dragometer. 55

2-2 Isotropic compression and Critical State data for Dog's Bay sand. 55

2-3 Variation of dilatancy with material state. 56

2-4 Critical State Line and state parameter as defined by Been & Jefferies (1985). 56

2-5 Undrained shearing tests on Toyoura sand. 57

2-6 Stress path of undrained shearing tests on Toyoura sand. 58

2-7 Behaviour of Toyoura sand during drained shearing. 59

2-8 Definition of state parameters, p'_e and p'_{cs}. 60

2-9 Critical State of Dog's Bay sand. 60

2-10 The effect of adding silt size fines to medium quartzic sand behaviour. 61

2-11 Effect of fines on Dog's Bay sand behaviour during compression. 61

2-12 Critical States for compacted samples of Botucatu soil. 62

2-13 Effect of fines on Toyoura sand behaviour. 62

2-14 Botucatu sandstone PSD and Critical State. 63

2-15 Comparison of behaviour of Botucatu sandstone with different soils. 64

2-16 PSD of Italian silt. 65

2-17 Oedometer compression curves for Italian silt. 65

2-18 Isotropic compression and Critical State for transitional soil. 66

2-19 Stress paths and normalisation for transitional soil. 67

2-20 Frequency distribution in till samples with progressive transport. 68
2-21 Comparison of grain size distribution of three subglacial sediments. 68
2-22 Definition of particle breakage parameters proposed by Hardin. 69
2-23 Development of particle breakage during isotropic compression and undrained shearing of Aio sand. 69
2-24 Particle breakage related to the state on the NCL and CSL for Dog's Bay sand. 70
2-25 Ring shear data on carbonate sand. 71
2-26 One dimensional compression tests on Petrolium coke. 72
2-27 Effect of strain level on particle breakage. 73
2-28 Grading state index, schematic diagram. 73
2-29 Critical State surface for crushable soils. 74
2-30 Three parts Critical State Line of crushable soils. 74
2-31 Creep tests at low stress level, schematic diagram. 75
2-32 Relaxation test, schematic diagram. 75
2-33 PSD increase with loading duration. 76
2-34 Constant rate of strain tests, schematic diagram. 76
2-35 Results of CRS oedometer tests on Batiscan clay. 77
2-36 Stress-strain behaviour of Saint-Jean-Vianny clay. 77
2-37 Strain rate dependency in Hostun sand. 78
2-38 TESRA and Isotach behaviour, schematic diagram. 78
2-39 Isotach behaviour on normally consolidated kaolin clay. 79
2-40 General TESRA behaviour in reconstituted Fukakusa clay. 79
2-41 Viscous flow model, proposed by Boulton & Hindmarsh, 1987. 80
2-42 Ring shear results on Dutch till. 80
2-43 Ring shear test on Ice Stream B-Antarctica. 81
2-44 Ring shear tests on Storgläciaren and two Rivers till. 82
3-1 Langjökull Glacier- Iceland (map). 89
3-2 Details of Vestari-Hagafellsjökull, showing flutes and drumlins. 89
3-3 Proglacial area of Langjökull and sampling pit. 90
3-4 Block sample trimming at the site. 91
3-5 Wrapping block samples by cling films. 91

3-6 Sealing of retrieved samples by applying paraffin wax. 92
3-7 Applying liquid nitrogen to freeze samples. 92
3-8 SEM image of undisturbed sample of Langjökull sediment. 93
3-9 SEM image of undisturbed sample of Langjökull sediment. 93
3-10 SEM image of undisturbed sample of Langjökull sediment. 94
3-11 SEM image of undisturbed sample of Langjökull sediment. 94
3-12 Particle size distribution of Langjökull sediment. 95
3-13 Particle size distribution of Langjökull sediment from the subglacial and proglacial sites. 95
3-14 Comparison of PSD of three subglacial sediments. 96
3-15 X-ray diffraction test for particles smaller than 63 microns. 96
3-16 X-ray diffraction test for particles between 63 to 295 microns. 97
3-17 X-ray diffraction test for particles between 295 to 1405 microns. 97
3-18 X-ray diffraction test for particles larger than 1405 microns. 98
4-1 Modified oedometer cell, used for one-dimensional compression tests. 127
4-2 Schematic figure of the standard triaxial cell and the triaxial cell set-up. 128
4-3 The high pressure triaxial cell and the high pressure triaxial cell set-up. 129
4-4 Schematic diagram showing the interior compartments of the high pressure triaxial cell. 130
4-5 Fully computer controlled triaxial cell, and a schematic digram showing its set-up. 131
4-6 Miniature local LVDTs for local strain measurement. 132
4-7 Calibration of exterior loadcell for the high pressure triaxial cell. 133
4-8 Trimming procedure of undisturbed samples of Langjökull sediment. 134
4-9 Mould used for preparing the remoulded samples. 135
4-10 General set-up of mould during sample preparation by sedimentation method (schematic). 135
4-11 Bishop's ring shear apparatus. 136

4-12 Placing the remoulded sample inside the pressure chamber of the permeameter. 137
4-13 The permeameter, schematic diagram. 138
4-14 The permeameter compartment with sample setting (schematic diagram). 139
4-15 Sample setting before placing in the permeameter. 140
4-16 The diffractometer available at the Earth Sciences department in the UCL. 140
4-17 Reflection of X-rays from two planes of atoms in a solid. 141
5-1 Particle size distribution of the natural sediment and artificially graded sediment. 152
5-2 Method of measuring shearing displacement in Bishop's ring shear apparatus, Θ represents the angular displacement. 152
6-1 Particle size distribution by sieve analysis before and after compresion tests on Langjökull sediment. 167
6-2 SEM images for sample which was isotropically compressed to 20MPa. 169
6-3 SEM images for sample which was isotropically compressed to 40MPa. 171
6-4 PSD before and after permeameter tests. 172
6-5 SEM images after permeameter tests LR250-1. 174
6-6 SEM images after permeameter tests LR250-2. 176
6-7 SEM images after permeameter tests LR250-2A. 178
6-8 SEM images after permeameter tests LR250-3. 180
6-9 PSD before and after undrained and drained shearing. 181
6-10 SEM image of remoulded samples subjected to undrained shearing. 183
6-11 SEM images of undisturbed sample subjected to drained shearing. 185
6-12 PSD before and after shearing by the ring shear apparatus. 186
6-13 Volumetric strain versus shearing strain during ring shear tests. 187
6-14 PSD before and after ring shear tests on artificially graded sample. 187

6-15 Volumetric strain during ring shear tests on naturally graded and artificially graded sample. 188
6-16 Isotropic compression tests on Langjökull sediment. 189
6-17 1D compression curves on Langjökull sediment. 190

7-1 Development of deviator stress during drained triaxial compression tests. 208
7-2 Volumetric strain versus axial strain during drained triaxial compression tests. 208
7-3 Deviator stress development during triaxial compression test of 100kPa. 209
7-4 Volumetric strain versus axial strain during undrained shearing of 100kPa. 209
7-5 Deviator stress development during undrained shearing. 210
7-6 PWP development in undrained shearing tests. 210
7-7 Deviator stress development in undrained shearing on remoulded samples. 211
7-8 PWP development in undrained shearing tests on remoulded samples. 211
7-9 Deviator stress development in undrained shearing on undisturbed samples. 212
7-10 PWP development in undrained shearing of undisturbed samples. 212
7-11 Stress ratio versus axial strain of triaxial compression tests on Langjökull sediment. 213
7-12 Stress paths of shearing tests in high confining pressure. 214
7-13 Stress paths of shearing tests in low confining pressure. 215
7-14 Critical state line in the v-ln p'plane. 216
7-15 Constant p' correction method, schematic diagram. 218
7-16 Change in void ratio on reference section during drained shearing. 218
7-17 Dilatancy during shearing tests on remolded samples. 219
7-18 Dilatancy during shearing tests carried out under 2MPa confining pressure. 219

7-19 Dilatancy during shearing tests, 10 MPa confinig pressure. 220
7-20 Young modulus change in the low strain range in drained shearing. 220
7-21 Shear modulus change in the low strain range in drained shearing. 221
7-22 Shear modulus change in the low strain range in drained shearing. 221
7-23 .Normalisation of shearing stress 222
7-24 Volumetric strain during ring shear tests.paths. 223
7-25 Angle of residual internal friction during ring shear tests. 223
8-1 Deviator stress and PWP change due to strain rate change. 235
8-2 Stress paths of triaxial shearing. 236
8-3 Effect of strain rate change on stress path. 237
8-4 Effect of shearing rate on the residual shearing strength. 238
8-5 Effect of shearing rate on the angle of internal friction. 239
8-6 Normal stress versus shear stress of ring shear tests. 240
8-7 Triaxial shearing results of Ice Stream B-Antarctica. 241
8-8 Test R1 on Ice Stream B-Antarctica sediment. 242
8-9 Test R2 on Ice Stream B-Antarctica sediment. 243
8-10 Test R2 on Ice Stream B-Antarctica sediment. 244
8-11 Effect of step change in strain rate on undrained compression R2. 245
8-12 Effect of step change in strain rate on undrained compression R3. 246

List of Tables

2-1 Evidence of subglacial deformation measured in situ. 53

2-2 Comparison of strain rates from subglacial investigation. 54

2-3 Values of strain rate, effective pressure and residual shear strength of ring shear tests on Dutch till. 54

3-1 Summary of Langjökull sediment mineralogy test. 99

5-1 Isotropic compression tests in the high pressure triaxial cell 153

5-2 Details of isotropic compression tests in the permeameter. 153

5-3 One-dimensional compression tests in the modified oedometer cell. 153

5-4 Triaxial shearing tests on Langjökull sediment at low pressures. 154

5-5 Details of triaxial shearing tests in the high pressure triaxial cell. 155

5-6 Details of bishop-type ring shear tests on langjökull sediment. 156

5-7 Change of shearing rate during test V3-60. 156

5-8 Shearing rate change during test BR350-var. 156

Notations

B	pore pressure coefficient.
B_r	relative breakage as defined by Hardins.
B_p	breakage potential as defined by Hardins.
B_t	total breakage as defined by Hardins.
C	cohesion or apparent cohesion.
e	voids ratio.
e_o	void ratio at the start of shearing.
e_c	void ratio at the critical state.
e_g	granular void ratio.
f_c	the ratio of volume of finesto total volume of solids.
I_G	grading index, defined by Wood.
N	the value of v corresponding to p'=1 kN/m^2 on the NCL.
M	the gradient of the critical state line in the p'-q' plane.
p'	mean effective stress.
p'_{cs}	equivalent effective mean effective stress on the CSL.
q'	deviator stress.
u	pore water pressure.
T_f, T'_f	the total and the effective shear strength.
σ_1	major principal stress.
σ_2	intermediate principal stress.
σ_3	minor principal stress.
σ'_1	major effective principal stress.
σ'_2	intermediate effective principal stress.
σ'_3	minor effective principal stress.
σ_f, σ'_f	total and effective normal stress at failure.
Φ,φ'	the angle of internal friction, the effective angle of internal friction.
v	the specific volume = 1+e.
Γ	the value of v corresponding to p'=1 kN/m^2 on the CSL.
λ	the critical state gradient in the v-ln p' plane.
Ψ	sample state parameter.
ε^0	strain rate during the test = change in strain dε, imposed in a time interval of dt.

IPCC Intergovernmental Panel of Climate Change.

NCL Normal Compression Line.

CSL Critical State Line.

CRS Constant Rate of Strain.

TESRA Temporary Effect of Strain Rate and Strain Acceleration.

Chapter One

Introduction

1.1 Introduction:

Moving glaciers are powerful geo-morphological features on this planet, which have distinctly altered many areas by their action. Glacier's advances and retreats have a great effect on global climate change and sea level changes which in turn affect all earth habitats. The effect of modern glaciers, particularly on global habitats and earth systems, can be viewed not only from their influence upon humans and habitats within their immediate locality but their much more pervasive influence on all global habitats due to the effect of modern ice masses on global climate and sea-level. By investigating how subglacial sediments deform, the research presented here contributes to the debate on glacier dynamics, which have a significant effect on global climate change and sea–level changes.

The growth and decay of glaciers and ice sheets has a profound effect on global sea-level, causing very large regional and global sea-level changes over the course of glacial cycles. The third assessment report of the Intergovernmental Panel of Climate Change (IPCC), 2001, stated that glaciers are projected to continue their widespread retreat during the 21st century. The Northern Hemisphere snow cover, permafrost, and sea-ice extent are projected to decrease further. The global mean sea level is projected to rise by 0.09 to 0.88m between the years 1990 and 2100. This rise is mainly due to thermal expansion of the oceans and the reduction in glaciers and ice caps. The impact of ice sheet growth on global climate is manifest in the equator-pole temperature gradient. Because ice sheets reduce the absorption of solar radiation, they will accentuate the thermal contrasts that already exist between polar and equatorial regions. Global atmospheric circulation will always react to the increased equator-pole temperature gradient created during glaciations, especially in the Northern Hemisphere (Benn & Evans, 1998).

The predictions of global glacial cover change for the next century, as it was outlined by the Intergovernmental Panel of Climate Change (IPCC) report (2001), are an increase in the Antarctic ice sheet, likely to take place during the 21st century, while the Greenland ice sheet is predicted to loose mass during this period and contribute to sea level rise. Ice sheets will continue to react to climate warming and contribute to sea-level rise for thousands of years after the climate has stabilized. Climate models indicate that the local warming over Greenland is likely to be one to three times the global average. Ice sheet models project that a local warming larger than 3°C, if sustained for millennia, would lead to a virtually complete melting of the Greenland ice sheet with a resulting sea-level rise of about 7m (IPCC, 2001). Changes in global climate produce only minor oscillations at the margins of the Antarctic ice sheet compared with the growth and decay of the northern hemisphere Laurentide (North America) and Fennoscandian (North-western Europe) ice sheets. The Greenland ice sheets, by contrast, probably fluctuate to a far greater degree than the Antarctic ice sheet in response to glacial/ interglacial climates (Benn & Evans, 1998).

Our knowledge of modern glacial conditions needs to be increased, if we are to understand and cope with the changing climate in the coming century. The need to understand glacier environment changes is so intense that it can only be done by studying all related factors leading to or causing glaciers' deformation and movement. Generally, changes in glaciers are mainly governed by two factors: the first factor is the glacier mass balance, which reflects the difference between net gains (accumulation) and losses (ablation) measured over a specified time period, usually one year. Changes in mass balance are climatically controlled (Hambrey, 1994). The second factor which controls changes in glacial environment is glacier dynamics. One of the most fundamental characteristics of glaciers and ice sheets is their ability to move. The deformation and sliding of glaciers under the force of gravity transfers snow and ice from accumulation areas and continental interiors to areas of ablation. In the early models adopted to simulate glacier flow, glaciers were thought to rest on clean bedrock. However, borehole studies in different glacial areas revealed the presence of a bed of

deformable sediment underneath some glaciers (Boulton & Hindmarsh, 1987; Blake et al., 1992; Humphrey et al., 1993; Iverson et al., 1994; Boulton et al., 2001). While the old common model assumed that glacier movement is generated by sliding processes, recent research has proved that a high percentage of glacier movement can be attributed to shearing processes within the saturated bed sediment (Iverson et al., 1994). Glacier deformations start at the base of the glacier or ice sheet, where ice and substrate are in intimate contact and where the change is greatest, leading to most glacial sediment deformation.

Some glaciers exhibit major periodic fluctuations in velocity over timescales, ranging from a few years to several centuries, swinging between phases of rapid and slow flow. The phase of rapid motion is termed the surge or active phase. A surge-type glacier experiences a dramatic increase in flow rate, which can be 10-100 times greater than normal flow rates. Measured glacier velocity can exceed 10 km/yr, as in the case of Jakobshaven Isbrae, Greenland, which is considered to be the fastest flowing glacier on earth (Tulaczyk, 2006A). Glacier surging remains an incompletely understood cyclic flow phenomenon. It is commonly accepted that fast flow during surge is a result of extreme subglacial water pressures. However, it is unknown whether fast flow is promoted and sustained by sliding at the ice-bed interface or by deformation of the weakened, saturated, subglacial sediment. The former implies decoupling at low effective pressures with rigid bed conditions, implying that a glacier may overlie soft sediment but need not cause pervasive deformation, while the latter requires coupling between the ice and the bed, promoting the theory of subglacial bed deformation as a substantial part of glacial deformation, which will be addressed in this research.

The subglacial bed experiences significant changes when a glacier is advancing or retreating, due to the deformational pressures exerted by the moving glacier. This process is significant in shaping the geo-morphological features and controlling modern drainage patterns (Flint, 1971;Bennett & Glasser, 1996). Channels, large and small, cut by meltwater streams are an

important part of the record of present and former glaciers. Of the world's rivers, the Mississippi and the Volga have been among the greatest drainage-ways for meltwater during glacial ages (Flint, 1971).

The implications of bed deformations are potentially far reaching in terms of understanding glacier dynamics and the stability of ice sheets. Bed deformation has been measured in an increasing number of sites of modern glaciers (eg., Breiðamérkurjökull- southeast Iceland, by Boulton & Hindmarsh, 1987; Tapridge Glacier- Yukon Territory, Canada, by Blake et al., 1992; Storglaciären- Sweden, by Iverson et al., 1995; Bakeninbreen, by Porter et al., 1997). In fact, sediments revealed by glacier retreat showed a clear stamp of deformation, the shearing caused by glacier movement resulting in the remoulding of the upper part of the sediment as was observed in the sediment revealed by Breiðamérkurjökull glacier, Iceland (Boulton & Hindmarsh, 1987). Studies on the behaviour of glacial sediment are limited, and those studies which took place concentrated only on investigating the ultimate strength of the sediments (Iverson et al., 1998; Iverson et al., 1999; Tulaczyk, 1999), without going into further details in interpreting their behaviour, from the geotechnical side, and the probable factors which affect their overall strength.

At present, the understanding of many aspects of glaciers remains poor. The process of glacier movement and the intricate relationship between ice motion and subglacial sediment continues to be poorly understood, mainly because only a limited amount of data from modern ice masses exist at present, detailed subglacial observations remain meagre and the precise rheology of glacial sediments under conditions typical of subglacial environments is not known. The study of subglacial sediment erosion processes, transport and depositions of modern glacial environments furnishes some evidence as to how these processes might operate, but more focussed studies on the behaviour of subglacial sediments, for example, need to be carried out. This thesis aims at improving the understanding of glacier motion by investigating the mechanical behaviour of a glacial sediment from Iceland using techniques and theories adopted from

geotechnical engineering. Glaciers on Iceland had their maximum Little Ice Age extension by 1890-1920. Glacier variations in Iceland since 1930 show a clear response to variations in climate during this period: most non-surging glaciers retreated strongly during the early half of the monitoring period, following the warm climate between 1930 and 1940. A cooling climate after 1940 led to a slowing of the retreat and many glaciers started to advance around 1970. A warming climate since 1985 led to an increased number of retreating glaciers, and all Icelandic outlet glaciers are retreating presently and the ice caps are loosing ice volumes due to accelerating summer melt. The estimated coverage loss per year is about 0.2% overall, which amounts to 20-30 km^2 becoming ice free every year.

This chapter which includes a general introduction to the subglacial environment, introduces the role of the subglacial bed in glacier movements, the formation of glacial tills and the factors influencing subglacial bed deformations.

1.2 The subglacial environment

The first impression of glacial environments indicates a complex and geologically ephemeral nature, yet beneath this apparent chaos exists a process-driven pattern. The conditions underneath glaciers are in continuous change, new particles are produced within the subglacial sub-environment incessantly, and they are frequently modified by crushing and grinding as a result of inter-particle and particle/bed contacts (Boulton et al., 1974; Brodzikowski & van Loon, 1991). To understand the role of the subglacial sediment in a glacier's dynamics, some important facts about the glacial environment need to be considered. Conditions at the ice-bed interface depend upon the stresses acting at the boundary, the temperature of the ice, the properties of the substrate and any subglacial water flow. Subglacial bed states are fundamental in specifying the probable mode of glacier movement. Essentially, ice masses can be subdivided into those which have hard or rigid beds and those with soft, mobile or deformable beds (Figure 1-1) (Boulton, 1996). In the former case, it is assumed that the glacier bed beneath the ice is rigid, smooth with zero permeability and is undeformable. This case is the

one most often modelled in the past. These beds are likely to be composed of unfractured bedrock of high intact shear strength or, if sediment-based, to be frozen and again impenetrable to meltwater. Under these conditions, if the ice is temperate, meltwater will move along the single basal interface and thus motion of the ice mass is likely to be predominately by basal slip (Weertman, 1957).

Where soft mobile beds occur, meltwater can penetrate the underlying sediment to a lesser or greater degree and the debris may be mobilised such that ice motion is largely accounted for by this underlying mobile bed. Unlike the rigid beds situation, several interfaces may temporally exist beneath the ice mass and act as shear zones to carry the pervasive or non-pervasive tangential shear stress imported to the mobile sediment by the overlying ice mass (Menzies, 1995).

The temperature distribution (thermal regime) of a glacier is of fundamental importance to its dynamics, both in terms of the way the ice deforms and with regards to the role that meltwater plays in lubricating the bed. Glaciers can be categorised depending on their thermal condition into cold bed and temperate or wet-based glaciers.

1.2.1 Cold bed ice and temperate bed ice conditions

Temperature conditions at the glacier-bed interface are ranging from areas with cold beds, where ice temperature is below the melting point, to temperate areas, in which ice is at its melting point. The behaviour of a glacier and its bed depends much on the temperature conditions, and for an easy classification, glaciers can be put into two groups, cold bed glaciers and temperate glaciers. In the first type, also called polar glaciers, the ice base is completely frozen, with basal interface temperatures well below melting point. The ice at the base is often white, debris-free and without cavities. In this case there is no free water at the sediment-ice interface and it is usually considered that the pressure on the sediment is equal to the overburden pressure of the ice mass (Menzies, 1995). When the glacier sole is below its

freezing point, the ice adheres to the underlying surface which may be rock or frozen sediment, exhibiting a strong ice–bed bond, stronger than any bonds within the ice sole. Therefore, any applied shear stress will cause deformation within the ice itself rather than at the ice-bed interface (Goldthwait, 1960). Where the ice is frozen to the bed, the erosion of the bed or deposition of sediment is inhibited (Boulton, 2006), and the motion of the ice in this case is due only to internal deformation of the glacier body in response to gravitational stresses (Figure 1-1, A).

Where temperate glaciers are concerned, the mechanism of the ice-bed deformation is completely different, mainly because of the difference of ground water existence in the system. For temperate glaciers, there are many water sources, surface meltwater being the main source of water in the glacial system (Shreve, 1972). Also of significance is the production of meltwater by geothermal heat at the glacier bed, melt from internal deformations generating heat conducted down the pressure melting gradient (Shreve, 1972). The ice at the base of wet-based, or temperate glaciers, is usually debris-rich. The thickness of the ice-debris layer and the concentration of debris vary depending on several influencing conditions. In this type of ice mass, meltwater usually fills the glacial cavities or it would form a thin layer at the ice-sediment interface. Unless the meltwater was drained, either by forming interconnected cavities to form a drainage channel or through conduits, then this water would be under constant high pressure, sometimes equal to the overburden pressure (Boulton & Hindmarsh, 1987).

The style of subglacial behaviour depends on a number of parameters, identified as ice-sheet velocity, basal shear stress, pore-water pressure, effective pressure, equal to the total pressure minus pore water pressure, and the geotechnical properties of the subglacial material (Hart, 1995). Where a deformable sediment, saturated by meltwater, exists beneath ice masses, deformation will occur when the applied shear stress imparted by the overlying moving ice overcomes the internal shear strength of the sediment (Figure 1-1, C) (Boulton, 1996). This process might be controlled by

more than one influencing parameter among which are the level of consolidation, grain size and porosity of the sediment (Menzies, 1995).

1.2.2 Origin of glacial sediments

Glacial sediments, also commonly called tills, refer to those sediments deposited by glaciers (see later). The variability of tills depends upon numerous factors, and usually the lithologic variety of rocks and minerals in the till, and their particle size are considered most important. These variables can be determined quantitatively, and therefore most of the applied classifications and descriptions of tills are based upon lithologic and granulometric parameters (Dreimanis, 1976).

Equally significant, is the origin or genesis of the till. It involves a sequence of events, beginning with the erosion of rocks and minerals, or merely deformation of them by a glacier or its meltwaters, followed by transport of this eroded material in or upon a glacier and then completed by deposition as till by various mechanisms. There are many variables involved in the above sequences, taking into consideration that some parts of till may go through this cycle several times (Dreimanis, 1976). Erosion, which is considered as one of the main mechanisms behind the formation of subglacial sediment, happens when a sediment particle is detached from its bed due to shear stresses exerted by the moving glacier, to enter the glacier transport. The converse situation, where the particle comes to rest as a result of rising resisting forces or falling shear stresses, is deposition (Benn & Evans, 1998). Erosion at the bed of glaciers comprises various processes: crushing, fracturing and abrasion, which combine to produce a sediment very different from that carried on the surface. Debris eroded in this fashion are initially transported in a basal zone of traction, where particles frequently come into contact with the glacier bed and are retarded, so that large forces are imparted on both the particle and the bed (Hambrey, 1994).

A till can be transported and deposited in a number of ways, and it is very important to recognize two principal types of till whose compositional characteristics are not so much governed by their environment of deposition

as by their entrainment and transportational history. The first type, the lodgement till, or basal till, is made of detritus carried in the basal or debris layer part, which comprises of probably 10-40m depth of the glacier, at the bed-glacier interface (Shilts, 1976), where the sediment density is high and mutual attrition of particles is severe due to the high frequency of clast to clast contacts. Shearing of differential movement of one clast with respect to another is dominant in this zone and drastically alters the physical characteristic of the debris during transport (Hart et al., 2004; Hooke & Iverson, 1995; Benn, 1995) . There is some disagreement on the formation of basal tills. Most geologists consider that basal tills have been deposited from the base of moving ice by a "plastering on" effect, producing what some refer to as a "lodgement till". Others consider that basal till was deposited by melting at the base of stagnant ice. Hart (1995) argued that deposition when the substrate is deformable is occurring by a combination of three different processes: melt-out at the ice-sediment interface, transportation of the sediment within the deforming layer due to glacial flow, and by basal shearing. Any of these methods may be valid, depending on the specific glacial regime. In any of these cases, it is assumed that particles were released from the ice by basal melting. Whatever the deposition mode, the resulting unstratified, unsorted mixture with a wide range of grain sizes material is known as "till" (Milligan, 1976; Flint, 1971). The second type of till is ablation till, comprising debris carried englacially or on the glacier's surface. The density of sediment carried in the englacial or supraglacial mode is much less than that of the basal portion so that clast attrition is reduced during transport, commonly leading to a coarser sediment with larger and more angular clasts than lodgement till (Shilts, 1976).

Tills consist predominantly of rock material that was not decomposed before deposition. Minerals such as hornblenders, micas, and plagioclase feldspars, notably susceptible to chemical decay, are conspicuous in till derived from rocks that contain those minerals. Most of the clasts, regardless of their size, are mechanically broken or abraded. These characteristics indicate that the related glaciers were eroding fresh rock rather than decomposed regolith (Flint, 1971).

The mechanical behaviour of subglacial sediment has not been fully interpreted yet. Limited studies on subglacial sediment geotechnical behaviour have been presented, and those studies concentrate on estimating the sediment ultimate strength without studying its full geotechnical properties and its behaviour within the modern Critical State framework (e.g. Kamb, 1991; Tulaczyk et al., 2000; Iverson et al., 1998). Understanding the rheology of tills is still vague in terms of the effect of shearing rate on the sediment behaviour during shearing. This mainly stems from the lack of sufficient geotechnical testing data which covers this subject.

1.3 Geotechnical theoretical aspects

This section aims to present the basic geotechnical theoretical aspects which are used to interpret the mechanical behaviour of sediments. It presents the essential theories in soil mechanics to describe stress-strain relationships in soil and solve problems of soil masses stability.

1.3.1 Stresses in soils

For a soil subjected to a given total stress, it is intuitive that the behaviour of the soil will, in some way, be dependant on the magnitude of the pore pressure. The principal stresses can be defined as those stresses acting normal to the principal planes, where the shear stress value is equal to zero and the stresses acting normal to theses planes are at their maximum (σ_1), intermediate (σ_2) or minimum (σ_3) value, taken to be positive in compression.

The principle of effective stress determines the effect of a pore pressure on the behaviour of a soil with a given total stress. The principle of effective stress was first stated by Terzaghi in 1936 which stated that the stresses in any point of a section through a mass of soil can be determined from the total principal stresses σ_1, σ_2 and σ_3 which act at this point. If the voids of the soil are filled with water under a stress u, the total principal stresses consist of two parts. One part u acts in the water and in the solid in every direction with equal intensity, which is called the pore water pressure. The balance: $\sigma'_1 = \sigma_1 - u$, $\sigma'_2 = \sigma_2 - u$, and $\sigma'_3 = \sigma_3 - u$ represents an excess over the neutral stress u and it has its seat exclusively in the solid phase of the soil. This fraction of

the total principal stress is called the effective principal stress. The Terzaghi fundamental effective stress equation can be written in a more general way as follows:

$$\sigma' = \sigma - u \quad .....[1\text{-}1]$$

where:

σ' is the effective stress

σ is the total stress.

u refers to pore water pressure.

In saturated soil, all measurable effects of a change of stress, such as compression, distortion and a change of shearing resistance, are exclusively due to changes in the effective stresses (Terzaghi, 1936).

1.3.2 Mohr- Coulomb failure theory

A knowledge of shear strength is required to solve problems concerning the stability of soil masses. If at a point on any plane within a soil mass the shear stress becomes equal to the shear strength of the soil, failure will occur at that point. The shear strength (τ_f) of a soil at a point on a particular plane was originally expressed by Coulomb as a linear function of the normal stress (σ_f) on the plane at the same point:

$$\tau_f = c + \sigma_f \tan \Phi \quad ..... \quad [1\text{-}2]$$

where:

c and Φ are the shear strength parameters, termed as the cohesion intercept or apparent cohesion, and the angle of internal friction, respectively (Atkinson & Bransby, 1978; Craig, 1974).

Changes of shearing resistance are due exclusively to changes in the effective stresses σ'

$$\tau'_f = c' + \sigma'_f \tan \Phi' \quad ..... \quad [1\text{-}3]$$

where the cohesion and the angle of internal friction are now represented by the symbol c' and Φ', implying that the equation is written in terms of effective

stresses. The failure criteria of Equations [1-2] and [1-3] given above are known as the Mohr-Coulomb failure criteria.

The shear strength of a soil can also be expressed in terms of the effective major and minor principal stresses σ'_1 and σ'_3 at failure. At failure, the line defined in Equation [1-3] will be tangential to the Mohr circle representing the state of stress, as shown in Figure (1-2), compressive stresses being taken as positive.

When analyzing a triaxial deformation experiment, the effective stress parameters q′ and p′ are more appropriate invariant quantities, where the mean effective pressure is

$$p' = \tfrac{1}{3}(\sigma'_1 + \sigma'_2 + \sigma'_3) \quad \text{.....[1-4]a}$$

p′ includes the intermediate principal stress σ'_2, which in the case of triaxial test is equal to the radial effective stress $\sigma'_r = \sigma'_2 = \sigma'_3$ and σ'_1 is equal to the axial effective stress σ'_a . The deviatoric stress can be expressed by:

$$q' = \sigma'_1 - \sigma'_3 \quad \text{.....[1-4]b}$$

For a purely frictional material, failure is governed solely by the angle of internal friction Φ'. By re-arranging [1-3] the ratio q′/p′ can be expressed as:

$$\frac{q'}{p'} = \frac{6 \sin \Phi'}{3 - \sin \Phi'} \quad \text{.....} \quad \text{[1-5]}$$

1.3.3 Critical State Framework

Normally consolidated clays, which can be defined as those clays which have never been under greater effective pressure than the current effective

pressure, in their equilibrium state, (with zero excess pore pressure), when they are compressed form a unique straight line in the specific volume (v) -ln p′ plane, known as the Normal Compression Line (NCL), as shown in Figure (1-3). The specific volume v is defined as the volume of the soil sample containing unit volume of soil grains and its relation with the void ratio as follows:

$$v = 1+e \quad \ldots\ldots\ldots\ldots [1\text{-}6]$$

where (e) is the void ratio of soils which is the soil mechanical property used to measure the packing of the grains of the soil, and can be defined as the ratio of the volumes of the void spaces and the mineral grains. In a saturated soil, the void spaces are completely filled with water and so the void ratio may be expressed in terms of water content (Atkinson & Bransby, 1978).

The initial curvature in the compression data in the v-ln p′ plane, is correspondent to the recompression process. After reaching the soil preconsolidation pressure, which is the maximum pressure the soil was subjected to during its history (Casagrande, 1936), the recompression curve ultimately joins the virgin compression or Normal Compression Line.

By applying a deviatoric stress, the sample ultimately reaches its failure, when the soil may continue to deform without further changes in stress or volume (Roscoe et al., 1958). This state is called "Critical State", which represent the basis on which the Critical State Model is built, by assuming that for a given soil the locus of the Critical State in v-q′-p′ space, forms a unique line, independently of how it is reached (drained or undrained shearing), called the Critical State Line (CSL). The projection of the CSL in the p′-q′ plane is shown in Figure (1-4), which is represented by a line with a gradient of M.

The projection of the Critical State Line on the v- p′ plane is a curve, however, the same data can be presented as a linear relationship by scaling the mean effective pressure axis in a logarithmic scale (Atkinson & Bransby, 1978).

The Critical State Line (CSL), in the v-ln p′ plane is usually a line with the same gradient as the Normal Compression Line (Figure 1-3), and may be represented by the equation:

$$v = \Gamma - \lambda \ln p' \quad \ldots\ldots\ldots \quad [1\text{-}7]$$

where:

v the specific volume of the sample.

λ the CSL gradient.

Γ the value of v corresponding to p′= 1.0 kN/m^2 on the CSL (Atkinson & Bransby, 1978).

The behaviour of clays is mainly dependent on their consolidation state. The difference between the stress paths of normally and over-consolidated clay samples, which they exhibit during shearing before reaching the failure state, can be extremely distinct. Stress paths followed in standard triaxial tests may also be represented in q′:p′:v space. For normally consolidated soils, which start their shearing stage from a point on the NCL, both undrained and drained tests define a curved three-dimensional surface, linking the NCL to the CSL (Roscoe et al., 1958). This surface, which defines all test paths for soils on the Normal Compression Line at the start of shearing, is called the Roscoe surface as shown in Figure (1-5). The shape of this surface is usually defined by the shape of undrained tests paths from the Normal Compression Line (Atkinson & Bransby, 1978).

To represent a possible stress path for a drained normally consolidated sample in the v-ln p′ plane, consider a sample which was isotropically compressed up to a certain pressure so it is on or near the NCL, point D in Figure (1-6). The path of the test expected for this sample could be any route which transfers the sample from its current state to the Critical State, on the CSL, which is usually associated with the sample being compressed and hardening during the shearing stage (Figure 1-6). Those samples which approach the CSL from the right side of it as in the sample described are termed “wet” of Critical State (Atkinson & Bransby, 1978).

Similarly, if the stress path of a sample which lies below and to the left of the CSL is considered, a sample which might be in the position of point E in Figure (1-6), is expected to expand and dilate till it reaches the CSL, after may be an initial compression at the early stages of shearing. This behaviour is the expected behaviour of heavily over-consolidated clays, and those samples which lie below and to the left of the CSL are considered "dry" of Critical State.

The failure of heavily over-consolidated clays in the q'-p'-v space defines another boundary state surface which starts from the tension failure surface and extends to the Critical State Line, intersecting with the curved Roscoe surface, called Hvorslev's surface, as shown in Figure (1-5). Here, we may also distinguish carefully two particular states attained by the over-consolidated soils. The first is the failure state, at which the deviator stress reaches a maximum, and the second state can be called the ultimate state, and it is that state at which large shear strains can occur with no change in stresses or volume. An ultimate state may or may not be achieved at the end of the test, and it appears from the data shown previously that over-consolidated clay and sand specimens often do not reach a well-defined ultimate state in triaxial tests (Atkinson & Bransby, 1978; Coop & Airey, 2003) and usually much larger strains are required to reach the Critical State as in the case of carbonate sand. The statements of the unique NCL and CSL, and Roscoe and Hvorslev surfaces, form the basis of the Critical State framework. Until recently it was assumed that all soil behaviour can be described using the Critical State framework, but new results on natural structured soils, and so called "transitional" soils (Martins et al., 2001), are questioning the universal applicability of that framework.

1.4 Research Aims and Objectives

The aim of this study is to provide a better understanding of glacial sediment mechanical behaviour, based on results from tests on samples that were collected from areas of the retreated margin of Langjökull- Hagafelsjökull glacier, a temperate glacier in Iceland. The research, which applies engineering knowledge to the problem of glacier motion, is at the interface

between soil mechanics and earth sciences. This approach is new and should yield interesting results for geologists and glaciologists to explore, as well as providing geotechnical engineers with valuable data to add to the database of granular soils. The objectives to be met to achieve the aim above are:

1. To evaluate the amount of subglacial deformation, which the sediment has suffered through its deposition and loading history, in order to achieve a better understanding of the role of the sediment bed deformation on glacier surging. This is achieved by studying the sediment particle crushability to evaluate the deformation characteristics of the retrieved sediment.
2. To investigate the validity of applying traditional geotechnical theories of soil mechanics to the behaviour of the sediment, in particular the validity of the Critical State framework in interpreting the sediment behaviour.
3. To explore the rheology of the sediment in terms of time dependency and viscous behaviour and the effect of shearing rate on the sediment mechanical behaviour.

1.5 Methodology

To achieve the aim of the study, a full investigation of the mechanical behaviour of the sediment has been undertaken. This includes a study of particle breakage of the sediment to explore the mechanisms governing this sediment's behaviour underneath the glacier, and the validity of coupling or decoupling behaviour. Particle breakage is studied for different patterns of stresses and different levels of strains, and monitored by sieving as well as monitoring the particle's deformation more closely by the use of a scanning electron microscope (SEM).

All possible deformation conditions under the glacier are investigated by subjecting the sediment to isotropic compression up to 250MPa by the use of a high pressure triaxial cell and a permeameter (see Section 4.3), and by shearing to different levels of strains, ranging from small strains, which can

be achieved in the triaxial cell to very high strains of about 50,000% by means of a Bishop's ring shear apparatus.

The validity of the Critical State framework in interpreting the behaviour of this sediment is scrutinized by performing shear tests in triaxial cells, with pressures ranging from low to moderate pressures, and up to 30MPa of effective confining pressure.

The viscous behaviour and shearing rate effect on the sediment behaviour is investigated by using variable shearing velocities on the sediment in a fully computer controlled triaxial cell equipped with LVDTs (Linear Variable Differential Transformers) for local strain monitoring. The effect of the shearing rate on the residual strength of the sediment was also examined by shearing the sediment with variable shearing velocities in a Bishop's ring shear apparatus.

1.6 Structure of the Thesis

The thesis consists of nine chapters. Chapter One introduces general information about the subglacial environment, types of glaciers and bed deformation. It also presents the basic geotechnical theoretical aspects which are used to describe the soil mechanical behaviour.

Chapter Two presents a review of the literature concerning subglacial stresses and deformations. The chapter also includes the application of the Critical State framework to granular sediments and its validity in interpreting different types of sediment behaviour, with a special reference to the behaviour of transitional soils. Particle breakability and crushability and its effect on cohesionless sediment behaviour is reviewed; a subject which is considered to be highly relevant in subglacial deformation. Literature on time dependency and shearing rate effect, is covered in Chapter Two as well, with special review of geophysical research on different subglacial sediments relating to this subject.

Chapter Three presents the sediment used in this research; the location of sediment retrieval, general description of the sediment, mineralogy, particle size distribution and sampling method.

Chapter Four covers the apparatus used in the testing programme, testing procedures and details of sample preparation.

The laboratory testing programme is presented in Chapter Five. This chapter lists all tests carried out on the sediment with details of sample properties. The chapter also discusses the methods for calculation and analysis of data to be presented in the following chapters.

Results and their discussion are presented in Chapters: Six, Seven and Eight. This includes data of tests investigating particle breakage in the sediment and its effect on the sediment mechanical behaviour (Chapter Six) and results concerning the mechanical behaviour of the sediment during shearing and the Critical State (Chapter Seven). Results of tests covering the investigation of shearing rate effect on the sediment mechanical behaviour are presented and discussed in Chapter Eight. This includes stress path tests which present shearing rate effects on the sediment mechanical behaviour, and Bishop's ring shearing data to investigate shearing rate effects on the residual strength of the sediment. The chapter also presents a new analysis of existing data of variable rate shearing tests carried out on the Ice Stream B-west Antarctica subglacial sediment (data from Tulaczyk, 1999). The results are re-analysed and used for comparison with the results obtained from testing Langjökull sediment.

The last chapter, Chapter Nine, presents the conclusions from the research, with recommendations for further studies.

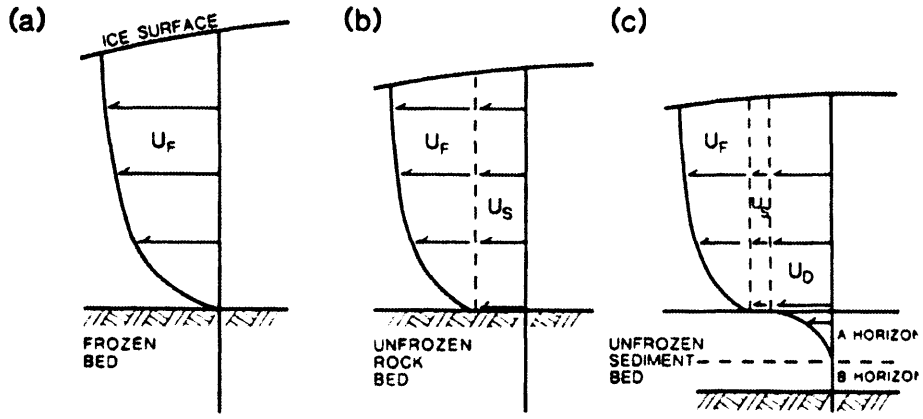

Figure (1-1): Ice Flow on different bed conditions, after (Boulton, 1996).
Ice Flow in this figure is from right to left.

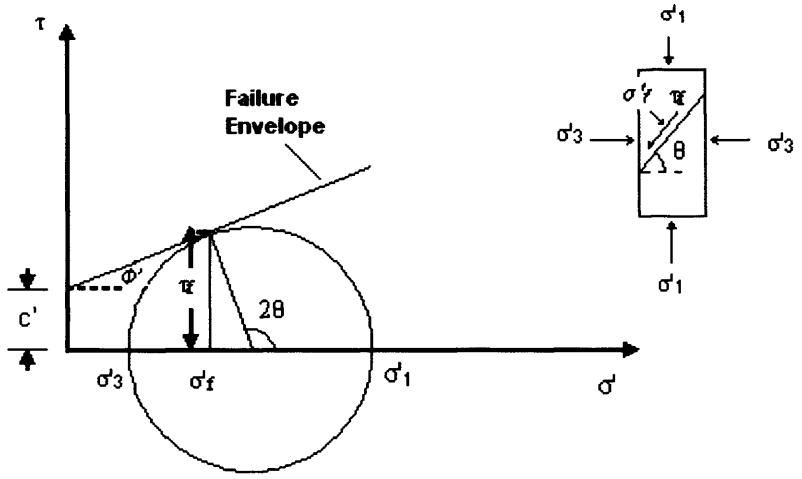

Figure (1-2): Stress conditions at failure.

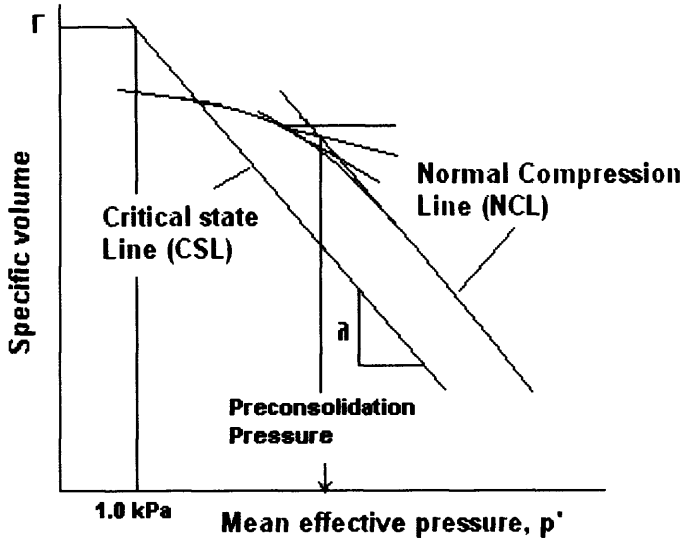

Figure(1-3): Schematic diagram showing the Normal and the Critical State Lines in the v-ln p′ plane.

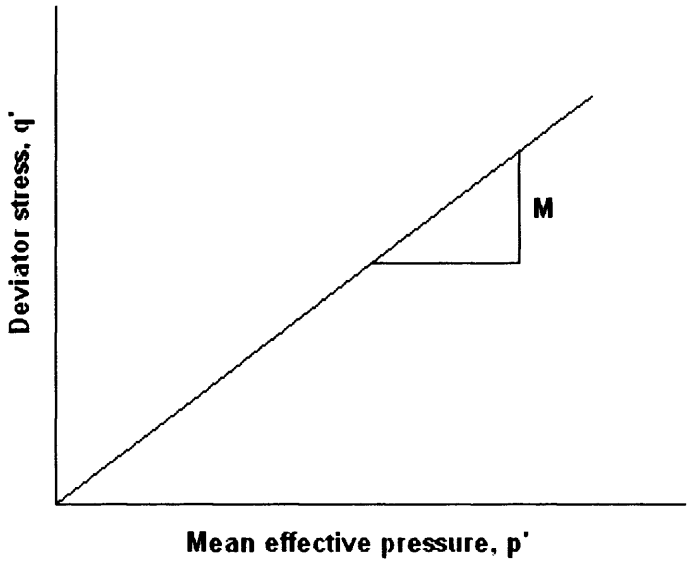

Figure (1-4): Schematic diagram showing the Critical State Line (CSL) in the mean effective stress(p′)- deviator stress (q′) plane.

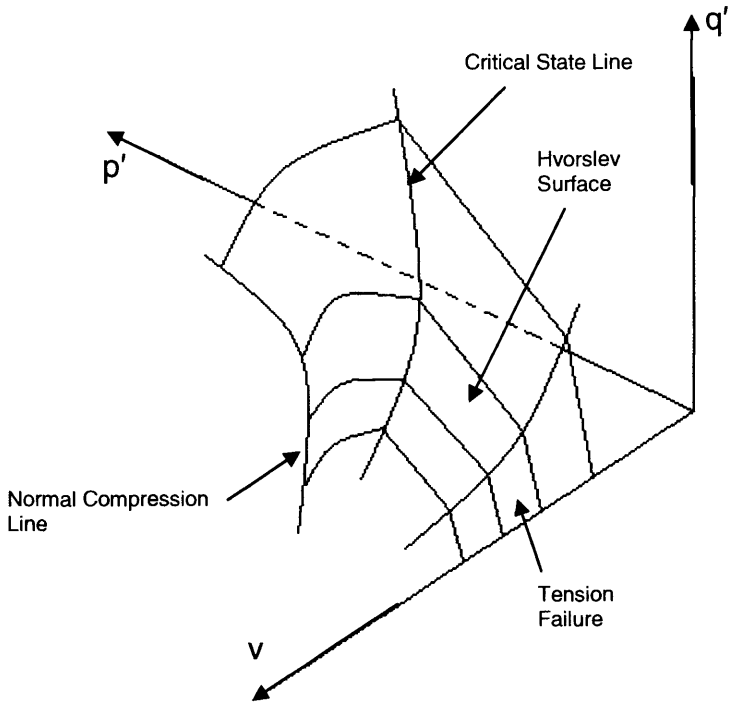

Figure (1-5): The Boundary surfaces in the q′:p′:v space, after Atkinson and Bransby, 1978.

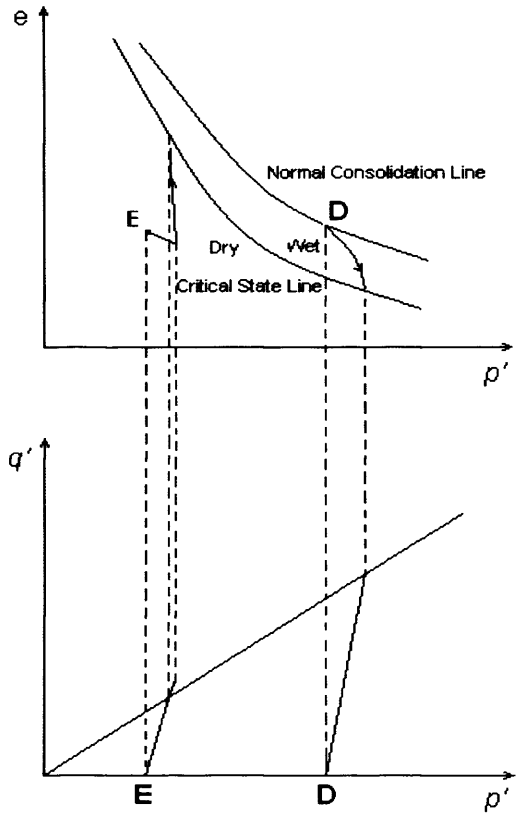

Figure (1-6): Stress paths for drained test on normally consolidated and over-consolidated samples of clay. Figure modified after (Atkinson & Bransby, 1978).

Chapter Two

Literature Review

2.1 Introduction

The discovery of the existence of subglacial sediments is a fundamental departure from past understanding of ice mass sliding. Not only do models of ice mass sliding have to be reconsidered in the light of the existence of deformable beds but, for the first time, an integration of glaciological conditions and sedimentological processes at the ice-bed interface is achieved. Studies on the behaviour of glacial sediments are limited, and those studies which took place concentrated only on investigating the ultimate strength of the sediments (e.g. Iverson et al., 1998; Iverson et al., 1999; Tulaczyk et al., 2000), without going into further details in interpreting their behaviour, and understanding the probable factors which are affecting their overall strength, as this would require geotechnical knowledge.

This chapter is divided into four main parts. In the first part, the most relevant literature in the geophysical sciences is reviewed, to give a good understanding of the subglacial environment stresses and deformations to which the sediment was subjected through its depositional and stress history. The second part of this chapter concentrates on reviewing the literature on the mechanical behaviour of granular materials and the application of the Critical State framework (Roscoe et al., 1958) in interpreting their behaviour, with special reference to the possible transitional behaviour of sediments. Particle breakage, which is a relevant subject in glacial sediment deformation, is discussed in the third part of this chapter. This includes presenting previous work results on the effect of sediment crushability on the mechanical behaviour of granular soils, and on glacial sediments in particular. Finally, the debate on the viscous behaviour of subglacial sediments, and the variable shearing strain rates imposed by glacier movement, is another significant issue in understanding the behaviour of subglacial sediment. The viscous behaviour, mainly the effect of shearing

rate on the behaviour of soils, is reviewed in the last part of this chapter, with reference to glacial sediments in particular.

2.2 Subglacial stresses and subglacial deformations

Subglacial deformation is a broad term that includes the pervasive deformation of some or all of a till layer, shear along discrete failure surfaces, and ploughing through the till of particles at the ice-till interface. Folds, faults, fractures and injection structures, apparently controlled by ice-induced shear, have been described in many tills. In general, the appearance of the till should reflect the type of deformation. However, there is no agreed criterion to distinguish a till that has been pervasively deformed to large strains from one that has not (Paterson, 1969).

The stress history of a glacial sediment is quite different to that of any other sediment. This difference was imposed on the sediment by the nature of its deposition, transportation and sedimentation. Glacial sediments, unlike other common sediments, were under unique conditions beneath glaciers when deposited and suffered incessant shearing due to the glacier's continuous movement and ice flow at the glacier's bed, which is one of the major causes of rock fracture and erosion during deposition. Subglacial erosion and abrasion of rocks are considered to be the main sources of debris in the basal layer of the glacier, and eventually the source of subglacial sediment (lodgement). Lodgement till is formed when the glacial debris is smeared into a deformable bed due to the movement of a glacier. In temperate glaciers, this sediment, which is sourced from the disaggregation of bedrock or incorporation of melt-out till, has been largely homogenised by shearing in the subglacial deforming layer (Dreimanis, 1976; Milligan, 1976; Boulton, 1976).

The effective pressure at the glacier bed determines the bed shear resistance to glacier movement and is fundamental to many aspects of subglacial sedimentary processes and glacier dynamics. The effective pressure at a temperate glacier bed is largely dependent on the extent to which melt-water can drain away. Therefore, an evaluation of pore water

pressures at the glacier bed is vital to estimate the effective stresses acting on the bed and the degree of deformation in the bed-sediment (Boulton & Dobbie, 1993). The pore water pressure regime underneath glaciers is explained in the next sub-section (2.2.1).

The shear deformation of sediments and the change in sediment structure due to high strains is likely to affect sediment properties such as shear strength and permeability. The response of a sediment to applied shear stresses will be dependent on basal conditions. Shear forces must be transmitted from the ice to the sediment. Coupling across the ice-sediment interface is unlikely to be uniform, and so the shear stress transmitted to a portion of the glacier may vary. The heterogeneity of the resulting deformation is probably more marked than in other geological environments (Murray, 1994). The bed coupling/decoupling is reviewed in sub-section (2.2.2).

Deformation may be pervasive (e.g. Boulton & Hindmarsh, 1987), and occur through a significant depth of basal material, or alternatively, discrete deformation may occur (Kamb, 1991), resulting in localised planes or regions of high strain with little strain occurring in the surrounding sediment. Clasts entrained at the ice-sediment interface may plough through the underlying sediment if the sediment yield strength is exceeded only locally. Ploughing represents an intermediate state between sliding and pervasive deformation (Murray, 1994).

2.2.1 Pore water pressure underneath glacier

The condition in which the underlying bed of a glacier is found is critical in studying the type of stresses and deformation exerted within this sediment. Under temperate glaciers, where meltwater can be found, sediments are usually fully saturated. The flow of meltwater beneath glaciers has normally been supposed to occur within a thin subglacial zone, either within channels immediately beneath the glacier, or as a thin sheet flow between the glacial sole and bed (Boulton & Dobbie, 1993). Measurements of pore water pressure by the means of boreholes showed the existence of high pore water

pressures in the bed sediment (Fountain, 1994). In most cases, as in the case of Langjökull Glacier, these pore pressures reach a value close to the value of the ice overburden pressure (Eyre, 2003; Fountain, 1994). The effective pressure at the glacier sole is largely dependent on the extent to which meltwater can drain away through the substratum, or through channels within the bed or the glacier sole itself (Boulton & Dobbie, 1993). It is generally assumed that most of the deformational processes of the sediment underneath glacier are taking place in undrained conditions. Based on these facts, Boulton & Dobbie (1993) concluded that the consolidation process in subglacial tills is usually incomplete, due to the existence of meltwater under glacier. This suggests that the state of consolidation of subglacial tills does not reflect the history of ice loading on the bed sediment.

2.2.2 Bed coupling/ decoupling and glacier movement

The major argument about glacier surging is about the mechanism in which the glacier is moving over its bed. It is still unknown whether fast flow is promoted and sustained by sliding at the ice –bed interface, or by deformation of weakened, saturated, subglacial sediments. The former suggests decoupling at low effective pressure, implying that a glacier may overlie soft sediments but need not cause pervasive deformation of them (Kamb, 1991; Fuller & Murray, 2000; Iverson et al., 1995; Iverson et al., 1999). The latter hypothesis emphases the role of the underlying bed deformation on glacier surging (Boulton & Hindmarsh, 1987; Alley et al., 1987; Tulaczyk et al., 2000; Hart & Smith, 1997), indicating a coupling of the glacier sole and its bed, suggesting that a glacier can deform its bed pervasively and that glacier movement is mainly attributed to this deformation. A number of devices, to be inserted into the subglacial bed from the glacial surface, to collect the necessary data for a better interpretation of the subglacial sediment behaviour, have been proposed by geophysical researchers. For example, the tiltmeter which investigates whether the sediment is actively shearing (Iverson et al., 1994), dragpools, which are used to measure sliding velocities (Blake, 1994) , the ploughmeter, which is used to measure the sediment field strength (Fischer & Clarke, 1997), and

the dragometer which was used for the same purpose (Iverson et al., 1994), where the till strength is measured by dragging an object through the till and measuring the force on the object (Figure 2-1). The argument against these techniques is that they neglect the role of pore water pressure development during the process of measuring the till strength (Iverson et al., 1994), making them appropriate only when the subglacial till is sufficiently permeable, so that excess pore water pressure does not develop during the test.

In-situ collected data from different glaciers (Table 2.1) indicate that glacier movements are mainly due to subglacial sediment deformation and that even during cycles of quiescence and rapid motion of ice, the ice remains coupled to its bed (Tulaczyk, 2006). This was confirmed as well by GPS (Global Positioning System) data of Whillans Ice stream- west Antarctica (Bindschadler et al., 2003), and the analysis which was presented by Tulaczyk (2006), based on the amount of waterflux available beneath the ice.

2.3 Behaviour of granular sediments within the Critical State framework

The concept of the Critical State framework (Roscoe et al., 1958), presented in the previous chapter, has been successfully applied to modelling the behaviour of sands (Coop & Lee, 1993), although the mechanisms in sands depend mainly on particle breakage.

Coop & Lee (1993) examined the behaviour of three types of sands: Dog's Bay sand, a carbonate sand; decomposed granite, and Ham River sand, a quartzic sand. In isotropic compression, a unique Normal Compression Line (NCL) was identified at high stress levels in the specific volume- logarithmic scale of mean effective pressure (v-ln p′) plane, regardless of the initial density of the samples (Figure 2-2). This was earlier observed on the behaviour of Chattahoochee River sand, a quartz sand, by Vesic & Clough (1968) (reported by Atkinson & Bransby, 1978). The plastic volumetric strain caused by compression down the Normal Compression Line is associated with particle breakage. The stress level at which this breakage starts and where the Normal Compression Line is encountered depends not only on the

strength of the particles but also on the density of the soil. Denser samples of each soil tend to exhibit higher yielding stresses than loose samples, resulting from the greater number of particle contacts in the dense soil and hence lower contact stresses (Coop & Lee, 1993).

A Critical State Line (CSL) has also been identified for sands that lies parallel to the Normal Compression Line (Figure 2-2). Critical State for sands is again governed by the particle breakage of the soil. The Critical State Line for sands, is identified as a parallel to the NCL, and may be defined by the same formula presented in Equation (1-7) for clays:

$$v = \Gamma - \lambda \ln p' \quad \ldots\ldots\ldots \quad [1\text{-}7]$$

The behaviour of less uniformly graded sands was also investigated through the addition of silt-sized particles. Both the gradient (λ) and the intercept (Γ), of the Critical State Line were found to be reduced (Coop & Lee, 1993). The spacing between the Critical State Line (CSL) and the Normal Compression Line (NCL), was also noted to be reduced by the addition of fines to the Dog's Bay sand (Coop & Atkinson, 1993). This will be discussed further in the next few sections.

2.3.1 Stress-dilatancy of granular materials

The stress path during shearing of granular sediments, like sands, depends on the internal state of the material. Dilatancy, is one of the features of deformation during sand shearing. When subjected to shear, a loose sand contracts and a dense sand tends to dilate. According to the Critical State framework, a dense or loose state is defined not only in terms of density but also of the confining pressure (Atkinson & Bransby, 1978 ; Li & Dafalias, 2000; Verdugo & Ishihara, 1996). This is because such a definition is relative to the Critical State Line in the v versus p′ space. The combination of stress and volume is usually referred to as "state". For a given e, for example, the sand will behave like a dense material for a sufficiently low p′ and like a loose material for a sufficiently high p′. Furthermore, for a sand that initially is either in the loose or dense state, there is an ultimate state of failure at which the

volumetric strain rate is zero (Li & Dafalias, 2000). This ultimate state is the well known Critical State (Roscoe et al., 1958) characterised by a unique combination of p′, q′ and critical void ratio e in a triaxial setting.

Consider two specimens of the same sand. One is in a loose state and the other in a dense state, accounting for both density and pressure. By subjecting shearing loading, the loose specimen contracts and the dense specimen dilates, as shown in Figure (2-3), in terms of undrained stress path in q′-p′ space.

Now consider a sand in dense state subjected to an undrained shear. As shear proceeds, the test path passes a so-called 'phase transformation state' (Li & Dafalias, 2000), and then approaches the critical state at a stress ratio $q'/p'=M$ (Figure 2-3).

Several attempts have been made to describe the state, on which the behaviour of the specimen will depend, in terms of contraction and dilatancy. Been & Jefferies (1985) defined a state parameter:

$$\psi=e-e_c \quad \ldots\ldots\ldots\ldots\ldots [2\text{-}1]$$

where:

e is the current void ratio

e_c is the critical void ratio on the Critical State Line in the e- ln p' plane corresponding to the current p', as shown in (Figure 2-4).

The state parameter ψ is a measure of how far the material state is from the Critical State in terms of density and whether the sample will be experiencing contraction or dilation during its shearing to reach its Critical State. Klotz & Coop (2001) proposed an alternative state parameter, based on the horizontal distance to the CSL, to avoid problems with the definition of the CSL at low stresses. Their state parameter is also a useful normalising parameter (see Section 2.3.2).

The steady state of sandy soils was further studied by (Verdugo & Ishihara, 1996). Undrained shearing data on Toyoura sand samples with the same

void ratio after consolidation, indicated that although these samples exhibited different stress- strain behaviour at the early stages when tested under different confining pressure, they tended to have the same ultimate strength at a large level of deformation (Figure 2-5). The data also illustrate the stress path dependence on the sample void ratio. While the loose samples exhibit pure compressive behaviour when sheared under relatively high confining pressure, a sample with the same density would exhibit some dilative behaviour before it reaches its Critical State, when sheared under lower confining pressure (Figure 2-6B,C).

It is also observed that at large levels of strain, stress-strain curves of drained sheared samples of a granular soil, sheared under the same confining pressure, would merge into a single one (2-7A), regardless of the sample initial void ratio. In terms of deviator stress and void ratio change during the test, the sample shows a change in void ratio, by compressing, in the case of a loose sample, or dilating, in the case of dense sample, as the deviator stress increases till it reaches a common void ratio and a common deviator stress for all tests, corresponding to the soil Critical State at this confining pressure (Figure 2-7B), (Verdugo & Ishihara, 1996).

2.3.2 State boundary surfaces

The yield surface of a given soil depends on its preconsolidation history and thus void ratio. In order to investigate the boundary surfaces, that is the Roscoe and Hvorslev surfaces, a scaling method of stresses is defined so as to account for the changes in the specific volume, or void ratio changes that occur during the test. One method, is by using the equivalent pressure p'_e on the Normal Compression Line at the current specific volume during testing (Atkinson & Bransby, 1978; Coop & Lee, 1993; Jovicic & Coop, 1997) as shown in Figure (2-8). Figure (2-9) shows normalised test paths for both drained and undrained tests conducted on Dog's Bay sand by Coop & Lee (1993) using this method. The value of p'_e at any specific volume can be given by the equation:

$$p'_e = \exp[(N-v)/\lambda] \quad .....[2\text{-}2]$$

where:

N is the value of v corresponding to p'= 1.0 kN/m^2 on the NCL

λ is the gradient of the Normal Compression Line in the v-ln p' plane.

The normalised stress paths clearly define the two state boundary surfaces, with the normally consolidated tests starting from the Normal Compression Line, represented by the point p'/p'_e=1.0 and ending at the Critical State Line which is also represented by a point in the normalised chart.

In some cases, a difficulty is encountered in defining the Normal Compression Line, as in the case of soils with transitional behaviour. The normalisation in such a case could be done by an equivalent pressure on the Critical State Line p'_{cs} for the soil as a state parameter instead of p'_e, in the above mentioned method. This approach was adopted by Klotz &Coop (2001). The method depends on specifying the equivalent pressure on the Critical State Line p'_{cs}.as shown in (Figure 2-8). The Critical State Line, can be defined from its position and slope in the v-ln p' space by the equation previously given in Section (1-3-4) :

$$v = \Gamma - \lambda \ln p' \text{.....[1-7]}$$

The normalised path can then be identified in the (p'/p'_{cs}) versus (q'/p'_{cs}). The Critical State Line in this case would be represented by a point which is encountered at (p'/p'_{cs})= 1.0.

2.4 The effect of the presence of fines on the mechanical behaviour of sediments

Fines content affects granular soil behaviour, as was shown by Coop & Lee (1993) and mentioned in Section (2-3). The effect of fines on the behaviour of granular sediments during compression depends on the type of fines and their plasticity as well as their percentage to the total weight of the sample. The addition of silt-sized fines to a sub-rounded to sub-angular medium quartzitic sand has been shown to increase the slope of the Critical State Line in the v-ln p' plane, as shown in Figure (2-10) (Been & Jefferies, 1985),

while in contrast Coop & Atkinson (1993) demonstrated that the addition of fines to a uniformly graded carbonate sand decreased the slope of the isotropic NCL (Figure 2-11). This might be an indication that the addition of fines may play different roles on different types of sands, or an indication of the role of the plasticity of the fines, as they were non-plastic in the case of Coop & Atkinson (1993). No information is however available on the plasticity data of the silty fines used by Been & Jefferies (1985). According to Pitman et al. (1994) the addition of plastic fines to a clean uniform sand increases the compressibility of the sediment, while the addition of non-plastic fines to the same sand does not have a significant effect. Furthermore, Pitman et al. (1994) conclude that the addition of up to 20% of either plastic or non-plastic fines moves the Critical State Line downwards while higher percentages start to move it up back towards the line without fines.

The other key difference between the addition of fines in the above-mentioned cases of quartizitic sand (Been & Jefferies, 1985), and the effect of fines on the behaviour of carbonate sand (Coop & Atkinson, 1993), is the stress levels which were used during test. While the tests on carbonate sand covered the range of pressures associated with particle breakage of carbonate sands, the quartz sand used by Been & Jefferies (1985), was examined at lower stresses, prior to the onset of particle breakage for the quartz sand, where the steady state or CSL is thought to be much flatter.

Coop & Airey (2003) found that, in general, NCLs are flatter for better graded sand (Figure 2-12). The effect of fines presence, which could be a result of excessive breakage of the sediment, may therefore lead to a dramatic change in the NCL of the sediment, as it is confirmed that the NCL of a soil is only appropriate to its initial grading, and not its current grading. Furthermore, if the soil has undergone any particle breakage in the ground, which could be the case for glacial sediments, then reconstituting the soil in the laboratory will not give the same behaviour as the soil in the ground, since the soil would now be starting with a new grading, not that at deposition (Coop & Airey, 2003). This is illustrated in Figure (2-12), where isotropic compression curves are shown for Rankin sand, a carbonate sand, for a first loading and

second loading. A flatter NCL was exhibited during the second loading of the sample, compared to the first loading, due to those fines created by particle crushing in the first loading stage of the sample.

Martins et al. (2001) conducted research on the effects of plastic fines on the compressibility of sandy soils. They showed that for a mixture of quartzitic sand and kaolin there is no unique Normal Compression Line even when pressures up to 3.5 MPa were reached, and the compression curves for samples of different initial densities did not seem to converge for any vertical stress applied. Such a behaviour, when the sediment exhibits no unique Normal Compression Line, was found in some types of soils like gap-graded sediments (Ferreira & Bica, 2006) and some well graded silts (Nocilla et al., 2006) The behaviour was termed as "Transitional behaviour" which will be discussed in the next section.

The effect of fines presence on the shearing strength of sands again depends on the type of fines. According to Georgiannou et al. (1990), the presence of a clay fraction of up to 20% in a mixed soil does not reduce the angle of shearing resistance at the Critical State, but the presence of clay reduced the stability of the fabric of sand, causing a reduction in undrained shear strength at quasi-steady state, which was defined by Ishihara (1993) as the state when the soil behaviour changes from contraction to dilation, with a temporary drop in shear stress.

The effect of non-plastic fines on Toyoura sand was investigated by Zlatovic & Ishihara (1995). Fines, which were made from crushing the same sand, were added to the sand with different percentages. Based on the results of undrained triaxial compression, it was observed that for the same void ratio, the soil weakened with an increase in silt-sized particles content up to 30%, as shown in Figure (2-13)A.

Mitchell (1976) & Kenny (1977) suggested that for such mixed soils, fine particles, because of their size, nature, or position, may not participate in the force transfer mechanism. And thus, the space they occupy should be

considered as a void. This led them to introduce another index known as the granular void ratio (e_g). which is computed by considering fines as voids as follows:

$$e_g = \frac{\text{Volume of actual voids + volume of fines}}{\text{Volume of coarse material}}$$

$$e_g = \frac{e + f_c}{1 - f_c} \quad \ldots\ldots\ldots\ldots\ldots [2\text{-}3]$$

where:

f_c is the ratio of volume of fines to total volume of solids

e is the void ratio.

Many researchers have used this index to provide a more consistent characterisation of such mixed materials. Ni et al. (2004) re-analysed the same data presented by Zlatovic & Ishihara (1995) by using this index. As shown in Figure (2-13)B, the new analysis showed a completely opposite trend to that shown in Figure (2-13)A. The conclusion which Ni et al. (2004) reached was that, although the silt fines are not contributing much to the undrained shear strength as if sand particles were to occupy the voids, they are not as weak as just acting as voids, but are providing some positive contribution to the Critical State shear strength. Ni et al. (2004) also studied the effect of adding plastic and non-plastic fines to clean sand on its strength. For a mixed soil containing plastic fines, the contribution appears to be a function of stress history. When the mixed soil is normally consolidated, the plastic fines are acting worse than voids. However, overconsolidation of the mixed soil seems to eliminate the negative role of these fines on the strength of the soil. The non-plastic fines however, generally contribute positively to the strength, with the stress history in this case, having little or no effect.

The use of a granular void ratio index in analysing properties of mixed soils should be used with some caution. According to its definition, the fines should be occupying the voids between hosting particles and do not contribute to forming the sample skeleton in the force transfer mechanism, so when the fines content exceeds a certain percentage (usually 20-30%), the

soil may become completely governed by the contacts between the fines, and the above definition may no longer be applicable (Chu & Leong, 2002).

2.5 Transitional behaviour of sediments

From the evidence shown in the last few sections, it is generally accepted that the Critical State framework (Roscoe et al., 1958) may be applied to most types of sands in the same way as for clays. Although the compressibility of clays and sands arises from two distinct mechanisms, the uniqueness of the Normal Compression Line and the Critical State Line in the v-ln p' plane is the main feature which can be found in both types.

Recently, some literature has presented a new pattern of behaviour of a different class of soils, which is intermediate to sands and clays; this has been termed "Transitional behaviour". This transitional behaviour may be an outcome of the addition of fines to sands, as in the case of a quartzitic sand and kaolin mixture which was tested by Martins et al. (2001), or of gap-graded soils as in the behaviour observed in residual Botucatu sandstone (Figure 2-14), (Martins et al., 2001; Ferreira & Bica, 2006). In soils with transitional behaviour, the compression curve location in the v-ln p' plane was dominated by the specimen's initial density, and there was no indication of any convergence of these curves into a unique compression line, at any vertical stress (Figure 2-15). Ferreira & Bica (2006) also studied the shearing behaviour of Botucatu sandstone by the means of triaxial tests. They found that the soil not only showed no unique Normal Compression Line even when subjected to isotropic pressures up to 25 MPa, furthermore, no unique Critical State Line was identified for the remoulded samples (Figure 2-14), not even in the p'-q' plane, indicating that the Critical State of a sample might depend on the initial void ratio of the sample as well (Figure 2-14).

Transitional behaviour was then found to describe the behaviour of some types of well-graded silts from the Po River in Italy (Nocilla et al., 2006). The natural soil, with 25% clay content, particle size distribution is shown in Figure (2-16). The same soil with three different clay contents was tested to investigate this effect on the soil behaviour. The tests demonstrated that a

behaviour similar to that exhibited by the gap-graded soils (mixed sand-clay, Botucatu sandstone) was shown by samples with low clay content (Figure 2-17). The soil showed an increase in NCL curves scattering with the decrease of clay content percentage (Figure 2-17). The silt soil with low clay content showed no indication of the uniqueness of the Normal Compression Line or the Critical State Line (Nocilla et al., 2006). A similar effect was exhibited on the CSL with the decrease of clay content. No clear CSL was detected by samples with 8% clay content (Figure 2-18).

The key feature of the behaviour of the gap-graded soils and the Po River silt, or more generally of transitional soils, is that they have no unique Normal Compression or Critical State Line. However, for one initial density the locus of "Critical States" may fall fairly close to a unique line (Nocilla et al., 2006; Ferreira & Bica, 2006). To validate the traditional Critical State framework for such a soil, Ferreira & Bica (2006) suggested that the framework can be applied using a family of parallel Critical State Lines depending on the initial specific volume. It was found that stress paths for different void ratios do not reach the same critical state, when normalisation of data is done following a unique Critical State Line (Figure 2-19, A). By normalising the data using the CSL corresponding to the sample void ratio, state paths for compacted samples of Botucatu soil seem to reach a unique Critical State (Figure 2-19, B). Particle breakage, in the case of those soils which demonstrated transitional behaviour, does not seem to be an important factor in their behaviour (Ferreira & Bica, 2006).

2.6 Particle breakage in subglacial sediments

In the glacial environment, sediment production, deformation and deposition cannot be separated conceptually. Sediments produced by the direct erosion of lithified material by glacier ice typically contain particles spanning a large size distribution, and are frequently characterized by high specific surfaces due to the presence of fine material. Deformation results in high strains within the basal sediment, often under high pore pressures and low effective pressures. Furthermore, sediment properties are altered by ice-basal processes, which are controlled by conditions at the bed. These basal

conditions are, in turn, affected by changes in sediment properties. The subglacial sediment system is characterised by a subtle interplay and feedback between sediment properties and basal processes (Murray, 1994).

Frequent interaction between particles, and between particles and a rigid bed, result in their substantial modification during transport. Inter-particle stresses are often high enough to cause fracture and abrasion of particles. In view of its importance in modifying debris, Boulton (1978) introduced the term "active transport" for debris transport in the basal shear zone of glaciers, in contrast to "passive transport", which refers to debris transport with little or no modification at higher levels within or on the glacier. There are two main effects on debris characteristics as a result of active transport: (a) particle breakage reduces the size of particles and creates distinctive grain size distribution; and (b) the form or morphology of particles is changed as a result of breakage or wear (Benn & Evans, 1998). The grain size distribution of sediments is a fundamental control on sediment deformation properties. The bimodal size (with two peaks in the grain size distribution) of rock fragments produced by the erosion processes of mechanical crushing and abrasion is reflected in the subglacial environment by the classic grain size distribution of subglacial sediment, which is usually rich in both fine and coarse material. Such distributions reflect progressive particle size reduction or comminution as particles are fractured under applied stresses during shear (Benn & Evans, 1998).

The progressive size reduction of subglacial debris during transport was studied by Dreimanis & Vagners (1971) by analysing the granulometry of tills with distance from known bedrock sources. They found that coarse modes are well developed close to the debris source, and fine modes increase in importance with increasing transport distance, but there appeared to be a lower size limit beyond which no further particle crushing occurred, regardless of transport distance (Figure 2-20) (Dreimanis & Vagners, 1971). The fine component reflects the terminal mode, or modes of the parent rock, and the proportion of coarse to fine material reflects the travel distance of material. Increased travel distance results in a depletion of clasts with

resultant progressive fining of sediments down glacier (Dreimanis & Vagners, 1971). The fine mode, varying from silt and sand sizes, reflects the texture of the mineral grains in the source rock and their physical properties under conditions of glacial crushing. The coarse mode is larger near the source but far from the source the fine mode is larger. Each mineral has a preferred ultimate grading to which it is crushed eventually when it is subjected to excessive crushing during glacial transport, This grading is defined as the "terminal grading" (Karrow, 1976). When minerals have been crushed to their terminal grading the till can be considered as mature.

Eyre (2003) compared the particle size distributions of three glacial sediments: Ice stream B- Antarctica, Breiðamérkurjökull- Iceland and Vestari-Hagafellsjökull from Langjökull-Iceland as shown in Figure (2- 21). The subglacial sediment from Ice Stream B, represents the clayey-type subglacial sediment which is different from the basaltic origin sediments from Breiðamérkurjökull and Langjökull. A comprehensive comparison between the two grain size distributions of the basaltic origin sediments shows that the travelled distance for Langjökull sediment from its source is more than this travelled by Breiðamérkurjökull sediment. This is reflected in the high percentage of fines in Langjökull sediment as indicated by the peak in the chart.

Field observations along with SEM observations emphases the fact that the subglacial sediment underwent subglacial stresses which caused their particles to be crushed (Boulton et al., 1974; Hooke & Iverson, 1995; Hart et al., 2004). This was also confirmed by micromorphological samples collected from Vestari-Hagafellsjökull, in Langjökull-Iceland, which showed clearly that the basaltic origin sediment suffered from breakage of its clasts. Furthermore, those samples showed clear evidence of sediment deformation from the finest to the largest grain sizes, indicated by the reworked components from the basalt parent rock. Some of these (clasts) were intact, but many had been highly altered into clay intraclasts that are subject to shearing processes (Hart et al., 2004).

Particle breakage occurs when the contact stresses between the grains generated due to an external force exceed the strength of the grains. This phenomenon happens in many soils with weak particles such as, volcanic soils (Miura & Yagi, 2003), carbonate sands (Coop et al., 2004; Coop & Airey, 2003; Sorensen, 2001; Georgoutsos, 2002; Nakata et al., 1999) and in glacial sediments (Hooke & Iverson, 1995; Boulton et al., 1974; Hart et al., 2004). The result of particle crushing is a significant change in particle grading and the textural and structural features of the sediment which will eventually affect the overall sediment mechanical behaviour. It has been advanced that extreme shearing may have caused some soils to reach characteristic "terminal" grain sizes for each mineral present, resulting in a "critical" particle size distribution that can evolve no more, not even if submitted to further shearing (Dreimanis & Vagners, 1971). In the following section, particle breakage and its effect on soil behaviour are presented as a geotechnical fact.

2.6.1 Particle breakage as a geotechnical concept

Soil particle crushing has become an increasingly important topic of soil mechanics research over the past decade. This is because the traditional idea was that within the geotechnical range the soil particle itself was never subjected to stresses high enough to make it break. This idea has been invalidated through the intensive study of the behaviour of some crushable sediments, like carbonate sand (e.g. Coop et al., 2004) and some volcanic soils in Japan (e.g. Miura & Yagi, 2003). Particle breakage occurs when the contact stresses between the grains generated due an external force exceed the strength of the grains.

To define particle breakage in a quantitative macroscopic way, the factors breakage potential B_p, total breakage B_t and relative breakage B_r factors have been proposed by Hardin (1985), as they are illustrated in Figure (2-22). **Breakage Potential, B_p,** is defined as the area between the original particle distribution curve and the American standard 74μm sieve size (or 63μm in British standards), [Area BCAB in the figure]. The area between the original and the final particle size distribution represent the **Total Breakage,**

B_t, [Area BCDB], while **Relative Breakage, B_r** is defined as the ratio between the two. This approach in defining particle breakage does not take into consideration the breakage of fine particles such as silts or clay particles, assuming that a significant breakage for these sizes of soil grains is unlikely to happen as it needs higher stresses than those needed for the bigger size particles.

Research has proven that particle breakage can lead to significant changes in the mechanical behaviour of sediments. As a result of breakage, sediments contain a higher percentage of fines than they would usually do, and thus would behave in a considerably different way than the original sediment before particle breakage (Coop & Atkinson, 1993; Nocilla et al., 2006) as highlighted in Section (2.4). The increase in percentage of fine particles depends on the level of strains reached during deformation (Coop, 1990; Miura & Yagi, 2003; Hyodo et al., 2002).

2.6.2 Particle breakage development during compression and shearing

The progress of particle breakage during compression and shearing of granular soils was investigated by many authors. Particle breakage associated with compression and shearing of silica sand was studied by Hyodo et al. (2002), who confirmed that particle breakage is usually initiated after reaching the yielding pressure during isotropic compression of the soil. However, particle breakage development during shearing is significantly larger mainly after the phase transformation state, and the major development of crushing occurs between the phase transformation and the Critical State (Hyodo et al., 2002), as shown in Figure (2-23), showing the increase of surface area development with confining pressure.

Tests on carbonate sand (Dog's Bay sand), conducted by Coop & Lee (1993), indicated that a unique linear relationship between relative breakage B_r, as defined by Hardin (1985), and mean effective stress, p′, was found in a B_r-log p′ space for both the Normal Compression Line (NCL) and Critical State Line (CSL), and suggests that a linear relationship between particle breakage and effective stress might exist independently of initial volumetric

state, stress path or stress level (Figure 2-24). In addition, it was found that particle breakage is accompanied by volumetric compression (Coop et al., 2004). In granular soils, the volumetric compression is directly related to particle breakage and it depends on stress level and uniformity of the sediment grading. Uniformly graded samples experience the same contraction in volume when sheared under the same vertical pressure, and eventually reach a stabilized volume. Well-graded samples exhibit less contraction under the same pressure, however the volumetric contraction will only cease when particle breakage stops and a stable grading is reached (Coop et al., 2004). This fact was clearly illustrated by the data obtained from shearing carbonate sand by means of a Bishop's ring shear apparatus to large strains, up to 150,000%, as shown in Figure (2-25). The shear strains measured in the ring shear device are notional strains and only reflect the deformation, but are typically used in plots as they make comparison easier. It is also worthwhile to note that this kind of deformation might be expected to simulate deformational conditions underneath glacier due to large deformational displacements taking place by glacier movement.

2.6.3 Critical or terminal grading of the sediments

Based on soil modelling and limited experimental data, McDowell and Bolton (1998) hypothesised that a linear Normal Compression Line for crushable soils is associated with the evolution of the soil grading. They also indicated that there are two factors dominating particle breakage: the size of the particle and the coordination number (number of contacts with neighbouring particles), which have opposing effects on particle survival. They emphasised the role of the successive fracture of the smallest particles under increasing macroscopic stress, providing a micromechanical insight into the existence of a linear compression line. One-dimensional compression data on Petroleum coke was reported by McDowell & Bolton (1998) to support the evolving particle size distributions during compression, indicated that a constant grading would eventually be reached, at high pressures. They also noted that this was associated by a change in curvature of the compression curve (Figure 2-26A, B), which they attributed to comminution limit for Petroleum coke. The finding of reaching constant grading at high stresses comprises

with Nakata et al. (2001) findings in one-dimensional compression of silica sand when a critical grading was observed at very high stresses.

The effect of the level of shearing strains on the evolution of soil grading was studied by Coop et al. (2004) by conducting shearing tests on Dog's Bay sand using Bishop's ring shear apparatus. These tests indicated that at very large strains, the particles of the soil would reach a stage when the contact stresses between the particles would be too low to cause any further breakage, and a constant grading should be reached. However, Coop et al. (2004) showed evidence that final grading curves may be different for different stress levels, so that a final constant grading, or critical grading, is dependent not only on the uniformity and absolute particle size of the initial grading, but also on the normal stress applied (Coop et al., 2004). This is clearly shown in (Figure2-27), which shows data of relative breakage versus shear strain during shearing of carbonate sand under different ranges of pressures. At very high strains, the sediment tends to reach a constant grading. The figure also indicates that different gradings are reached under different stress ranges, this was indicated by the higher relative breakage achieved by those samples sheared under higher stresses. The figure also illustrates that samples which were subjected to higher normal stresses would reach their critical grading at lower shearing strains.

A critical or terminal grading is consistent with the observation of glacial sediment grading modes and the idea of preferred terminal grading existence for each mineral, to which the mineral could be crushed during glacial transport (Karrow, 1976). Particle breakage in glacial sediment is dependent on strains caused by glacial transport, and when these strains are high enough, most minerals will be reduced to their terminal grading. This is the case when the sediment is considered to be mature. The sediment, when reaching its mature state, will deform at constant void ratio and exhibit no further contraction.

2.6.4 Geomaterials with changing grading

The change in the physical properties of the subglacial sediment while deforming, for example the evolving particle size distribution, is an issue which needs to be covered when characterising its mechanical behaviour. Sediments which are composed of crushable particles will change irreversibly as particle breakage occurs and the grading will become progressively uniform until it reaches its terminal grading where the sediment cannot evolve anymore. The breakage coefficient introduced by Hardin (1985) does not incorporate the idea of a limiting grading or a terminal grading. Wood (2006), proposed a coefficient which considers the terminal grading for crushable sediments. The grading state index I_G is based on the concept of the existence of a limiting grading for each soil type, and measures the state of the current grading of the sediment according to the final grading, by using the ratio of the area [ABC] to the area [ABD], as shown in Figure (2-28). When I_G=1, the soil has reached its critical grading and no crushing can occur anymore. The absolute narrowest grading consists entirely of one size of material which is the size of the largest particles in the sediment, represented by the grading curve AB when ($d=d_{max}$), where the value of the grading index is assumed equal to 0. For intermediate gradings, the grading index is equal to the ratio of areas under the current grading curve and the area under the fractal limiting grading curve, and the value of I_G is between 0 and 1.

The difference between the proposed grading state index, I_G, and the relative breakage proposed by Hardin (1985), is that the critical or terminal grading for the granular material is considered in the definition of I_G, while the relative breakage definition assumes infinite breakage of the sediment particles, which is unreasonable in reality. For a crushable soil, the grading state index will increase monotonically with crushing depending on the properties of the material, such as particle mineralogy and particle shape, and on environmental parameters such as density of packing, stress level and mobilised friction. Wood (2006) tried to apply the concept of I_G in modelling the behaviour of crushable soils. In order to link particle breakage with the mechanical response, he assumed that the elastic properties of the soil do

not change to first order, and that the Critical State angle of friction also remains constant with crushing. In fact, particles crush and progressively fill the voids, the maximum and minimum void ratios will fall (Wood, 2006; Daoudji & Hicher, 2006), and the Critical State Line would be expected to be affected (Luzzani & Coop, 2002; Coop et al., 2004).

If the range of stable packing, defined by maximum and minimum void ratio, has become denser, then the Critical State Line should correspondingly drop in the compression plane. Wood (2006) argued that since the grading state index (I_G) of crushable soils is rising during crushing and the material is changing, the defined Critical State Line should not be for a single material. These observations were reinterpreted in the form of a critical state surface (Figure 2-29) linking the specific volume, mean stress and grading state index.

A section through this surface gives a three-part Critical State Line, as shown in (Figure 2-30A), which is identified in the specific volume- log mean effective stress plane. The steep slope, which is usually observed once crushing has started (Coop & Airey, 2003; Martins et al., 2001; Coop & Lee, 1993), is a consequence of the accelerating fall of the critical state void ratios as the crushing stress is exceeded and the grading state index (I_G), increases (Wood, 2006). This three-part Critical State Line can also be observed in data from triaxial tests on Chattahochee River sand (Vesic & Clough, 1968) (Figure 2-30B). As particle crushing proceeds, the grain size distribution for the sand is changing, and the location of the Critical State Line is dropping in the void ratio-mean effective pressure plane until particle crushing ceases and the sediment has reached its terminal grading. At this stage the accelerating drop of the Critical State Line in this plane will also cease (Figure 2- 30) and the slope of the Critical State Line will decrease.

Wood's (2006) work is preliminary and purely theoretical, but it seems to fit existing data for crushable sands. From what was covered in this section we can conclude that studying the subglacial crushable sediment at any stage of its existence under glacial will represent the behaviour of this sediment at this

specific stage and it is not characterising the mechanical behaviour of the history of this sediment or its behaviour afterwards as this sediment is under continuous change. The Critical State of such soil is thus expected to be completely dominated by its current grading and pressure range, and the study of glacial sediment crushability should be a significant part of its characterisation.

2.7 Time dependent behaviour of sediments and shearing rate effects on the sediment behaviour

Soil properties undergo changes with time, some insignificant, but others very important. Time dependent processes may result in compositional and structural changes that lead to softening, stiffening, strength loss, strength gain or altered conductivity properties. The need to predict what the properties and behaviour will be months to hundreds or thousands of years from now based on what we know today is a major challenge in geoengineering. In the following, a limited review of rate effects on soil behaviour is presented.

When soil is subjected to a constant load, it deforms over time and this is usually called creep (Figure 2-31). The inverse phenomenon, usually termed stress relaxation, is a drop in stress over time after a soil is subjected to a particular constant strain level (Figure 2-31). Creep and relaxation are two consequences of the same phenomenon.

The time dependent deformation response of a soil may assume a variety of forms owing to the complex interplays with the soil structure, such as, stress history, drainage conditions and change in temperature and pressure with time. The magnitude of time dependent effects increases with increasing plasticity and water content of the soil. Strain rate-dependency has been investigated extensively in the past decades. Research has shown that rate effects have great influence on the stress-strain behaviour of clays (e.g. Tatsuoka et al., 2002; Graham et al., 1983; Leroueil & Marques, 1996; Tavenas et al., 1978; Vaid & Campanella, 1977), however, research which have investigated rate effects on granular soils are limited; e.g. Tatsouka et

al., (2000) on sedimentary soft sanstone, Santucci de Magistris (1998) on Metramo silty sand, and on Hostun sand by Cazacliu et al. (1998) and Matsushita et al. (1998 a,b). The limited studies of shearing rate effects on granular soil's behaviour may be attributed to the fact that this phenomenon (time dependency) is clearer in clayey soils, and strain rate effects are usually found to be considerably smaller for sands, even though new evidence by Tatsuoka (2006) shows that at large strains they cannot be neglected. On the other hand, particle breakage can contribute to the time-dependent deformation of granular soils (Leung et al., 1996; Takei et al., 2001; McDowell, 2003; Gasparre et al., 2003). It was observed that the amount of particle breakage increases with load duration (Figure 2-33) (Leung et al., 1996). This was confirmed by microscopic observations revealing that angular protrusions of the grains were ground off, producing fines. The fines filled the voids between larger particles and crushed particles progressively rearranged themselves with time.

2.7.1 Constitutive Modelling-The ISOTACH-Type Behaviour

Increasing attention has been paid to the rate dependency of clays since the introduction of various continuous loading testing procedures. The Constant Rate of Strain (CRS) testing method (Hamilton & Crawford, 1959; Smith & Wahls, 1969; Janbu et al., 1981), which can be carried out in both oedometer and triaxial apparatus, can be used to investigate strain rate effect. In the CRS test, a total strain rate is enforced and kept constant throughout the experiment. Strain rate can be defined as:

$$\varepsilon^0 = d\varepsilon/dt \qquad \ldots\ldots\ldots \qquad [2\text{-}4]$$

where:

ε^0 strain rate during the test.

$d\varepsilon$ change of strain imposed in a time interval of dt.

The stress response is then measured in order to obtain a stress-strain relationship. Figure (2-34), shows a schematic diagram of CRS test result for a soil where the larger the strain rate, the stiffer the soil, a typical strain rate

dependency behaviour of soft clays. If a soil is rate independent, the three curves will coincide. CRS tests are used to characterise the influence of strain rate on the preconsolidation pressure and the stress-strain behaviour. The general observation is that the faster the loading rate, the higher the effective stresses for a given strain.

Results from oedometer tests on different natural clays by Leroueil et al. (1985), indicated that this behaviour was controlled by a unique relationship between the vertical effective stress, strain and strain rate. This unique relation is denoted "isotach behaviour", as shown in Figure (2-35). The figure shows typical CRS oedometer tests on Batiscan clay. It illustrates the influence of strain rate on both the Normal Compression curve and the yield pressure. An increase in strain rate shifts the compression curve to the right and result in an increase in yield pressure. Tavenas & Leroueil (1977) suggested that the effect of time and strain rate on the preconsolidation pressure can be generalized to the entire limit state surface of the soil. Based on this, the rate dependency of the peak strength envelope can be explained by the rate dependency of the preconsolidation pressure obtained from one-dimensional conditions.

Figure (2-36) shows the effect of strain rate on the stress-strain response for overconsolidated Leda (Saint-Jean-Vianney) clay during undrained CRS shearin tests (Vaid et al., 1979). The results show clearly that the greater the strain rate, the greater the peak strength. Similar observations have been reported by Tavenas et al. (1978) for overconsolidated Saint-Alban clay, Lefebvre & Leboeuf (1987) for structured Grande-Baleine clay, and Zhu et al. (1999) for soft Hong kong marine deposits.

2.7.2 TESRA Behaviour (Temporary Effect of Strain Rate and Strain Acceleration)

The viscous behaviour in sands and granular materials is not as clear as in clays and soft rocks. Most constant rate of strain tests conducted on sands showed no significant rate effects on the stress-strain relations (e.g. Anders et al., 2004; Yamamuro & Lade, 1993). Matsushita et al. (1998b) studied the

rate dependency of the stress-strain behaviour of Hostun and Toyoura sands by performing drained plane compression tests and triaxial compression tests. The rate dependency was investigated in two loading situations; tests where the strain rate for each test was kept constant, and tests where the strain rate was changed stepwise (Figure 2-37). In tests where the axial strain rate was kept constant, the stress-strain relationships were essentially independent of the constant strain rate, which varied by a factor of up to 500. However, there was a temporary overshoot or undershoot in the shear stress when strain rate was changed stepwise in variable strain rate. This behaviour has been called (TESRA) behaviour by Tatsouka et al. (2002), which stands for "Temporary Effect of Strain Rate and strain Acceleration". The stress-strain relationship temporarily overshoots the unique relationship for the constant rate of strain curve when the strain rate is increased stepwise. After having exhibited clear yielding, the stress-strain relationship gradually rejoins the unique relationship for the constant rate of strain curve. Similarly, when the strain rate is decreased stepwise, the stress-strain relation undershoots temporarily and eventually rejoins the unique relationship for the constant rate of strain curve.

Figure (2-38) shows a schematic diagram illustrating both isotach and TESRA viscous behaviour. The change in strain rate in the isotach behaviour would coincide with a permanent change in the stress stain curve. This can be illustrated by the data obtained from the consolidated undrained test conducted on normally consolidated kaolin (Tatsuoka et al., 2002) (Figure 2-39). Viscous soil behaviour can also occur as a combination of temporary and persistent viscous effect as in the behaviour observed in triaxial compression of very dense Chiba gravel, cement–mixed sand and reconstituted normally consolidated stiff Fujinomori clay (Tatsuoka et al., 2000).

Oka et al. (2003) performed a series of undrained triaxial compression tests on both normally consolidated and overconsolidated reconstituted samples of Fukakusa clay, where the strain rate was changed step wise during the tests to investigate the immediate and persistent viscous effects. The results for

the normally consolidated samples show that at low stress levels the effect of strain rate changes on the stess-strain relationship appears to be persistent and the viscous behaviour can be defined as isotach (Figure 2-40). Then at higher stress levels effects of strain rate changes become temporary with overshooting and undershooting of the persistent CRS curves, a feature which appears to become more and more apparent as failure was approached. However, in contrast to what has been seen for clean sands the path upon strain rate change did not decay completely to a single unique CRS curve, instead some of the viscous effect was still persistent after large straining. Furthermore, the persistent CRS curves are seen to separate and appear to show a unique stress-strain relationship for a given strain rate. A similar pattern is observed for the effective stress path. In addition, the permanent CRS effective stress paths appear to approach a unique Critical State Line, but there are observed differences in undrained strength. However, the Critical State Line was found to be strain rate independent for most soils. Leroueil & Marques (1996) also reported that the effective angle of shearing resistance at peak strength was more or less independent of strain rate and could therefore conclude that an observed reduction in undrained strength of both normally and overconsolidated clays with reducing strain rate was due to creep driven pore water pressure changes as it was also suggested by Soga & Mitchell (1996) and Vaid & Campanella (1977).

2.8 Shearing rate in subglacial environment

The fact that glaciers are moving on a deformable bed of sediment, implies that researchers had to review their models of glacier movement to take into consideration all the factors which can contribute to sediment deformation which is accounted for most of the glacier movement (e.g.: Boulton & Jones, 1979; Truffer *et al.,* 2000; Blake, 1992) . As the role of subglacial deformation was confirmed, it became necessary to build a new model based on the rheology of the subglacial sediment which takes into consideration the deformation conditions under glaciers. As it was discussed in the previous sections from this chapter, the sediment under temperate glaciers is usually assumed to be; fully saturated, ice free and under high pore water pressure,

which sometimes supports all the dead weight of the glacier leaving the sediment under low effective pressure. With glaciers moving, the sensitivity of till to deformation under different shearing strain rates (viscous rheology) needs to be addressed, especially with a case like subglacial deformation when the strain rate can vary from almost nil to as high as $73yr^{-1}$ in ice streams. Table (2-2) presents a comparison of some of the strain rates found under investigated glaciers.

The rheology of till has been a major concern during the last few years, some studies suggested that the subglacial sediment is deforming as a nonlinear viscous material arguing that only by adopting such a behaviour will the sediment deformation be extended to a relatively deep thickness of subglacial sediment, as in the study under Breiðamérkurjökull- a glacier in Iceland (Boulton & Hindmarsh, 1987), and the evaluation of a Dutch till behaviour (Dobbie, 1992) using the ring shear apparatus to conduct shearing tests with different shearing rates. On the other hand, research on Ice stream B-Antarctica (Tulaczyk et al., 2000), Storglaciären-Sweden (Iverson et al., 1998) and Black Rapid Glacier- Alaska (Truffer et al., 2000), suggested that a Mohr-Coulomb failure envelope rheology model for the subglacial sediment deformation is reasonable. These suggestions were derived from geotechnical testing of the sediment and site observations and investigation. Hindmarsh (1997) and Fowler (2002, 2003) proposed that experimental results represent the behaviour of small till samples, but that till behaves viscously over length scales that are relevant to determination of ice –flow rates in glaciers and ice sheets. However, a comparison between in-situ rheology of till under Whillans Ice stream- west Antarctica with the rheology of the same till determined on small laboratory samples, indicated that the rheology of the subglacial till is independent of scale (Tulaczyk, 2006). In the following section, a review of Boulton & Hindmarsh (1987) flow relation is presented, as it represents one of the pioneer studies which emphasised the role of strain rate on subglacial deformation. The contradicting studies are reviewed in section 2.8.2.

2.8.1 Boulton & Hindmarsh experiment under Breiðamerkurjökull

Boulton & Hindmarsh (1987) established a flow law for till from field experiments on subglacial shearing carried out near the terminus of Breiðamérkurjökull in Iceland. The till under Breiðamérkurjökull is typical of sandy tills produced by erosion of igneous bedrock (Boulton & Dobbie, 1998). Their experiments monitored the deformation process and its relation to glacier movement using a series of strain markers and piezometers inserted into subglacial till from tunnels excavated in the ice. The strain rate and effective pressure were averaged over the thickness of the deforming bed and plotted along with the calculated shear stress. Two rheological models were fitted to these data by direct mathematical modelling, a nonlinear viscous material and a nonlinear Bingham material (Figure 2-41). Boulton & Hindmarsh (1987) suggested that in most circumstances the nonlinear viscous model is the more useful. It takes the form

$$\varepsilon^{\circ} = 3.99 \left(\frac{\tau}{10^5}\right)^{1.33} \left(\frac{p'}{10^5}\right)^{-1.8} \quad \text{.....[2-5]}$$

where τ and p′ are in Pa and ε° is in yr^{-1}.

The majority of subsequent models for the deforming bed have assumed a flow law of this form with a linear or weakly non-linear rheology (e.g. Alley et al., 1987b; Alley, 1989b; Alley et al., 1989; MacAyeal, 1989).

Dobbie (1992), proposed a similar model based on laboratory results from ring shear tests on Dutch till, which is mainly composed of overconsolidated clay. She argued that the flow law presented by Boulton & Hindmarsh (1987) is based on values of shear strain rate and effective pressure averaged over the deforming layer, and ignores the vertical distribution of effective pressure thus masking the effect of any non-linearity. Dobbie (1992) presented her model of the Dutch till flow law, which was built on studying the viscous behaviour of the till by observing the change in the residual strength of the sediment with changes in the shearing rate (Table 2-3) and (Figure 2-42).

The flow law presented by Dobbie (1992) took the form:

$$\varepsilon^{\circ} = 10^{13.1} \left(\frac{\tau^{13.7}}{p'^{15.9}}\right) \quad \text{.....[2-6]}$$

The larger values of the exponents in this formula indicate that the system is more sensitively dependant on shear stress and effective pressure than the one presented by Boulton & Hindmarsh (1987).

2.8.2 Contradicting studies (studies supporting plastic deformation model)

The viscous model presented by Boulton & Hindmarsh (1987), suggested that the subglacial sediment under Breðamérkurjökull is exhibiting a viscous behaviour, emphasises the role of strain rate on the deformation of the subglacial sediment. It urged researchers to conduct more in-situ observations and laboratory tests on subglacial sediments from different glacial areas, to establish their own models and to test the validity of the viscous model.

As a result, sixteen controlled strain direct shear tests on freshly cored subglacial sediment from the base of Ice Stream B –Antarctica, a clay-rich till, were conducted. Results showed no clear viscous behaviour exhibited by the sediment. The tests were conducted under (0.017 bar) 1.7 kPa normal stress, with different shearing displacement (0.09, 0.86, and 5.2) $m.d^{-1}$ (metres/day) (Kamb, 1991). Tulaczyk et al. (2000) adopted more geotechnical testing in investigating the rheology of Ice Stream B till, using triaxial tests (which will be discussed thoroughly in Chapter Eight) and ring shear tests with variable shearing displacement rates were conducted. Although, the shearing displacement rate in the ring shear tests was increased twice by a factor of 10 from an initial low value of 0.1m/d, no clear change in the residual strength of the sediment was detected (Figure 2-43). Based on these results, Tulaczyk et al. (2000) suggested that the till mechanical behaviour under Ice stream B is strongly dependent on effective stress and it shows no dependency on strain rate, supporting the use of Coulomb plastic rheology in modelling this till behaviour. Iverson et al. (1998) studied the behaviour of two tills by using the ring shear apparatus: the first

sediment was collected from beneath the margin of Storglaciaren (4% clay, 21% silt and 75% sand & gravel) and the Two Rivers till of the lake Michigan Lobe (32% clay, 30% silt and 38% sand & gravel). The results showed no clear viscous behaviour, indicating that also Coulomb- plastic behaviour is more reasonable for these two sediments (Figure 2-44a, b).

Studies which suggest the plastic rheology of the subglacial till were also supported by some field observation studies in different glacial areas. Studies based on field collected data in Black Rapid glacier (Truffer et al., 2000), Storglaciären glacier- Sweden (Iverson et al., 1994) and Vestari-Hagafellsjökull- Langjökull in Iceland (Eyre, 2003) all favoured the plastic rheology of subglacial sediment in interpreting their role in glacial movements.

From a geotechnical point of view, viscous and plastic deformations cannot be dissociated. A soil is usually assumed to follow an elasto-plastic behaviour, and its viscous properties determine whether strain rate effects are significant or not. In this thesis the effect of strain rate on Langjökull sediment behaviour during shearing will be investigated. The thesis will also address the effect of strain rate on the sediment residual strength. A new geotechnical analysis for existing data from Ice-Stream B- Antarctica will be presented for comparison. The strain rate effects on the sediment behaviour are presented and discussed in Chapter Eight.

Table (2-1): Evidence of subglacial deformation measured *in situ.*

Glacier	Nature of Subglacial sediment deformation	Basal motion due to sediment deformation	Ice thick-ness (m)	Other data and inferences	Source
Black Rapids Glacier **Alaska**	Decollment at depth >2m	100% of basal motion 50-70% of total glacier motion	600	Till 7.5 m thick	(Truffer M., Harrison W.D., & Echelmeyr K.A. 2000)
Trapridge Glacier **Yukon Territory, Canada**	Strain distributed in topmost 0.3m	25-45%		Coarse grained till	(Blake, Clarke, & Gerin 1992)
Columbia Glacier **Alaska**	Deformation to depth of 0.65m. Strain rate increases with depth		950	Till carries 13kPa of 100kPa average basal shear stress	(Humphrey et al. 1993)
Breiðame-rkurjökull **Iceland**	Net strain distributed to a depth of 0.38-0.45m in till. Net strain decreases with depth	67-85%	8	Coarse grained till	(Boulton & Hindmarsh 1987) (Boulton, Dobbie, & Zatsepin 2001)
Storglaciaren, **Sweden**	Till deforming to a depth of 0.35m	~26%	95	Coarse grained till supports 55kpa shear stress. Till lies in rock basins. Rock knobs probably support much of the stress.	(Iverson, Jansson, & Hooke 1994)
Ice Stream B, **Antarctica**	Till deforms 5-6m Till deforms to at least 2m	17% or 31%	~1000 1058 1027	Inferred from seismic velocities High porosity till (40%) Shear dilation inferred	(Alley et al. 1986) (Engelhardt & Kamb 1997)

Table (2-2): Comparisons of strain rates from subglacial investigations.

Site/Tiltmeter	Maximum Strain Rate yr^{-1}	Minimum Strain Rate yr^{-1}	Depth of deformation m
Vestari-Hagafellsjökull Langjokull(Eyre, 2000)	4.6	2.4	0.1
Ice Stream B- Antarctica (Paterson, 1994)	73	----	----
Breidamerkurjökull (Boulton and Hindmarsh, 1987)	27.8	9.35	0.5
Trapridge (Blake *et al.*, 1992)	36	4.1	0.45
Storglaciaren (Iverson *et al.*, 1995)	25	25	0.34

Table (2-3): Values of strain rate, effective pressure and residual shear strength of the ring shear tests conducted on the Dutch till by Dobbie (1992).

Displacement Rate (ms^{-1})	Strain rate (yr^{-1})	Effective pressure (kPa)	Residual Shear strength (kPa)
4.7×10^{-8}	150	100	28.1
4.7×10^{-8}	150	120	41.5
4.7×10^{-8}	150	140	51.2
4.7×10^{-8}	150	200	86.0
4.7×10^{-7}	1500	100	40.4
4.7×10^{-7}	1500	140	62.8
4.7×10^{-7}	1500	150	66.9
4.7×10^{-7}	1500	300	151.1
4.7×10^{-7}	1500	400	207.3
4.7×10^{-6}	15000	100	52.2
4.7×10^{-6}	15000	200	109.0
4.7×10^{-6}	15000	300	153.6
4.7×10^{-6}	15000	400	222.5

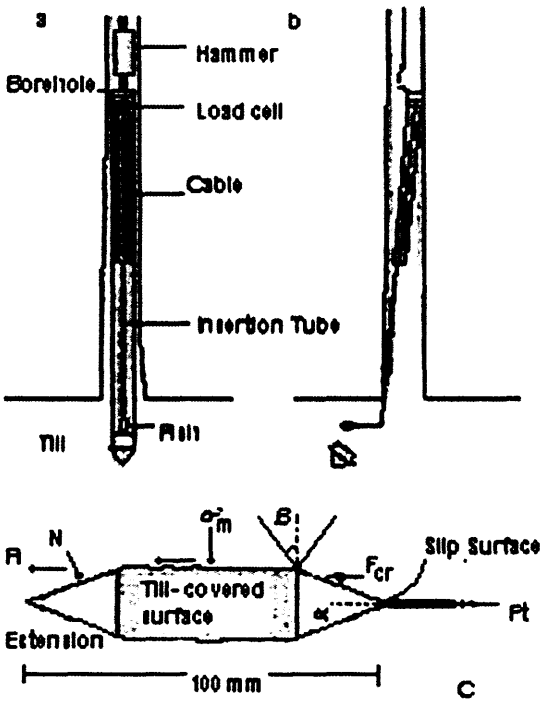

Figure (2-1):
Sketch of dragometer;
(a) immediately after insertion and (b) in operation.
(c) Cross section of fish moving from left to right through till. Slip surface lie approximately parallel to surface defined by ß (Iverson et al., 1994).

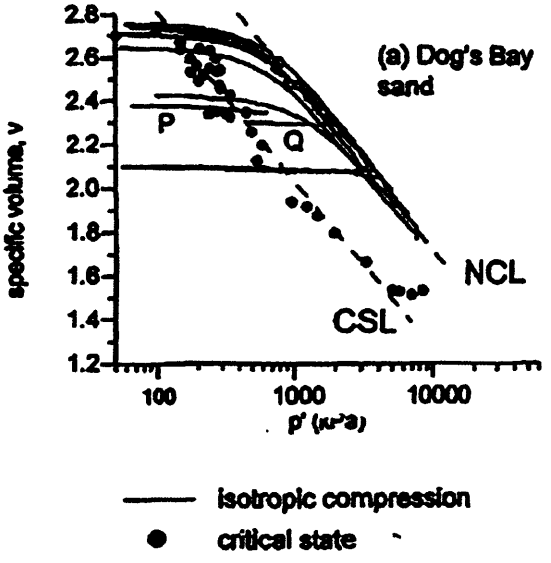

Figure (2-2):
Isotropic Compression and Critical State data for Dog's Bay sand (Coop & Lee, 1993).

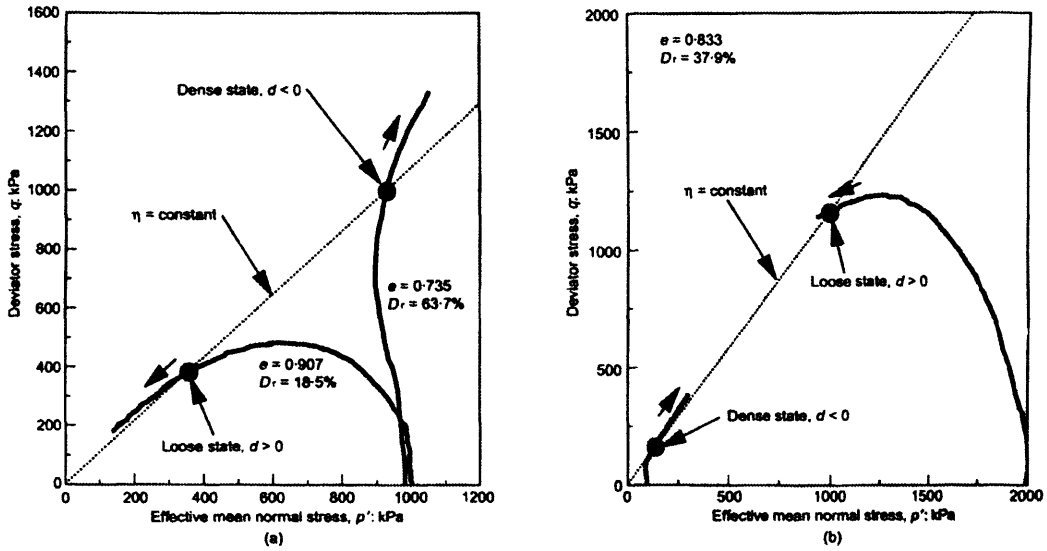

Figure (2-3):
Variation of dilatancy with material state, (Verdugo & Ishihara, 1996). Undrained response of a sand with (a) different densities and (b) the same density but under different confining pressures.

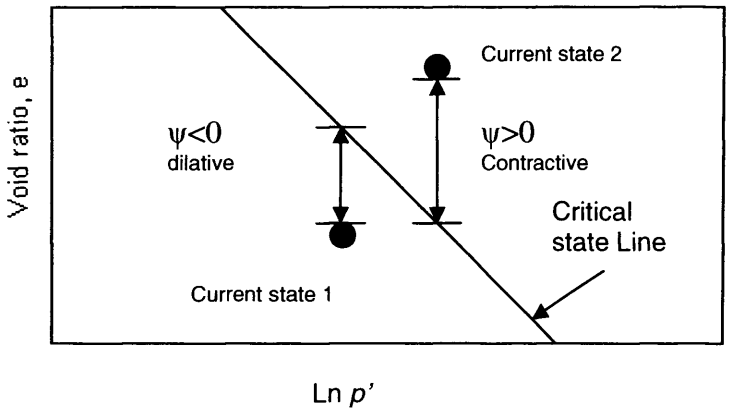

Figure (2-4):
Critical State Line and state parameter ψ as defined by Been & Jefferies (1985).

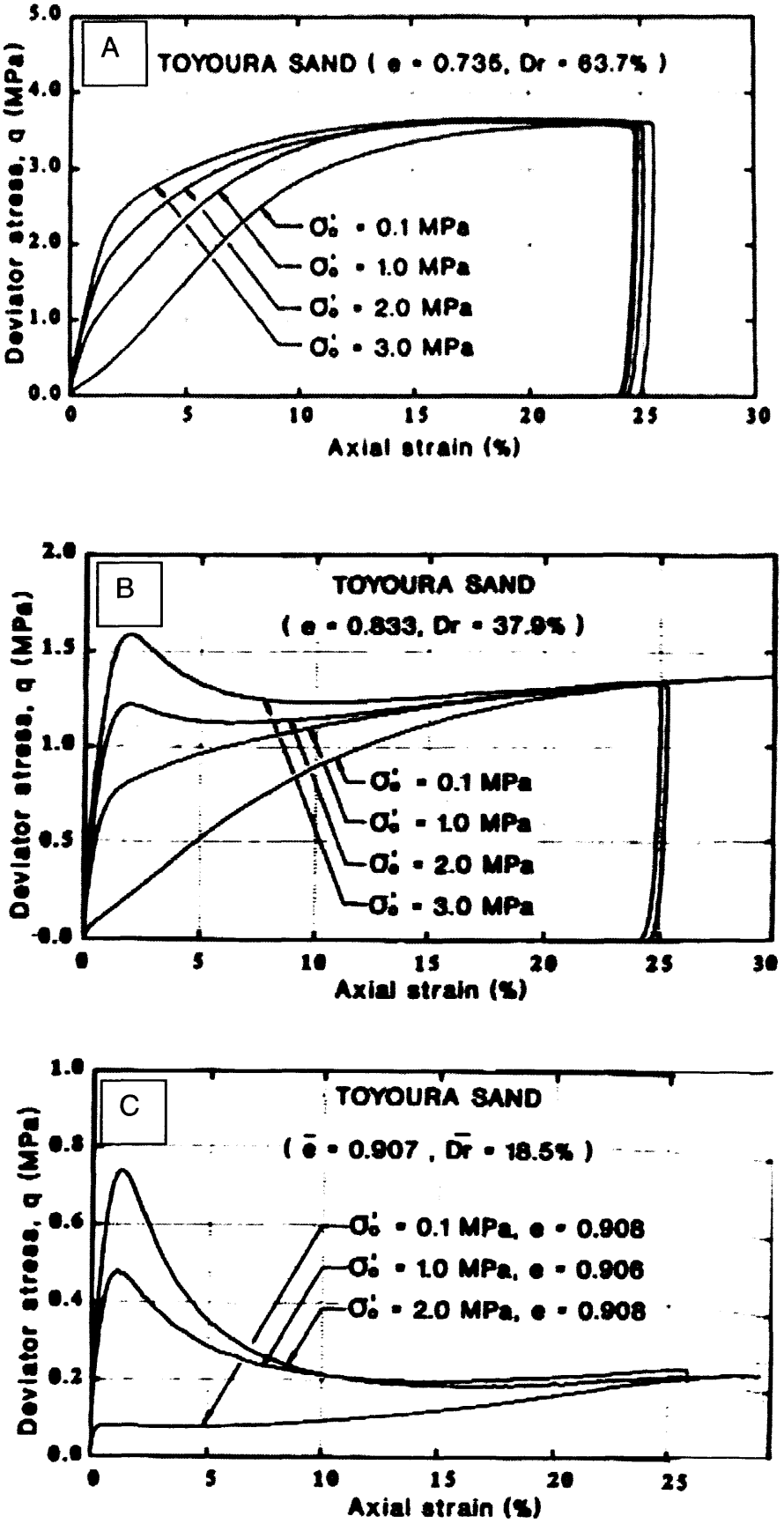

Figure (2-5): Undrained shearing tests on Toyoura sand (Verdugo & Ishihara, 1996).

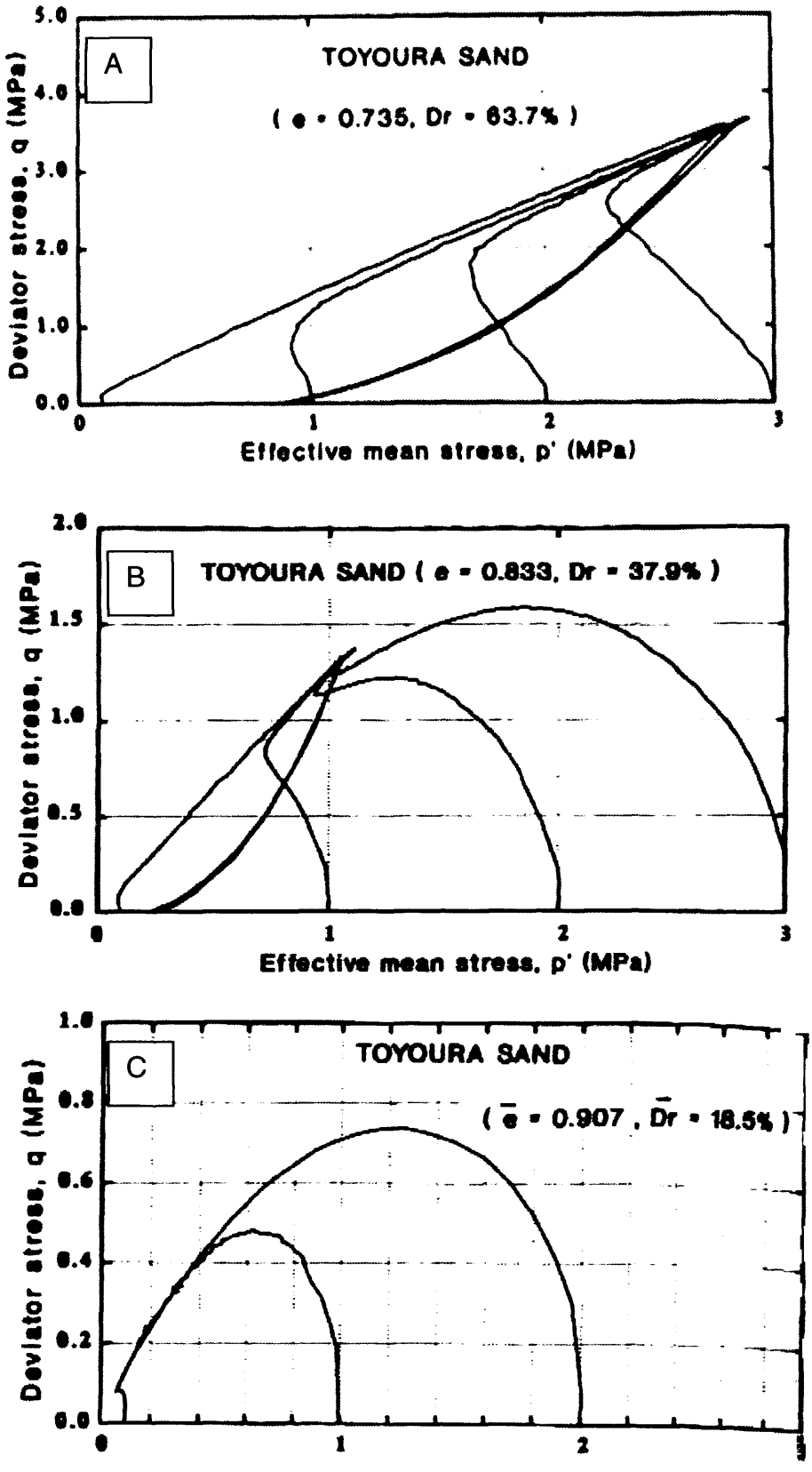

Figure (2-6): Stress paths of undrained shearing tests on Toyoura sand (Verdugo & Ishihara, 1996).

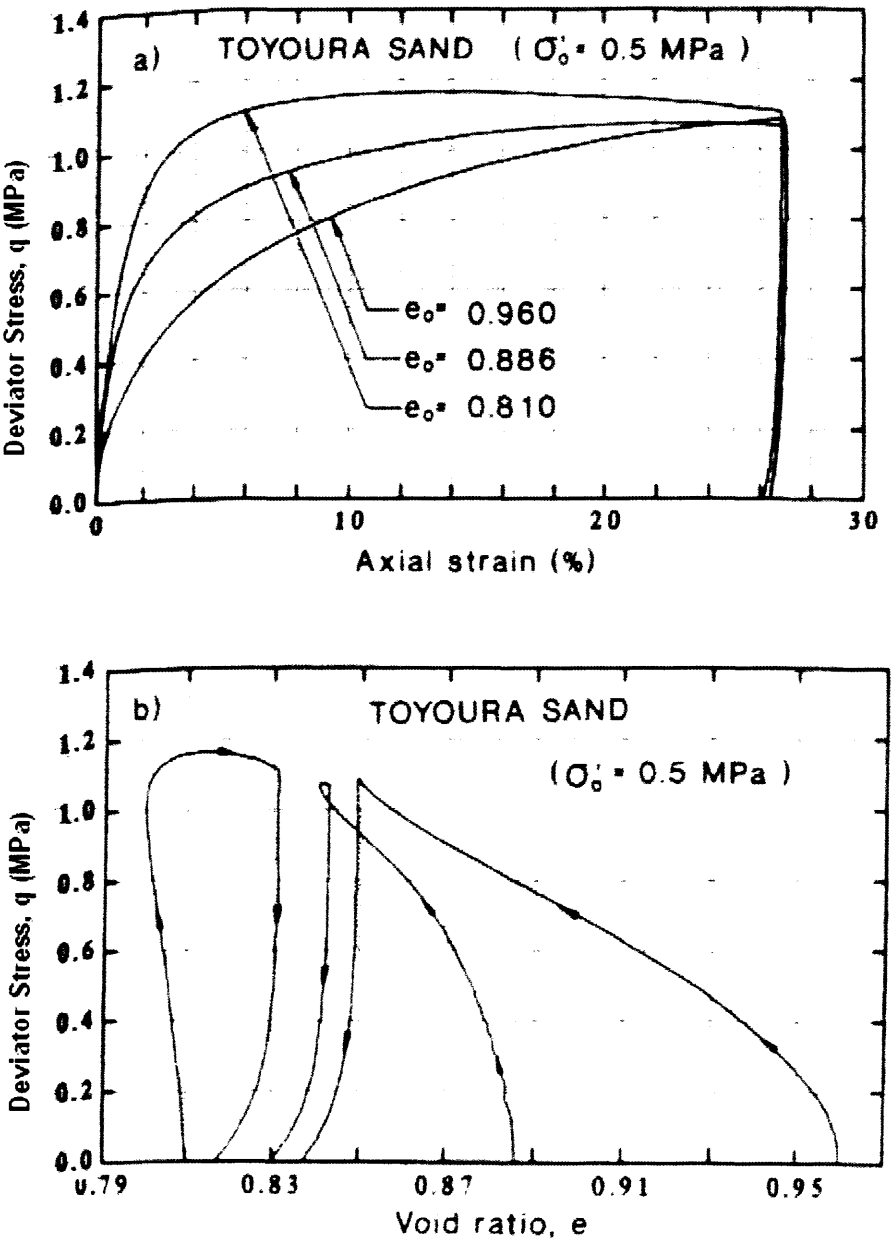

Figure (2-7): Behaviour of Toyoura sand during drained shearing (Verdugo & Ishihara, 1996).

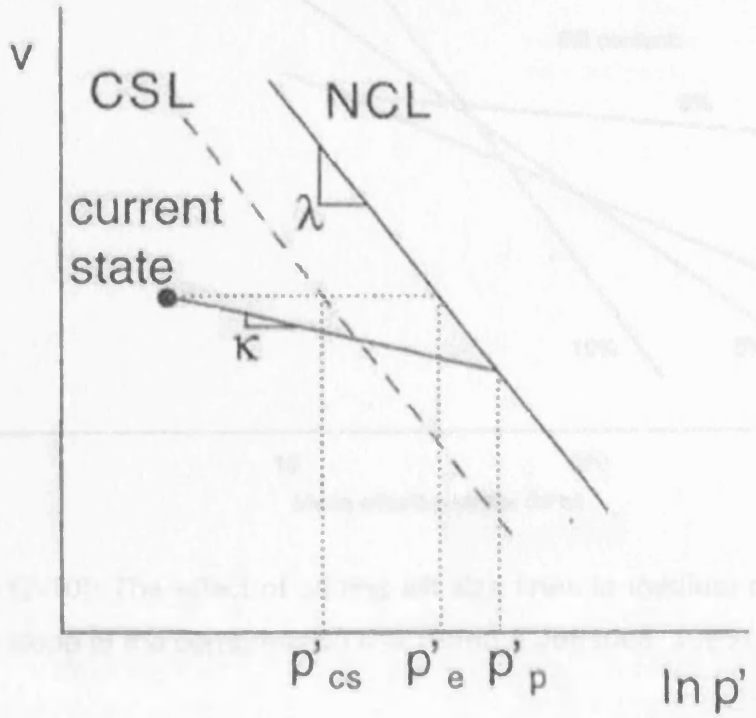

Figure (2-8): Definition of state parameters p'_e and p'_{cs} (Coop & Airey, 2003).

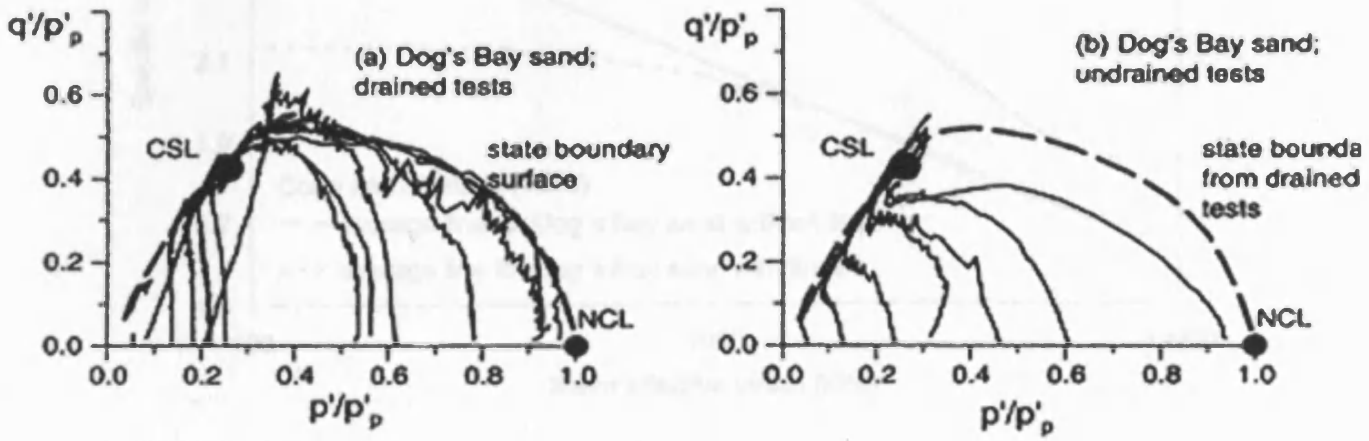

Figure (2-9): Normalised shearing data for Dog's Bay sand (Coop & Lee, 1993). (a) Drained tests (b) undrained tests

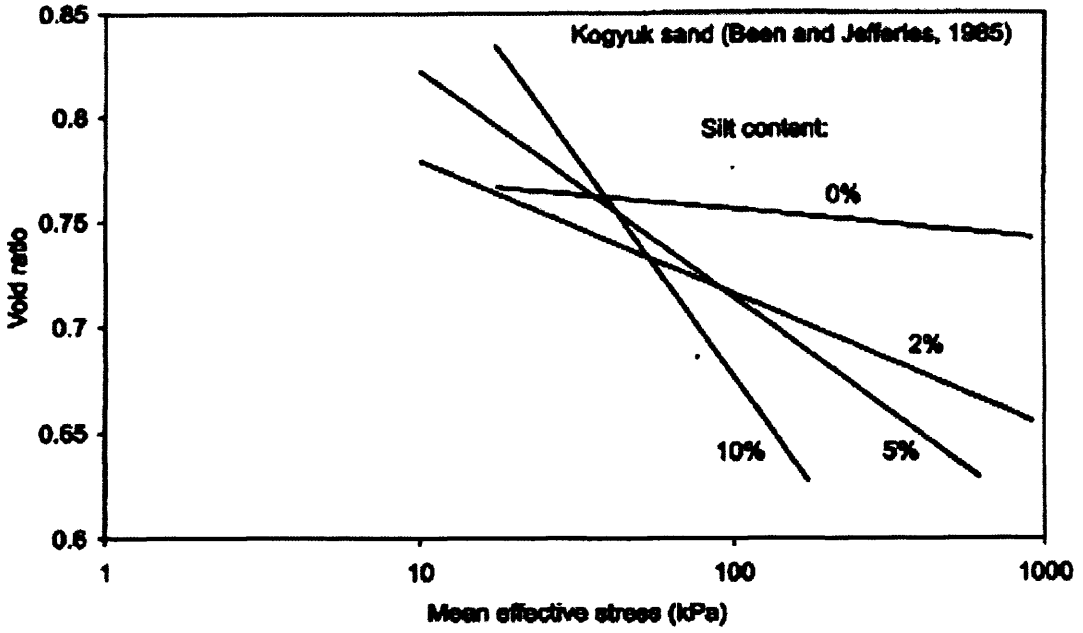

Figure (2-10): The effect of adding silt size fines to medium quartzic sand on the slope of the compression line (Been & Jefferies, 1985).

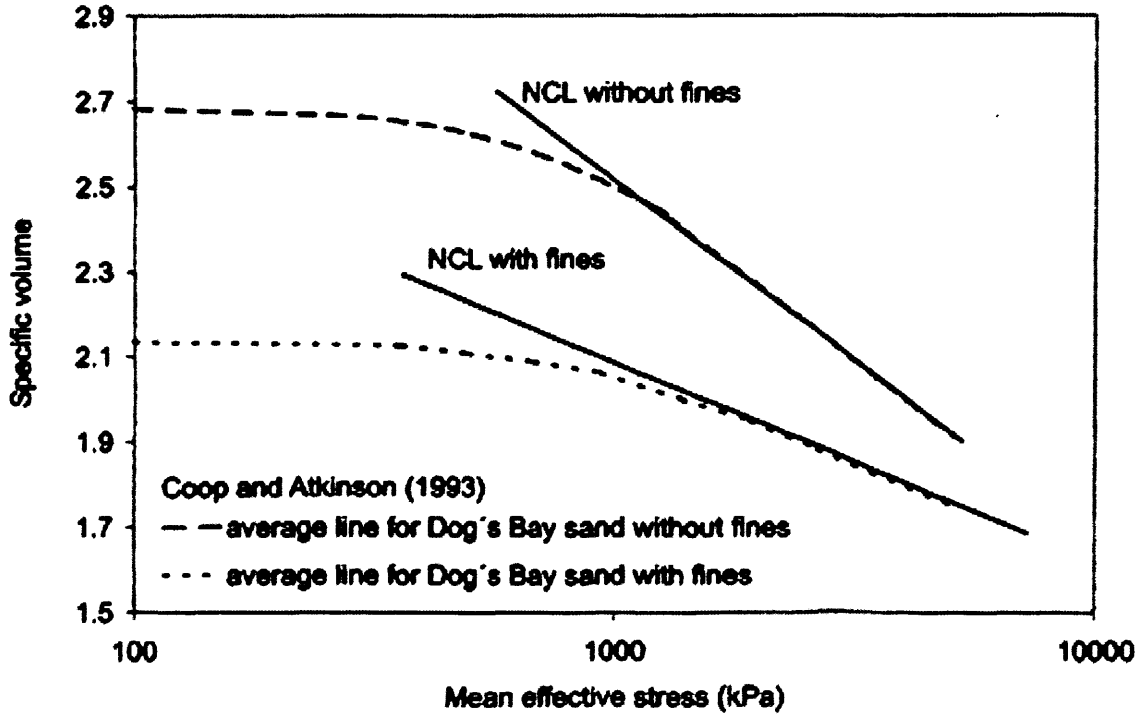

Figure (2-11): The effect of adding fines to Dog's Bay Sand on its compressibility behaviour (Coop & Atkinson, 1993).

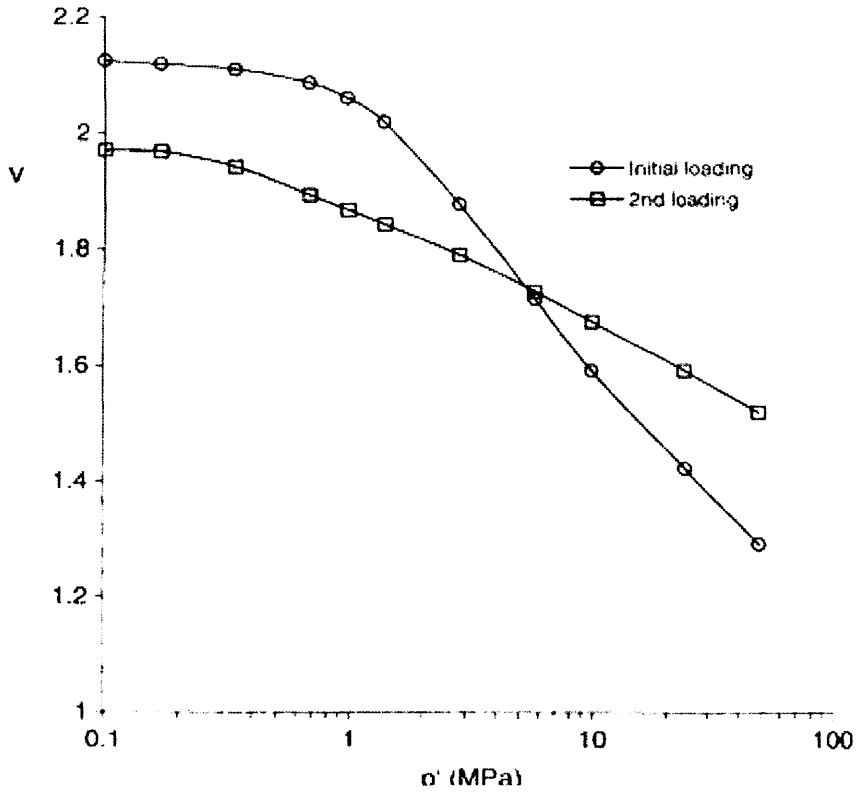

Figure (2-12): The effect of the initial grading on compressibility behaviour of soils (Reported by Coop & Airy 2003, after Pan 1999).

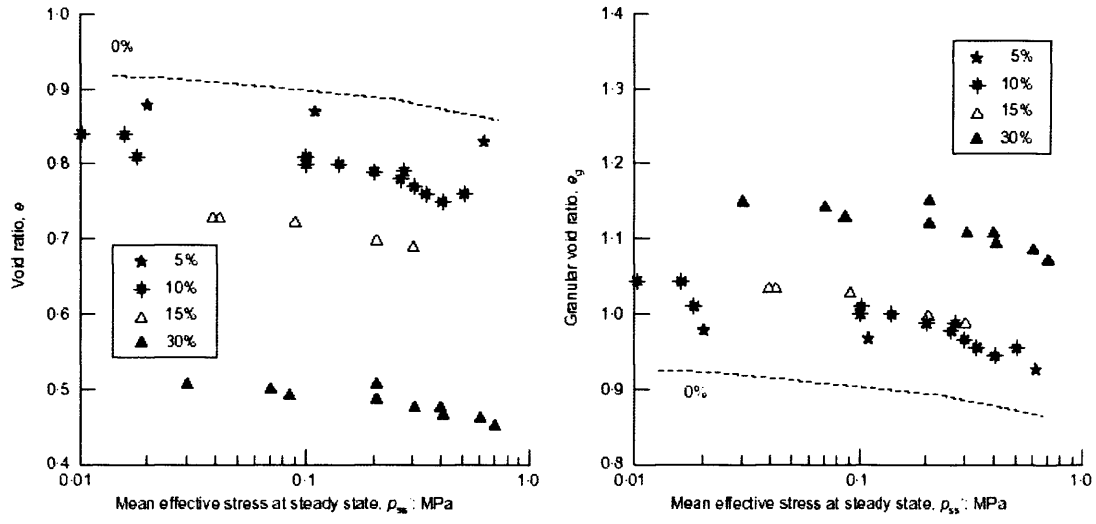

Figure (2-13): The effect of addition of fines to Toyoura sand on the steady state line. (a) using void ratio for analysis (b) using granular void ratio in analysis (Ni et al., 2004).

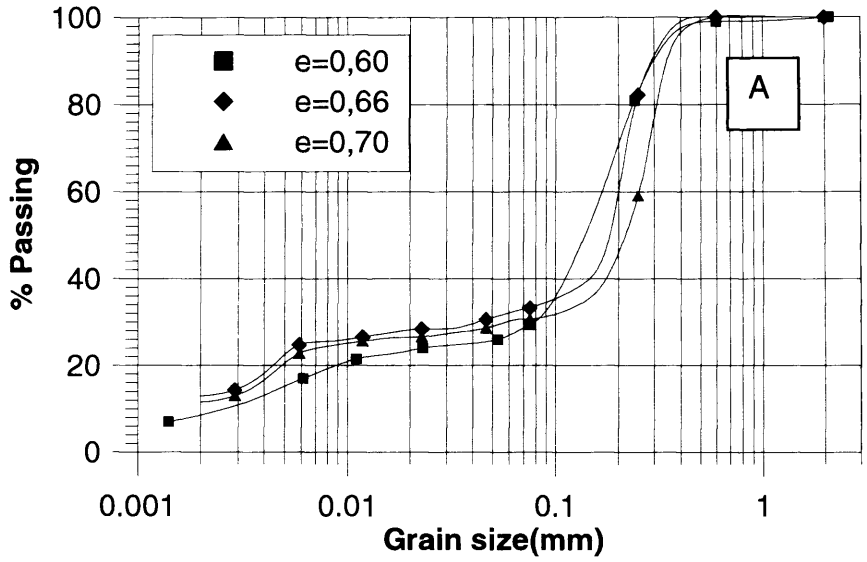

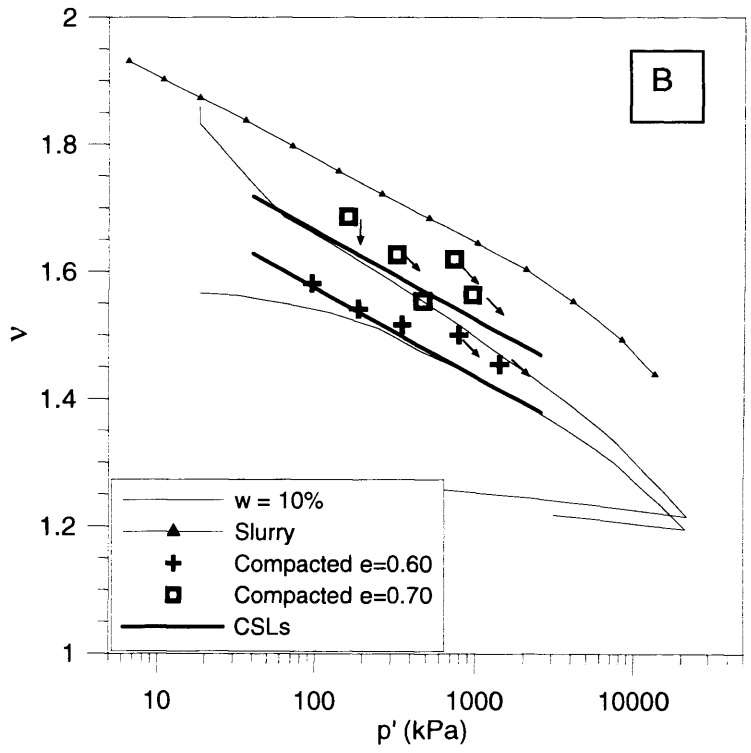

Figure (2-14): Botucatu sandstone (A) particle size distribution. (B) Critical States of compacted samples (Ferreira & Bica, 2006).

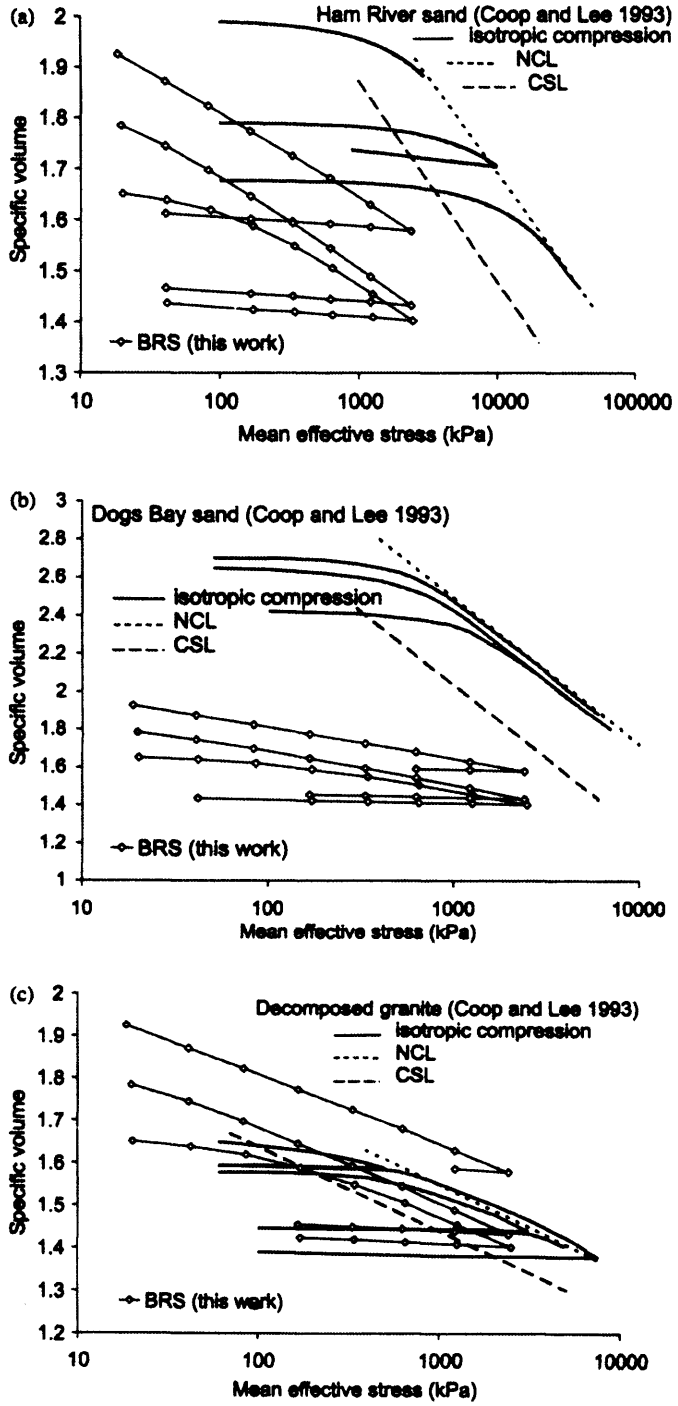

Figure (2-15):

Comparison of the behaviour of Botucatu sandstone (Martins et al., 2001) and soils tested by Coop & Lee, 1993 (a) Ham River sand (b) Dog's Bay sand and (c) Decomposed Granite. BRS refers to Botucatu residual soil.

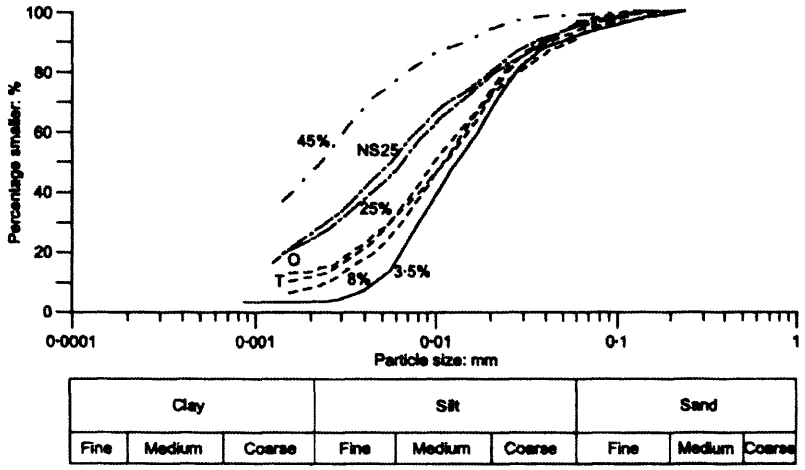

Figure (2-16): Particle size distribution of the Italian silt tested by Nocilla et al. (2006).

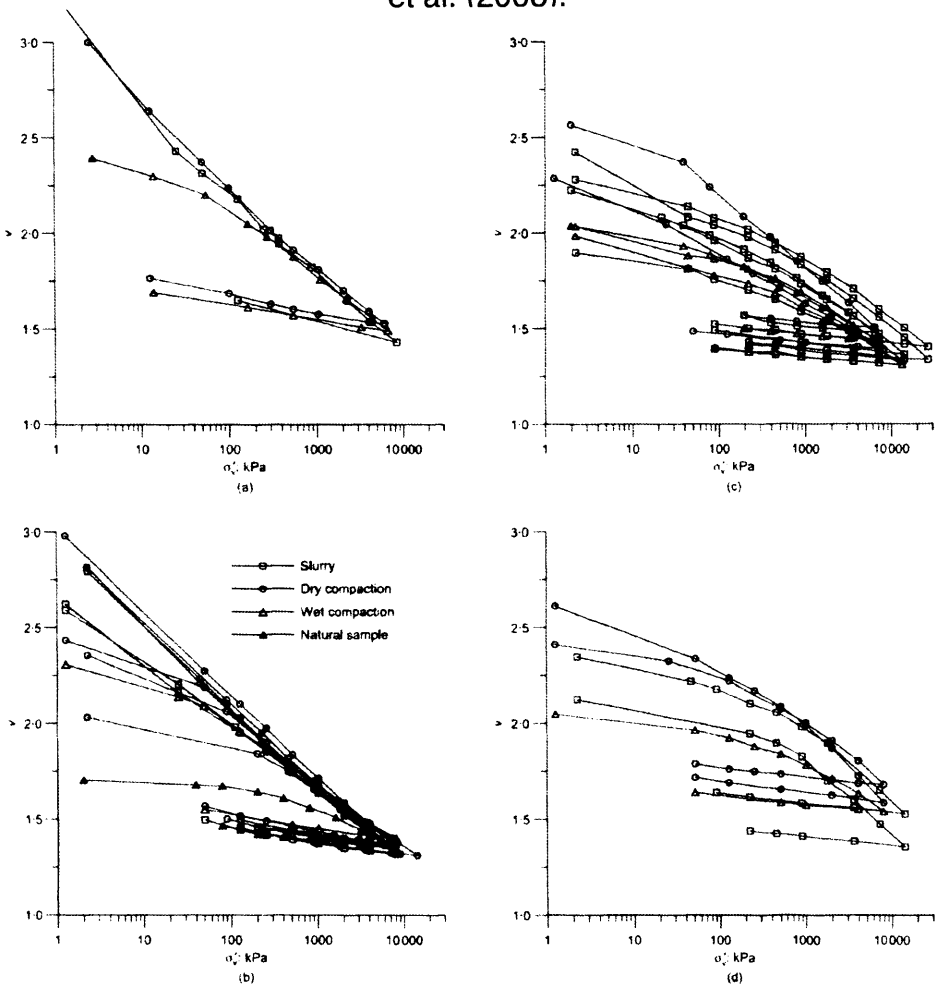

Figure (2-17): Oedometer compression curves for an Italian silt. The figures show the change in compression behaviour with the change of clay content in the soil (a) 45% clay content (b) 25% clay content (c) 8% clay content and (d) 3.5% clay content (Nocilla et al., 2006).

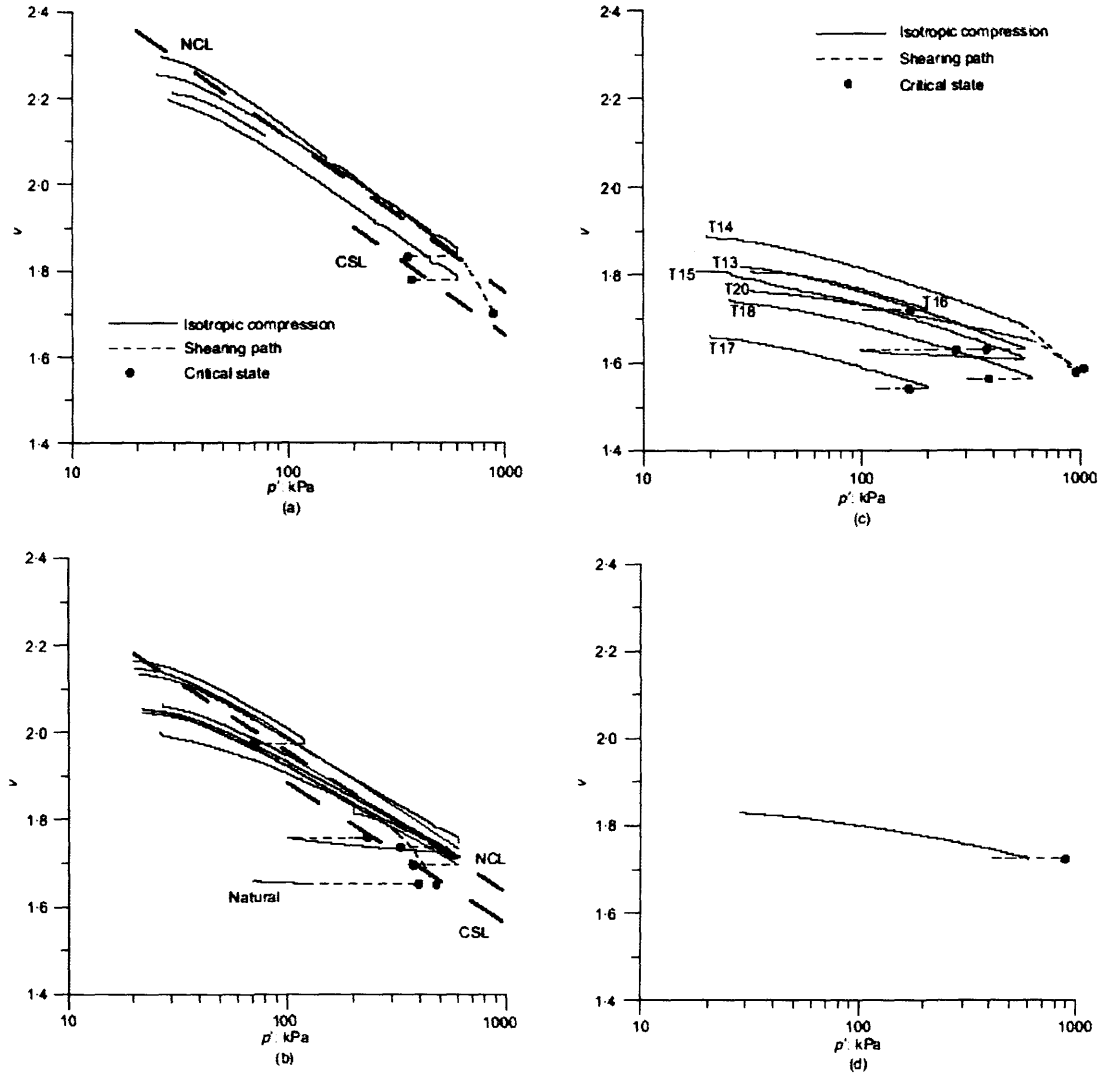

Figure (2-18): isotropic compression data and Critical State for soil tested by Nocilla et al. (2006): (a) 45% clay content (b) 25% clay content (c) 8% clay content (d) 3.5% clay content.

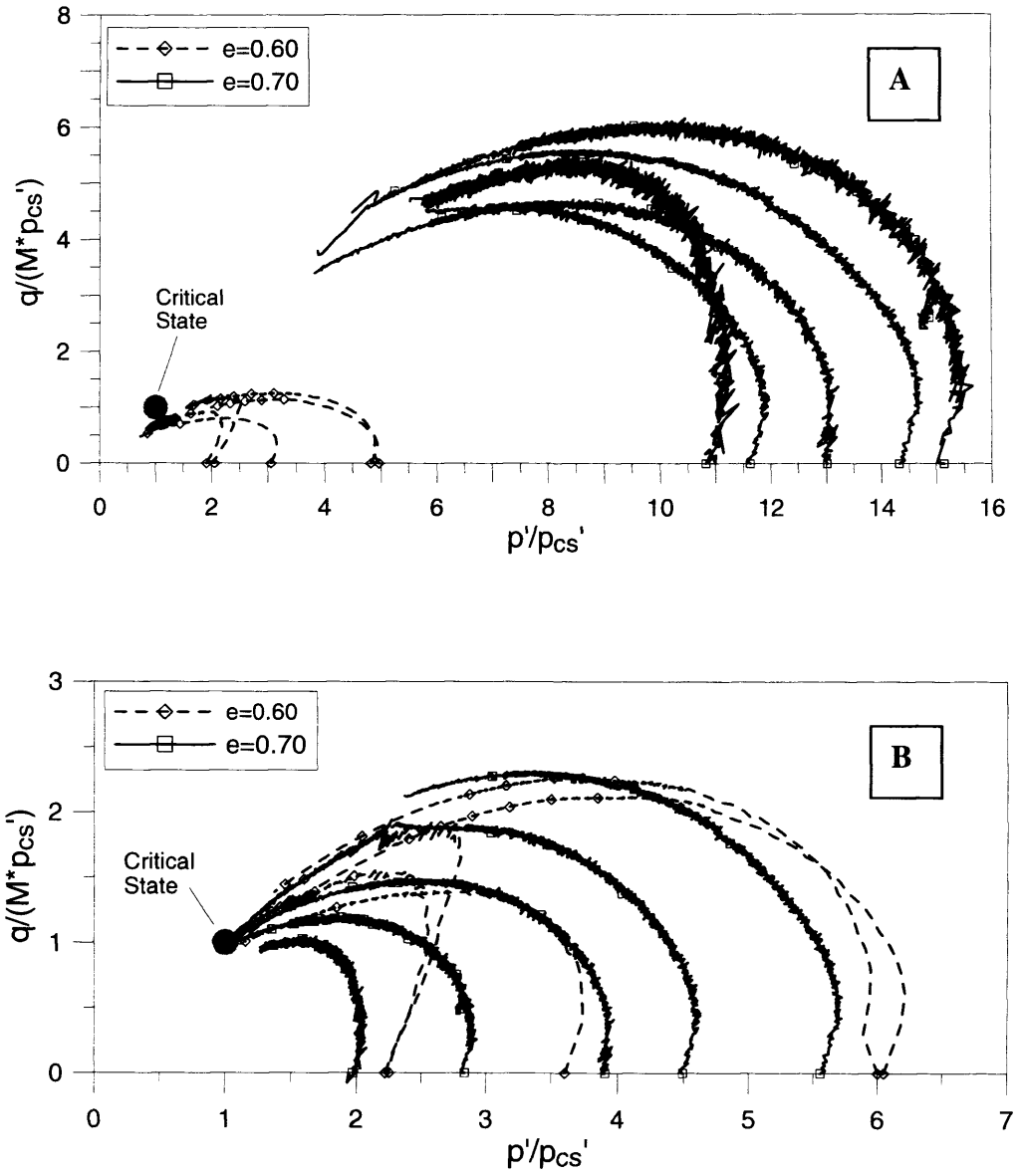

Figure (2-19):
(a) State paths for compacted samples of Botucatu soil using one CSL, two initial densities were used, with voids ratio of 0.6 and 0.7.
(b) State paths for compacted samples of Botucatu soil using a set of parallel CSLs (Ferreira & Bica, 2006).

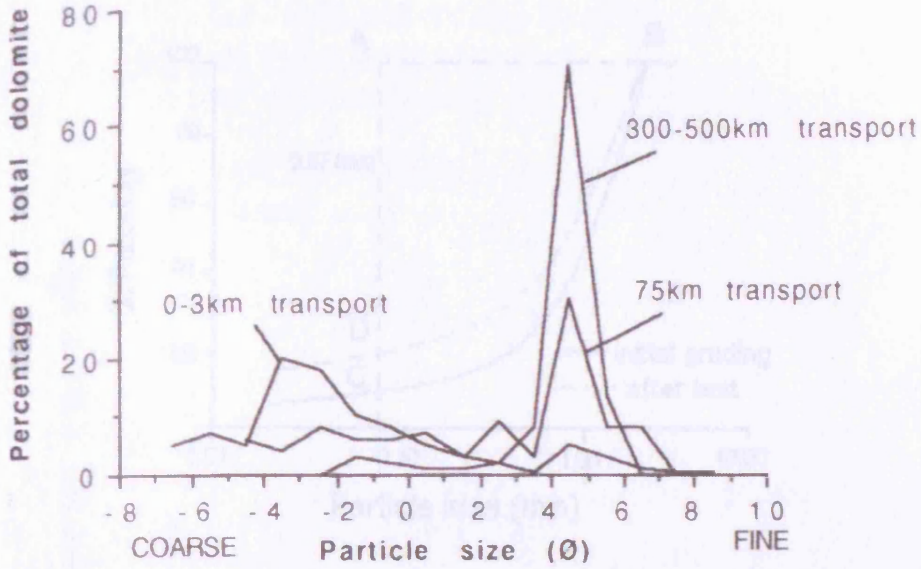

Figure (2-20): frequency distributions of dolomite in till samples from the Hamilton-Niagara region, Canada, showing the effect of progressive particle crushing during transport (modified after Dreimanis and Vagners, 1971).

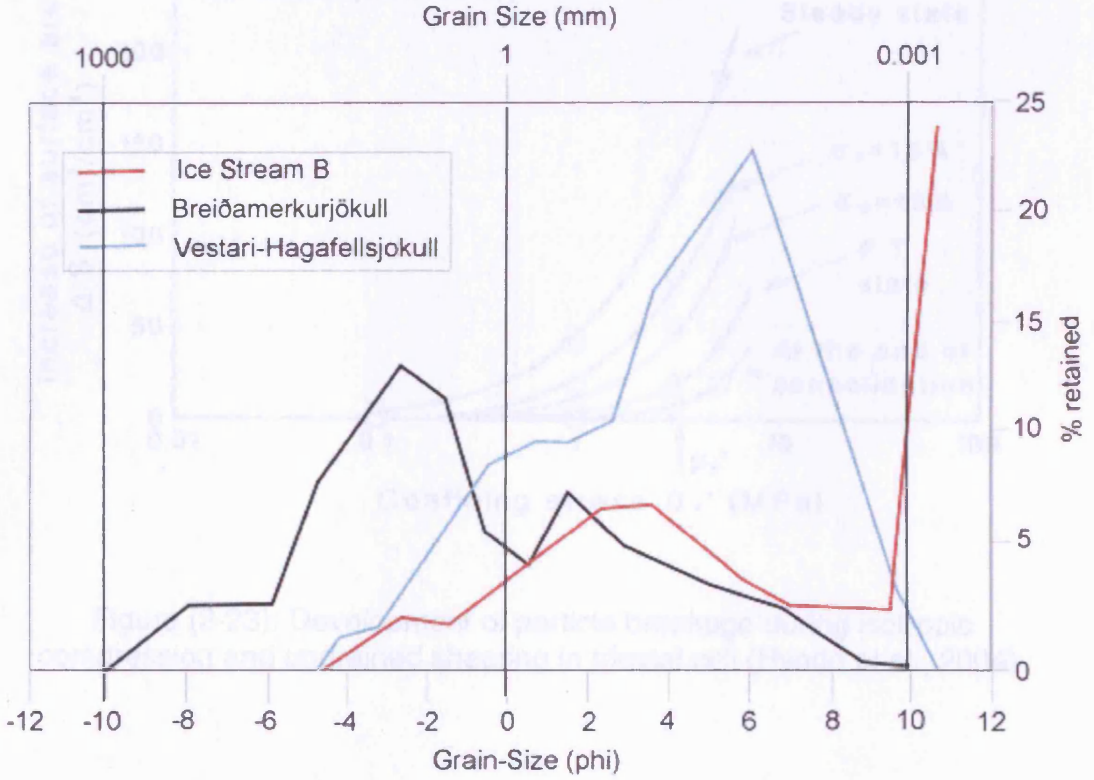

Figure (2-21): A comparison of grain size distribution of three subglacial sediments (Eyre, 2003).

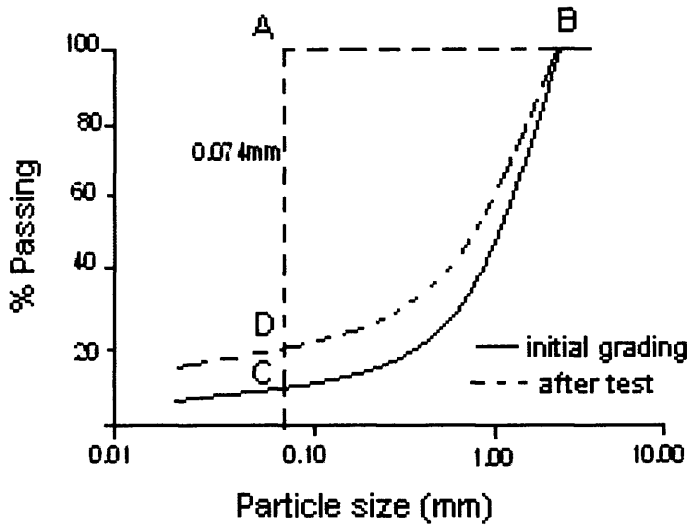

Figure (2-22): Definition of particle breakage parameters proposed by Hardin (1985).

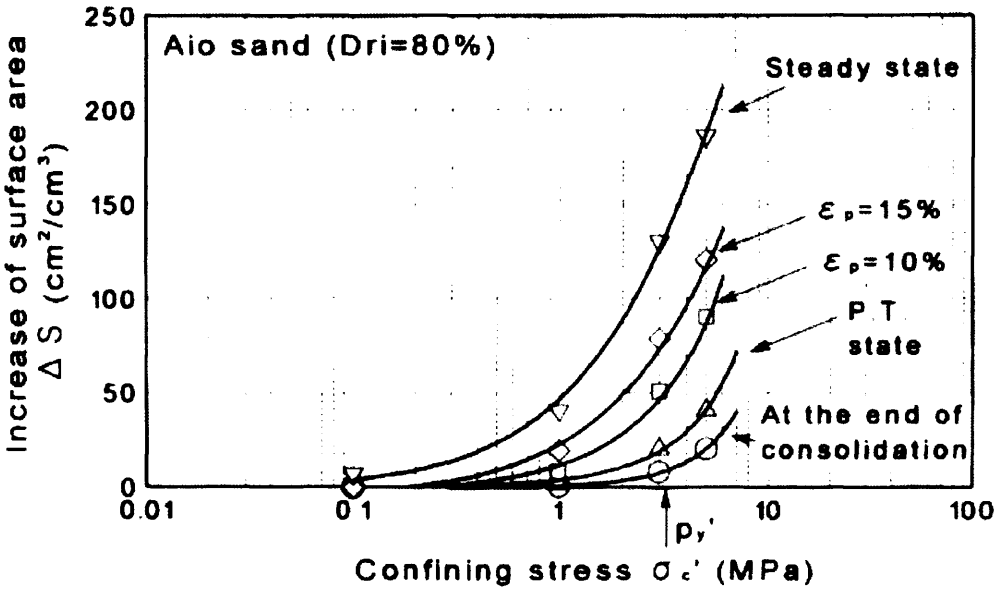

Figure (2-23): Development of particle breakage during isotropic compression and undrained shearing in triaxial cell (Hyodo et al., 2004).

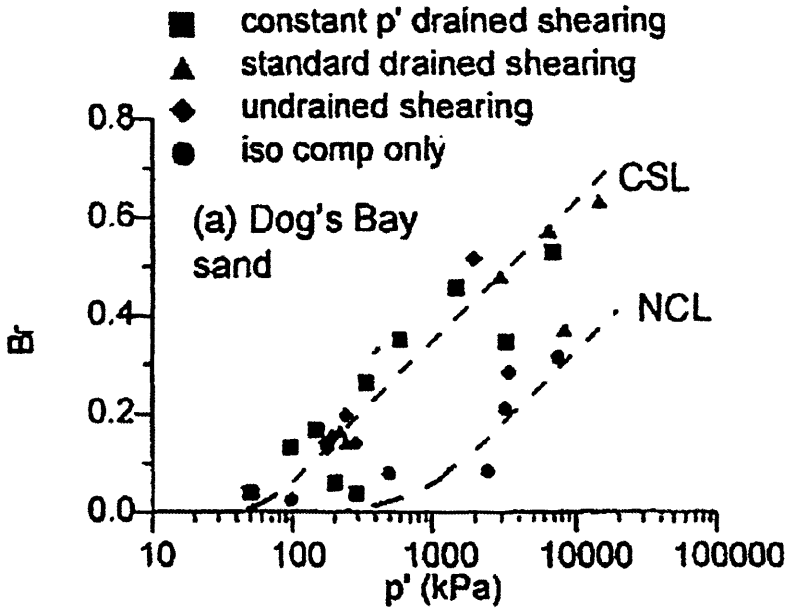

Figure (2-24): Particle breakage related to the state on the NCL and CSL for Dog's Bay sand (Coop & Lee, 1993).

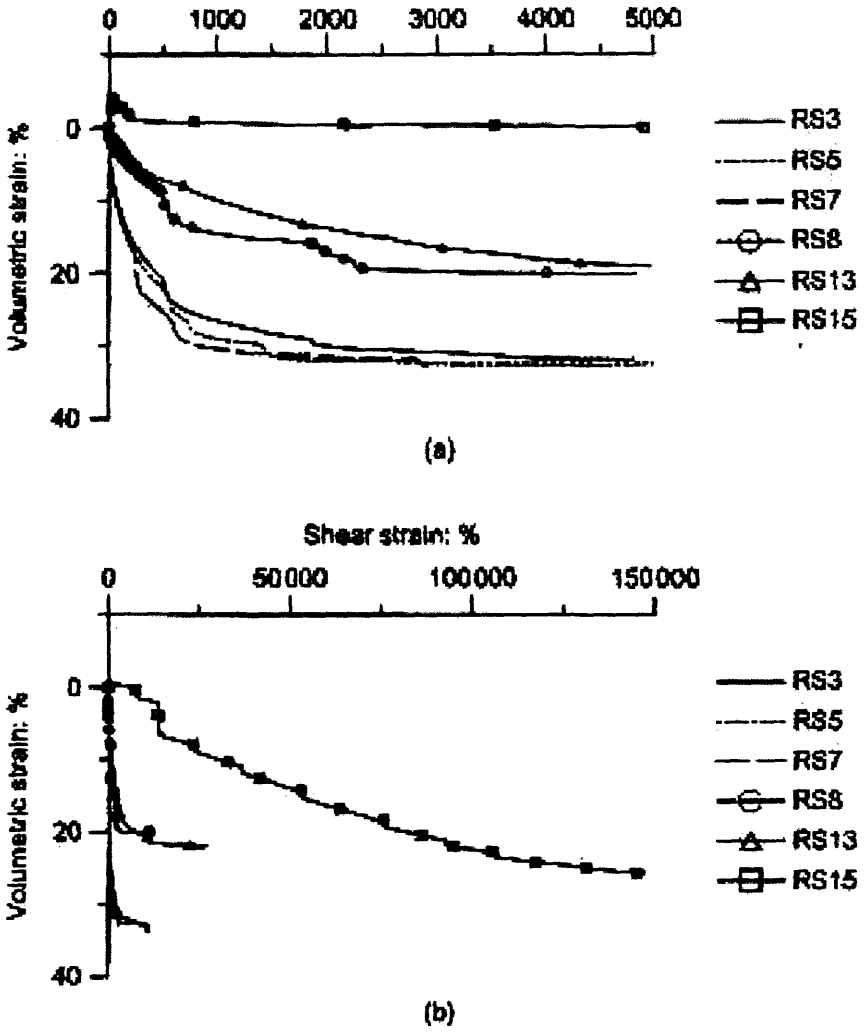

Figure (2-25):
Ring shear data on carbonate sand showing sample volumetric strain development with shearing strain.

- RS3, RS5 and RS7 are uniformly graded samples sheared under vertical pressure range of 650-860kPa.
- RS8 was a well graded sample sheared under the same range of vertical pressure.
- RS15 was sheared under low vertical pressure 60kPa.

(Coop et al., 2004).

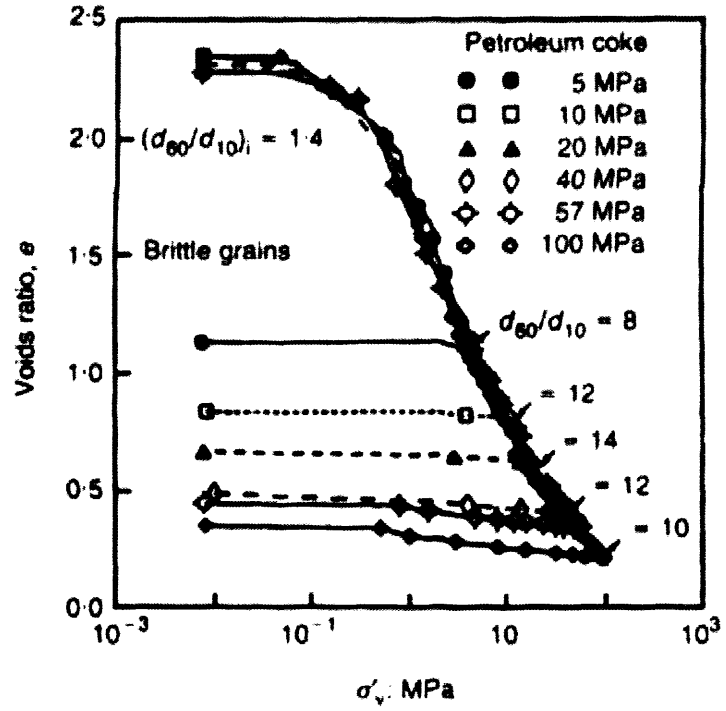

(a)

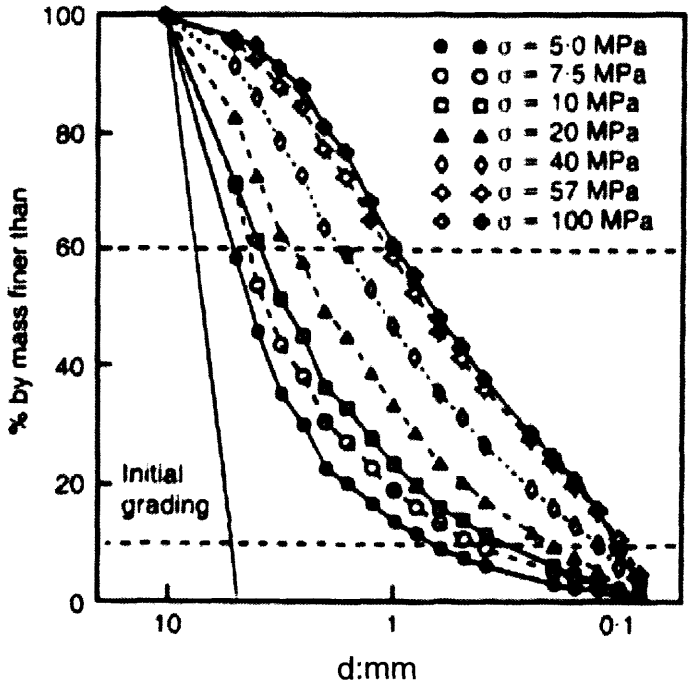

Figure (2-26): One dimensional compression tests on Petroleum coke, as reported by MacDowel & Boulton (1998).

A) compression curve in the void ratio (e)- vertical effective stress plane (σ'_v).

B) The evolvement of the soil grading with increase in stress.

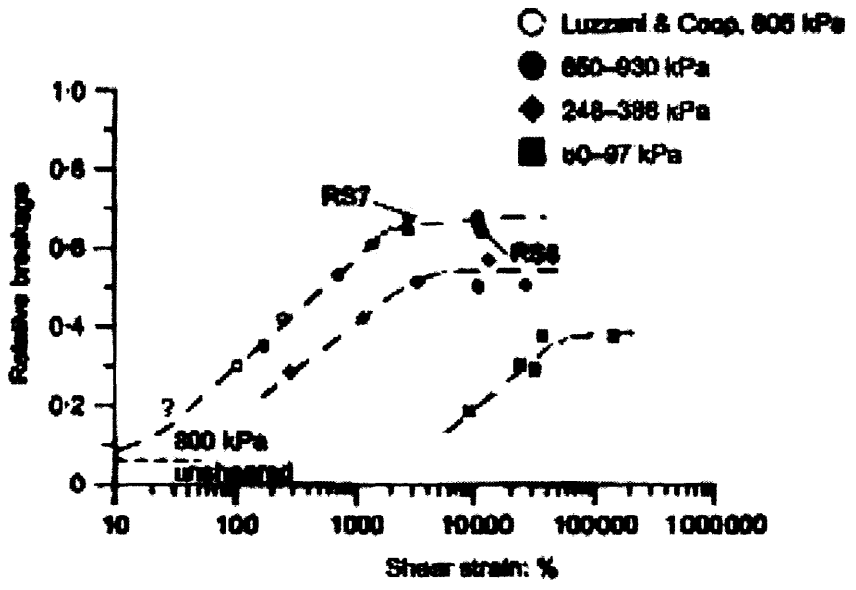

Figure (2-27): The effect of strain level and applied normal stress on particle breakage in carbonate sand (Coop et al., 2004).

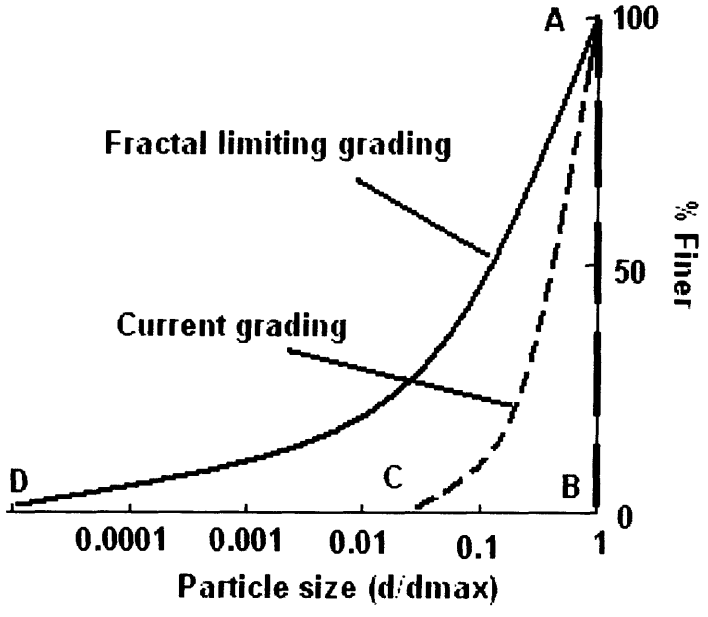

Figure (2-28): Grading state index, I_G= area ABC/area ABD, (Wood, 2006)

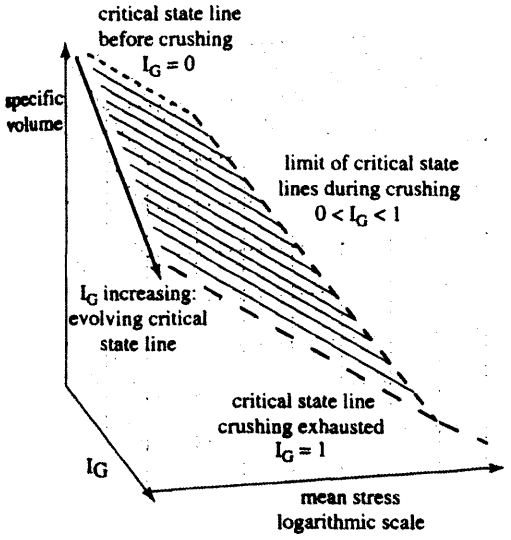

Figure (2-29): Critical state surface for crushable soils in space of: specific volume, mean stress and grading state index (Wood, 2006).

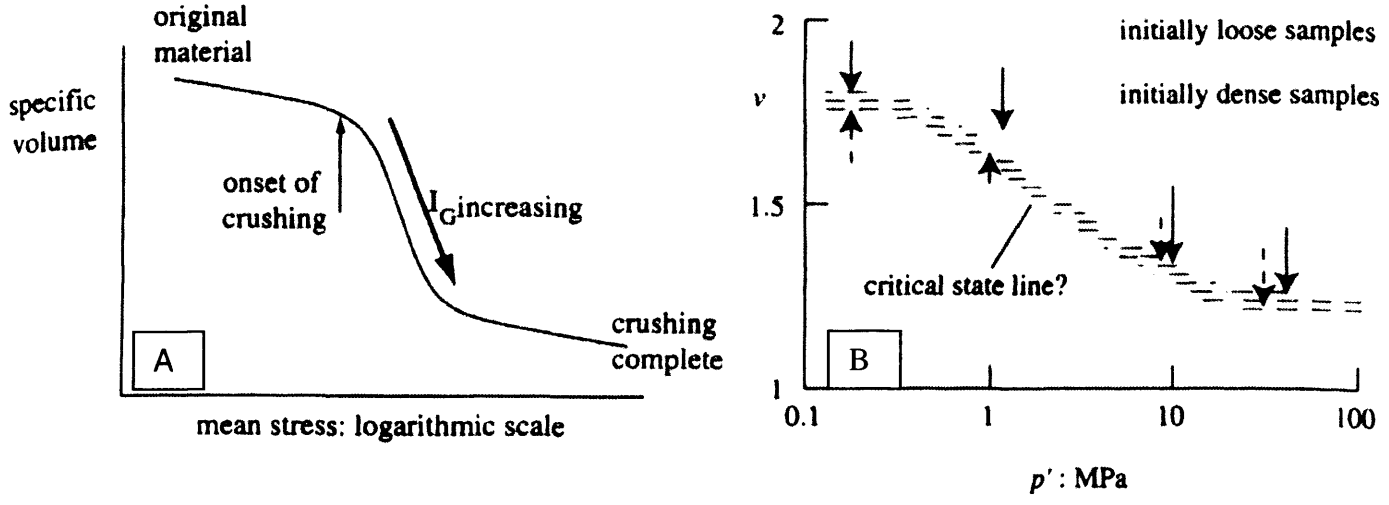

Figure (2-30):

A- Schematic figure showing the three part Critical State Line section through the critical state surface for crushable soils proposed by Wood (2006).

B- Ultimate state for triaxial tests on Chattahochee River sand: semi-logarithmic compression plane (data from Vesic & Clough, 1968)

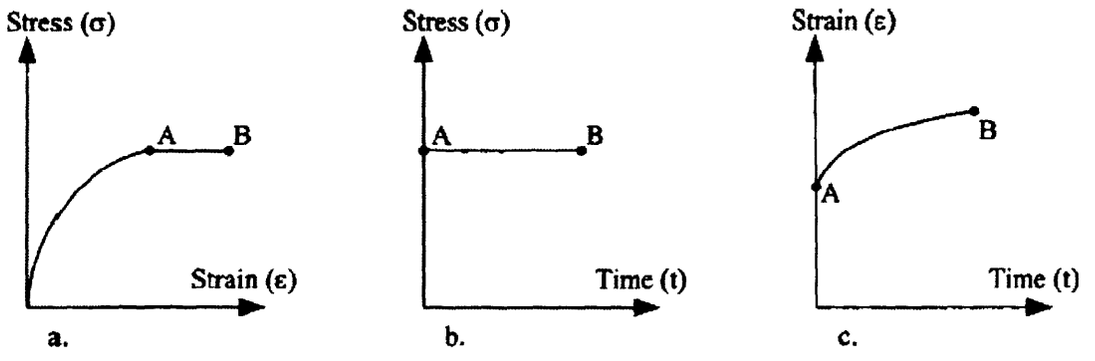

Figure (2-31): Schematic diagram showing creep test data performed at a low stress level: (a) Stress-strain relationship; (b) stress history; and (c) strain history.

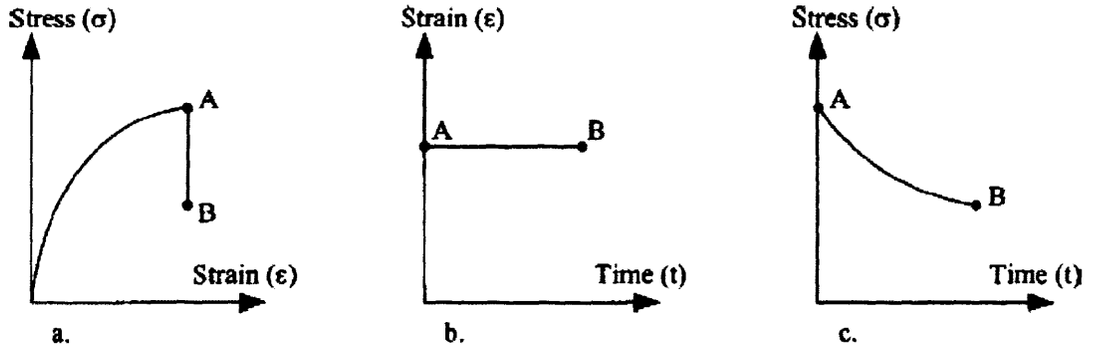

Figure (2-32): Schematic diagram showing relaxation test data (A-B): (a) Stress-strain relationship; (b) strain history; and (c) stress history.

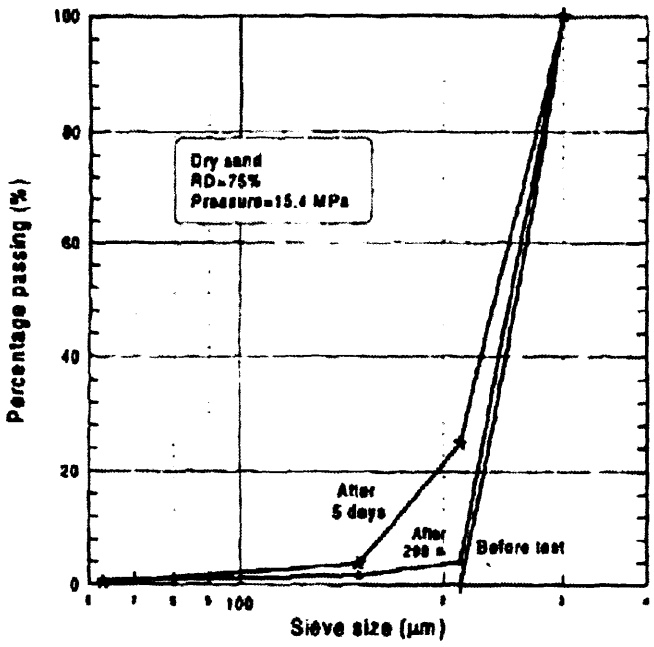

Figure (2-33): Particle size distribution (PSD) increase with loading duration. The figure shows the PSD of the sample before loading, 290 seconds after loading and 5 days after loading (Leung et al., 1996).

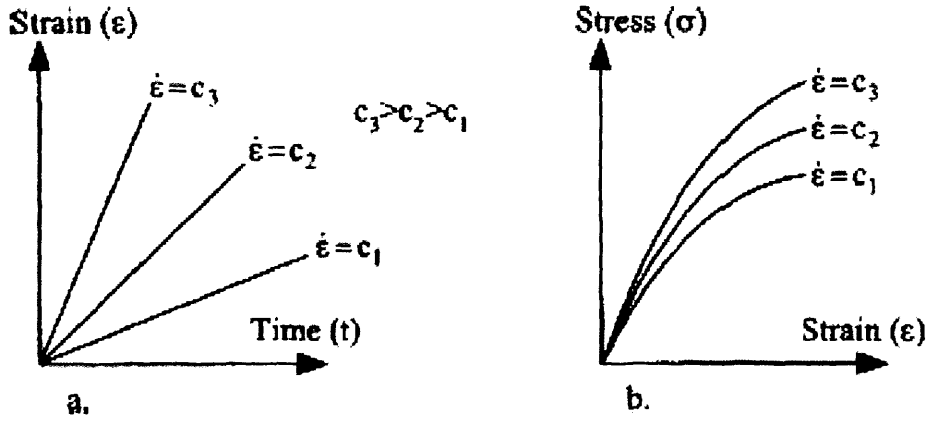

Figure (2-34): Constant Rate of Strain tests (a) Strain rate is kept constant during test (b) Stress- strain response due to different strain rate shearing.

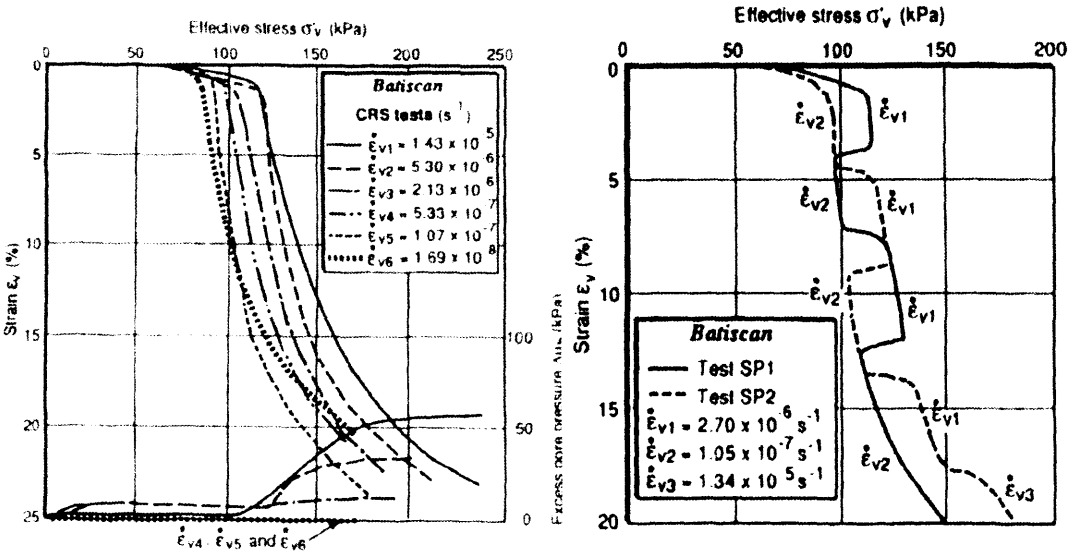

Figure (2-35): Results of CRS oedometer tests on Batiscan clay (Leroueil et al., 1985).

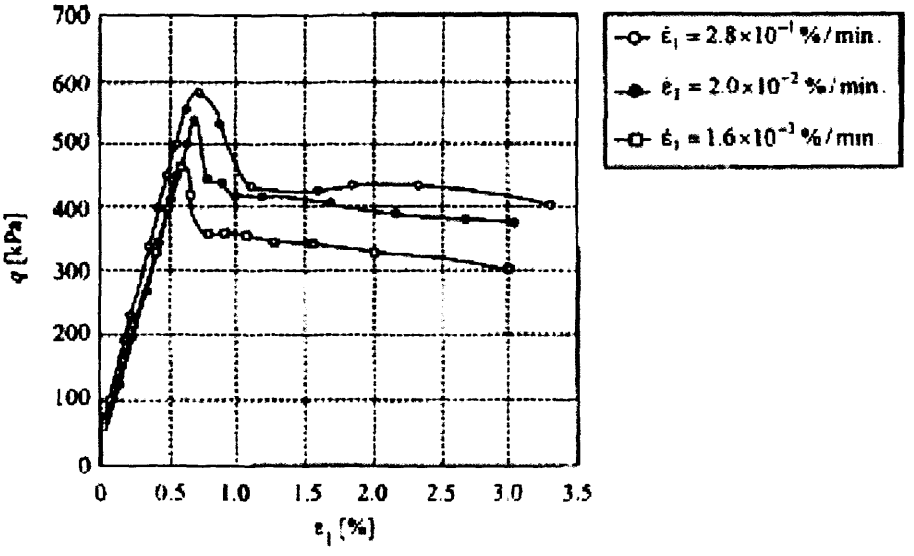

Figure (2-36): Stress- Strain behaviour of Saint-Jean-Vianny clay in undrained constant rate of strain test (Vaid et al., 1979).

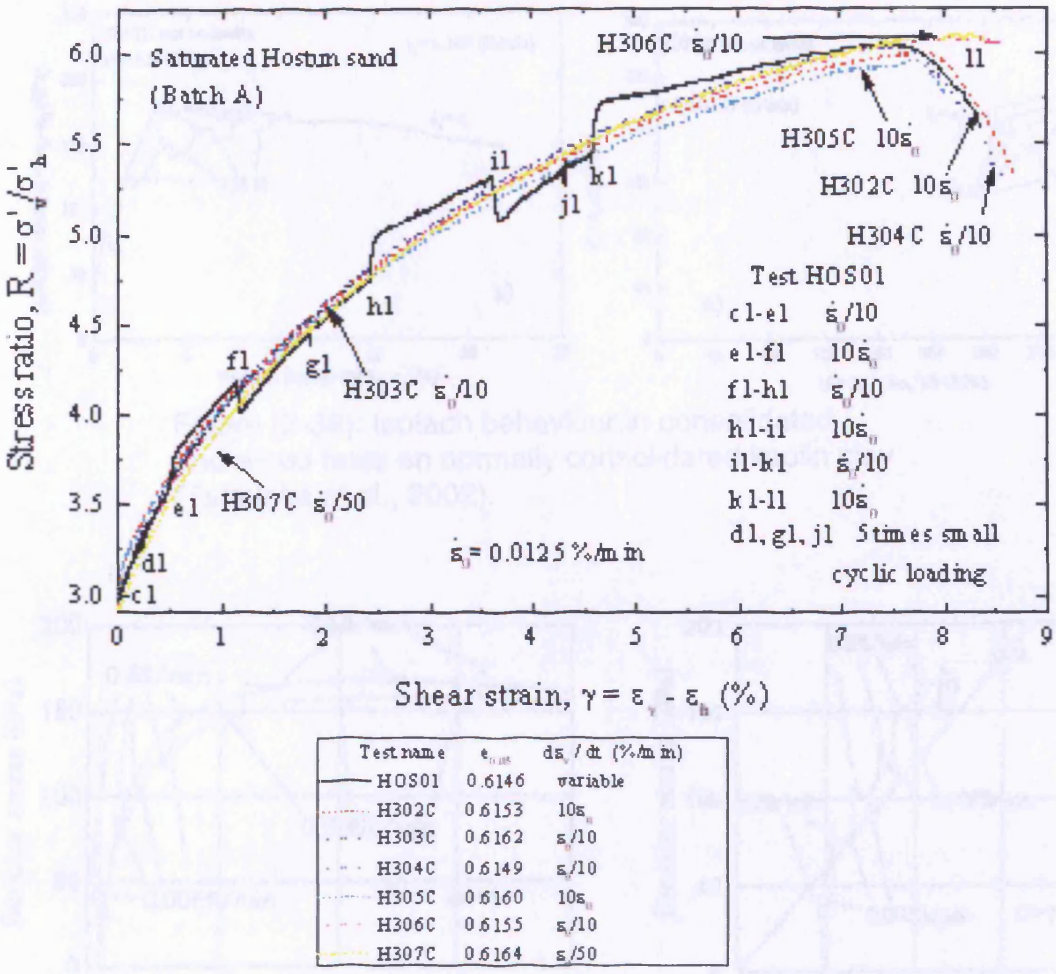

Figure (2-37): Strain rate dependency in Hostun sand. The figure shows the data of six CRS with one variable strain rate test (Matsushita et al., 1998a).

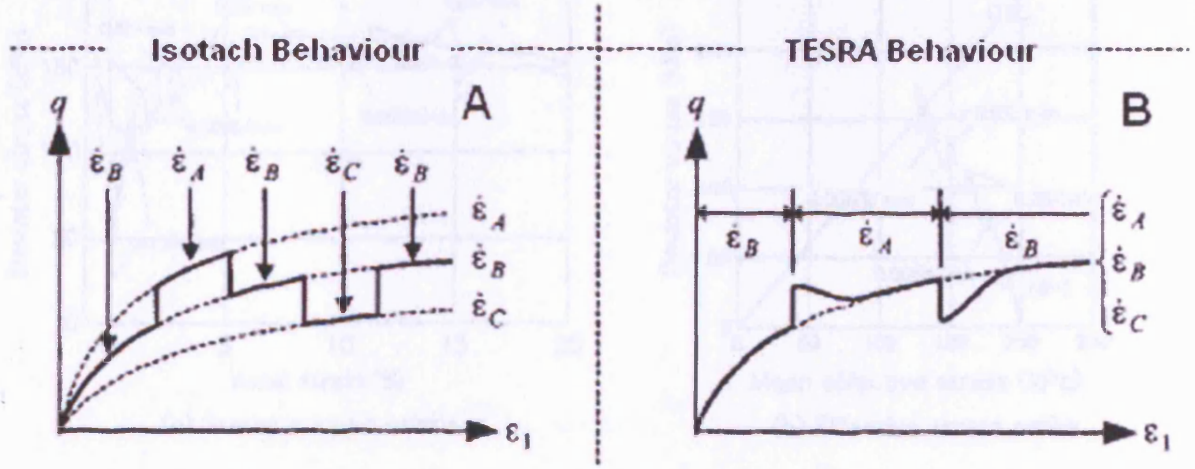

Figure (2-38): Schematic diagram illustrating the detecting of (A) Isotach behaviour (B) TESRA behaviour from variable strain rate.

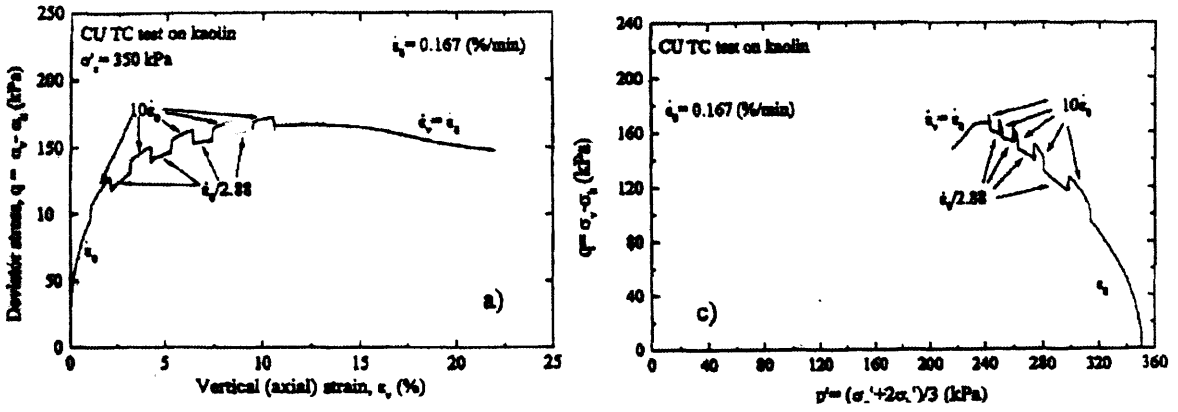

Figure (2-39): Isotach behaviour in consolidated undrained tests on normally consolidated kaolin clay (Tatsuoka et al., 2002).

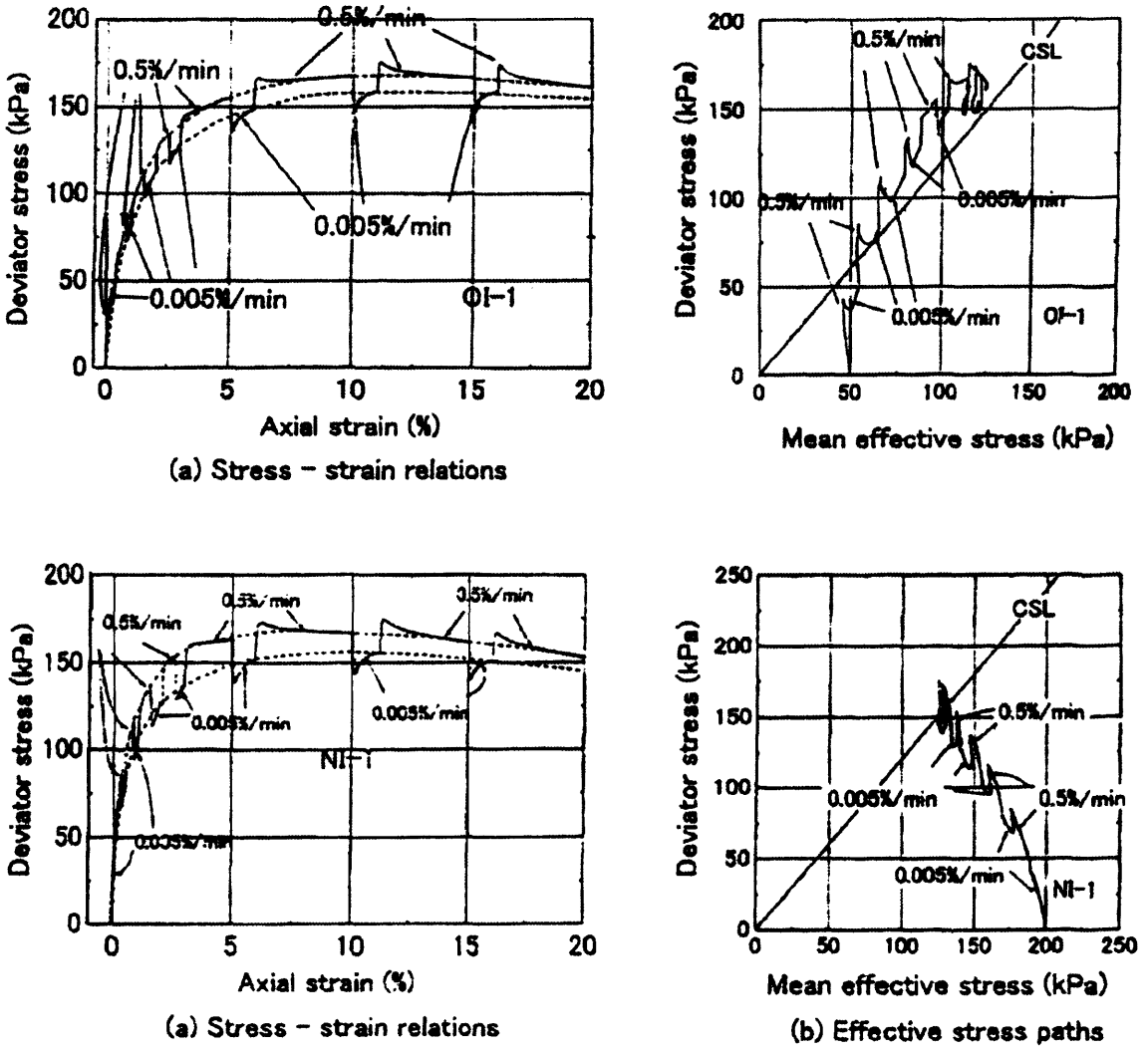

Figure (2-40): General TESRA behaviour in consolidated undrained tests on overconsolidated (top) and normally consolidated (down) reconstituted Fukakusa clay (Oka et al., 2003).

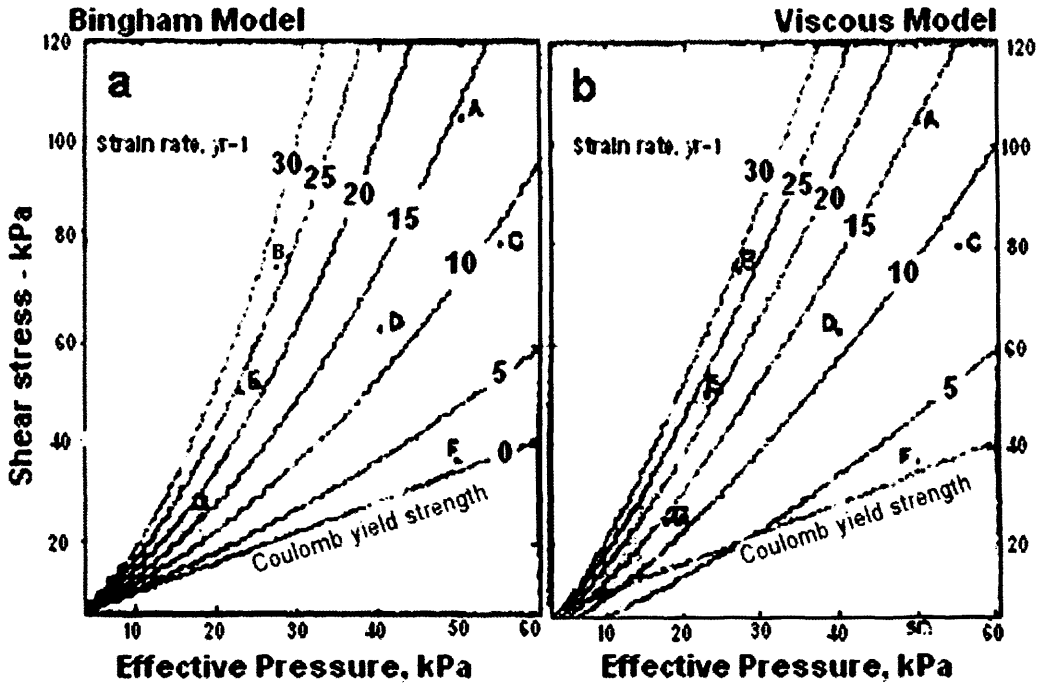

Figure (2-41): Relationships between shear stress, strain rate and effective pressure at Breiðamérkurjökull, to which Bingham fluid (a) and non-linearly viscous fluid (b) models have been fitted. The Mohr-Coulomb failure criterion for the till has also been plotted. (Boulton & Hindmarsh, 1987)

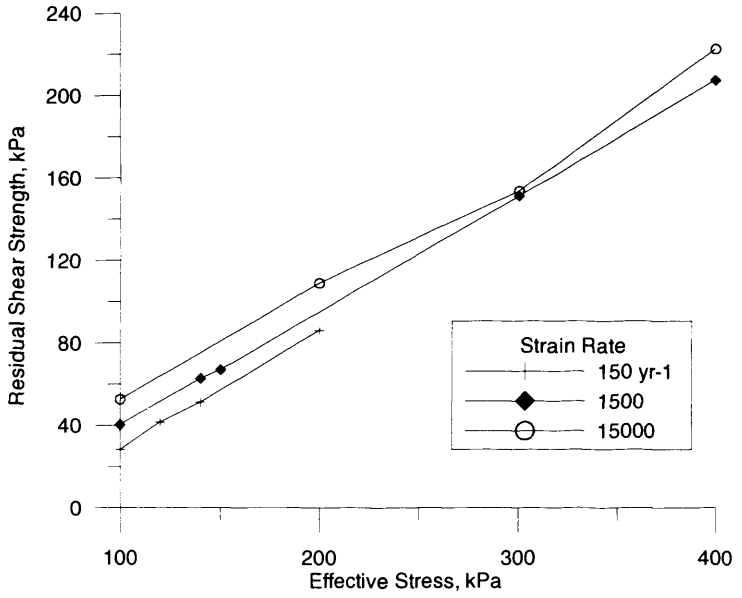

Figure (2-42): Results from ring shear tests on the Dutch till, conducted by Dobbie (1992).

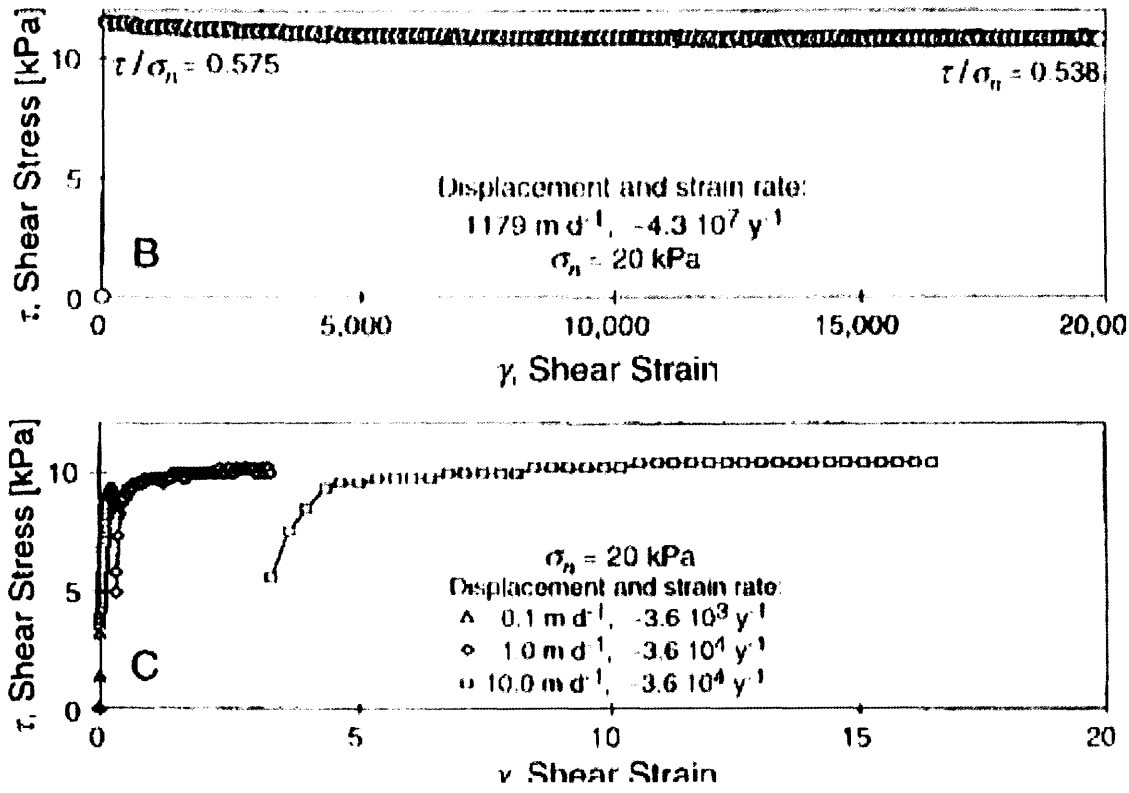

Figure (2-43): Tulaczyc et al. (2000) data from ring shear tests on sediment from beneath Ice stream B-Antarctica.
A- Shear stress (open circles) and sample thickness change versus shear strain in ring shear test. Total normal load 20 kPa.
B- Results of ring shear test in which the relative displacement rate was increased twice by a factor of 10.

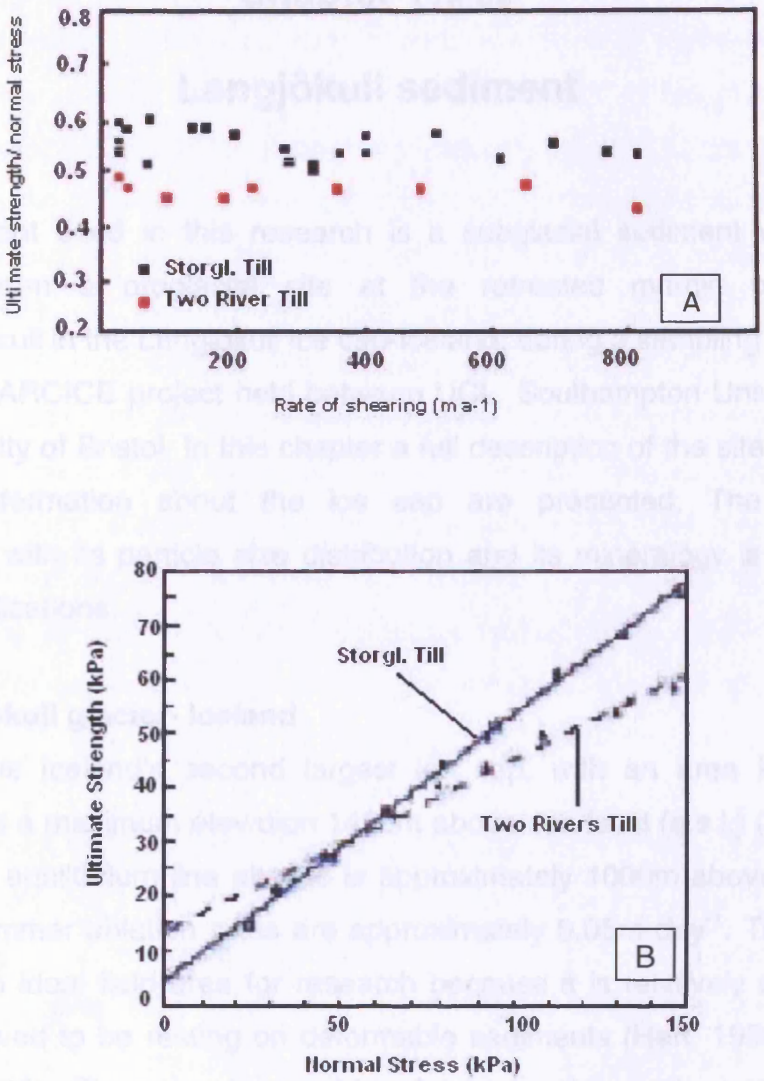

Figure (2-44): Results of ring shear tests on Storglaciaren and Two Rivers Till (Iverson et al., 1998).

Chapter Three

Langjökull sediment

The sediment used in this research is a subglacial sediment which was retrieved from a proglacial site at the retreated margin of Vestari-Hagafellsjökull in the Langjökull ice cap-Iceland, during a sampling expedition part of the ARCICE project held between UCL, Southampton University and the University of Bristol. In this chapter a full description of the site and some relevant information about the ice cap are presented. The sediment description with its particle size distribution and its mineralogy is discussed with its implications.

3.1 Langjökull glacier- Iceland

Langjökull is Iceland's second largest ice cap, with an area in 1973 of 953km^2 and a maximum elevation 1450m above sea level (a.s.l.) (Björnsson, 1978). The equilibrium line altitude is approximately 1000m above sea level and net summer ablation rates are approximately 0.05m day^{-1}. The ice cap provides an ideal field area for research because it is relatively accessible, whilst believed to be resting on deformable sediments (Hart, 1995; Fuller & Murray, 2000). The area is considered to be volcanically active but no postglacial volcanic activity has been pinpointed (Sigurdsson, 1998). The Hagafell ridge separates Vestari-Hagafellsjökull and neighbouring Eystri-Hagafellsjökull glaciers (Figure 3.1), and the outlets drain the majority of the southern sector of the ice cap. These two glaciers are the only outlets of the ice cap to have a recorded history of surging (Eyre, 2003).

The two glaciers last surged simultaneously in the winter of 1979/1980 (Sigurdsson, 1998) and Eystri-Hagafellsjökull also surged in 1998-2000. Following such surge activity the two outlets provide important field sites in terms of considering the contributions of basal motion and/or sediment deformation to the overall glacier velocity in both surging and non-surging conditions. The behaviour of the subglacial sediment from the proglacial

fields of these outlets glaciers provides a good source of comparison with data collected from other Icelandic glaciers, to decide whether all Icelandic glaciers can be considered to behave similarly in terms of subglacial sediment rheology and deformation. In particular, the results presented here will be useful to determine whether the work of Boulton & Hindmarsh (1987), which proposed a viscous model for deformations in subglacial sediments based on data from Breiðamérkurjökull (see Section 2.8), is relevant to all Icelandic glaciers or whether this is just confined to Breiðamérkurjökull. In addition the research presented here may provide insights into the validity of studying the mechanical behaviour of a sediment which is retrieved from proglacial conditions and whether it will accurately reflect the behaviour of the sediment under subglacial conditions. This will be achieved by taking in consideration all the deformational factors which might cause significant change to the sediments geotechnical properties during its transport under glaciers.

The margin of Vestari-Hagafellsjökull is lobate, with a low surface slope (approximately 3.8°) and extends over a large Holocene basalt lava field, which contains numerous glacial landforms in the proglacial area including flutes and drumlins (Hart, 1995) as shown in Figure (3-2). The ice is thought to be temperate throughout with implication that meltwater may directly reach the glacier bed. Details of the sampling area and methods are given below.

3.2 Sampling and sample storage

Undisturbed samples of till which lay underneath the glacial sole are usually difficult to obtain, and the methods available, up to this time, do not ensure high quality undisturbance of samples retrieved. The hot water drill method is one of the most used to retrieve subglacial samples. This method was used in different cases such as in Ice stream B- West Antarctica, where it was used to retrieve subglacial sediment with the help of a 6m piston corer, under about 1000m of ice layer (Tulaczyk, 1999). The 5cm diameter sample of sediment was considered to be undisturbed. However, microscopic examination of till thin sections suggested that the sample had experienced some disturbance during acquisition.

To avoid the disturbance which is associated with the retrieval procedure, which may affect the evaluation of the sediment behaviour by laboratory geotechnical testing, sampling from proglacial areas was considered. The site chosen for sampling was in the proglacial region near the Vestari-Hagafellsjökull margin (Figure 3-3). In general, thicknesses of the sediment layer in the proglacial area were highly variable and lay in pockets on the bed rock, ranging in thickness from a few centimetres to approximately 5m - with most being no more than 1 or 2 metres thick. The pit from which the samples were collected was on the eastern side of the river approximately 30 m south of the glacier toe. At this location 10 block samples were collected by the UCL Earth Science Department team in the year 1998-1999, as it proved the most effective method for collecting high quality undisturbed samples. Care was taken to avoid sampling from the topmost 0.4 m of the lodgement till, which is likely to have been remoulded by shear deformation, erosion and some fluvial disturbance (Boulton, 1976). Block samples of 30x30x40cm^3 were retrieved. The sediment blocks were cut by digging a trench on all sides of the sample and carefully trimming it to the right size (Figure 3-4). Moisture content was preserved by wrapping the sample with a cling film and layers of muslin soaked in paraffin wax (Figures 3-5, 3-6). The orientation of the samples was noted. These samples were undisturbed as samples can be, and therefore it was considered that they had retained most of the original natural structure and fabric of the soil. Liquid nitrogen was applied to the samples to freeze them immediately for easier handling and transportation (Figure 3-7). The freezing technique is considered one of the practical methods in preserving the granular material structure (Mimura, 2003), and is unlikely that the soil mechanical properties is going to be affected due to freezing, especially for a sediment which is expected to have been subjected to many cycles of freezing during its history.

3.3 General description of the Langjökull sediment

The sediment retrieved has a colour ranging from grey to dark grey. It can be described as a well graded (poorly sorted) cohesionless sediment with a high presence of clasts, the clasts being sometimes larger than 100mm in diameter and sometimes present in the form of isolated boulders. The larger

particles of the sediment can be described as having a sub-angular sub-rounded shape. The sub-rounded shape might be due to the nature of the subglacial deformations, with shearing that might have caused abrasion and breakage of the sediment particles. The sediment in the proglacial site was water-saturated with relatively high void ratios considering the well graded nature of the sediment. The field void ratio was found to be around 0.57. Scanning electron microscopy images of undisturbed samples (Figures 3-8 to 3-11), confirms the sub-angular sub-rounded shape of the sediment particles and the high voids in the sediment's undisturbed fabric.

3.4 Particle size distribution and specific gravity

Particle size distribution analysis was carried out by the author in the laboratories of the UCL Civil Engineering Department. For particle sizes larger than 63 microns, both dry and wet sieving was used (the particle size distribution procedure with the mesh size used will be discussed in the next chapter). A hydrometer analysis was used for particles less than 63 microns in size. The particle size distribution for the tested sediment in this research is shown in Figure (3-12).

The results obtained for the particle size distribution of the sediment is consistent with the particle size distribution of samples retrieved from the same location, which were presented by Eyre (2003) as shown in Figure (3-13) and the results of laser granulometry carried out on the sediment by the Department of Geology at Royal Holloway and Bedford college (see appendix A). The specific gravity of the sediment, determined using the procedure described by the British Standard (BS1377), was found to be equal to 3.107, which is a relatively high value compared to well known soils. Figure (3-14) shows a comparison of particle size distributions between three subglacial sediments collected from: Langjökull Glacier (Vestari-Hagafellsjökull-Iceland), Breiðamérkurjökull (Iceland) and Ice-stream B (Antarctica). The latter subglacial sediment is a clayey sediment. A simple comparison between Langjökull sediment and Breiðamérkurjökull sediment, both of basaltic origin, shows that the tested sediment in this research (Langjökull Sediment), is richer in fines than the Breiðamérkurjökull sediment.

3.5 Mineralogy

The sediment's mineralogy was determined by the means of X-ray diffraction, available at the UCL Earth Sciences Department. The sample was tested according to the particle sizes. Particles larger than 1405 microns, which represent the very coarse sand size, were tested separately. Coarse to medium sand size particles, represented by the particles between 1405 and 295 microns, and the fine sand size particles, for particles between 295 and 63 microns, composed the second and the third specimens, while the fines (<63 microns) represented the fourth specimen. The four specimens were prepared by grinding the particles to very fine sizes before they were examined by the X-ray diffractometer (Make: PANalytical, Model: X'Pert Pro). The histogram of 2Θ against its occurrence for all four samples of Langjökull sediment are presented in Figures (3-15) to (3-18) (see Section 4.6.4 for explanations on interpreting X-ray diffraction tests).

The aim behind testing each size of particles separately is to identify the minerals present in each size and whether the parent rock is the same for all particle sizes. This would also clarify some important aspects about particle breakage of the sediment, by comparing the mineralogy of different sizes of particles for a better judgement on the evolution of the finer particles.

The X-ray diffraction test results showed the presence of three glacial feldspar minerals which are usually present in sediments of basaltic origin. These are: Labradorite, which is a combination of Anorthite ($Ca\ Al_2\ Si_2O_8$) and Albite ($Na\ [Al\ Si_3O_8]$), Augite ($Ca\ Mg\ O_6Si_2$) and Forsterite ($Mg_{1.626}\ Fe_{0.37}\ SiO_4$). The percentage of each of these minerals in the tested samples is shown in Table (3-1). This result revealed that this sediment is of a typical clean basaltic composition which is mainly dominated with feldspar and pyroxenes.

The X-ray diffraction test results for the particles finer than 63 microns showed no trace of clay mineralogy. This confirms that the mineralogy of these particles is very much the same as the larger ones. The absence of

clay minerals in the samples as well as the presence of Augite, give an indication of the type of weathering which this sediment was subjected to (Flint, 1971). Usually clay minerals form when a chemical weathering is involved in the formation process of the sediments, and the absence of these minerals is an indication of the non-attendance of this type of weathering in the formation of this till. The survival of Augite, which is a mineral susceptible to chemical decay, in the composition of this sediment, in fact, confirms that a mechanical weathering was responsible for the formation of this sediment rather than a chemical one, which also emphasis the role of subglacial deformations on the formation of this sediment. In this till, which was derived from rocks that contain those minerals, most of the clasts, regardless of size, were mechanically broken or abraded. These characteristics indicate that the related glaciers were eroding fresh rock rather than decomposed minerals.

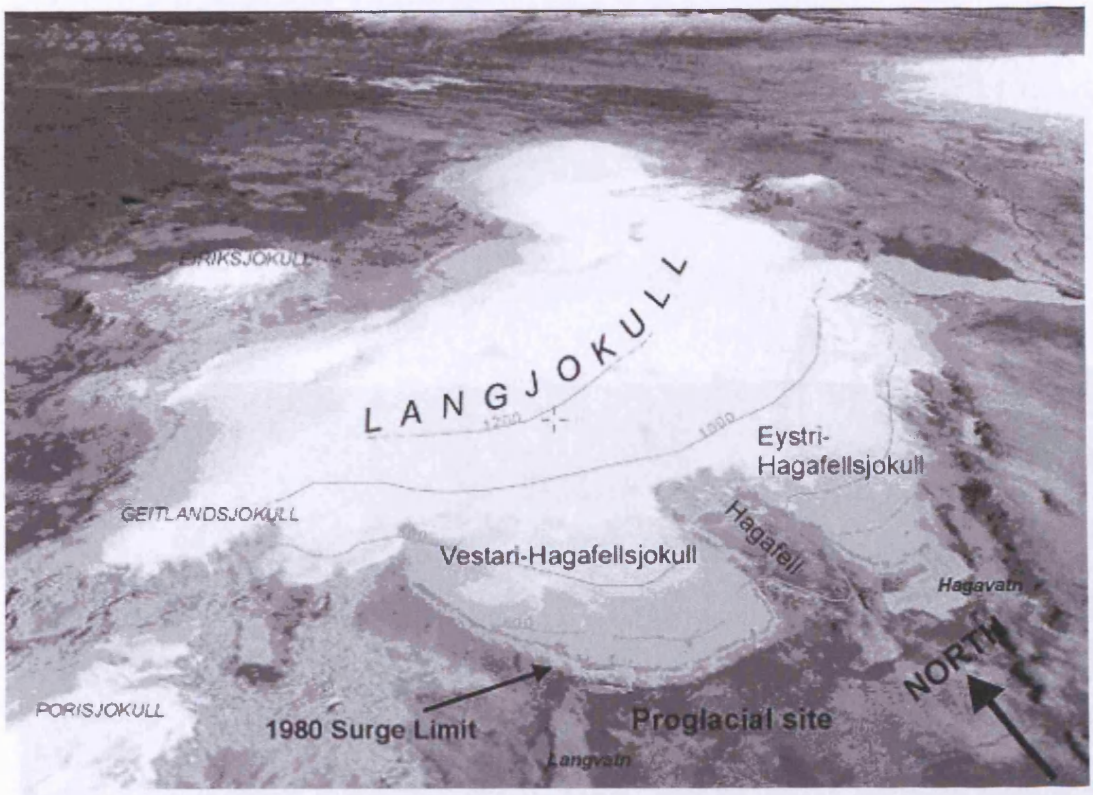

Figure (3-1): Langjökull Glacier- Iceland.

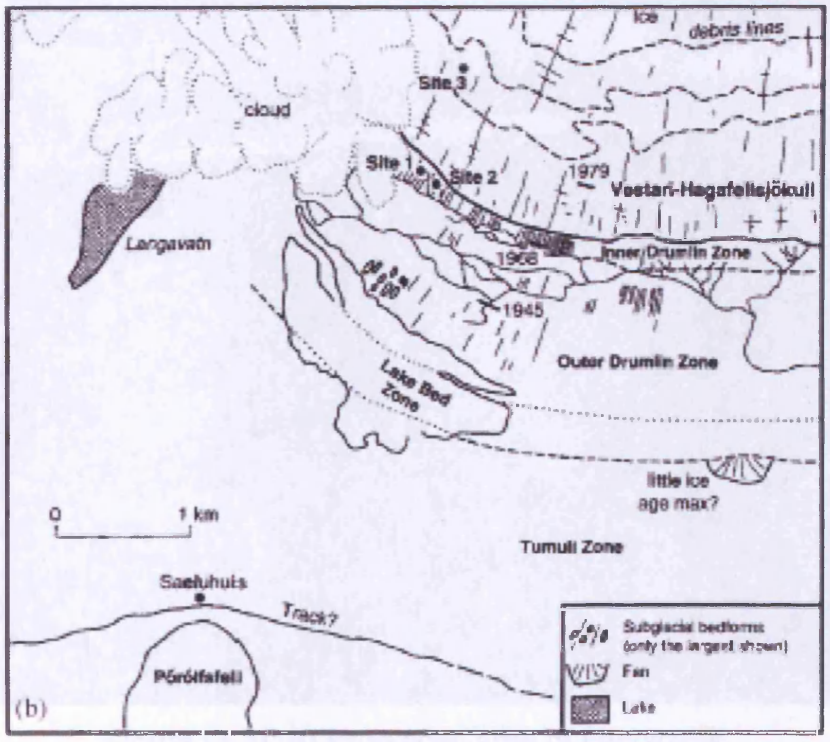

Figure (3-2): Details of Vestari-Hagafellsjökull, showing flutes and drumlins (Hart, 1995).

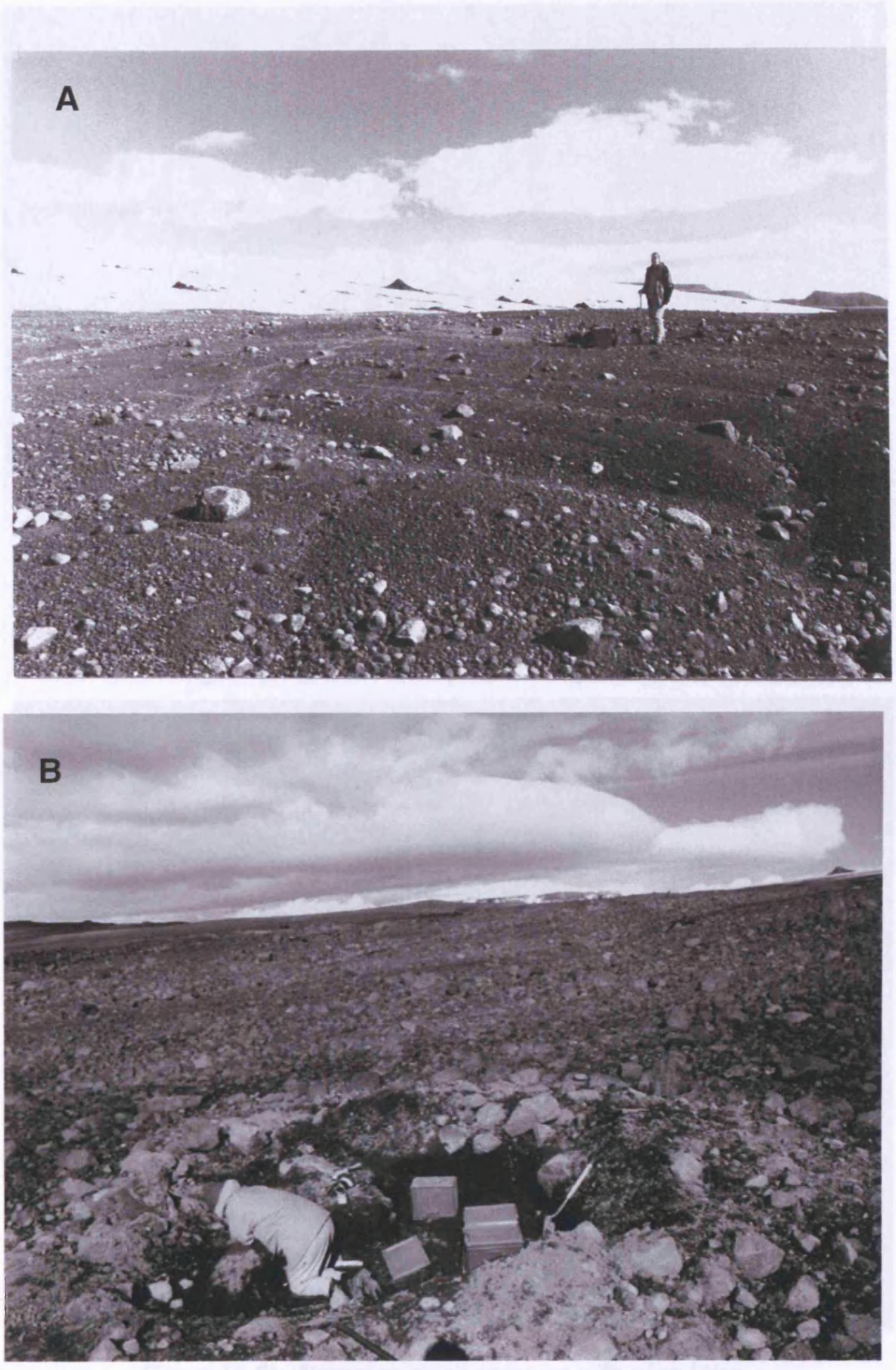

Figure (3-3): A) Proglacial area of Langjökull.

B) The sampling pit.

Figure (3-4): Block sample trimming at the site.

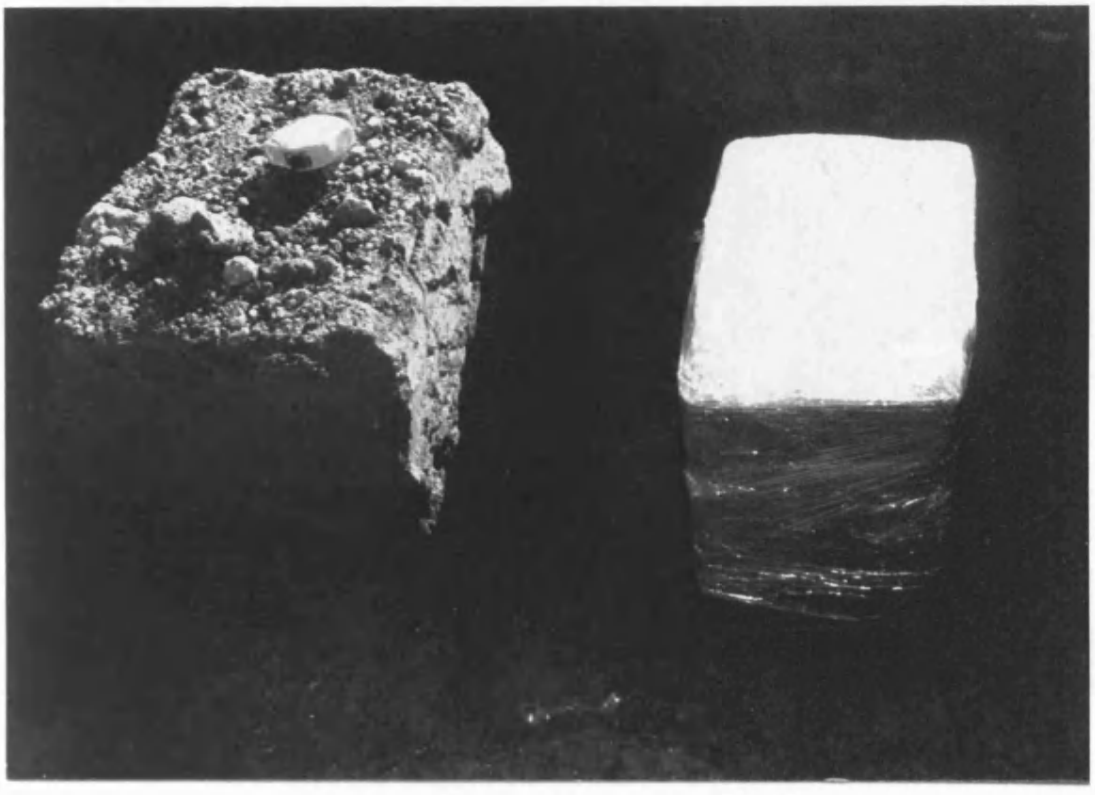

Figure (3-5): Wrapping block samples with cling films.

Figure (3-6): Sealing of retrieved samples with paraffin wax.

Figure (3-7): Applying liquid nitrogen to freeze the samples.

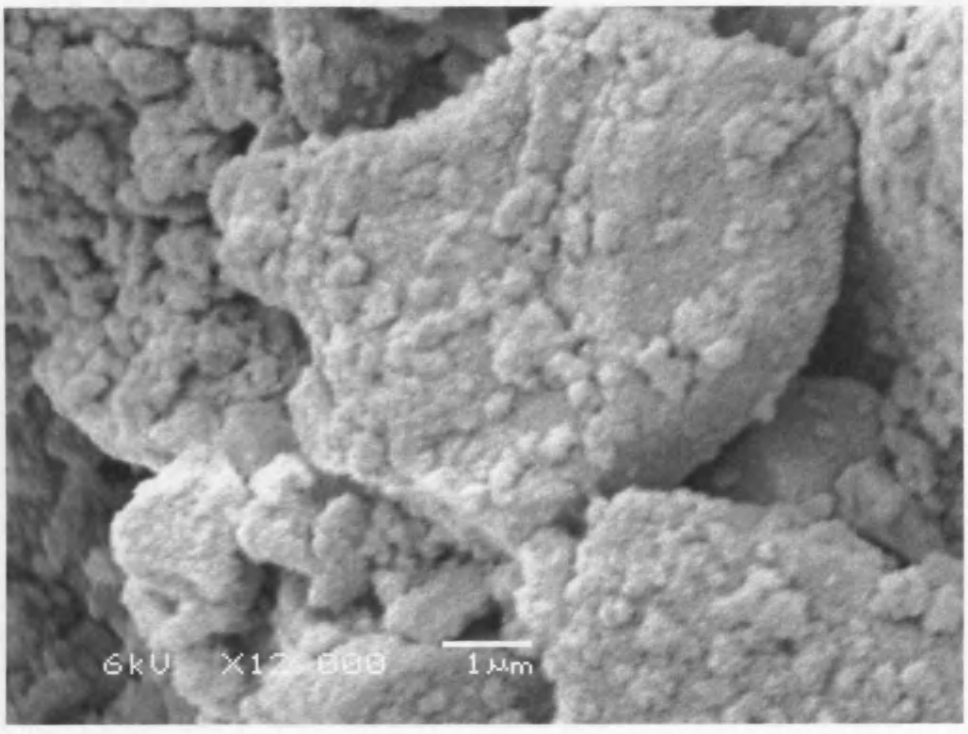

Figure (3-8): Scanning electron microscope image showing the sub-angular sub-rounded particle shape of Langjökull sediment.

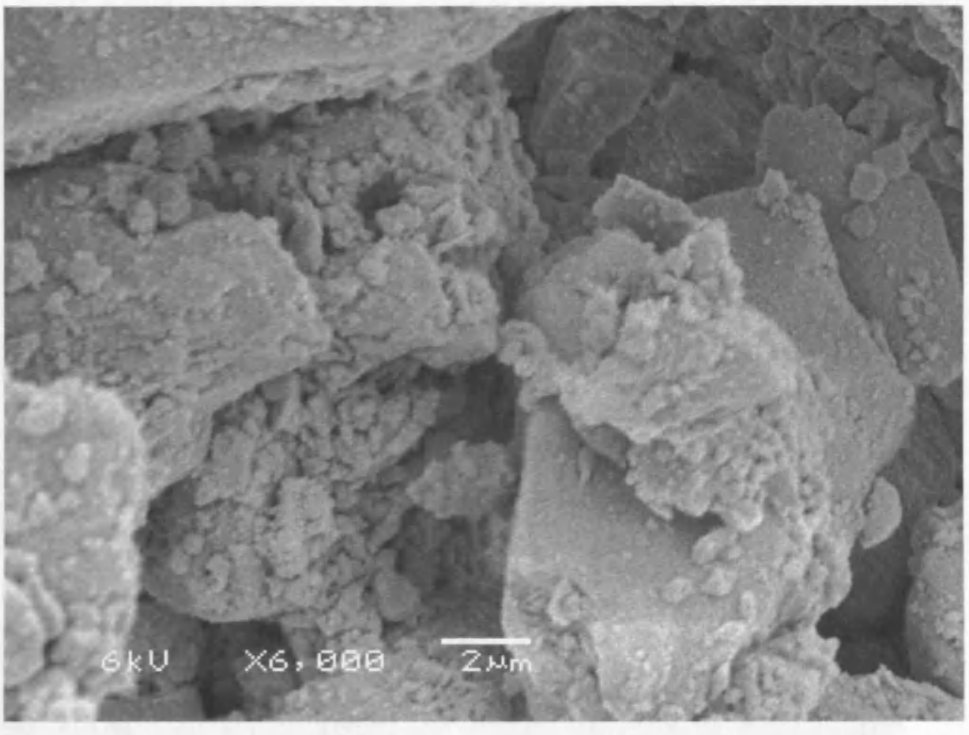

Figure (3-9): Scanning electron microscope image of an undisturbed sample of Langjökull sediment showing the range of particles' sizes of the sediment.

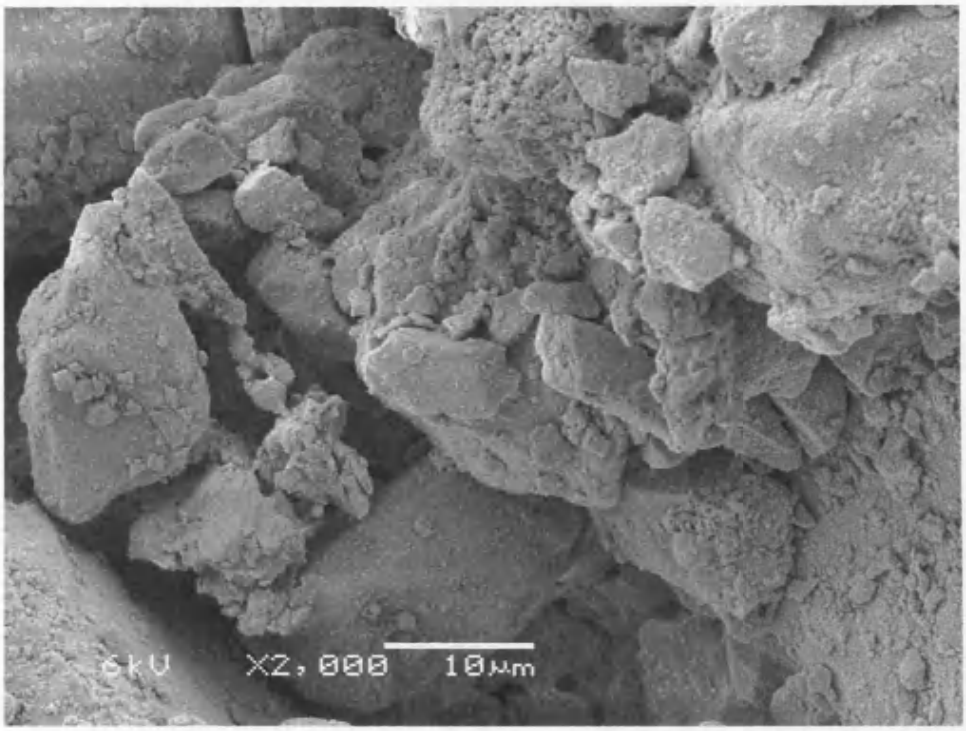

Figure (3-10): Scanning electron microscope image of an undisturbed sample illustrating the high void ratio in the undisturbed fabric of the sediment.

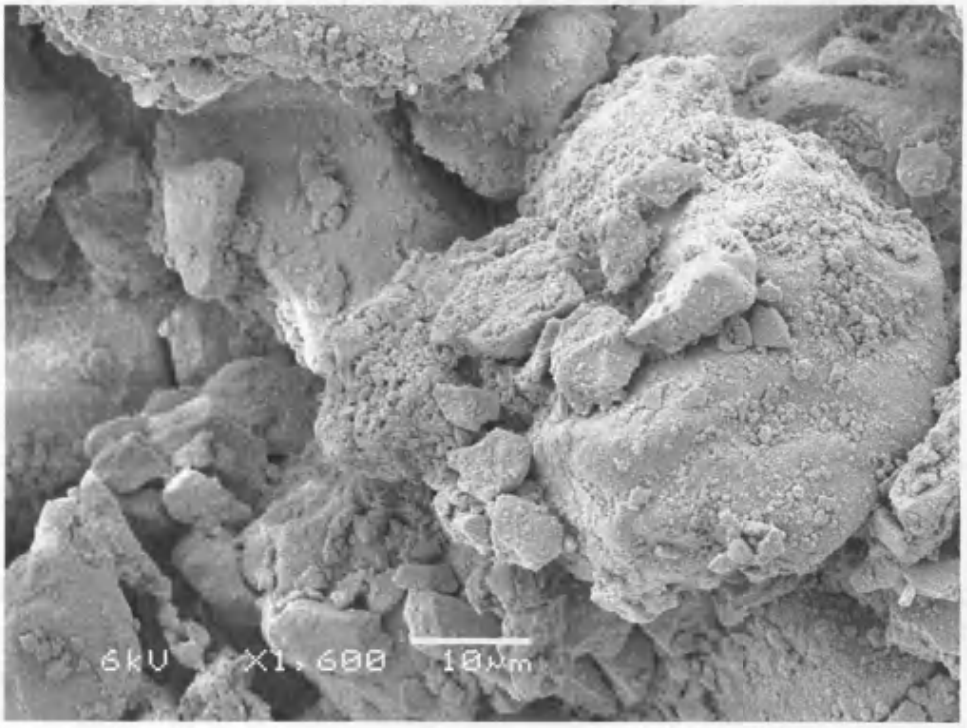

Figure (3-11): Scanning electron microscope image of an undisturbed sample of Langjökull showing the sediment's particles size range and shape and the voids in the sediment's undisturbed fabric.

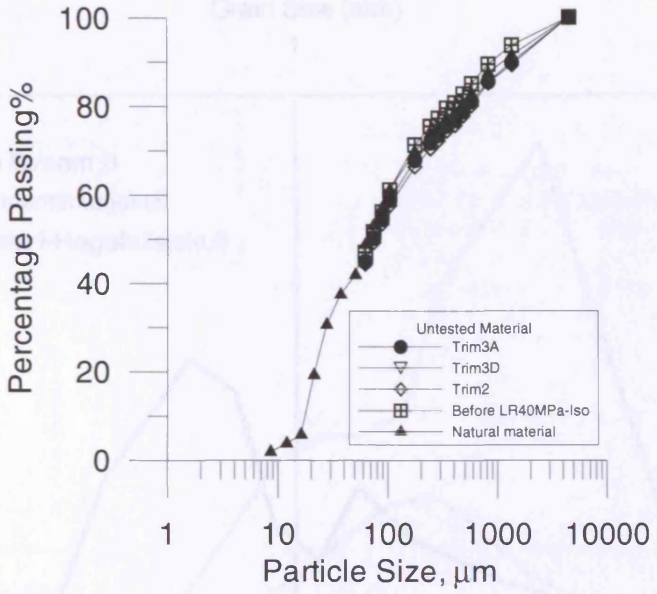

Figure (3-12): Particle size distribution of Langjökull sediment.

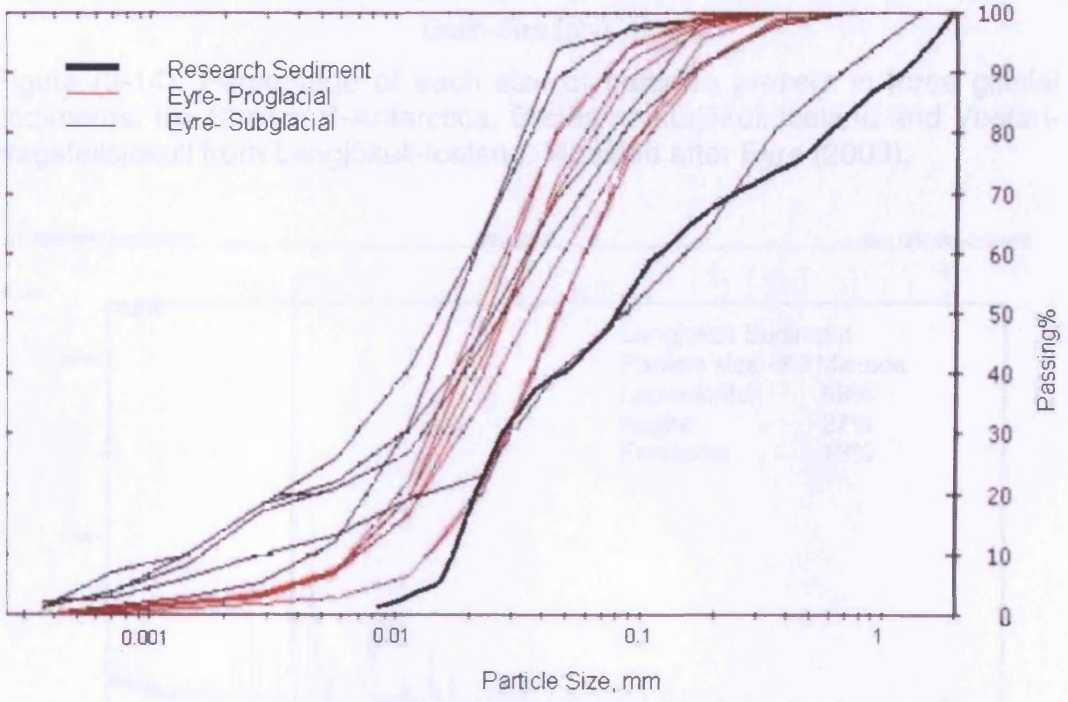

Figure (3-13): Particle size distribution of Langjökull sediment, carried out by the author and particle size distribution of Langjökull sediment from the subglacial and proglacial sites which were presented by Eyre (2003).

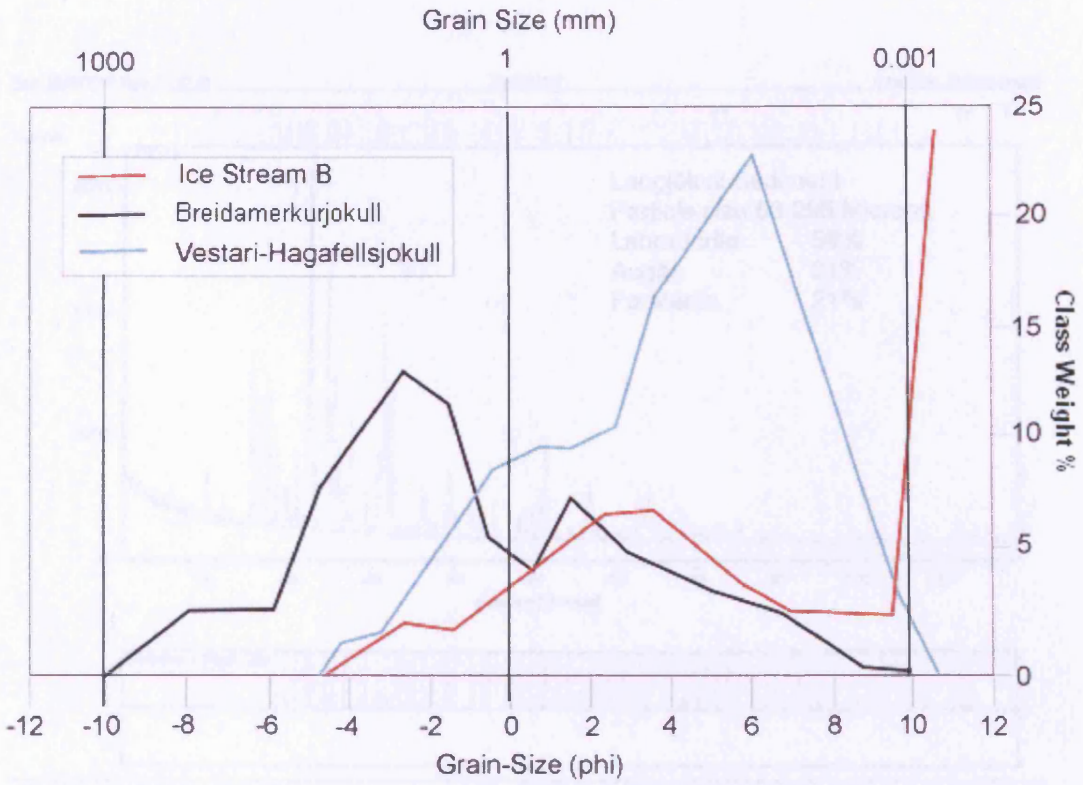

Figure (3-14): Percentage of each size of particles present in three glacial sediments: Ice Stream B-Antarctica, Breiðamerkurjökull-Iceland and Vestari-Hagafellsjökull from Langjökull-Iceland. Modified after Eyre (2003).

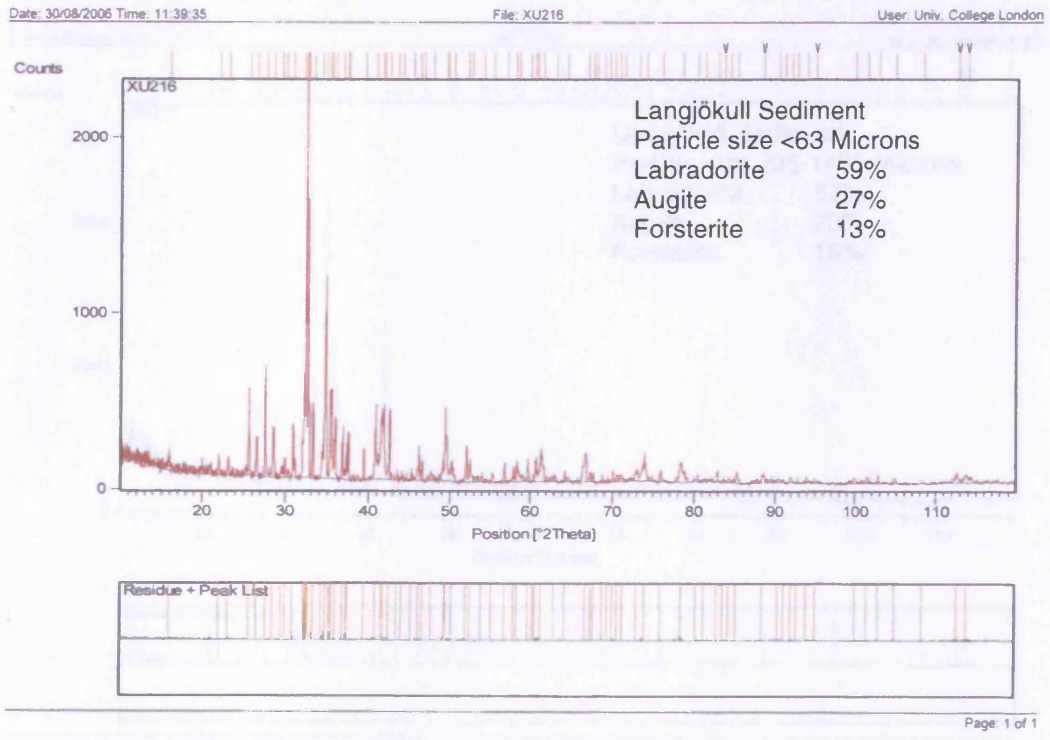

Figure(3-15): X-ray diffraction test results for particles smaller than 63 microns.

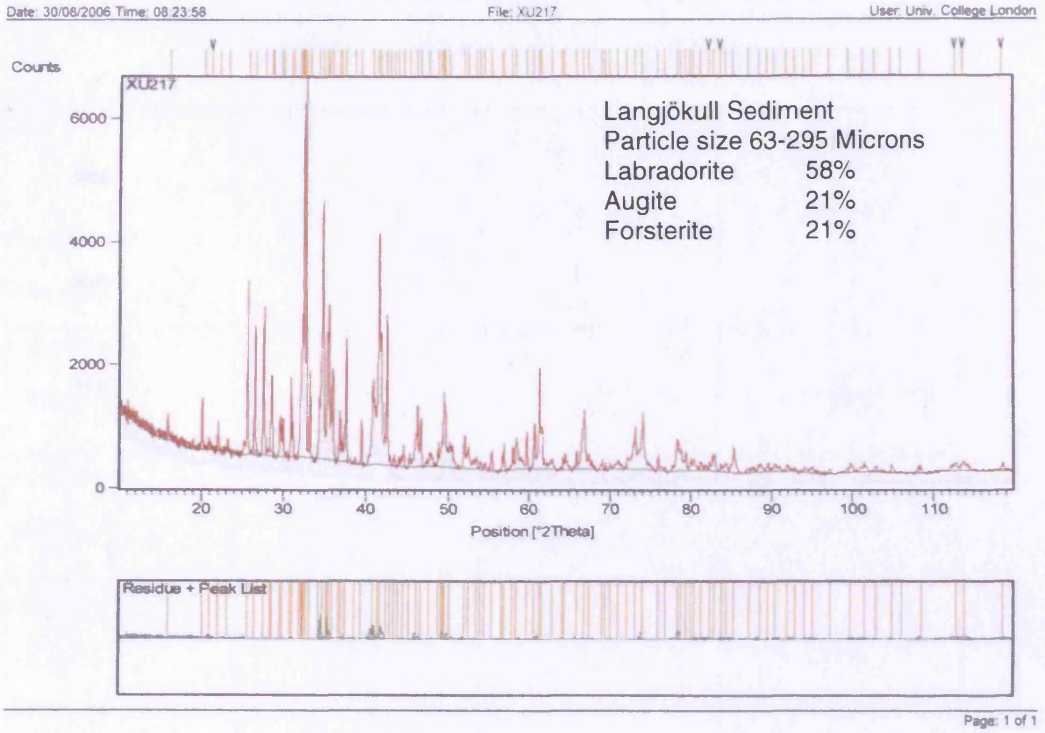

Figure (3-16): X-ray diffraction test results for particles between 63 and 295 microns

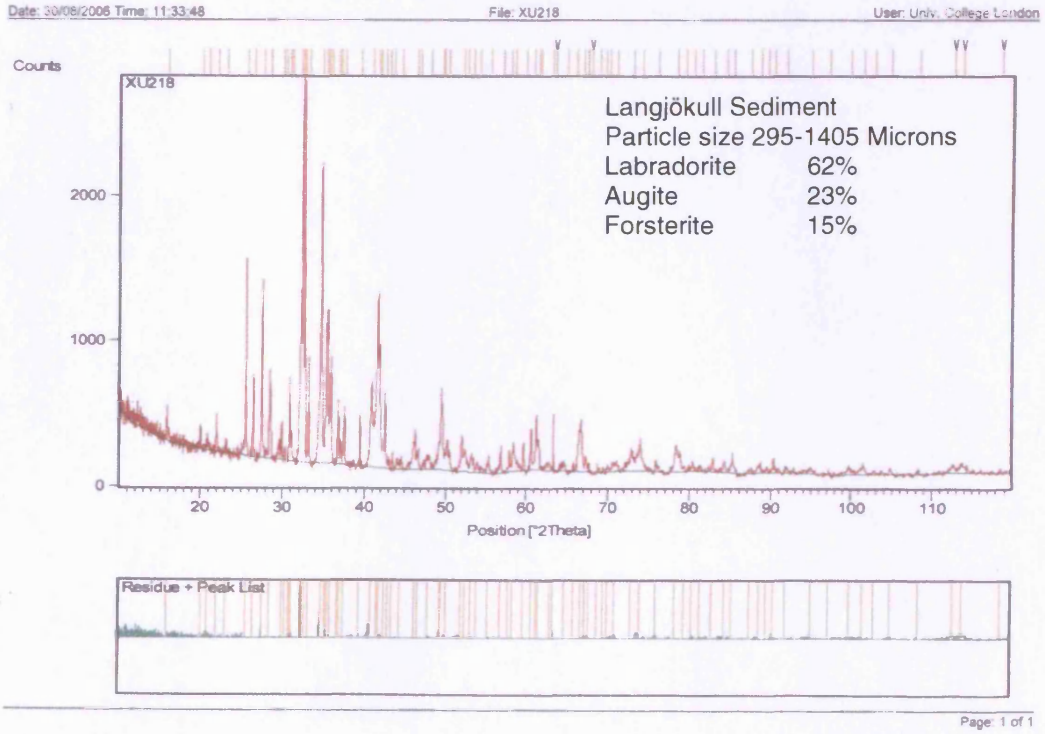

Figure (3-17): X-ray diffraction test results for particles between 295 and 1405 microns

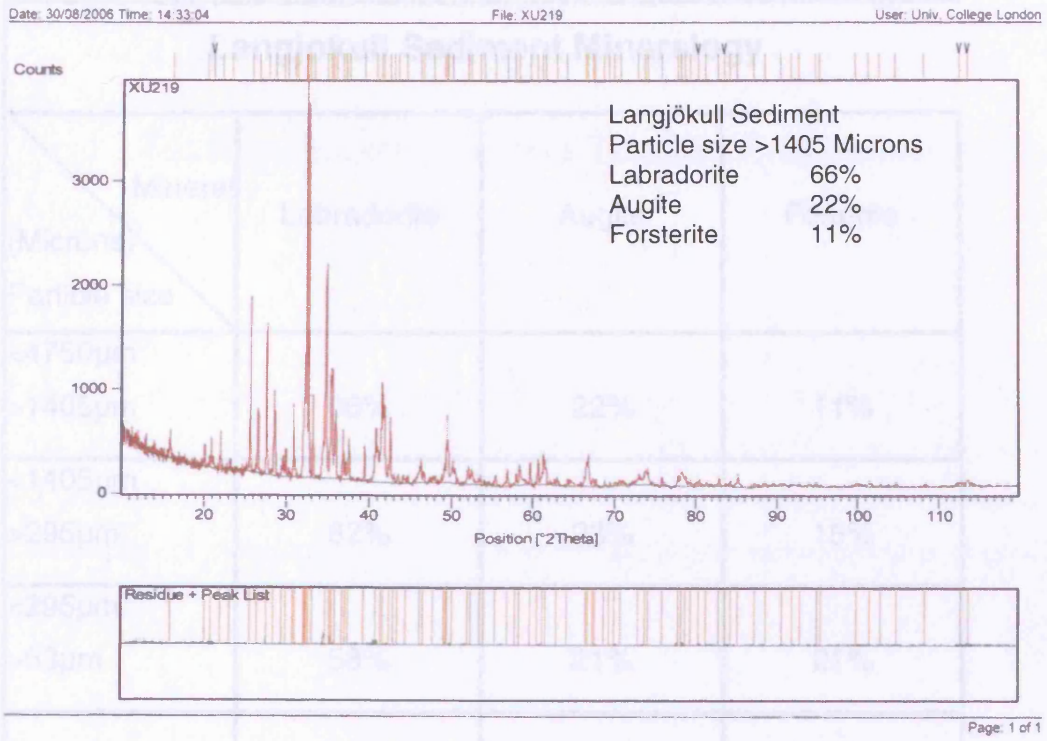

Figure (3-18): X-ray diffraction test results for particles larger than 1405 microns

Table (3-1): Summary of Langjökull sediment mineralogy test

Langjokull Sediment Mineralogy			
Mineral / (Microns) Particle size	Labradorite	Augite	Forterite
<4750µm >1405µm	66%	22%	11%
<1405µm >295µm	62%	23%	15%
<295µm >63µm	58%	21%	21%
<63µm	59%	27%	13%

Chapter Four

Testing Apparatus and Testing Procedure

4.1 Introduction

This chapter describes the experimental testing program in detail, and includes a full description of the laboratory soil testing equipment which has been used to characterise the mechanical behaviour of Langjökull subglacial sediment. A combination of standard and unconventional testing procedures were employed to investigate:

1. The Critical State of the sediment and the validity of the Critical State framework to describe its behaviour.
2. The crushability of the sediment's particles.
3. The rheology of the sediment.

To achieve these aims, a high pressure triaxial cell was used to investigate the compression and shearing behaviour of the sediment, as well as for monitoring the crushability of its particles. The so-called permeameter (high pressure triaxial system), which is traditionally intended for testing rocks, was used to investigate the compressibility of the sediment under very high isotropic compression pressures up to 250MPa. The effect of high shearing strains on the sediment's particle breakage was investigated using a Bishop-type ring shear apparatus. This apparatus was also used to monitor strain rate effects on the residual strength of the sediment. A fully computer controlled triaxial cell equipped with high accuracy local LVDTs (Linear Variable Differentials Transformers) to monitor small deformations in the sample was used to define the sediment's rheology, by studying the effect of shearing strain rate on the sediment behaviour during shearing. Finally, the oedometer apparatus was used for one-dimensional compression tests. The standard oedometer cell was used

along with a modified small cell to reach higher pressures (up to 20MPa) than those permitted by the standard apparatus. In this chapter, the above mentioned apparatuses are fully described, with full description of the testing procedure used for each apparatus.

4.2 Modified oedometer cell for one-dimensional compression

A standard oedometer loading frame and cell (BS:1377, 1990) was first used to investigate the sediment behaviour during one-dimensional compression. Due to the limited pressure range reached by the standard oedometer (≈1MPa for a 75mm diameter sample), the standard oedometer loading frame was used along with a special oedometer cell which was modified at UCL to enable application of higher stresses to the sample. The cell, which comprises of a 20mm diameter and 10mm height sample confining ring, is shown in Figure (4-1). Reducing the area of the sample enabled applying higher stresses up to 20MPa. Boundary effects were reduced by applying some grease on the interior surface of the ring to reduce friction. Two porous discs were used one at the bottom of the sample and one at the top to ensure two-way drainage during compression. Loading was carried out in a similar way to the standard consolidation test.

Remoulded samples were prepared by pouring a saturated sediment mixture (slurry) into the sample ring to achieve a high void ratio for the tested sample. The initial density of the sample was determined from the dry weight of the sediment poured in the ring and the interior sample ring volume. Undisturbed samples were prepared by trimming the frozen sediment to the ring size. The sample was weighed and the water content was determined from the material left from the trimming process. The sample volume was assumed to be equal to the interior volume of the sample ring. All tests were carried out with the oedometer ring containing the sample being submerged in water bath.

4.3 The use of triaxial cell to investigate the compression and shearing behaviour of the sediment

Triaxial tests were carried out using first a standard triaxial cell which was used for preliminary investigation of the sediment behaviour, then the high pressure triaxial cell (see sub-section 4.3.2) was used to reach pressures higher than those permitted by the standard cell. The sediment rheology was investigated using a fully computer controlled triaxial cell (see sub-section 4.3.3) equipped with local transducers for small sample deformation monitoring. These will be described in this section.

4.3.1 Standard Triaxial Cell

A standard basic soil triaxial cell (Figure 4-2), which takes a cylindrical sample with 38mm in diameter and 76mm in height, was used for preliminary triaxial shearing tests to define the sediment's behaviour up to its Critical State. The cell could be pressurised up to 1MPa of cell pressure by using compressed air through an air-water interface system. The main advantage of this cell was the ease of operation and the facility it provides in controlling drainage and applying back pressures to the sample while shearing. This is one of the features which favours the use of this cell on the use of other shearing apparatus available like the shear box apparatus, for simulating the undrained deformation of the sediment under glaciers. The system of this cell comprises of a 100ml Imperial College volume gauge which was used as an air-water interface for the cell pressure while a 50ml capacity gauge was used for the back pressure and for monitoring sample volume changes. Each of the volume gauges and the cell pressure interface was connected to the base of the cell through a valve and a transducer (Maywood instrument transducers, type p-102). A 1000psi (6895 kPa) pressure transducer was used to monitor the cell pressure while a 200psi (1379 kPa) maximum pressure transducer was used to monitor the pore water pressure. The cell was filled through the same channel used for drainage, with the top vent valve open.

The applied deviatoric force on the sample (see equation [1-4]b), was measured using a 3kN capacity internal submersible load cell, Wykenham Farrance type (STALC3). The shearing was applied by driving down the ram of the cell by means of the motorised frame. The ram passes through an opening in the top platen of the cell which also has an air release valve. The ram opening is lined with ball bearings to allow the ram to pass through with minimum friction.

The shearing rate could be specified prior to shearing by choosing the combination of gears of the loading frame driving motor. This process would only allow constant rate of shearing tests to be performed. The shearing load was applied by driving the ram downward against the sample's top cap. A ball bearing fitting was used between the loading frame and the ram to eliminate any misalignment effect. The shearing displacement was monitored using an exterior 25mm range LVDT (MPE Transducer type HS with spring return armature). All transducers, LVDT and volume gauges, were calibrated regularly (see section 4.3.5). The electrical signals from the transducers were fed into a SERVO conditioning unit and then were processed into a multiple precision data acquisition unit based on national instrument-data logging card, run by Lab View and acquisition software written by R. T. Cox in 1998.

4.3.2 High pressure triaxial cell

The high pressure triaxial apparatus (Figure 4-3), was used to apply higher pressures, up to 70MPa of confining pressure. This cell is available in the UCL Earth Sciences Laboratory (Mineral, Ice and Rock Physics (MIRP)). The cell (Wykeham Farrance 40030) is manufactured of high strength material to support a working pressure of 700 kg/cm^2, (10,000psi) with a ram diameter of 50.8mm. The cell which comprises of two interior compartments (Figure 4-4) uses silicone oil as its confining medium. The specially hardened steel ram is precision-ground and set in PTFE seals to minimise friction. The ram also has a special balancing arrangement whereby the ram is drilled to allow a connection between the main chamber and the second upper point so that the upthrust on the ram

from the pressurising fluid is balanced out. The unit is clamped together by means of eight stainless steel nuts which clamp the chamber to the base (sealing being effected by an "o" ring). With the sample placed in position and any drainage connection made up, oil can then be pumped into the chamber via the cell pressure channel which is connected to a hydraulic pump. Any air is removed via the de-airing coupling (port A) and the auxiliary position (port B), by slightly undoing the connections, one at a time until air free oil escape is obtained before closing them again. While shearing and as the piston moves down under load, air escapes from point E and oil is fed into the space behind the piston "collar", this all being part of the ram balancing system.

The cell pressure was controlled by a 50ml pressure intensifier cylinder and monitored by a 10,000 psi (68950 kPa) controller transducer (Maywood instrument type P102) with a resolution of 0.06 volts/MPa. Back pressure was controlled by another 50ml intensifier which was calibrated to monitor the sample volume change. The back pressure was applied at the base of the sample and monitored by a 10,000psi (68950 kPa) transducer (Maywood instrument type P102) with a resolution of 0.16 volts/MPa, which is located between two high pressure valves, for cell and intensifier isolation purposes. Both the cell pressure and back pressure were controlled by a feed back to the intensifier from the controller transducers. The transducers provide a pressure monitoring on which a displacement of the intensifier piston will be initiated accordingly to achieve the desirable pressure.

The shearing load was applied by the means of a mechanically operated Wykenham Farrance loading frame. The motorised gears controlled the upward (or downward) displacement of the loading platform, pushing up the cell against the loading frame. The motorised gears and the controller allow full control of shearing displacement rate. The loading frame supports the exterior heavy duty compression 25ton (250kN) capacity loadcell (Tedea series Model 100), which is placed on the top of the cell ram cap via a cylindrical stainless steel fitting with

inner- curved bases. A hemispherical fitting is attached to the loading frame to avoid any misalignment in loading. The recorded force by the exterior load cell would also include the resultant of the friction force generated by the driven ram through the cell opening, plus the force resulting from the applied pressure inside the cell which will be exerted on the base of the ram. This should be deducted from the total reading of the load cell to obtain the net deviatoric force. All transducers' signals, except for the local LVDTs, were fed into a SERVO conditioning unit and then were processed into a multiple precision data acquisition unit based on national instrument-data logging card, run by Lab View, and acquisition software written by R. T. Cox in 1998.

The back pressure system can be filled with water by using a Bishop's ram-type pump which can be isolated from the high pressure system by a valve (Figure 4-3 B). Both cell pressure and back pressure are controlled by an electro-hydraulic and electro –pneumatic closed loop SERVO with a SERVO controller system (type SEBL). The base of the cell has seven holes, one at the base of the sample pedestal for the back pressure system, a second connected to the cell pressure channels and the cell pressure intensifier. Three of these holes were used to pass through the local LVDTs and strain belt electrical connections. The sample cap was made of aluminium to avoid applying excessive load to the sample. The cylindrical shaped sample cap has a curved top to avoid misalignment of ram loading to the sample.

Shearing displacement was recorded by the means of an external LVDT (25mm range) (MPE Transducer LSC Type HS with spring return armature). In some tests, sample deformation was also monitored by the means of local LVDTs (two with range$\pm$ 7.5mm) (RPD type D5/300HK). Those were attached to the sample by using special aluminium mounts manufactured at UCL (see Figure 4-6). Electrical signals from the local LVDTs were fed into two inline amplifiers and were processed into a multiple precision data acquisition unit. Radial strain was

monitored by using a strain belt, which was designed for this purpose and used strain gauges (Figure 4-6 C).

4.3.3 Fully computer controlled triaxial cell

A computer controlled hydraulic triaxial testing system from the UCL Civil and Environmental Engineering department was used to investigate shearing rate effects on the sediment behaviour. This triaxial cell allows fully computer controlled stress paths to be carried out at controlled rate of strain or controlled rate of stress. The general set-up of the triaxial cell is shown schematically in Figure (4-5). This triaxial testing system was principally designed by the Geotechnical Engineering Research Centre at City University, with a few modifications made at UCL, which included the introduction of high resolution miniature local LVDTs to improve the accuracy of strain rate measurements in the small strain region.

The triaxial cell is similar in design to the original hydraulically operated stress path cell designed by Bishop & Wesley (1975). The cell consists of a water filled main chamber for applying a uniform radial confining pressure to the sample. The cylindrical sample is placed on a pedestal inside the cell and is separated from the cell water by a thin membrane. A hydraulically activated loading piston applies the axial force to the base of the sample, which in turn reacts against a submersible load cell fixed at the top. The cell accommodates a 38mm diameter sample fitted with local strain gauges. Sample drainage is permitted through the base pedestal only. For the measurement of pore water flow and for the purpose of saturation, the drainage line is connected to a combined volume gauge and back-pressure system. The drainage line from the base pedestal consists of short thin stiff tubing in order to minimize the compressibility of the drainage system, which could significantly influence the pore water pressure response.

The hydraulic pressure system in the triaxial cell consists of a constant air pressure source, computer controlled air pressure controllers and use of air-

water interfaces to achieve the regulation of the back-pressure, ram pressure and cell pressure. The main air pressure is supplied by a vane-compressor, which maintains a continuous pressure between 800 and 950kPa. Three air pressures controllers give three independent pressure sources used for the cell pressure, axial ram pressure and back-pressure. Each pressure controller is adjusted on an individual basis using feed back loops from the load cell and the pressure transducers connected to the cell water and the sample pore water respectively. The triaxial system uses accurate multi-stage pressure controllers attached to stepper motors, where each step of the motor corresponds to a change in pressure of about 0.4kPa.

The cell chamber was filled with water directly from the mains water supply. A 50ml Imperial College type volume gauge was used as drainage reservoir, which was also used as sealed air-water interface for regulating the pore/back-pressure. The piston movement was regulated using an accurate constant rate of strain pump, which is connected directly to the ram pressure line. The secondary displacement system consists of a Bishop's ram driven by a small stepper motor with a 1:25 reduction through a gear box. The stepper-motor is regulated by a so- called clicker box, which switches on and off at manually controllable intervals from 160 cycles/min to 10 cycles/min corresponding to axial displacement rates of 0.6mm/hr and 0.0375mm/hr respectively. However, bedding errors and the presence of dissolved air in the ram pressure line will influence the accuracy of the constant rate of straining displacement system.

For data acquisition and control of pressures in the triaxial system, a Spectra micro-ms measurement system was used in connection with a Pentium processor PC. The Spectra box (model SBL-11) was manufactured by Intercole System Ltd. and features 32+ input channels, internal instrumentation amplifier, auto calibration, auto ranging and programmable integration. A triaxial control software written in q-Basic^{TM} code and developed over several years by Mathew Coop (Imperial College) was used for the calibration and monitoring of

transducers, control of stress paths and recording of data. Special attention was paid to the voltage supply, amplification of output signals and earthing of cables. Since the LVDT output signal is proportional to the excitation voltage, it is highly beneficial to have as high as possible excitation with as little as possible fluctuation in order to increase the resolution. A single Farnell stabilised voltage supply (type L30) was used to excite all the transducers with 9.7 volts, which is close to the 10 volts capacity of the spectra box and transducers. The output signal of the 3kN submersible load cell (Wykenham Farrance type STALC3) was amplified before reaching the Spectra box for higher resolution purposes. The two external displacement transducers, axial displacement and volume gauge, were both of the RPD LDC type with built-in amplification.

4.3.4 Small strain local instrumentation

For an accurate measurement of strain, high resolution submersible miniature local Linear Variable Differential Transformers (LVDTs) were used to measure local strains in the sample (Figure 4-6 A, B). Those LVDTs were directly attached to the membrane surrounding the soil sample. Two axial miniature LVDTs were placed diametrically opposite on the sample to cancel out strain non-uniformities. For the LVDTs used in the high pressure cell, the same design was used with some modification to survive the high cell pressure. Holes in the LVDT body were made to ensure balanced pressure application inside and outside the LVDT body. The linear range for those local LVDTs used in the high pressure triaxial cell is 15mm, while 10mm linear range was used in the fully computer controlled triaxial cell which were a slightly modified version of the standard RDP D5/200W transducer (Sorensen, 2006).

A strain belt fitted with four strain gauges was used to monitor the radial strain of the sample in the high pressure triaxial cell (Figure 4-6 C), while a third miniature LVDT was incorporated into a radial strain belt attached around the centre of the sample in the computer controlled cell to be able to determine

shear strains and volumetric changes at very small strains for comparison with the pore water flow.

The transducer body of each local axial LVDT was mounted onto the top part of the sample by gluing the mounts directly onto the membrane, while the unguided armature extended downwards and rested on a flat surface mount glued onto the lower part of the sample. The floating type set-up has been described by Cuccovillo and Coop (1997). These local LVDTs have very high resolution allowing measurement of strain in the order of 10^{-4}% depending on the set-up.

4.3.5 Calibration of instrumentations

Calibration of all the test instrumentations was done regularly to ensure accurate data feeding. A Budenburg calibration kit was used to calibrate all pressure transducers, as well as calibrating some of those against each other's reading. Exterior LVDTs were calibrated by using a micrometer with a resolution of 0.01mm for higher accuracy travel distance. The calibration of the local LVDTs was done by re-zeroing the LVDT while the armature was out of the LVDT body to ensure using maximum range of the LVDT, before the calibration. All strain transducers were calibrated over their full working range.

Calibration of the Imperial College type volume gauges was carried out by the volumetric flow from a manually operated Bishop ram, which in turn had been calibrated against a burette with a resolution of 0.02ml. For the high pressure triaxial cell, volume change of the sample was done by monitoring the change in the intensifier piston displacement. This was achieved by recording the change of voltage signal when the piston was fully forward (empty intensifier cylinder) and when the piston was fully back (full intensifier cylinder). The total volume of the intensifier cylinder was measured with a 50 ml cylinder, and assuming a linear range over the full volume of the intensifier.

For the standard triaxial cells, the load cells were calibrated using dead weights over their initial linear range up to a load of 0.5kN, while the exterior load cell for the high pressure cell was calibrated on its full range of loading by using a proving ring and the same loading frame as shown in Figure (4-7).

4.3.6 Sample preparation for the triaxial cell tests

Remoulded as well as undisturbed samples were tested in the triaxial apparatus. The remoulded samples were made with variable void ratios. Local LVDTs were used to monitor small strains during the tests conducted in the fully computer controlled cell and some tests which were carried out in the high pressure triaxial cell. In this section, the methods of sample preparation for the samples which were tested in the triaxial apparatus are presented. This includes preparation procedures for both undisturbed (intact) samples, and remoulded (reconstituted) samples.

(a) Undisturbed samples

The undisturbed block samples were kept frozen until the time of testing. Each block was cut into small cubes with suitable dimensions for easier trimming to the size of the triaxial test samples. The tested samples had to be trimmed to 38mm diameter and 76mm height cylindrical specimens. The trimming of the undisturbed samples was carried out on frozen sediment as it was almost impossible to do this if the sediment was left to thaw first. Trimming took place in a cold room (-20°C) with the help of a trimming frame which was used to hold the small block of sediment. Cheese wire and hacked back saw were used for trimming with the help of the heating gun which was used to apply some heat to the sample surface before using the cheese wire and the saw to shave the surface of the sample (Figure 4-8). The trimming procedure was very difficult due to the presence of moderate size particles in the sediment. The cheese wire would often snap or pull the particle out causing some disturbance to the sediment fabric, defeating the undisturbed nature of the sample. The sample

was then cut to the right height. Measurements of the sample were taken using callipers (to the nearest 0.01mm). The diameter was measured at the top, middle and bottom of the sample, with the average value being used in the calculations. Some of the trimming material was used for water content determination. The trimming was placed in a 100°C oven for 24hrs, with its weight being recorded before and after drying.

Before the test, a latex membrane (thickness= 0.3mm), in the case of standard triaxial test, or a relatively thick rubber jacket in the case of high pressure triaxial test (thickness= 0.5mm), was used to isolate the sample from the cell fluid. Some back pressure was applied in the back pressure channels with the back pressure valve to the sample open, to ensure the saturation of the channels before installing the sample. A saturated porous disk was put on the pedestal before placing the sample. Two o-rings on the sample cap and the sample pedestal were used to guarantee the sample isolation. The local LVDTs' mounts were then glued (using superglue) to the sample membrane, before closing and filling the cell wit the confining fluid.

(b) Remoulded samples

The remoulded samples were prepared using the material left from trimming the undisturbed samples. Particles with a size larger than 4.75mm were first removed from the sediment. For those samples which were intended for particle breakage monitoring, dry sieving was carried out before and after testing to record the change in particle size distribution of the sample.

All remoulded samples (except the loose sample), were prepared by adding water to the dry sediment to achieve the desirable water content (about 10%). The weight of the sediment was calculated to achieve the desirable void ratio of the sample. The sediment was then statically compacted in three layers in a mould made to measure (Figure 4-9). The sample was then removed from the mould, which can be opened vertically for an easier handling to the sample, and weighed. Although care was taken to control the void ratio of the sample during

preparation, by calculating the exact weight needed for each layer, and compacting the layer to a pre-calculated thickness, some disturbance could not avoided while placing the sample rubber jacket, resulting in some reduction in void ratio of the sample. Sample measurements were then taken using callipers in the same way the undisturbed sample measurements were taken. Placing the membrane and attaching the LVDTs mount was done in the same way as described for the undisturbed samples.

A different method was used to prepare one remoulded sample which was supposed to be prepared in a very loose state. The sample was prepared by the sedimentation method. In this method, a mould which can be opened vertically and has a tube connection at the side was used (as shown in Figure 4-10). The mould was placed directly on the sample pedestal of the triaxial cell with the sample rubber jacket fitted inside the mould to the sample pedestal by a two o-rings. Two (Jubilee Ring) ties were used to secure the two parts of the mould together, after applying some sealant grease between the jacket and the base of the mould. A vacuum was then used to suck the air between the mould and the jacket before using the back pressure system to half fill the jacket and the mould with some water. An accurately known amount of dry soil, which had already been mixed with water and left under vacuum, to ensure full saturation of the sediment, was then gradually lowered into the half filled mould by using a small spoon. Care was taken not to apply unnecessary pressure to the sample while the sediment was placed into the mould to achieve the maximum void ratio for the prepared sample. When the mould was full with the saturated sediment, the sample cap was placed on the sample and fitted to the sample jacket by using 38mm o-rings. At this stage, the mould was be kept in its position, surrounding the sample. A small negative back pressure was then applied to support the sample, before the mould was finally removed. Sample dimensions were then measured. The amount of sediment which was left from the total prepared sediment was dried and the exact weight used for the sample determined for

initial void ratio calculation. A schematic figure showing the general set-up to prepare a sample using this method is shown in Figure (4-10).

The sample prepared by the sedimentation method was found to be with a void ratio of about 0.49, which was lower than some samples which were prepared by the general compaction method described previously. This might be due to the small negative back pressure applied to the sample during preparation, which resulted in some reduction in sample volume, taking into consideration the high packing ability of this sediment due to its well graded nature.

Another draw back for this method of sample preparation was the particle segregation during lowering the sediment in the half water filled mould. Again, this method proved unsuitable to prepare very loose samples for this kind of sediment, being a well graded sediment. Only one sample was prepared by this method for this study.

4.3.7 Triaxial tests testing procedure

Tests using the triaxial apparatus were done according to the British Standards (BS 1377: Part 2: 1990) for soil testing. Isotropic compression tests and shearing tests were conducted on the sediment under variable effective pressures. The test procedure usually included the saturation stage, consolidation stage, and finally the shearing stage, for those tests which were intended for shearing.

4.3.7.1 Testing procedure by standard and high pressure triaxial cells

Tests using both the standard triaxial cell and high pressure triaxial cell were carried out following a similar procedure due to the lack of computer control. The sample was placed on the pedestal for testing after ensuring full saturation of the back pressure channels. A saturated porous disk was placed between the pedestal and the sample to ensure uniform distribution of back pressure water on the sample cross sectional area, as well as preventing any blockage of the

channels with the sediment particles. A membrane in the case of standard testing, or a rubber jacket in the case of high pressure testing, with two o-rings at the top and bottom of the sample were used to isolate the sample from the surrounding cell fluid. The local strain transducers were then fitted to the sample when used. The distance between the mounts was measured centre to centre.

The cell was then closed and filled with water in the case of the standard cell or silicone oil, in the case of the high pressure triaxial cell. The saturation stage followed. Stages of cell pressure increments were applied to the sample while the sample was isolated from the back pressure system, the change in pore water pressure was monitored and the B value was calculated from the equation (Skempton, 1954):

$$B = \frac{\text{Cell pressure increment}}{\text{Change in pore pressure}} \quad \text{.....[4-1]}$$

The saturation process was ended when a B value of 0.97 or higher was achieved. When a lower value of B was obtained, a back pressure, slightly lower than the cell pressure, was applied to the sample. The difference between cell pressure and back pressure in the case of standard test was chosen to be 10kPa, and 100kPa in the case of high pressure triaxial. The valve of the back pressure to the sample was closed and another stage of cell pressure increment was applied when the water flow from the volume gauge to the sample faded.

The consolidation stage followed. It was done by increasing the cell pressure by the specified consolidation pressure, with pore water flow prohibited. When the pore water pressure had fully developed, the valve to the volume gauge was opened and the pore water flow was permitted. The consolidation stage would be considered to be completed when the volume gauge reading stabilised.

Usually, multiple consolidation stages were conducted when a high pressure test was carried out. This was done by repetition of the same procedure described above by increasing the cell pressure gradually until the desired cell pressure for shearing was reached. Consolidation at each cell pressure increment was done. Sometimes, the sample was left overnight for creep monitoring, before starting the shearing stage.

The shearing stage was either drained with the pore water flow permitted to the volume gauge, or undrained with the valve to the back pressure system closed and no pore water flow permitted. The shearing was carried out with a shearing displacement rate of 0.05mm/min for the undrained tests, and 0.0167mm/min for drained tests to avoid pore water pressure development during the drained tests.

The sample was retrieved with the back pressure valve closed to maintain the final water content of the sample. The sample total weight was recorded before it was left in the oven until a constant weight was reached. The final water content was then determined. The final void ratio was calculated assuming a fully saturated sample at the end of the test from the equation:

$$e_f = w\, G_s \qquad \text{.....[4-2]}$$

where:

e_f the sample final void ratio.

w water content of the sample.

G_s specific gravity of the sediment, (measured as 3.107, see Section 4.5.1).

The value of the determined final void ratio was compared with the calculated one, which is based on initial sample weight, dimensions and water content. A backward calculation was done to determine the initial void ratio of the sample.

The dry weight of the sample was also used, when available, to double check the initial void ratio of the sample (detailed equations are given in Chapter 5).

4.3.7.2 Testing procedure by fully computer controlled triaxial cell

The testing procedure in the fully computer controlled triaxial cell slightly differed from that followed in the standard and high pressure cells. The availability of complete computer control allowed a continuous increase in both radial pressure and back pressure, with a specified rate and specified difference between the radial and back pressure value during saturation stage.

After ensuring sample saturation by achieving a B value of 0.97 or higher, a suction cap was connected before the consolidation stage was commenced. The suction cap was connected while the back pressure was on. With the Bishop's ram connected to the suction cap channel, the ram pressure (the pressure in the chamber under the sample pedestal) was gradually increased until it was equal to the cell pressure. The sample would then move upward until the sample cap touched the load cell. The water trapped between the suction cap and the load cell was gradually removed by turning the wheel of the Bishop's ram. This stage was done carefully to avoid applying any axial stress to the sample. When the suction cap was fully connected, the sample's upward movement stopped. The Bishop's ram was disconnected while the suction valve channel was left open to atmosphere.

The consolidation stage took place afterwards, by continuously increasing the radial pressure, rather than in multiple stage increments as in the tests conducted in the standard and high pressure cells. The pore pressure was held constant during consolidation with the pore water flow to the volume gauge permitted, while an increase in radial pressure and ram pressure was applied by the same rate and value.

The shearing stage followed. This was done by increasing the ram pressure by the means of the clicker box which enables changes in the shearing rate during testing. After test termination, the suction cap was disconnected. This was done by connecting the Bishop's ram to the suction cap channel. The deviatoric stress (q') value was then gradually lowered to zero. Water was pumped in stages by the means of Bishop's ram while the ram pressure was decreased gradually. When the cell pressure became higher than the ram pressure and the suction cap was fully disconnected, the sample pedestal would move downward. The ram pressure chamber valve was turned off before the cell pressure was released. This process was done with the pore water flow prevented to maintain the final water content of the sample for final void ratio calculation. Sample retrieval and determination of water content and void ratio was done in the same way as in the tests conducted by standard and high pressure cells.

The axial local strain gauges were fitted by gluing the mounts to the sample on the middle third of the sample. This was done after zeroing their reading with the armature out to ensure full use of their linear range. They were positioned so that their reading is close to zero. The process of zeroing the local strain gauges was carried out again before the shearing stage commencement. This ensured the use of the local strains maximum resolution for the small strains region measurement.

4.4 Ring shear apparatus

Ring shear tests were conducted using the Imperial College ring shear apparatus also known as the Bishop-type ring shear apparatus. The Bishop ring shear apparatus was designed by A.W.Bishop, Imperial College to accommodate for the measurements of residual strength of clayey material. The design and principles of operation of the ring shear apparatus are described in detail by Bishop et al. (1971).

The ring shear device, shown in Figure (4-11), was used to study the crushability of Langjökull glacier sediment deformed to high strain levels. The device shears a remoulded confined sediment specimen between horizontal parallel rough platens, with built in porous stones to provide drainage. The specimen, about 22mm in thickness, occupies a chamber that consists of two metal rings, an outside ring with a radius of 76.2mm, and an interior ring with a radius of 50.8mm. The specimen chamber is placed in a water reservoir to ensure saturation of the sample during the test. This reservoir is open to the atmospheric pressure which makes these tests "drained", in the vernacular of geotechnical testing.

The specimens were sheared by rotating the platen in contact with the base of the specimen at a controlled rate with a variable-speed electric motor and gear boxes. The upper platen that grips the top of the specimen is kept from rotating by two diametrically positioned roller platens that extend from the perimeter of the plate and press on load cells. These load cells measure the resistance to shearing. An adjustable counterweight balances the weight of the lever arm, main shaft and torque arm. The lower walls adjacent to the specimen move with the rotating base; the upper walls are fixed and held by an independent assembly called the yoke. The adjusting screw at the top of the yoke either lifts the upper walls above the lower walls by a fraction of a millimetre forming a gap, or presses the upper walls against the lower walls. A proving ring with strain gauge was mounted in the axis of the yoke to record the vertical frictional force on the upper walls that arises due to shearing. A uniform stress normal to the shearing direction was applied by the base of the torque arm, which was loaded with dead weights hung on a lever arm. Two LVDT transducers were placed in a vertical position in contact with the normal load platen to monitor the change in sample height during testing.

4.4.1 Testing procedure in the Bishop-type ring shear apparatus

Before each test, lower porous disc and lower and upper confining rings were assembled on the base platen, and the confining rings were fixed in place with locking screws.

After the sieving stage, the sediment was placed in the ring shear apparatus after water was added to it to form a uniform mixture similar to a paste. Care was taken not to add excessive water to the sample at this stage to avoid segregation of the particles while placed in the chamber. The sediment was then levelled to a uniform thickness of about 22mm and the top platen was carefully placed to the rest on top of the sample. Measurements (using a Vernier scale) of the relative position of the top platen to the upper confining rings made it possible to determine the initial sample height with the load from the top platen (equivalent to a normal stress of 1.2kPa). The torque arm was subsequently placed in position and fixed to the main shaft. The water reservoir was then filled with distilled water before applying the normal pressure. The main shaft and lever arm were balanced by the counterweight.

The weight of the dry sediment used for each sample was calculated accurately to give a good estimation of the sample's initial density. All samples were left overnight after applying the normal pressure and before starting the shearing stage. Shearing velocity was controlled by the gear box system, and shearing displacements were measured by using the angular displacement scale. Variable shearing displacement rates were used in one of the ring shear tests to investigate the viscous behaviour of the sediment, while the rest of the tests were carried out by using a constant shearing rate equal to 0.89mm/min.

Generally, the gap was kept closed during the tests to avoid excessive soil loss, with some intervals when the gap is opened to get a measurement of the torque. As the test preceded, the lateral torque forces, recorded by the lateral load cells, would experience some distort. This was adjusted by using the adjusting nuts at

the back of each load cell so that the output readings of the load cells measuring the torque forces are as close as possible to each other.

After the termination of each test, the sample was unloaded and left for about 12hrs before it was retrieved from the apparatus. Following previous studies finding that particle breakage is more concentrated in the middle zone of the sample (Sorensen, 2001; Georgoutsos, 2002; Coop et al., 2004), a scooping device was used to retrieve the sample into three zones. The top layer, defined as zone 1, was scooped out with a brass device reaching down to a depth 2.5mm above the confining ring split. The middle zone, which extends to 2.5mm below the split, was divided into two sub-layers depending on their location relative to the split. Finally the bottom layer, defined as zone 3, was scooped out and after removing the whole base and transferring it to the sink, the remainder of the soil was retrieved by washing it out using a wash bottle. The soil from each zone was retained in appropriate beakers, before oven drying to determine the retrieved dry mass of each zone. Wet sieving of the retrieved sample was carried out to examine evidence of particle breakage. The interval of gap opening during tests, which is used to record the actual shearing resistance of the sediment, may have resulted in a loss of some sediment particles through the gap. This lost sediment was also retrieved for weight comparison purpose.

4.5 High pressure permeameter (high pressure isotropic pressure system)

Very high isotropic pressures were applied to the sediment by using the so-called permeameter. The permeameter (Figure 4-12) comprises of a pressure chamber which is manufactured of high strength materials to support very high working pressures up to 300MPa. The cell uses silicone oil as its confining medium. The cell takes a sample holding frame and caps for samples with similar dimensions to those for the triaxial cell.

The sample is held in a stainless steel frame which holds the upper cap to the lower cap by two stainless steel bars and nuts (Figure 4-14). Two rubber jackets

with four o-rings (two at each side of the sample), are used to isolate the sample from the confining fluid. The distribution of the back pressure is achieved by using a metal disc with uniformly distributed small holes and channels. A relatively thick porous fibre disc (thickness around 1mm) is also used between the metallic disc and the sample to prevent any blockage of the metal disc holes. After placing the sample between the two stainless steel caps, and tying up the frame nuts, the sample frame with the fitted sample was lowered inside the pressure chamber which is securely sealed by the o-ring and the breech nut. Back pressure connections are fitted to the sample holder.

Back pressure can be applied to the sample via the sample caps (in this research back pressure was applied via the upper cap only) which are connected to two channels of back pressure system. All pipes and connections of back pressure system were manufactured from stainless steel pipes which can support the designed working pressure. Back pressure can be applied to the top of the sample using a computer controlled intensifier (50ml) and a valve. A controller transducer (maximum pressure 10,000psi (68950kPa), Maywood instruments transducer type p-102) was used to supply a feed back reading, the intensifier piston would then move accordingly to achieve the desired pressure. A second transducer was used on the same line, between the sample and the back pressure controlling valve to enable pore water pressure monitoring while sample isolation. The volume change of the sample was monitored by measuring the displacement of the piston of the back pressure intensifier which was calibrated for this purpose in the same way as it was calibrated in the high pressure triaxial cell. The intensifier cylinder can be re-filled with water via a special priming pump used for this purpose, which is isolated by a valve from the high pressure system.

The cell pressure is applied by using a controlled electrical powered 3kbar (300,000kPa) pump. The cell pressure is monitored in two ways, by a pressure gauge (resolution 100bar/div), as shown in Figure (4-13), with a resolution of

10MPa per division, and by an inline controller transducer (Intersonde Transducer type XR17) with maximum pressure 3000bar (300MPa), which logs the data to the computer. The desired cell pressure is achieved by a feed back reading from the controller transducer which is sent to the pump controller. The pump will initiate pumping the fluid until the desirable pressure is achieved. This system ensures developing higher pressures but does not enable lowering the cell pressure afterwards. To release the cell pressure at the end of the test, the pump needs to be switched off.

All transducers were fed into a servo conditioning unit and then were processed into a multiple precision data acquisition unit based on national instrument-data logging card, run by Lab View and acquisition software written by R. T. Cox in 1998.

4.5.1 Test procedure in the permeameter

All samples used in the permeameter were remoulded specimens. The cylindrical samples which had similar dimensions to those used in the triaxial cell, were prepared in the same way described in section (4.2.6 part B). Sample dimensions, weight and moisture content were determined in the usual way.

Two rubber jackets were usually used to avoid any leakage through the jacket. The sample was placed on the lower cap and two or more o-rings were placed after applying some thread sealant material to improve the sealing properties between the jacket and the cap. This was done with both sample caps. To avoid applying any excess load to the sample via the weight of its caps, the sample was fitted to the upper cap in a hanging position (see Figure 4-15) and the nuts of the sample frame bars were tightened up. The back pressure channel via the sample upper cap was filled with water to ensure less air in the channels during the saturation stage. This helps avoid long saturation time for the sample. The sample with its frame was lowered to the cell and the cell securely sealed by an o-ring and a breach nut. The back pressure channel connection was made after

applying a very small back pressure to ensure better air release from the channels.

The cell was then filled by specifying some pressure in the pump controller. At this stage the valve to the intensifier was kept closed. From experience, it has been found that the sensitivity of the cell pressure pump controller is about 5-8MPa, so the smallest initial pressure which should be applied should be within this range. Both saturation and compression stage were done in a similar way to those done in the high pressure triaxial cell, with the only difference that the cell pressure could not be reduced and could only be released at the end of the test before retrieving the sample. The sample final water content was determined and samples to be examined by the SEM were obtained after the sample was dried.

4.6 Additional Tests

To determine the sediment physical properties some tests were carried out. These tests are: specific gravity test, particle size distribution by both sedimentation and sieve analysis, X-ray diffraction test and scanning electron microscopy (SEM) tests. These tests will be described in the following sections.

4.6. 1 Specific gravity (particle density) test

The test to determine the specific gravity of the sediment was carried out according to the British Standards (BS1377: part 2: 1990). Soil passing a mesh size 4.750 mm was used in this test. The value used as specific gravity of the sediment was taken as the average value of three individual tests. The test was carried out in a temperature controlled room with temperature $20\pm0.5C^{\circ}$. The weight of a 50 ml clean stoppered bottle (Pycnometer) was recorded, it was then then filled with distilled water and left for four hours before placing its stopper and weighing again (W_a). Care was taken to wipe the pycnometer outside surface from any spillage of water before weighing. The temperature of its content was recorded.

The oven dried sediment sample (at last 10gm of weight) was placed in the pycnometer and the weight of the sample was determined to the nearest 0.001gm (W_o). The pycnometer was then half filled with distilled water and its contents subjected to vacuum for no less than two hours until no air bubbles were seen to be escaping the distilled water covered sample. At this stage more distilled water was added to fill the pycnometer. The pycnometer was left in the temperature controlled room for four hours before placing its stopper and weighing it with its content (W_b).

The specific gravity of the sediment was determined as follow:

$$\text{Specific Gravity} = W_o/(W_o + W_a - W_b) \quad \text{.....[4-3]}$$

Where:

W_o is the mass in grams of sample of oven dry soil

W_a the mass in grams of pycnometer filled with water.

W_b the mass in grams of pycnometer filled with water and soil.

The average of three values found for Langjökull sediment was 3.107.

4.6.2 Particle size distribution of Langjökull sediment

The particle size distribution for the natural sediment was determined by carrying out a sieving analysis for particles larger than 63μm while a sedimentation test was carried out to determine the particle size distribution for those particles smaller than 63 microns. Sieving was also used to monitor particle breakage.

4.6.2.1 Sieve analysis

The mesh sizes used for the sieve analysis were:

4750, 1405, 853, 599, 500, 420, 353, 295, 250, 180, 106, 90, 75 and 63 microns.

Dry sieving was carried out using a mechanical shaker which was used for twenty minutes over two sets of sieves for each analysis. Care was taken to break any bonding between sediment particles by crushing any aggregated particle by hand before the sieving stage.

Sometimes, wet sieving was used. This was done using the same set of sieves under tap water. A brush was used to disaggregate the particles of the sediment while washing on the mesh till clear water through the mesh is obtained. The sediment over each mesh was then dried in the oven with 105C° before the dry weight of sediment was determined for the sieve analysis. Consistent results were obtained from both wet and dry sieving indicating the validity of both methods with the tested sediment.

4.6.2.2 Sedimentation test

The sedimentation test for particles passing the mesh 63 microns was carried out by using the hydrometer method which was calibrated according to the British Standard (BS 1377: Part2: 1990). Sample preparation was carried out according to the British Standard (BS 1377: Part 1: 1990). A specimen of 50 gm of Langjökull soil passing 63μm was used with sodium hexametaphosphate solution, which acted as a dispersion agent for the sedimentation test.

4.6.3 Scanning electron microscopy (SEM) sample preparation

SEM monitoring samples were prepared from the dry samples. A reasonable size of sediment was cut from the sample, taking care not to affect or change the sample fabric. The sample was glued by quick hardening epoxy to a 10mm diameter stub which was then placed on the SEM stage. Liquid silver paint was applied to the sample edges, at the contact line between the sample and the stud. The sample was then gold-coated before being ready to be examined. All samples were examined by the SEM under high vacuum unless stated otherwise.

4.6.4 X- ray diffractometer

A Langjökull sediment mineralogy test was carried out using the X-ray diffractometer available in the UCL Earth Sciences department (Figure 4-16). X-ray diffraction is one of the most important characterization tools used in solid state chemistry ad materials science. X-rays are electromagnetic radiations of wavelength about 1 Å (10-10 m), which is about the same size as an atom. They occur in that portion of the electromagnetic spectrum between gamma-rays and the ultraviolet. Each crystalline solid has its unique characteristic X-ray powder pattern which may be used as a "fingerprint" for its identification. During an X-ray diffraction analysis, X-ray beams are reflected off the parallel atomic layers within a mineral over a range of diffraction angles (Figure 4-17). Because the X-ray beam has a specific wavelength, for any given 'd-spacing' (distance between adjacent atomic planes) there are only specific angles at which the exiting rays will be 'in phase' and therefore, will be picked up by the detector producing a peak on the 'diffractogram'. Just like a 'fingerprint', every mineral has its own distinct set of diffraction peaks that can be used to identify it.

When the incident beam strikes a powder sample, diffraction occurs in every possible orientation of 2theta (Figure 4-17). The diffracted beam may be detected by using a moveable detector such as a Geiger counter, which is connected to a chart recorder.

A Langjökull sediment sample was prepared to be tested by the X-ray diffractometer according to its particle size: fine particles, passing the sieve size 63 micron; particles of size between 295-63 micron; particles of size between 1405-295 micron and particles larger than 1405 micron. Each sample was prepared by grinding the particles into powder before it was examined in the X-ray diffractometer.

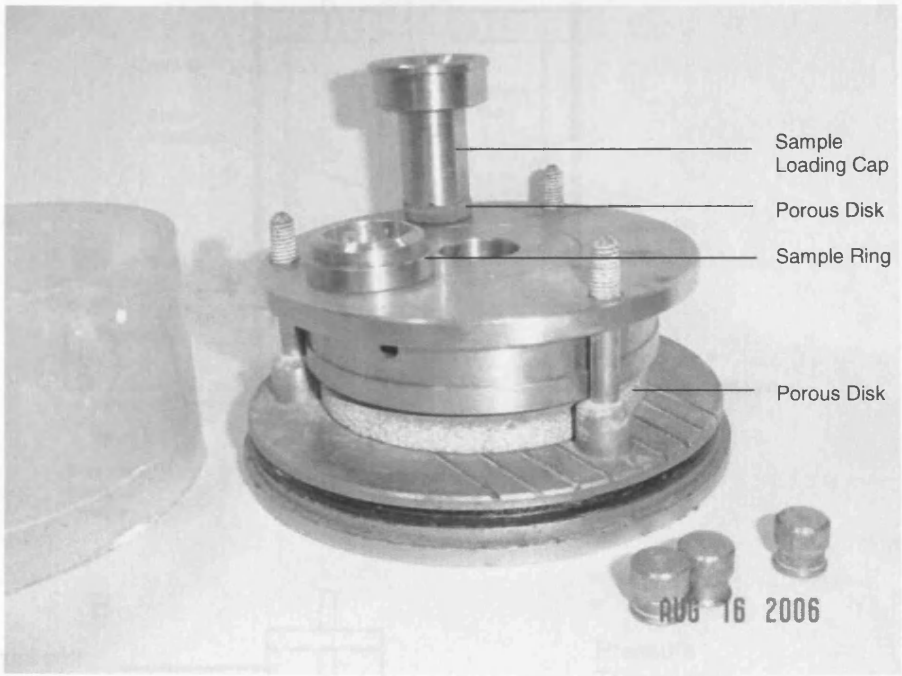

Figure (4-1): Modified oedometer cell, used for one-dimensional compression tests to 20Mpa.

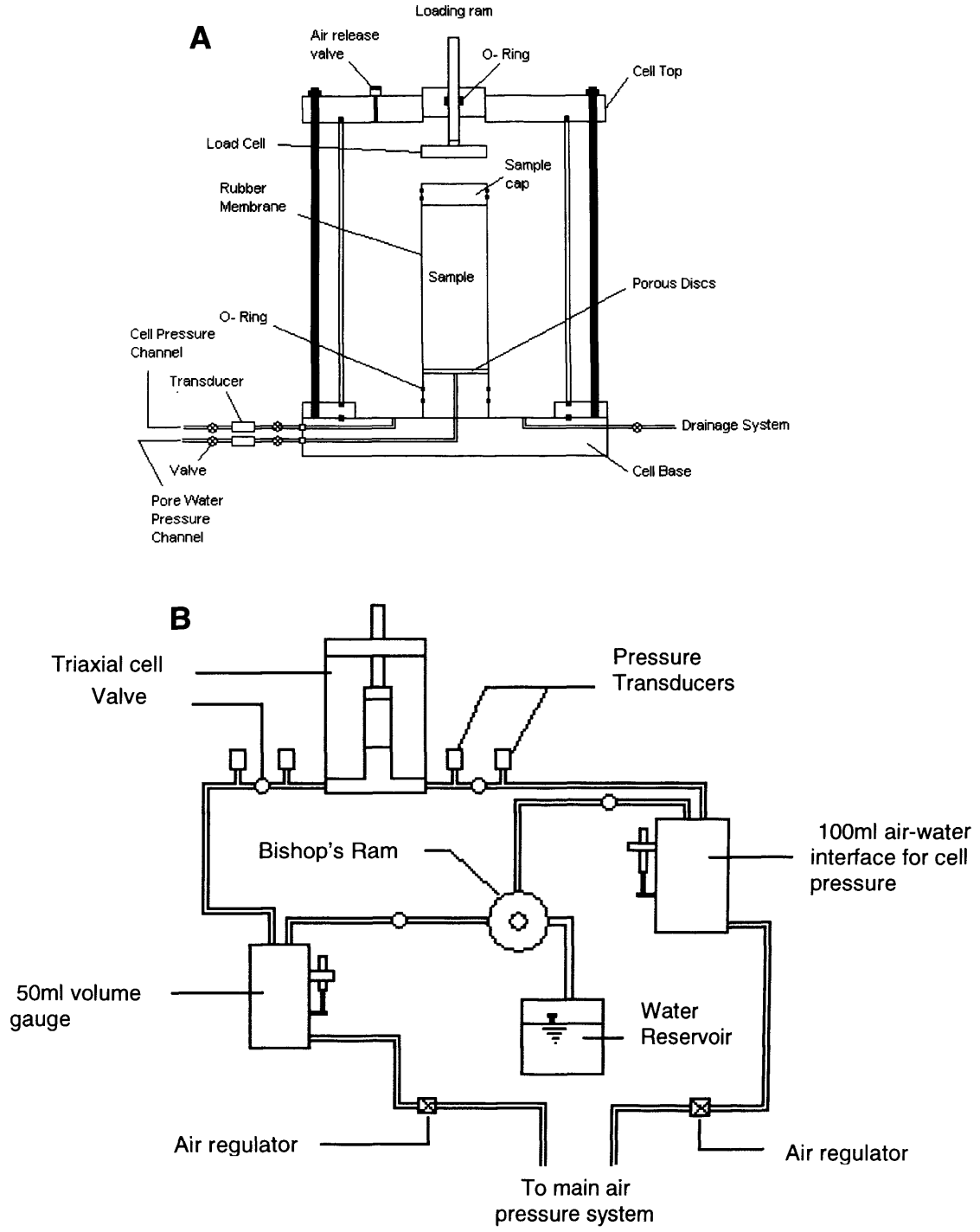

Figure (4-2): A-Schematic figure showing the standard triaxial cell.

B- Standard triaxial cell set-up.

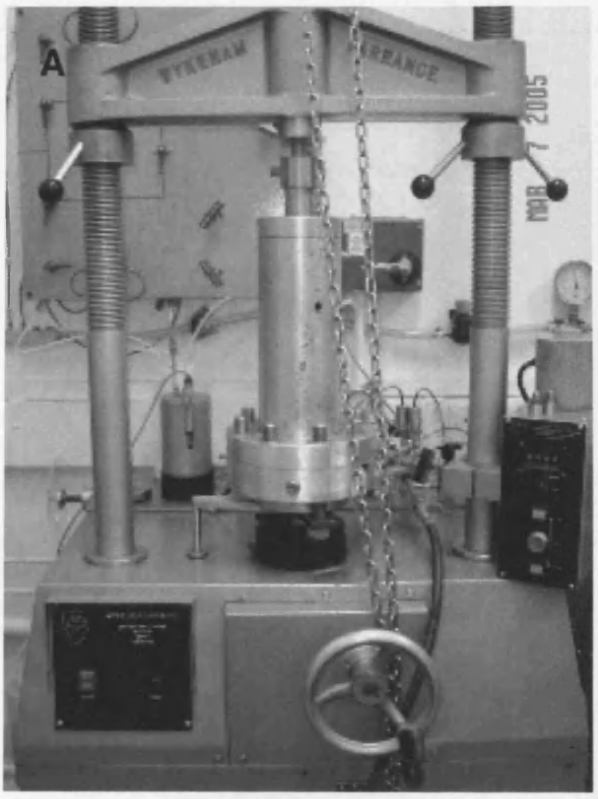

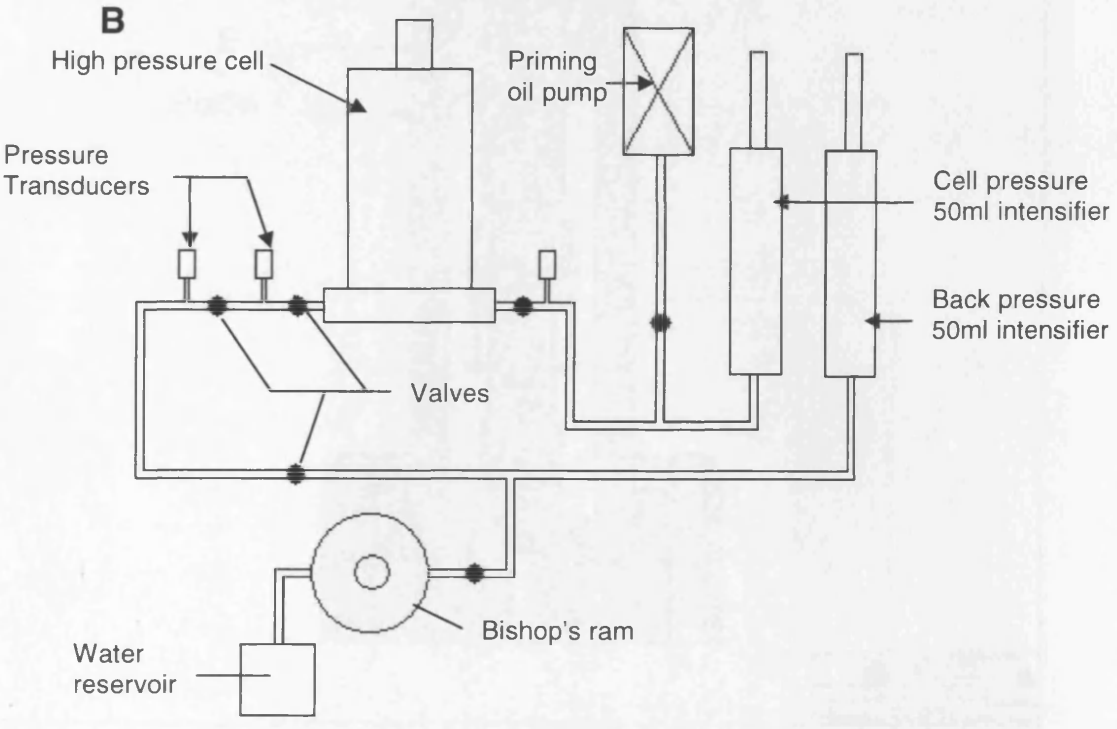

Figure (4-3): A- High pressure triaxial cell with its loading frame

B- Schematic diagram showing the HP cell plumbing work.

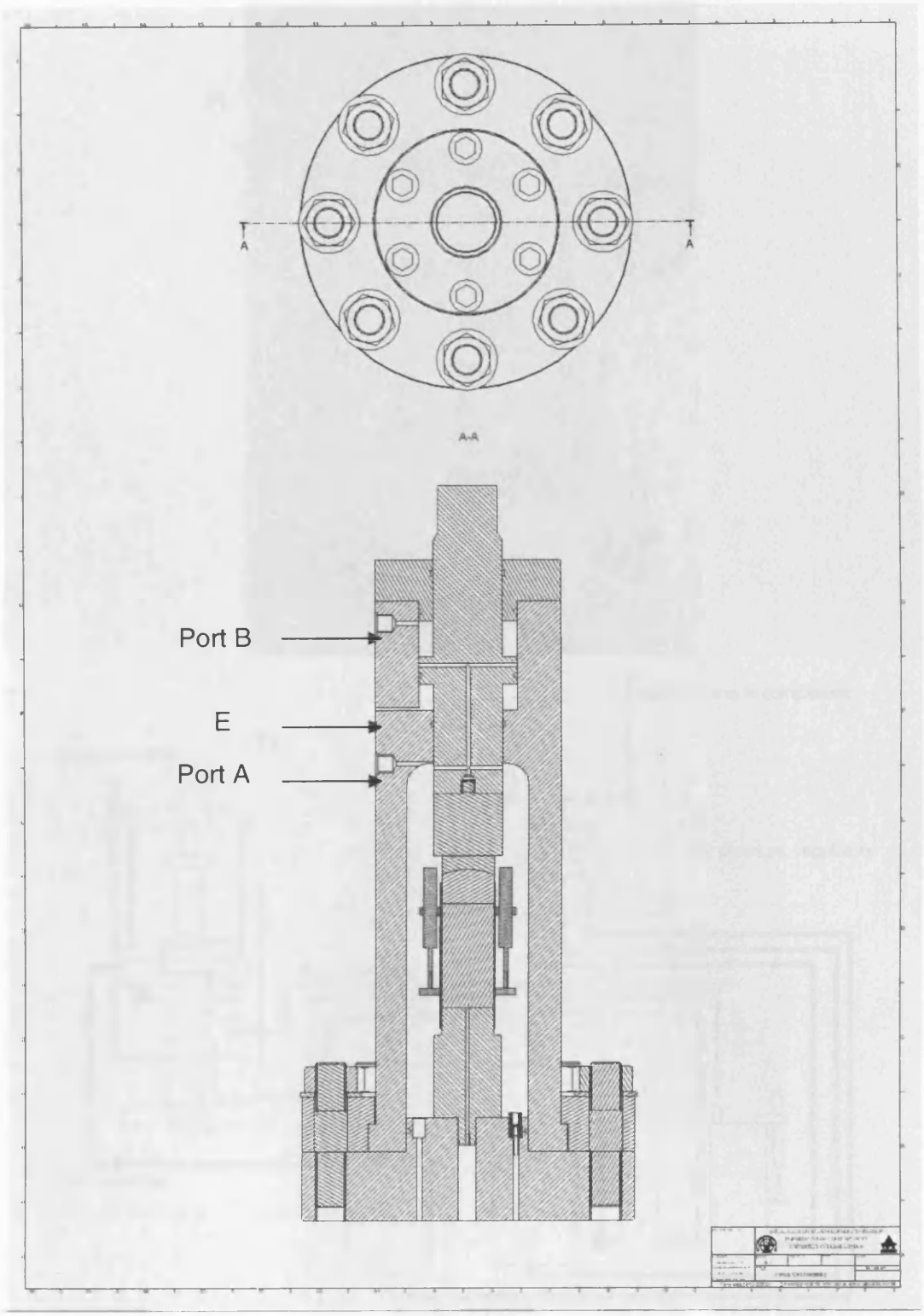

Figure (4-4): Schematic diagram showing the interior compartments of the high pressure triaxial cell.

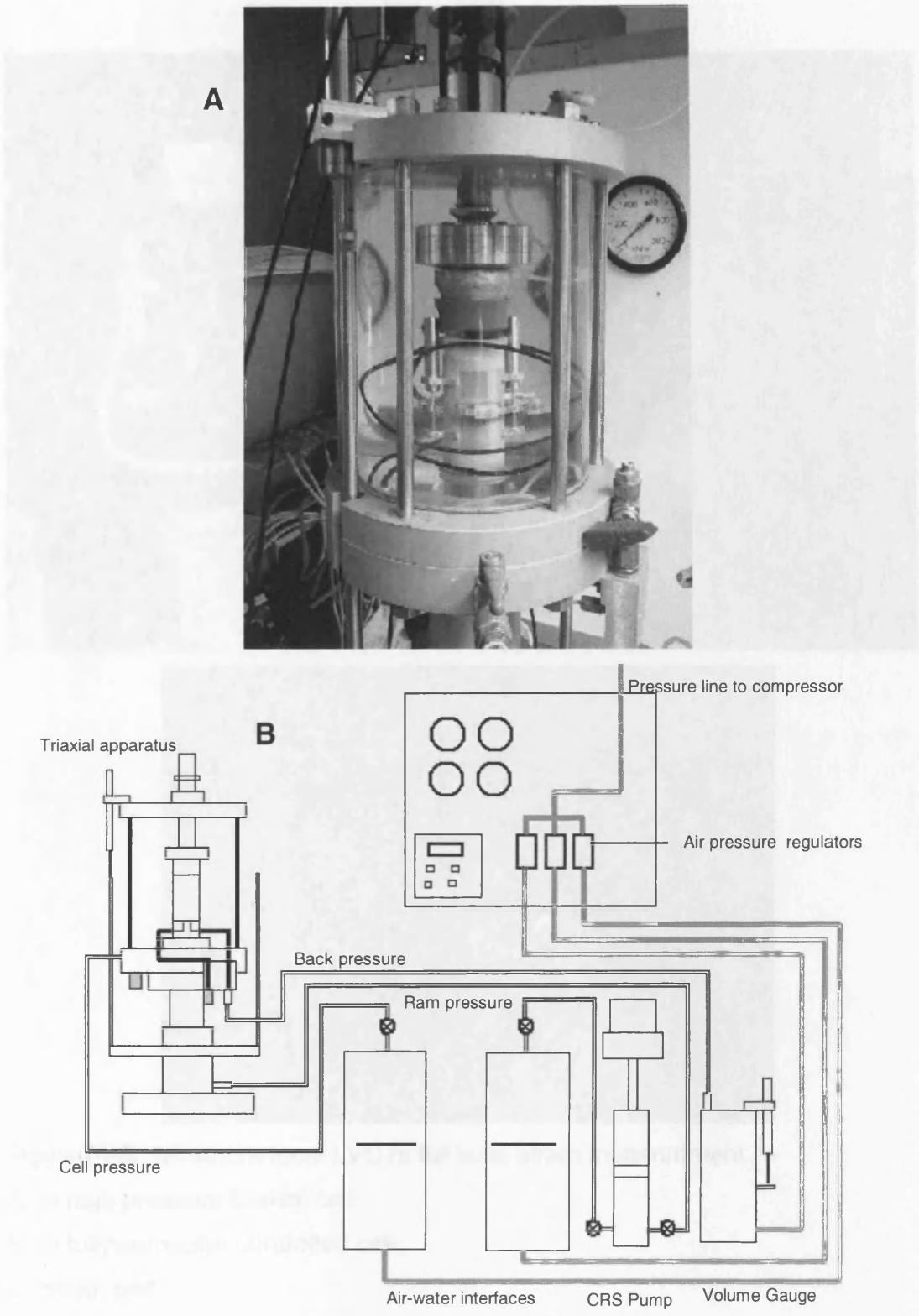

Figure (4-5): A- Fully computer controlled triaxial cell, with local miniature LVDTs.
B- Set-up of the fully computer controlled triaxial cell.

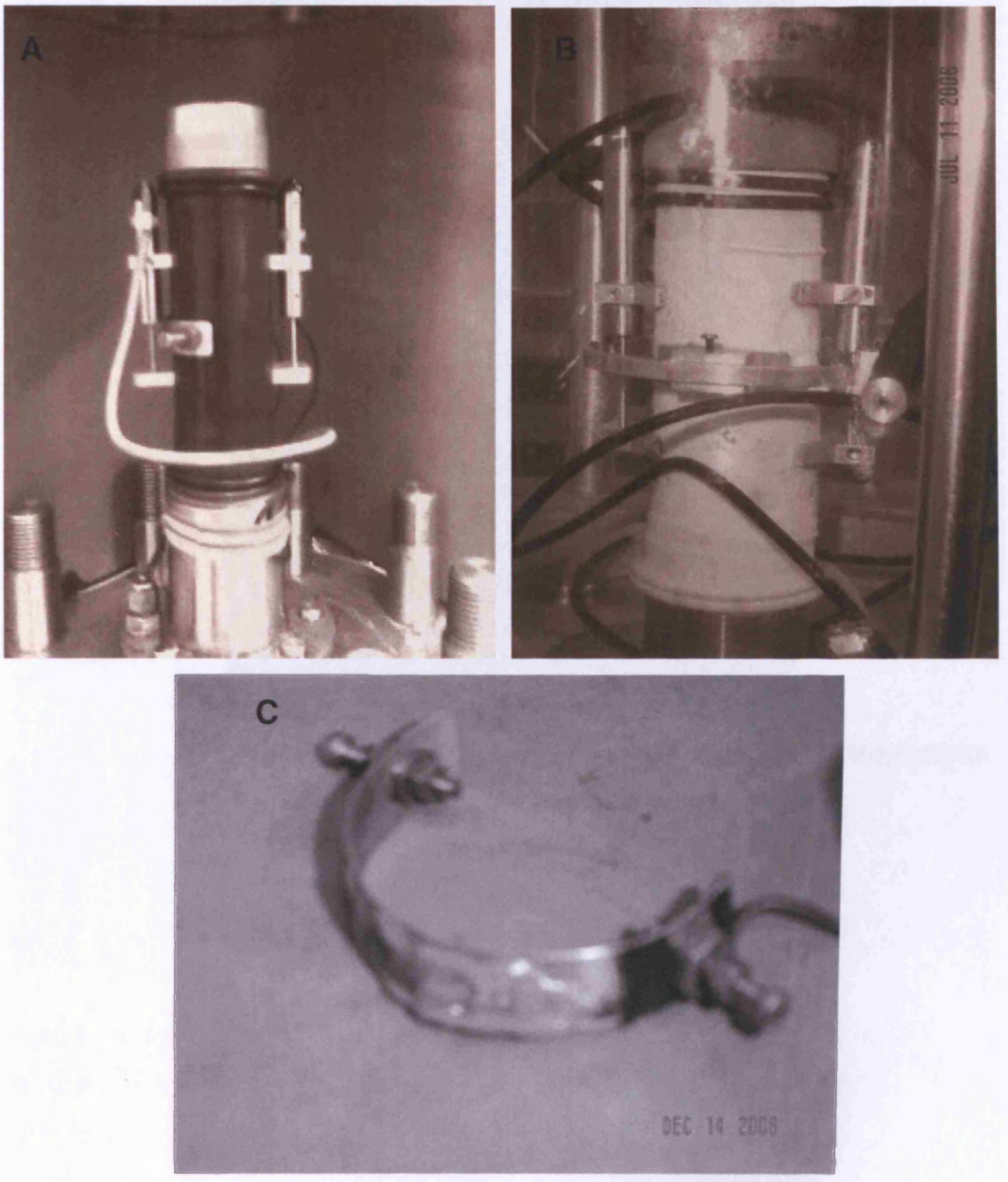

Figure (4-6): Miniature local LVDTs for local strain measurement.

A. In high pressure triaxial cell.

B. In fully computer controlled cell.

C. Strain belt.

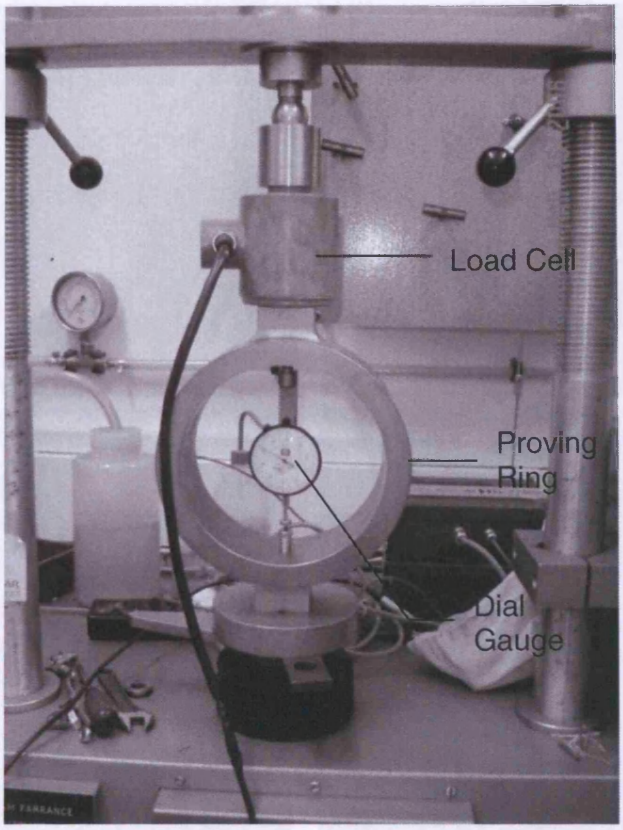

Figure (4-7): Using a proving ring in the calibration of the exterior Load cell for the high pressure triaxial cell.

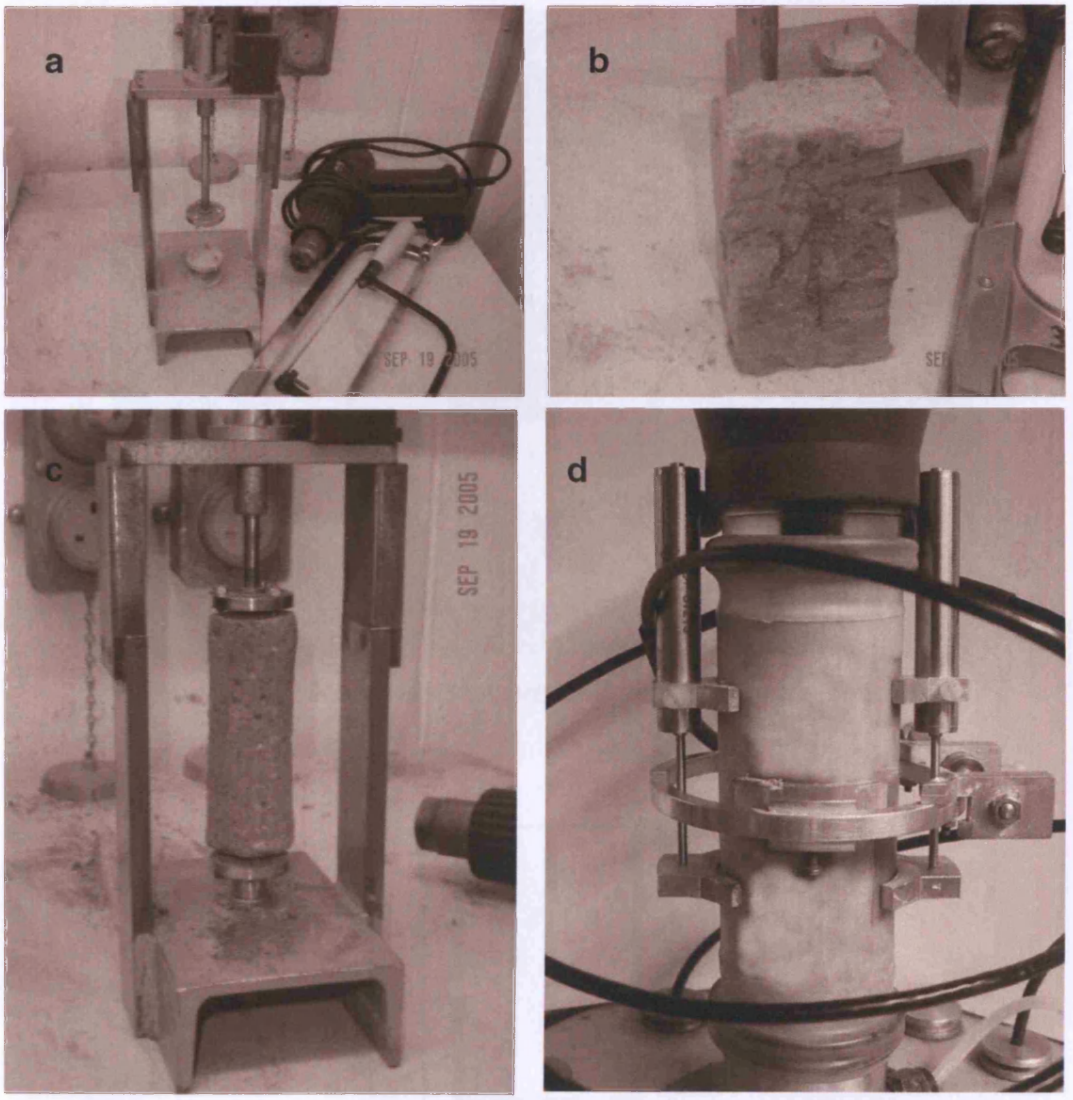

Figure (4-8): Trimming procedure and tools used for trimming undisturbed samples of Langjökull sediment (a,b &c). The figure also shows sample setting with its local LVDTs (d).

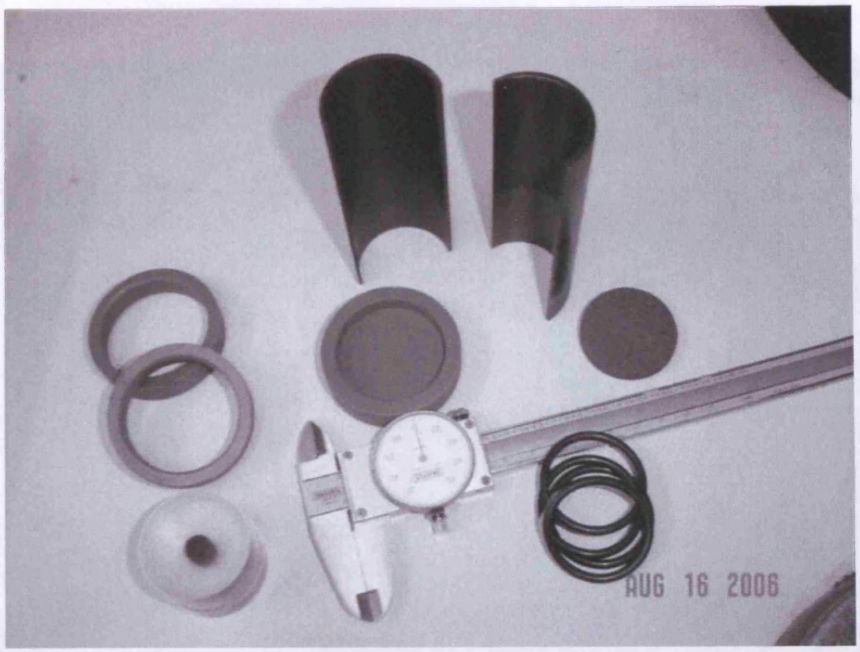

Figure (4-9): Mould used for preparing the remoulded samples.

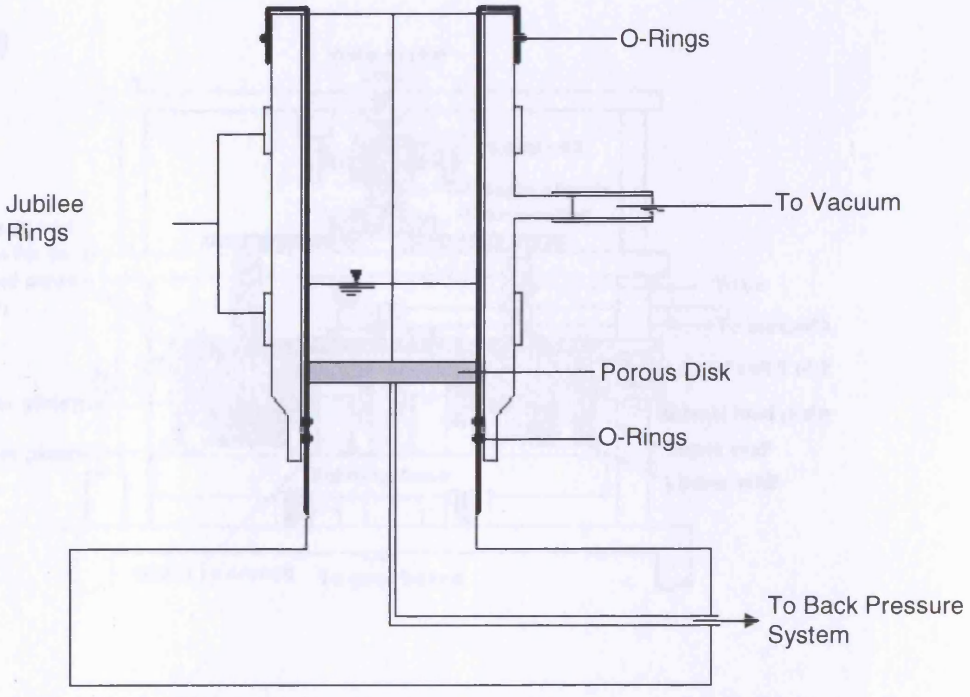

Figure (4-10): Schematic figure showing the general set-up of the mould during sample preparation by sedimentation method.

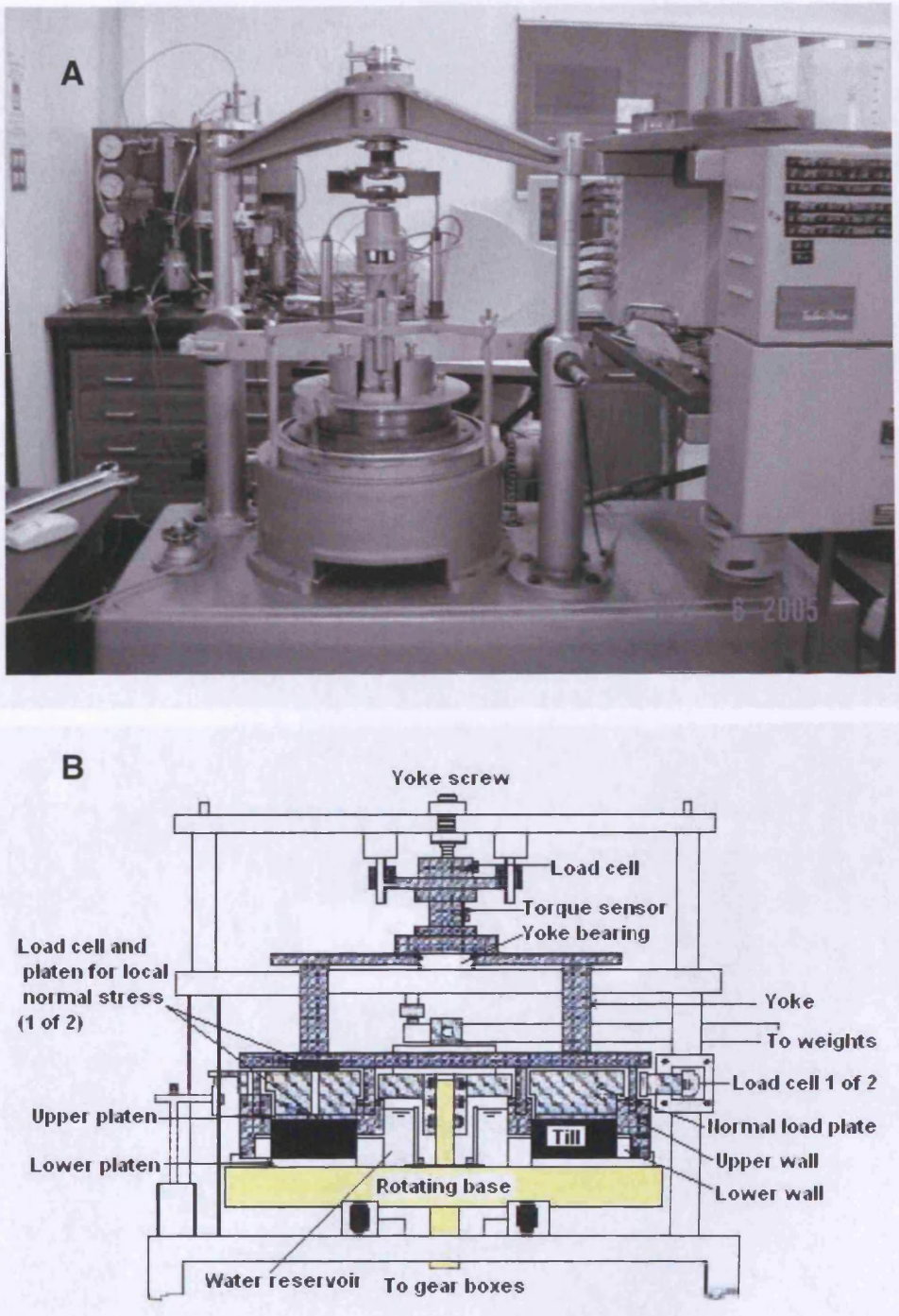

Figure (4-11): A- Bishop's ring shear apparatus at Imperial College.
B- Mid-section of the apparatus.

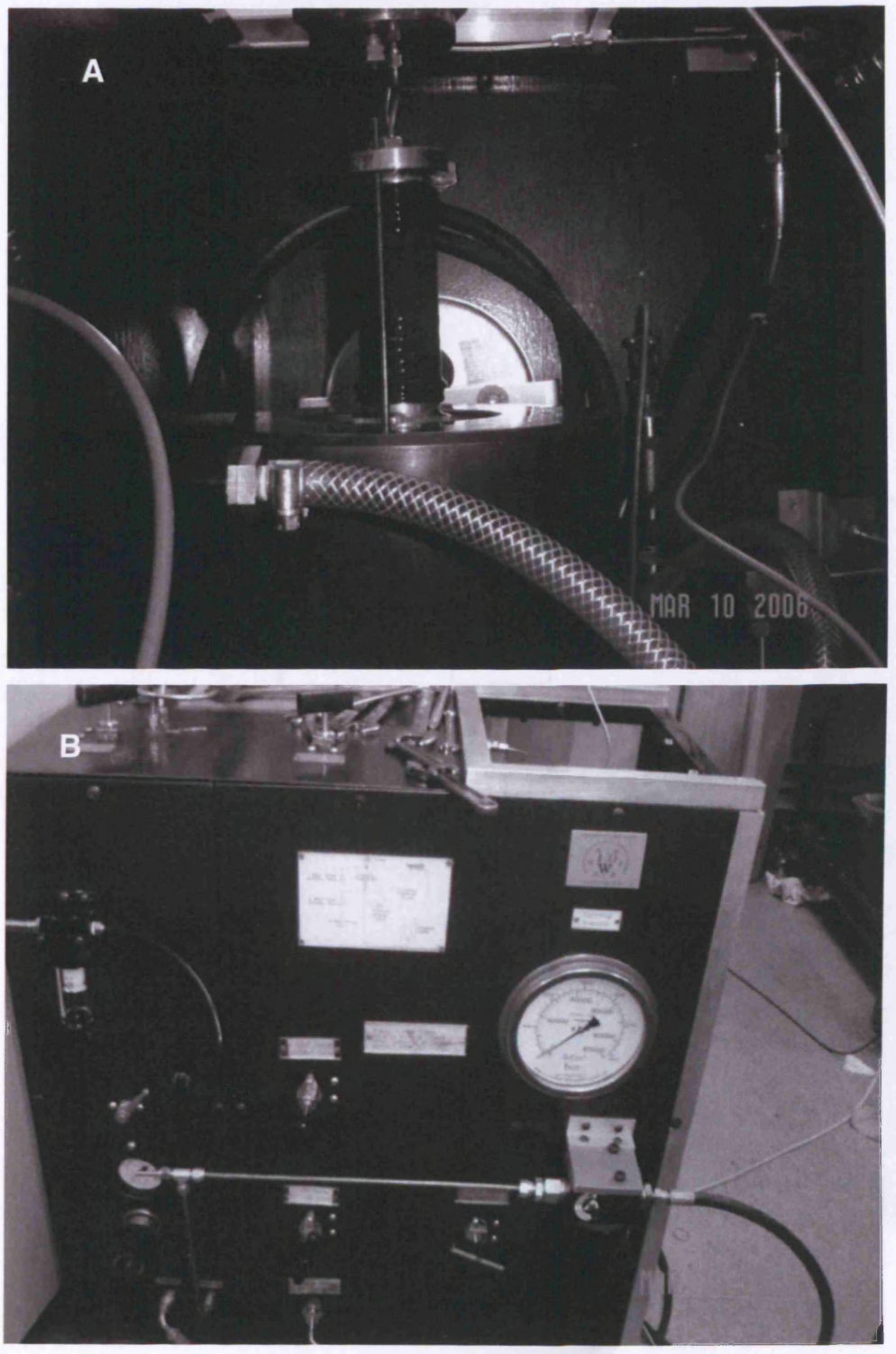

Figure 4-12: A. Placing the remoulded sample inside the pressure chamber of the permeameter. B. The permeameter.

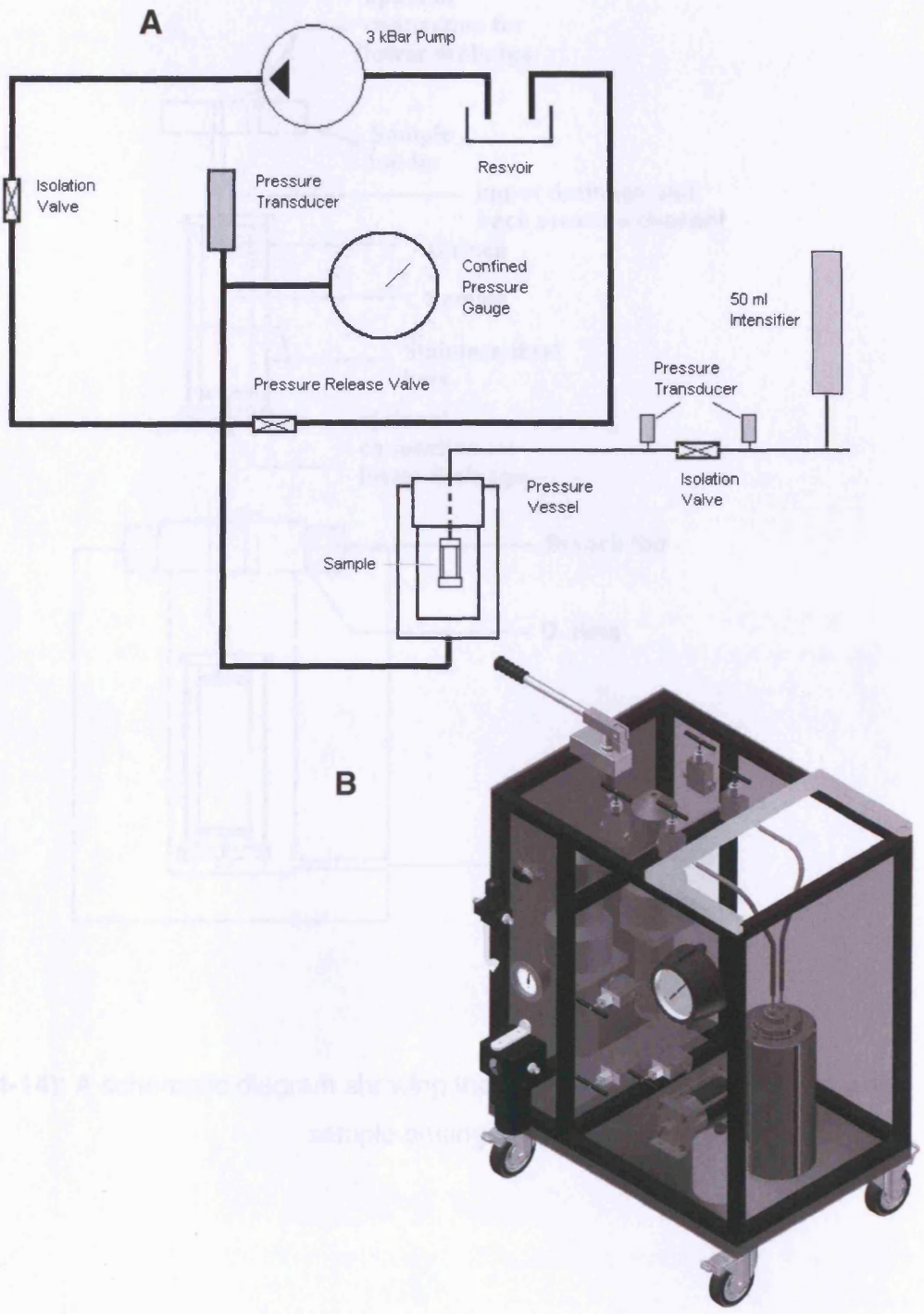

Figure(4-13): The permeameter, A- Set-up.
B- Schematic diagram.

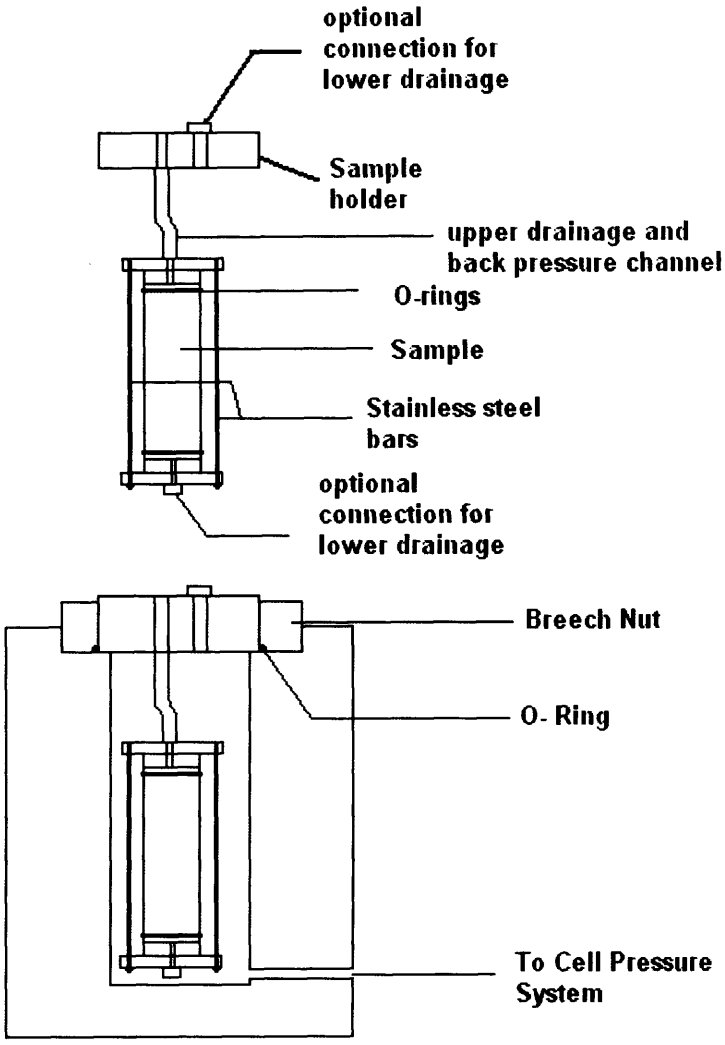

Figure(4-14): A schematic diagram showing the permeameter compartment with sample setting.

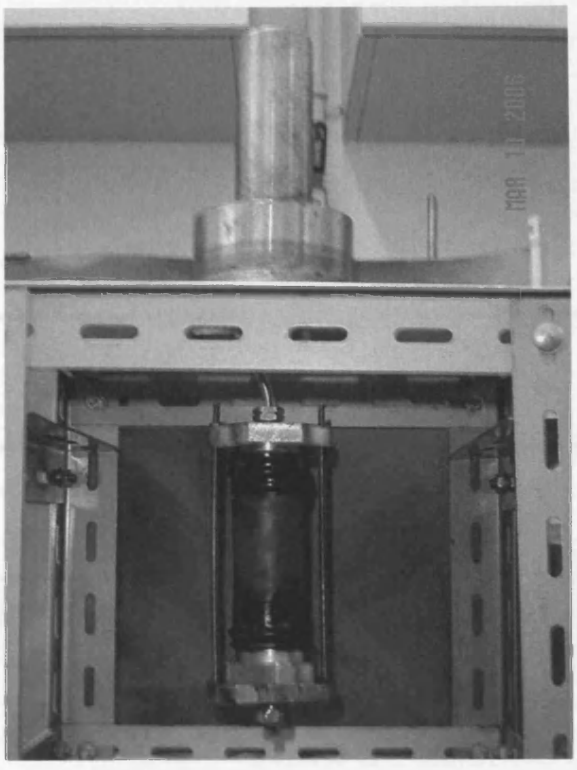

Figure (4-15): Sample setting in the permeameter, the figure also shows the procedure by which the sample frame is fitted while the sample is in a hanging position to avoid any excess load application to the sample.

Figure (4-16): The diffractometer available in the Earth Sciences department at UCL.

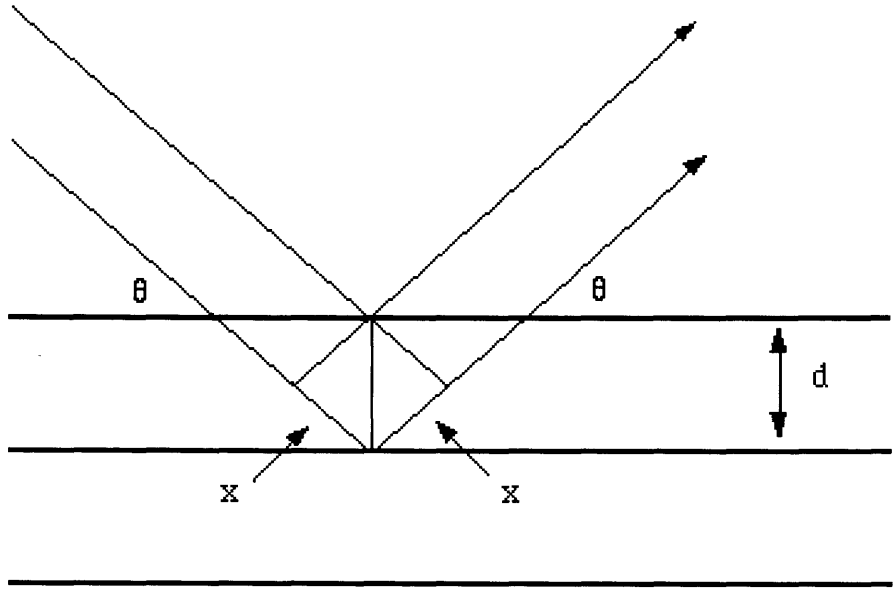

Figure (4-17) Reflection of X-rays from two planes of atoms in a solid.

Chapter Five

The mechanical behaviour of Langjökull glacial sediment

5.1 Introduction

This chapter describes the experimental research work that was carried out on the Langjökull sediment and explains the purpose behind each test. It can thus serve as reference for the following chapters (Six, Seven and Eight), where the test data are analysed in detail. The study of the mechanical behaviour of the sediment focussed on two main issues: firstly whether applying traditional soil mechanics theories to the sediment's behaviour is valid, and this was done by analysing test data within the Critical State framework proposed by Roscoe et al. (1958) (see Section 1.3.3); secondly particle breakage was monitored in selected tests, to investigate the relation between particle breakage and the sediment's behaviour in terms of its yielding in compression and its Critical State in shearing. A brief study of the viscous behaviour was carried out, and data of the effect of varying the shearing rate on the shearing behaviour of the sediment are also presented. Finally, details of the data analysis calculations and the methods applied for data correction are discussed in this chapter.

This chapter has been constructed as follows: the following section describes the testing materials and type of samples used in the testing programme. Section 5.3 describes and lists all compression tests performed on the sediment; this includes isotropic compression tests and one-dimensional compression tests. Shearing tests by the means of triaxial cells are discussed in Section 5.4. Three different cells were used: a conventional standard cell, a high pressure cell and a fully computer controlled triaxial cell. Shearing tests using a Bishop's type ring shear apparatus are presented in Section 5.5. The last section presents data for the tests which were carried out to investigate the shearing rate effect on the sediment behaviour. Details

of the testing equipment and general testing procedure were given in Chapter Four.

5.2 Tests on Langjökull sediment

In this study both remoulded and undisturbed samples of the natural sediment were used to investigate the sediment's mechanical behaviour. In addition, artificially graded samples made of selected particles of the sediment were tested to investigate the effect of grading on the mechanical behaviour. Particles retained on a mesh of 295 microns were used for all samples stated as artificially graded samples in this chapter. The grading of both the natural sediment and artificially graded sample are shown in Figure (5-1).

5.3 Compression tests on Langjökull sediment

Isotropic compression tests and one-dimensional compression tests were carried out on both natural undisturbed and reconstituted samples of Langjökull sediment, and on an artificially graded sediment to investigate the compressibility behaviour and the effect of grading on the sediment's compression behaviour. High (up to 40MPa) to extremely high isotropic compression pressures (up to 250MPa) were applied to the sediment by the means of the high pressure triaxial cell and the permeameter described in Section 4.4. Particle breakage during compression was monitored by the sieving method for some selected tests. Remoulded samples were sieved before and after test to compare any change in particle size distribution of the sample. For the undisturbed samples the particle size distribution after test had to be compared to the particle size distribution of the sediment obtained from sample trimming.

Additional tests were performed on the artificially graded soil to study the effect of grading on the compressibility of the sediment.

5.3.1 Isotropic compression tests by the means of the high pressure triaxial cell

Table (5-1) presents details of isotropic compression tests carried out on the natural samples of Langjökull sediment. One test was carried out on an undisturbed sample (LU-ISO) to reach a pressure of 37MPa while the rest of the tests (LR-ISO, LR-10MPa-ISO, LR-30MPa-ISO, and LR-40MPa-ISO) were carried out on remoulded samples to reach maximum pressures of 22, 10, 30 and 40MPa respectively. An additional sample, LR-ISO(loose), was prepared by using the sedimentation method described in Section (4.2.6.B) to achieve the loosest state possible. Tests which were selected for particle breakage monitoring were sieved before and after test, as indicated in Table (5-1). Some selected tests were closely examined by using the scanning electron microscope to characterise the change in particle properties of the sediment and identify potential breakage.

The void ratio of the sample at any time during testing was calculated as follows:

$$\text{Void ratio (e)} = \frac{\text{Volume of voids } (V_v)}{\text{Volume of Solids } (V_s)} \quad \text{.....[5-1]}$$

The change in volume of voids was monitored by the change in pore water content which also corresponded to the sample's volume change. The volume of solids was calculated as follows:

$$V_s = \frac{\text{Sample's dry weight}}{\text{Sediment's specific gravity}} \times \text{water density } (1\text{gm/cm}^3) \text{.....[5-2]}$$

(The mean effective stress p′ was calculated as:

p′= total pressure- pore water pressure, as indicated in equation [1-1].)

The water content of the retrieved sample was determined by the oven drying method and the final void ratio of the retrieved sample was calculated by using Equation (4-2). This was used as a check to be compared with the final void ratio calculated from test data and initial weight, dimensions and water

content of the sample. Results from these tests are analysed and discussed in Chapter Six.

5.3.2 Isotropic compression tests by the permeameter

To reach very high isotropic pressures, higher than those permitted by the high pressure triaxial cell, the permeameter was used to test four samples. Two tests (LR250-2 and LR250-2A) were performed on remoulded samples of void ratios of 0.45 and 0.42 respectively. Another two samples with lower void ratio (e=0.35) were also tested to investigate the effect of sample initial density on the compressibility and particle breakage of the sediment. All these samples were sieved before and after testing and were further examined by the scanning electron microscope after test to observe the deformational characteristics of the sediment particles under such high pressures. The sample's void ratio and effective pressure at any time during the test are calculated in a similar way to that described in Section 5.3.1. Details of tests carried out in the permeameter are shown in Table (5-2). Results from the permeameter tests are analysed and discussed in Chapter Six.

5.3.3 One-dimensional compression tests

The modified oedometer cell described in Section (4-2) was used to test samples of the sediment and artificially graded samples. Test results were used to characterise the sediment's compression behaviour during one-dimensional compression and identify the role of grading on its compressibility. It was intended to carry out high pressure isotropic compression tests on the artificially graded sediment for comparison, but due to the high angularity of the specimen particles which resulted in tearing of the sample double-layered jacket before reaching the desired high pressures this was not possible. Five tests were conducted using the modified oedometer cell: three on sediment samples: one undisturbed (LU-Oedo), and two remoulded (LR1-Oedo) and (LR2-Oedo), and two on artificially graded samples (ART1-Oedo) and (ART2-Oedo) with two different initial void ratios of 0.90 and 0.97 respectively to investigate the effect of sample's initial density on the compression behaviour. Initial void ratios for the remoulded

samples were calculated by determining the dry weight of the sediment which was poured in the consolidation ring, and dividing it by the volume calculated from the ring's interior diameter and height. The undisturbed sample was prepared by trimming the frozen sample to size. Details of tests conducted in the modified oedometer cell are shown in Table (5-3). Results from the one-dimensional compression tests on the Langjökull sediment is analysed and discussed in Chapter Six.

5.4 Shearing tests by triaxial cell apparatus

The mechanical behaviour of the sediment during shearing was investigated by using three triaxial cells: a conventional triaxial cell; a high pressure triaxial cell and a fully computer controlled cell, those apparatuses have been described in Section 4.3.

Two undisturbed (LU1-CU and LU2-CU) and three remoulded samples (LR2-CU, LR3-CU, and LR4-CU) were tested in the conventional triaxial cell. The samples were consolidated before applying undrained shearing, within the limit of the range of pressures permitted by this cell. The sediment's behaviour under undrained shearing with relatively low pressures, compared to the ones permitted by the high pressure cell, is more realistic in simulating the sediment behaviour under glaciers, as the pore water pressure under glacier is expected to be very high, thus, the sediment under glaciers is deforming under low effective pressure and usually in undrained conditions.

A number of drained tests were performed in the conventional cell, however data obtained from those tests were unreliable. Consequently, one drained test on a remoulded sample of the natural sediment was additionally carried out at low pressure (100kPa) by using the fully computer controlled triaxial cell (LR100kPa-CD), which is more reliable than the conventional cell. All these tests are listed in Table (5-4). The last test which was carried out by the fully computer controlled triaxial cell (V3-60kPa), was conducted on a remoulded sample which was consolidated under 60kPa of isotropic confining pressure before it was subjected to undrained shearing with

variable shearing rate; this will be discussed in the last section of this chapter.

The main reason behind using the high pressure triaxial cell was to achieve sediment yielding, as this is usually associated with particle breakage in granular materials (Coop & Lee, 1993). The range of pressures permitted by the conventional cell (up to 1MPa) was not enough to achieve any breakage in the sediment and thus any yielding. The shearing test data of the high pressure triaxial shearing were also necessary to define the Critical State Line of the sediment in the v-ln p′ plane, as it was difficult to define it clearly from the data obtained from tests conducted in the conventional cell only. The difficulty stems from the fact that the Critical State Line location of granular materials is unclear in the low pressure range and it is slightly curved towards the specific volume axis (Verdugo & Ishihara, 1996; Coop & Lee, 1993).

Remoulded as well as undisturbed samples were tested in the high pressure triaxial cell under drained and undrained conditions (Table 5-5). Some selected samples were sieved before and after testing, or only after testing in the case of undisturbed ones, to monitor particle breakage. The scanning electron microscopy facility was also used for selected samples for further examination. The shearing rate for the undrained tests was chosen to be 3.0mm/hr, while this rate had to be lowered to 1.0mm/hr for the drained tests to avoid the development of pore water pressure during shearing. Details of the shearing tests conducted in the high pressure triaxial cell are listed in Table (5-5).

Results from these tests are analysed and discussed in Chapter Seven. The triaxial shearing data analysis was carried out by calculating both the deviator stress, q′, and the mean effective pressure p′. Axisymmetric conditions were assumed so that:

$$\sigma_1=\sigma_a \quad \& \quad \sigma_2=\sigma_3=\sigma_r$$

The deviator stress, which means the difference between the axial stress σ_a and the radial pressure σ_r, is calculated from the axial force (F) applied to the sample during shearing divided by the sample's current area (A_s).

$$q' = \sigma_a - \sigma_r \quad \text{.....[5-3]}$$

$$q' = F / A_s \quad \text{.....[5-4]}$$

Sample dimensions were calculated after the consolidation stage which was carried out in multiple pressure stages. These dimensions were used in the shearing stage calculations of the axial strain and deviator stress. The sample's dimensions after consolidation were determined by calculating both the axial and radial strains experienced by the sample during the consolidation stage based on the total volumetric strain experienced during consolidation, measured from the volume gauge. In the case of isotropic consolidation and assuming soil isotropy, where:

$$\varepsilon_a = \varepsilon_r \quad \text{.....[5-5]}$$

$$\delta\varepsilon_a = (1/3)\,(\delta\varepsilon_v) \quad \text{.....[5-6]}$$

where:

ε_a is the axial strain experienced by the sample during consolidation.

ε_r is the radial strain experienced by the sample during consolidation.

ε_v the volumetric strain during consolidation stage, calculated from the volume gauge reading.

The calculated sample dimensions obtained from the above-mentioned equations, were compared to the strain values obtained from the local strain measurements when local instrumentation was used, to check the accuracy of the calculated sample dimensions.

As the shearing proceeds the sample's cross-sectional area changes. This requires some correction for the deviator stress calculation. For undrained shearing tests, with no sample volume change, the estimation of the actual sample area can be calculated as follows, assuming a uniform sample diameter during deformation:

$$A_s = V_c / h \quad \text{.....[5-7]}$$

where:

A_s is the sample's cross-sectional area at any time during shearing (deformed).

V_c the sample's volume when shearing is commenced (after consolidation stage).

h the sample's deformed height, which is calculated from the sample height after consolidation and the current exterior axial strain as follows:

$$h = h_c(1- \varepsilon_a) \quad \text{.....[5-8]}$$

where:

h_c is the calculated sample's height after consolidation stage.

ε_a is the axial strain, calculated from the exterior axial LVDT reading.

For drained shearing tests, the sample's volume change during shearing should be considered in the sample's cross-sectional area correction. The sample's cross sectional area is calculated as follows:

$$A_s = V_c\ (1- \varepsilon_v)\ /h_c(1-\varepsilon_a) \quad \text{.....[5-9]}$$

Where:

ε_v is the volumetric strain of the sample due to shearing, calculated from volume gauge reading.

The mean effective stress, p', is calculated as follows;

$$p' = (1/3)\ (\sigma'_a+2\sigma'_r) \quad \text{..... [5-10]}$$

In the triaxial test, $\sigma'_a = q'+ \sigma'_r$,

thus,

$$p' = (1/3)\ (3\ \sigma'_r +q') \quad \text{.....[5-11]}$$

Young's modulus has been calculated in the drained shearing tests where local LVDTs were used for local strain measurements. According to Hooke's law, when $\delta\sigma_r=0$ as follows:

$$E' = \delta\sigma'_a/\delta\varepsilon_a \quad \text{.....[5-12]}$$

Or:

$$E' = \delta q'/\delta\varepsilon_a \quad \text{.....[5-13]}$$

In the case when $\delta\sigma_r$ is not equal to 0.

Shear strains were calculated assuming symmetry in the triaxial cell tests,

$$\delta\varepsilon_s = (2/3)\ (\varepsilon_a-\varepsilon_r) \quad \text{.....[5-14]}$$

The shear modulus is then calculated from the equation:

$$G' = \delta q'/3\delta\varepsilon_s \quad \text{.....[5-15]}$$

5.5 Ring shear tests

A Bishop-type ring shear apparatus available at Imperial College was mainly used to investigate the sediment particle breakage when it is sheared to very high strains. The fact that subglacial sediments experience high shearing strains due to glacier movements make ring shear tests a more representative simulation than those carried out by triaxial cell due to the shear strain's limitation in the triaxial cell. It is also possible to reach a residual condition in the ring shear apparatus. One drawback which needs to be considered in ring shear data is the fact that tests in this apparatus are done in drained conditions, which are not the expected environmental conditions underneath glaciers. However, to estimate the residual strength of glacial sediment is still a critical issue that needs to be addressed to understand its overall mechanical behaviour.

All tests conducted in the ring shear apparatus were carried out on remoulded samples. Two tests, BR350 and BR570, were carried out on samples of the sediment. Those samples were consolidated prior to shearing under 350 and 570kPa normal stress respectively, and were sheared with low speed to avoid any pore water pressure development during shearing. Both samples were sheared to reach more than 50,000% shear strain, where the shear strain represents the displacement divided by the height of the sample at the beginning of the shearing stage. A third test was carried out on an artificially graded sample (ART570) to investigate the effect of grading on the sediment's shearing and crushing behaviour. The bigger particles resulted in a relatively high initial void ratio of the sample, here calculated as 0.94. The sample was consolidated under 570kPa normal stress before shearing was commenced. A higher shearing speed was used during shearing of this sample as it was unlikely to develop any excess pore water pressure during shearing due to the size of its particles and based on results by Ferreira et al. (2006) which seem to show that there is no affect of the shearing speed on particle breakage.

The shearing velocity and shearing displacement during the test were measured from the angular displacement of the lower ring of the apparatus in a known episode of time. The shearing strain was then calculated from:

$$\varepsilon_s = (d_s / h_c)*100 \quad \text{.....[5-16]}$$

where:

h_c is the sample's depth after the consolidation stage.

d_s is the shearing displacement measured on the sample centre line represented by the average distance of the interior and the exterior apparatus radius, which was also used to calculate the sample's virtual length (Figure 5-2).

Details of the tests conducted by the ring shear apparatus are shown in Table (5-6). The last test which was conducted by this apparatus was carried out on a sample of the sediment using variable shearing rate to investigate the effects of shearing rate on the residual strength of the sediment. This will be discussed in the following section. Results from these tests are analysed and discussed in Chapter Six.

5.6 Effect of shearing rate on the sediment's behaviour

To investigate the shearing rate effects on the sediment shear strength, two tests with variable shearing rate were carried out. The fully computer controlled triaxial cell was used to carry out an undrained shearing test (V3-60). The undrained conditions and low effective stress for this test were chosen to simulate the conditions underneath glaciers. Details of the test are given in Table (5-4). The sample was consolidated under 60kPa prior to shearing. The shearing rate was changed stepwise. Table (5-7) shows the change of shearing rate sequenced with axial strain during this test.

To investigate shearing rate effects on the residual strength of the sediment, test (BR350-Var) was conducted in the Bishop-type ring shear apparatus on a sample of the sediment, using variable shearing rate. Table (5-8) lists the shearing rates used during this test.

Results obtained from these tests are analysed and discussed in Chapter 8.

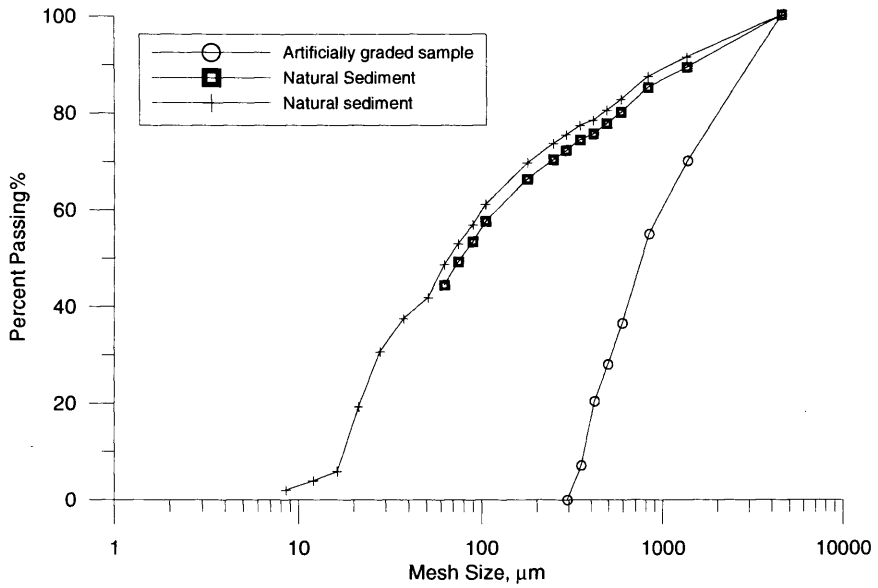

Figure (5-1): Particle size distribution of the natural sediment and the artificially graded sediment.

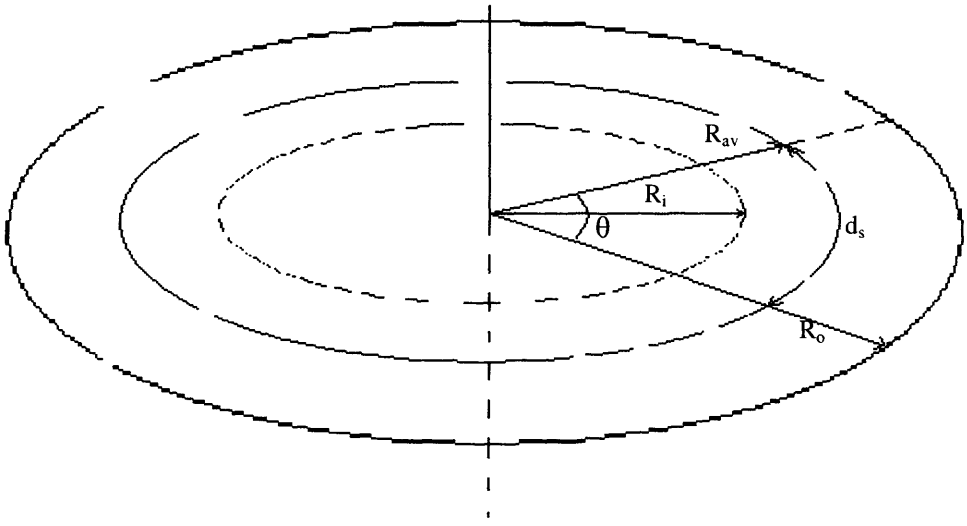

Figure (5-2): Method of measuring shearing displacement in Bishop's ring shear apparatus. Θ represents the angular displacement.

Table (5-1): Isotropic compression tests in the high pressure triaxial cell.

Test	Sample	Max. Pressure MPa	Initial Void Ratio	Final Void Ratio	Retrieved Sample Void Ratio	Remarks
LU-ISO	Undisturbed	37.0	0.57	0.29	0.27	
LR-ISO	Remoulded	22.0	0.49	0.38	0.39	SEM
LR-10MPa-ISO	Remoulded	---	---	---	---	Sieved- SEM
LR-30MPa-ISO	Remoulded	30.2	0.42	0.30	0.28	Sieved
LR-40MPa-ISO	Remoulded	40.0	0.52	0.29	0.28	Sieved - SEM
LR-ISO*(loose)	Remoulded	19.5	0.47	0.35	0.30	Sieved

* This sample was prepared by sedimentation while applying back pressure

Table (5-2): Details of isotropic compression tests in the permeameter.

Test	Sample	Maximum Eff. Pressure MPa	Initial Void Ratio	Final Void Ratio	Retrieved Sample Void Ratio	Remarks
LR250-1	Remoulded	234.0	0.35	0.10	0.066	Sintering
LR250-2	Remoulded	248.3	0.45	0.26	0.17	
LR250-2A	Remoulded	249.5	0.42	0.23*	0.18*	
LR250-3	Remoulded	249.0	0.35	0.100	0.10	Sintering

* The back pressure system channels experienced some leakage which resulted in a reduction in the retrieved sample's void ratio.

Table (5-3): One-dimensional compression tests in the modified oedometer cell.

Test	Initial Void Ratio	Max. Pressure MPa	Final Void Ratio	Retrieved Sample Void Ratio
LU-Oedo	0.57	16.3	0.48	----
LR1-Oedo	0.50	19.8	0.37	0.34
LR2-Oedo	0.61	20.9	0.43	0.43
ART1-Oedo	0.90	14.7	0.59	-----
ART2-Oedo	0.97	19.3	0.56	0.50

Table (5-4): Triaxial shearing tests on Langjökull sediment at low pressures.

Test	Test description	sample	Effective Cell Pressure kPa	Initial Voids ratio	After consolidation Voids ratio	Final Voids ratio	Shearing Rate mm/hr
LU1-CU*	Consolidated undrained shearing	Undisturbed	496	0.58	0.43	0.43	3.0
LU2-CU*	Consolidated undrained shearing**	Undisturbed	215	0.58	0.50	0.50	3.0
LR2-CU*	Consolidated undrained shearing	Remoulded	329	0.48	0.45	0.45	3.0
LR4-CU*	Consolidated undrained shearing	Remoulded	101	0.52	0.50	0.50	3.0
LR3-CU*	Consolidated undrained shearing	Remoulded	449	0.40	---	---	3.0
LR100kPa-CD+	Consolidated drained shearing	Remoulded	104	0.51	0.49	0.47	1.0
V3-60kPa+	Consolidated undrained shearing	Remoulded	60	0.61++	0.50	0.50	Variable

* void ratio of retrieved sample was not determined for these tests.
** There was some stress relaxation times during test.
+ Test was conducted in the computer controlled triaxial cell.
++ Although the sample initially was very loose, it experienced some reduction in void ratio during installation and saturation, the initial void ratio before consolidation based on the retrieved sample data is 0.50.

Table (5-5): Details of triaxial shearing tests in the high pressure triaxial cell.

Test	Sample type	Test description	Initial e	At start of Shearing	Final e	Strain Rate mm/hr	Effctive Cell P MPa	Retrieved sample voids ratio
LU2MPa-CD	Undisturbed+	Consolidated Drained shearing	0.56*	0.38	0.36	1.0	2.0	0.35
LU10MPa-CD**	Undisturbed	Consolidated Drained shearing	0.56	0.33	0.29	1.0	10.0	0.27
LU10MPa-CU	Undisturbed+	Consolidated Undrained shearing	0.58	0.33	0.33	3.0	10.2	0.33
LR2MPa-CD	Remoulded+	Consolidated Drained shearing	0.45	0.37	0.35	1.0	2.0	0.33
LR2MPa-CD(Dense)	Remoulded+	Consolidated Drained shearing	0.40	0.36	0.34	1.0	2.1	0.33
LR10MPa-CD**	Remoulded+	Consolidated Drained shearing	0.50	0.33	0.29	1.0	10.0	0.28
LR20MPa-CD	Remoulded+	Consolidated Drained shearing	0.52	0.33	0.27	1.0	20.0	0.27
LR30MPa-CD**	Remoulded+	Consolidated Drained shearing	0.57	0.31	0.27	1.0	30.1	0.25
LR10MPa-CU**	Remoulded	Consolidated Undrained shearing	0.47	0.37	0.37	3.0	10.0	0.33
LR20MPa-CU	Remoulded+	Consolidated Undrained shearing	0.49	0.30	0.30	3.0	20.1	0.30
LR30MPa-CU	Remoulded	Consolidated Undrained shearing	0.51	0.28	0.28	3.0	30.0	0.28

* The sample experienced some reduction in void ratio when the membrane was placed, initial void ratio due to reduction was 0.50.
** Sample was sieved before and after test for particle breakage monitoring.
+ with the use of local LVDTs and strain belt.

Table (5-6): Details of Bishop-type ring shear tests on Langjökull sediment.

Tests	σ_n kPa	Shearing speed mm/min	Initial void ratio	Void ratio when shearing is commenced	Max. shear strain%
BR350	350	0.87	0.42	0.300	52086%
BR570	570	0.87	0.37	0.29	50283%
ART570	570	2.35	0.94	0.80	7796%
BR350-var	350	variable	0.36	0.27	49978%

Table (5-7): Change of shearing rate during test V3-60.

Exterior Axial Strain %	Strain rate yr^{-1}
0 – 0.515	60
-- 2.09	67
-- 2.60	8.7
-- 3.73	67
-- 6.90	9.0
-- 15.66	9.0
--15.80	50
--17.43	68

Table (5-8): Shearing rate change during test BR350-Var.

Angular displacement, degrees	Displacement mm	Total accumulative displacement, mm	average velocity, mm/hr
1350	1496	0-1496	0.957
43.6	48	-1544	0.007
46.4	51	-1596	0.918
1080	1197	-2793	8.307
1440	1596	-4389	107.6
1260	1396	-5785	1.161
1440	1596	-7381	107.6

Chapter Six

Particle Breakage in Langjökull Sediment

6.1 Introduction

During its history, a sediment may have been deposited, eroded and/or transported, and these mechanisms will have affected the size and shape of its particles. The particle size distribution is thus a reflection of these diverse mechanisms, and by studying how particular distributions are created we may understand better the origins and history of some sediments. The Langjökull sediment has a well-graded (poorly sorted) particle size distribution. The particle size distribution of a glacial sediment is an indicator of the crushing history undergone by this sediment, which can in turn be linked to the stress and strain history of the deposit. The nature of sediment grading will also influence its mechanical behaviour, as will be illustrated in Section (6.5).

Existing studies of the mechanical behaviour of granular sediments have shown that yielding and the compression behaviour are dependent on the soil particle crushability and its initial grading (Coop & Atkinson, 1993; Coop & Lee, 1993). This makes studying the sediment's crushability and its current grading necessary to define its previous, present and future behaviour. The programme of tests which was used to study the Langjökull particles' crushability can be summarised as: isotropic compression tests to very high pressures (high pressure triaxial apparatus, permeameter), triaxial shearing tests at low to high confining stresses, and finally studying the sediment's crushability at high shearing strains by using the ring shear apparatus.

In this chapter particle crushability is presented and discussed through the results obtained from the laboratory testing programme carried out on Langjökull sediment. The chapter is constructed as follows: particle breakage of the sediment induced by pure isotropic compression is presented in

Section (6.2). Section (6.3) discusses the sediment's particle breakage during shearing while the sediment's breakage potential and the effect of its grading on its crushability are presented in Section (6.4). Finally, the effect of the sediment's grading on its behaviour during compression is discussed in the last section in this chapter.

6.2 Particle breakage of Langjökull sediment induced by pure isotropic compression

The breakage potential of the particles of the Langökull sediment was first investigated in pure compression, by performing a series of isotropic compression tests in the high pressure triaxial apparatus and the permeameter described in Sections (4.3.2) and (4.4) respectively. The aim of this series of tests was to characterise the development of particle breakage with stress level, by identifying a Normal Compression Line in a plot of relative breakage, B_r, against mean effective stress, p', similarly to what Coop & Lee (1993) had done for the carbonate Dog's Bay sand. Isotropic compression tests to 10, 20 and 40MPa were performed on the sediment. Particle size distributions of the samples were determined before and after testing for each test; results of the sieve analyses are shown in Figure (6-1). As the results indicate, in all three tests the difference in the particle size distributions for particles larger than 63μm is very small, of magnitude equivalent to that of the scatter. This indicates that there is no or insignificant breakage in particles larger than 63μm during isotropic compression up to 40MPa. Scanning electron micrographs of the sample which was compressed to 20MPa showed no indication of particle breakage (Figure 6-2), however scanning electron micrographs of the sample which was compressed to 40MPa, shown in Figure (6-3), seem to show that some breakage occurred in the smaller-sized particles (5-10μm), though it was difficult to quantify it. It is not thought that this amount of breakage, and in that size range, would alter the mechanical behaviour of the till significantly.

These tests were carried out on samples with various initial densities, but it is unlikely that it affected the overall result which can be concluded from these

tests. Previous work on crushable sediments showed that a sample's initial density has a great effect on the stress level at which breakage starts and where the Normal Compression Line is encountered, but it is unlikely to affect the position or the slope of the Normal Compression Line, in the v- ln p' plane (Coop & Lee, 1993). Denser samples are expected to show higher yield stresses than loose samples, resulting from the greater number of particle contacts in the dense soil sand hence lower contact stresses. None of all three samples which were isotropically compressed seems to show the usual amount of breakage which is encountered with yielding.

The breakage potential under isotropic conditions of the Langjökull sediment was tested further by compressing it in the permeameter apparatus that allowed reaching a pressure of 250MPa. This very high pressure is unrealistic in terms of stress applied to the sediment by a glacier (equivalent to 25km) and may represent a sample buried at about 25km below ground level, but these tests were carried out for the purpose of determining whether the soil particles eventually break under high stresses. Four tests in total were performed, two on medium density samples (e=0.41-0.43) and two on dense samples (e=0.35). The particle size distributions for the tested samples are shown in Figure (6-4) along with the initial (natural) distribution. Samples 2 and 2A, which were tested from relatively looser states, show insignificant breakage for the particles larger than 63μm, similarly to what was found for lower stresses. Scanning electron micrographs (Figures 6-6 and 6-7) show that some limited amount of breakage occurred in the finer fraction. Samples 1 and 3 however, which were tested from denser states, show a different behaviour. Instead of shifting upwards, a characteristic of particle breakage, the particle size distribution curve shifted downwards, indicating that the tested samples gained larger particles during testing. Scanning electron micrographs of the tested samples show indeed that cold-welding occurred between the particles during testing, with small-sized particles (less than 1μm) being "absorbed" by the larger particles (Figures 6-5 and 6-8). The dense state at the start of compression must have facilitated high stress contacts between particles, and thus sintering. The heavier

particles resulting from the process are reflected in the location of the grading curve post-testing, which was determined by weight.

The behaviour found for the dense samples above may give an insight into the process of lithification that happens in soils subjected to large overburden pressures. However, this is unlikely to happen under glaciers as the conditions underneath glaciers are always associated with high pore water pressure and low effective pressure (Eyre, 2003; Fountain, 1994). The main output of these tests is that the particles of the Langjökull sediment do not break even under very high pressures. Typically in sandy materials yield is associated with the onset of significant particle breakage (Coop & Lee, 1993) but here the absence of breakage seems to hinder any yielding process. The null breakage potential in compression for these sediments can either be due to the mineral characteristics of the particles, even though particles of basaltic origin are typically fragile, or to other reasons that need to be identified.

6.3 Particle breakage of Langjökull sediment induced by shearing

Particle breakage can be induced by shearing, which is a more likely process to have happened in the glacial sediments during deposition and transport. To investigate the sediment's particle breakage during shearing, shearing tests on the sediment were carried out in the high pressure triaxial cell, and ring shear tests were performed to very high strains in a Bishop-type ring shear apparatus.

Again the sieving method and scanning electron microscope images were used to detect any breakage which might take place during testing. Samples were sheared in drained and undrained conditions in the high pressure triaxial apparatus with constant cell pressures up to 10MPa. It was shown above that the isotropic compression stage did not cause any breakage in the particles of the sediment larger than 63μm, so it was assumed that at the start of shearing the grading was the same as the initial grading before testing. The particle size distribution curves for the samples before and after testing, in Figure (6-9), show that the drained and undrained shearing at

confining pressures of 10MPa and drained shearing at confining pressure up to 30MPa did not cause any more breakage of the particles than the isotropic compression. This was also confirmed by SEM images on samples which were sheared under a confining cell pressure of 10MPa in both drained and undrained condition , as shown in Figures (6-10) and (6-11).

To overcome the shearing strain limitation in the triaxial cell, which might be the reason behind the lack of particle breakage in the previous shearing tests, a series of tests was then carried out in the Bishop-type ring shear apparatus to reach very high notional strains, up to 50,000%, as defined by Equation (5- 16). This magnitude of strain is typically enough to break hard particles such as quartzitic particles (e.g. Leighton Buzzard sand; Smalley et al., 2004; Jefferson et al., 1997; Klotz & Coop, 2002). Two samples were tested, the first one under a normal stress of 350kPa (sample BR350) and the second one under 570kPa (sample BR570). It was not possible to test samples under high normal stresses due to limitations of the apparatus. Figure (6-12) shows the particle size distribution curves before and after testing: the grading did not change during shearing, which again reflects that no particle or a very insignificant proportion of particles larger than 63μm was crushed during the shearing. The volumetric strain versus shearing strain for both tests is shown in Figure (6-13). The limited volumetric strain, which is usually associated with particle breakage, is another indication of the lack of particle breakage during the tests (Coop et al., 2004).

6.4 Effect of sediment grading on its breakage potential

Results of both compression and shearing discussed in the previous sections showed that neither compression under extremely high pressures nor shearing to very high shearing strains can cause significant breakage in the Langjökull sediment. Considering the basaltic origin of the sediment, this was an unexpected result. Past research on sands (Hardin, 1985) has shown that typically in a soil the larger particles are more likely to be broken than the smaller particles. The Langjökull sediment contains up to 50% fines which may account for the fact that breakage does not occur easily in that soil. There is a strong suspicion that not only the amount of fines but the whole

particle size distribution is responsible for the behaviour of the sediment. In order to verify this hypothesis compression and shearing tests were carried out on a soil artificially composed of the biggest particles of the Langjökull sediment. The particle size selected passed through a 475mm sieve and retained by a 295μm sieve. A sample (ART570) was tested in the Bishop-type ring shear apparatus under a normal stress of 570kPa to reach a strain equal to 7,800%. The particle size distribution curves before and after testing the sample are shown in Figure (6-14), along with the natural distribution of the Langjökull sediment. Unlike what was seen in previous tests a shift of the particle size distribution curve occurred upwards, demonstrating an increase in the number of fines and thus breakage of the sample particles. The grading curve obtained is less well graded (poorly sorted) than the natural sediment, but it is imagined that by shearing the sample to higher strains it may have become coincident with the natural particle size distribution curve.

The test had to be stopped at 7,800% strain because significant compression occurred during the shearing that caused the thickness of the specimen to reduce to a value that was too low and could cause damage to the apparatus. The volumetric response of sample ART570 is shown in Figure (6-15), plotted with the curve for sample BR570. Particle breakage is necessarily accompanied by a decrease in volume (increase in volumetric strain), as seen in the plot for sample ART570 which reached 25% volumetric strain at 7,800% shear strain. Virtually no compression occurred in sample BR570, which may be an additional proof that the sample did experience no or insignificant breakage. The figure also shows that at the stage when test ART570 was terminated, the sample was still experiencing volumetric compression, which indicates that further shearing would probably have caused further particle breakage to the sample, and maybe by further shearing a state where the sheared sediment would reach a grading similar to that of the natural sediment could have been achieved.

The above mentioned tests illustrate clearly that Langjökull sediment in its current grading has suffered incessant breakage during its history of transport and deposition so that a "critical" or "terminal grading" for the

sediment has been reached (Dreimanis & Vagners, 1971; Karrow, 1976; Coop et al., 2004; McDowell & Boulton, 1998) and no further breakage for this sediment can be achieved under any pressure or strain. This complies with the results of compression tests on petroleum coke reported by McDowell & Bolton (1998) which indicated that the soil eventually reached a constant grading at high stresses (these data discussed in Section 2.6.3), which is what these tests on Langjökull sediment have proved, by exhibiting no particle breakage when subjected to high and extremely high isotropic pressures in the high pressure triaxial cell and the permeameter.

The results obtained from the shearing tests to very high shearing strains, are also in agreement with those results obtained on carbonate sand (Coop et al., 2004) and discussed in Section 2.6.3. The hypothesis that there is a constant or "critical" grading that can be reached by shearing a sediment to very high strains when no further grading evolution can be achieved by imposing any further shearing strains, again complies with the fact that Langjökull sediment during its depositional and transportation history has been subjected to large shearing strains which have imposed their deformational stamp on the sediment, reflected in the current grading (Dreimanis, 1976; Karrow, 1976). This was confirmed by the behaviour of the artificially graded sample which exhibited significant breakage compared to the naturally graded samples, which proves that the "non breakable sediment" is an outcome of the grading rather than an outcome of mineralogy.

The depositional and transport history of glacial sediment seems to be a crucial factor in defining the sediment's grading and subsequently its overall behaviour. This was also confirmed by results obtained from ring shear tests on another subglacial sediment which was collected from Breiðamérkurjökull-Iceland. This sediment, although from similar basaltic origin to that of Langjökull, exhibited behaviour distinct from that observed in Langjökull sediment, showing a clear tendency for its particles to break under relatively low stress (500kPa), and to reach a constant grading at about 350% shear strain (Altuhafi et al., 2006). This result gives an indication of the effect of

sediment transport history on the sediment, which would be reflected in the grading of the sediment, as Breiðamérkurjökull sediment represents a more uniformly distributed (well sorted) sediment with larger particles, compared to Langjökull, an indication of smaller transport distance from the source (Dreimanis, 1976; Karrow, 1976).

6.5 Effect of sediment grading on compression behaviour

It is widely accepted that the compression behaviour of granular materials is governed by particle breakage (Coop & Lee, 1993; Hyodo et al., 2002; McDowell & Bolton, 1998). It is also generally found that for a given granular sediment, irrespective of initial density, the compression curves all tend towards a common compression line at high stresses. This unique compression line is termed the Normal Compression Line (Coop & Lee, 1993), this was discussed in detail in Section 2.3. This hypothesis should be further investigated and questioned when dealing with sediments like Langjökull sediment, which proved that it cannot experience further particle breakage under any high stress or high level of shearing strains.

The isotropic compression tests which were carried out on the natural sediment of Langjökull were conducted on samples of various initial densities (see Tables 5-1 and 5-2). The compression curves obtained from these tests are shown in Figure (6-16). Multiple parallel compression curves were obtained from those tests depending on the initial sample's density. These curves did not seem to converge at any level of pressure even when 250MPa of compression pressure was reached. The sediment also showed no clear yielding point and a very stiff unloading curve. The lack of significant breakage and non-uniqueness of the NCL meant that it was not possible for the Langjökull sediment to define a clear unique relation between the relative breakage Br and mean effective stress p′ as was defined for carbonate sand (Coop & Lee, 1993). The non-uniqueness of the Normal Compression Line has also been reported in previous literature in some gap-graded residual soils (Ferreira & Bica, 2006) and some types of well graded silts (Nocilla et al., 2006), or by addition of fines to sand (Martins et al., 2001). This behaviour was termed "transitional" behaviour of soils. The location of the

compression curves of soils with transitional behaviour is totally dependent on the initial density or void ratio of the sample, which seems to be the case for Langjökull sediment.

From previous studies on the evolution of subglacial sediment grading, a progressive size reduction of subglacial debris is expected during transport, with coarse modes of the sediment expected to be found near its source (Dreimanis & Vagners, 1971). In this study, another question was considered, whether the Langjökull sediment had in any time during its history and before reaching its terminal grading behaved in a similar way to those well known granular crushable sediments. To answer this question, the compressibility of artificially graded samples made of coarse particles was investigated by one-dimensional compression tests on two samples of different initial densities (ART1-Oedo) & (ART2-Oedo), with initial void ratios equal to 0.90 and 0.97 respectively (see Table 5-3). The high initial void ratio of these samples, when compared to samples of the natural sediment (highest void ratio around 0.6), is a reflection of the uniformity of the artificially graded sample. The compression curves obtained from these tests along with three tests of natural sediments are shown in Figure (6-17). The figure illustrates clearly the difference between the behaviour of the two types of samples. Again the natural sediment's behaviour in one-dimensional compression is similar to that obtained from isotropic compression tests, showing no clear yielding point and no indication of convergence to form a unique compression line, with a stiffer curve obtained from the undisturbed sample. On the other hand, the artificially graded samples showed a clear yielding point at a pressure of about 6MPa and a clear tendency to converge to form a unique compression line.

The sediment's evolving particle size distribution during transport and deposition would probably affect its mechanical behaviour. If a more uniform sediment is considered, for example near the source, as the particles of the sediment crush and progressively fill the voids the sediment will experience a reduction in the maximum and minimum void ratio (Wood, 2006; Daoudji & Hicher, 2006). This will cause a corresponding drop in the position of the

Normal Compression Line and Critical State Line of the sediment. Thus, the steep Normal Compression and Critical State Lines which can be defined for crushable granular soils may be a result of multiple drops in the position of these lines due to the change of the material properties (Wood, 2006; Daoudji & Hicher, 2006) (see section 2.6.4). In the case of Langjökull sediment, the sediment seems to have reached its terminal grading. Hence, the grading state index of the sediment, as it was defined by Wood (2006), is equal to 1, and the position on which the sediment is deforming in the e-log p' plane, if the three-part critical state line hypothesis defined by Wood (2006) is considered, is at the third and final part, where the sediment would show a more flattened Normal Compression and Critical State Line compared to the second part, which coincides with the particle breakage stage (see Figure 2-27).

On the other hand, the compression behaviour exhibited by the artificially graded sample represents the behaviour of the same sediment before reaching the current state. In other words, it represents a state when the grading index is less than 1, and when particle breakage still governs the sediment behaviour. This is illustrated in the tendency to form a unique Normal Compression Line with a higher slope than that exhibited by the natural sediment and the clear yielding point which is associated with particle breakage on set (Coop & Lee, 1993; Wood, 2006; Hyodo et al., 2002).

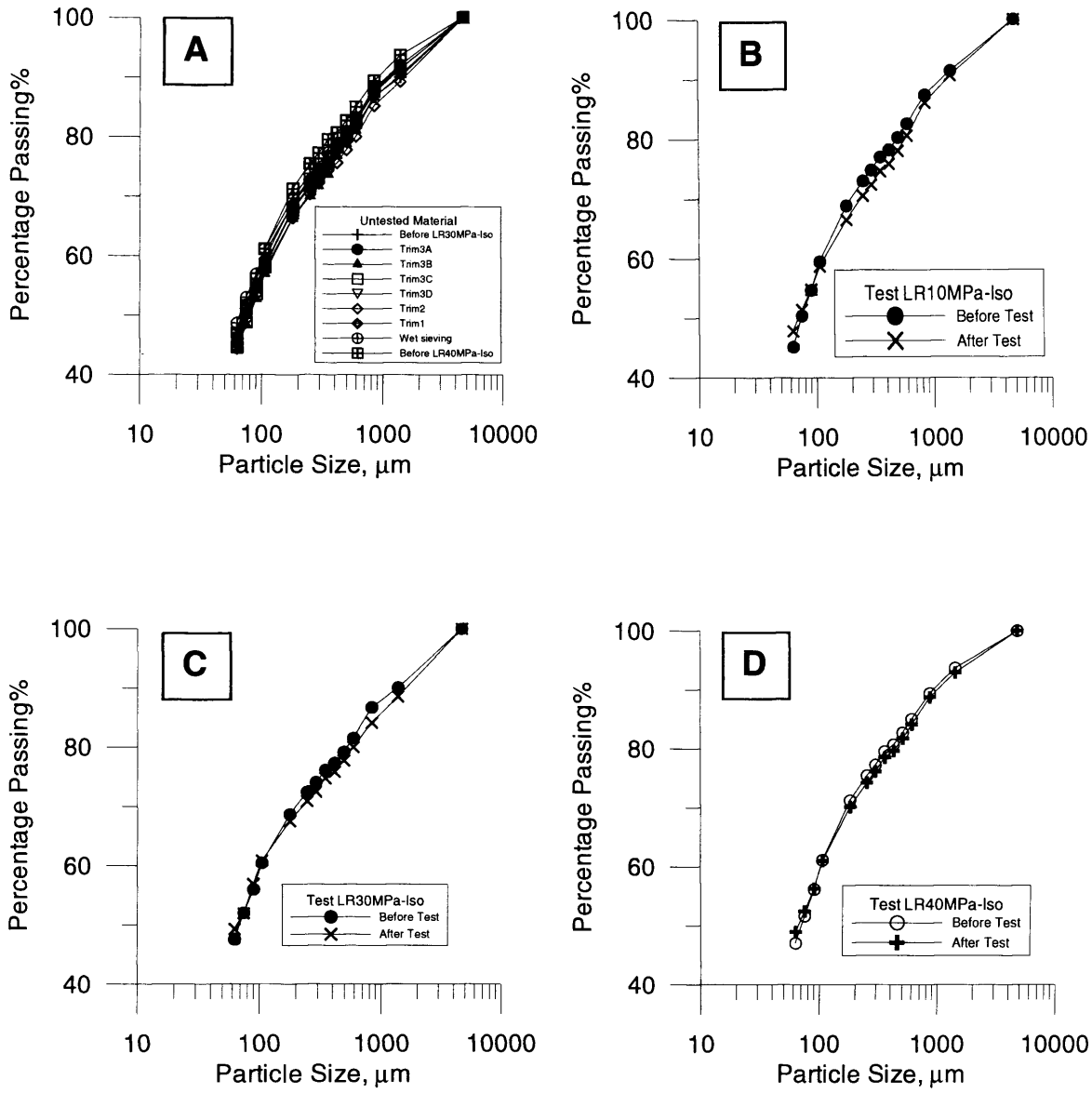

Figure (6-1): A) Natural particle size distribution by sieve analysis. B) Before and after isotropic compression tests up to 10MPa. C) Before and after isotropic compression tests up to 30MPa. D) Before and after isotropic compression tests up to 40MPa.

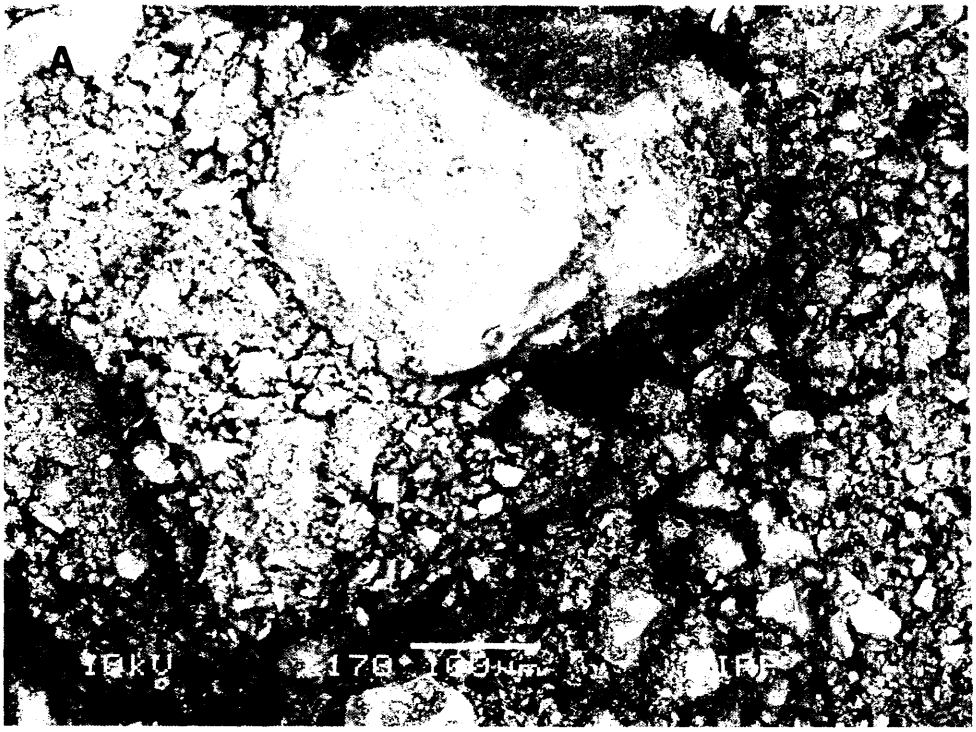
A

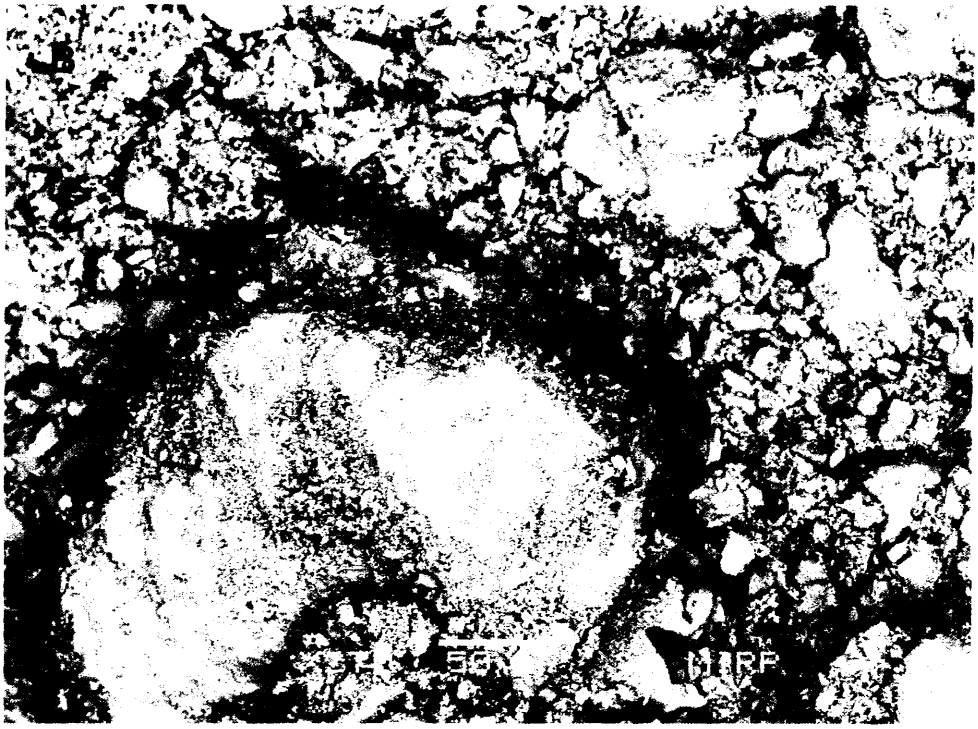
B

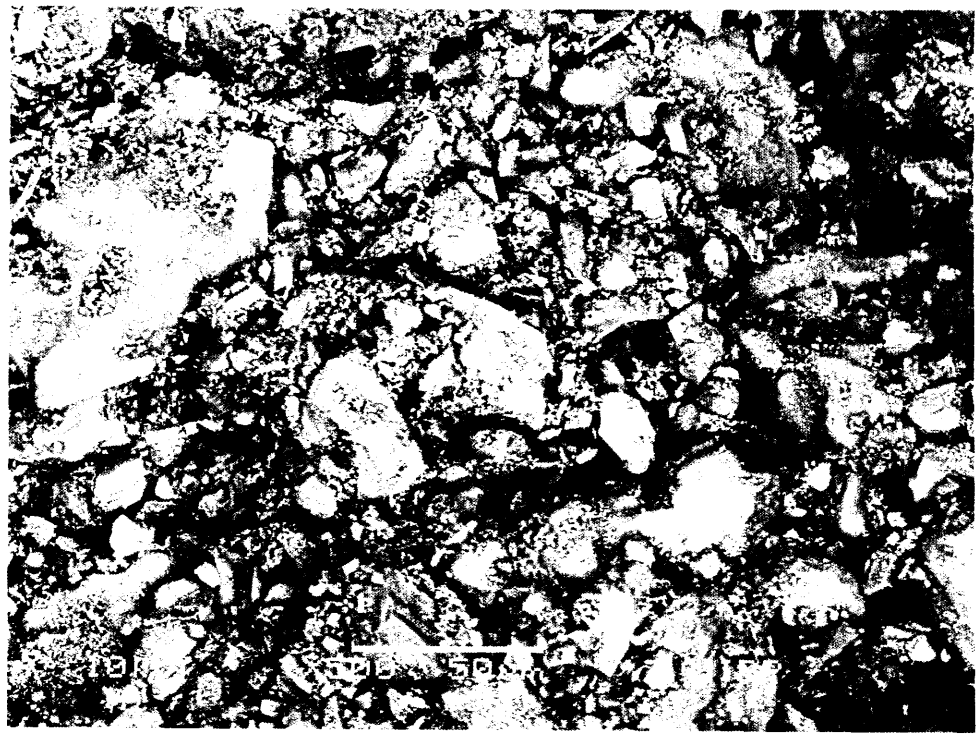

Figure (6-2): Scanning electron microscope images from a sample which was isotropically compressed up to 20MPa, increasing magnification from A to D.

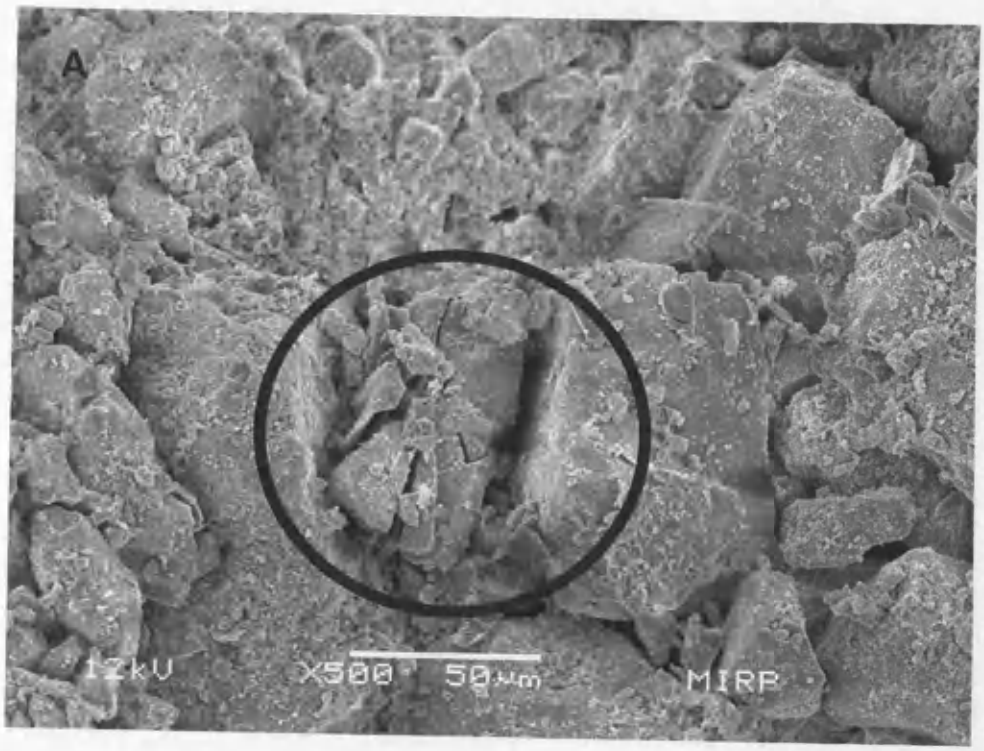
A
12kV
X500
50µm
MIRP

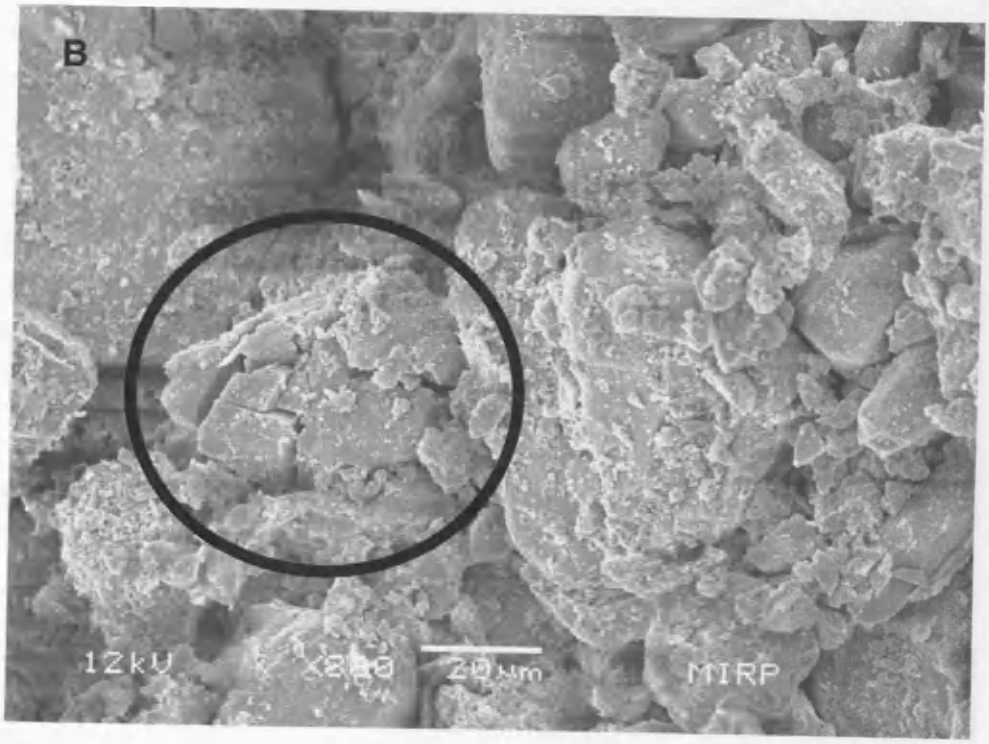
B
12kV
20µm
MIRP

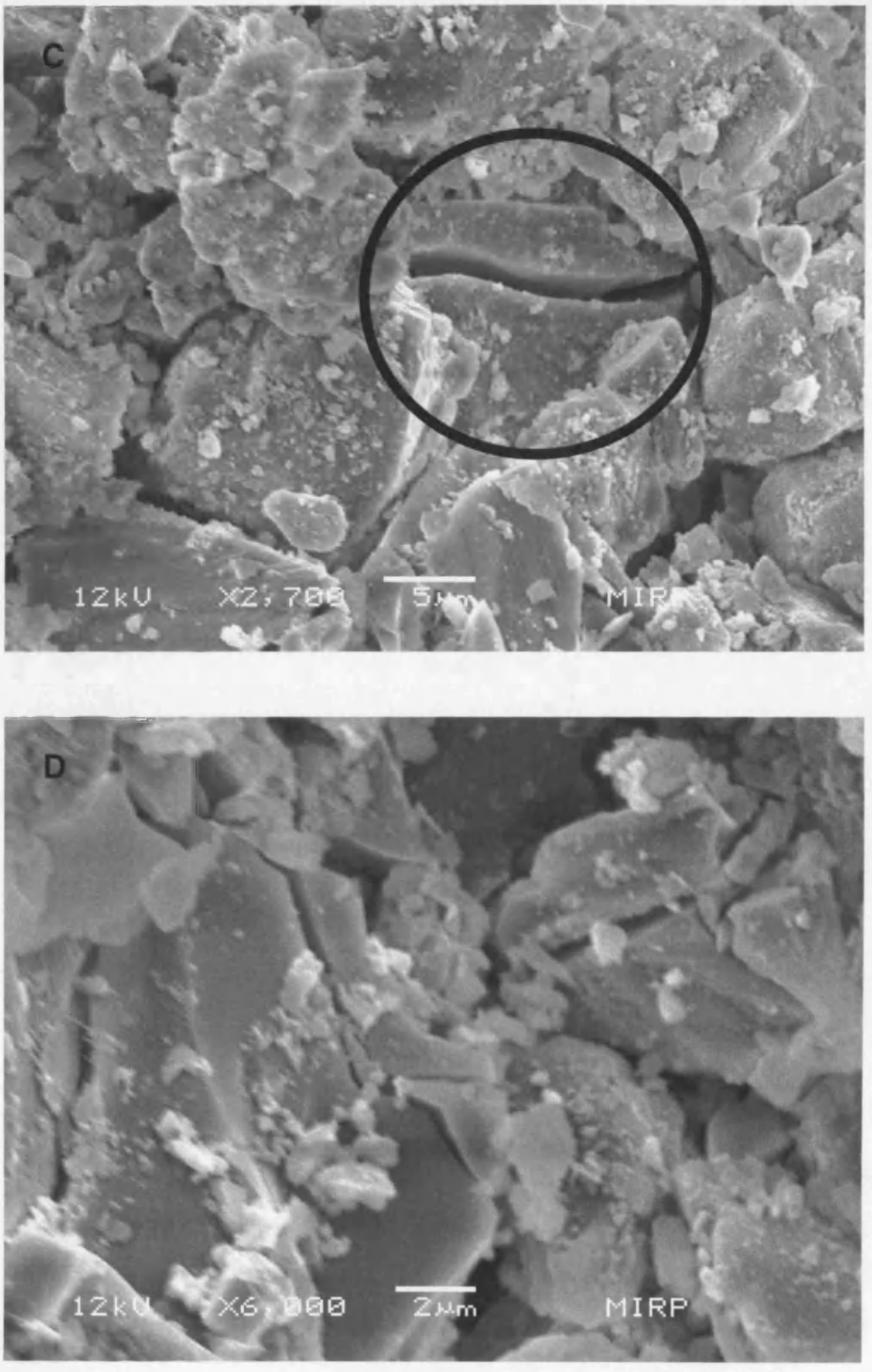

Figure (6-3): Scanning electron microscope images from a sample which was isotropically compressed to 40MPa, increasing magnification from A to D.

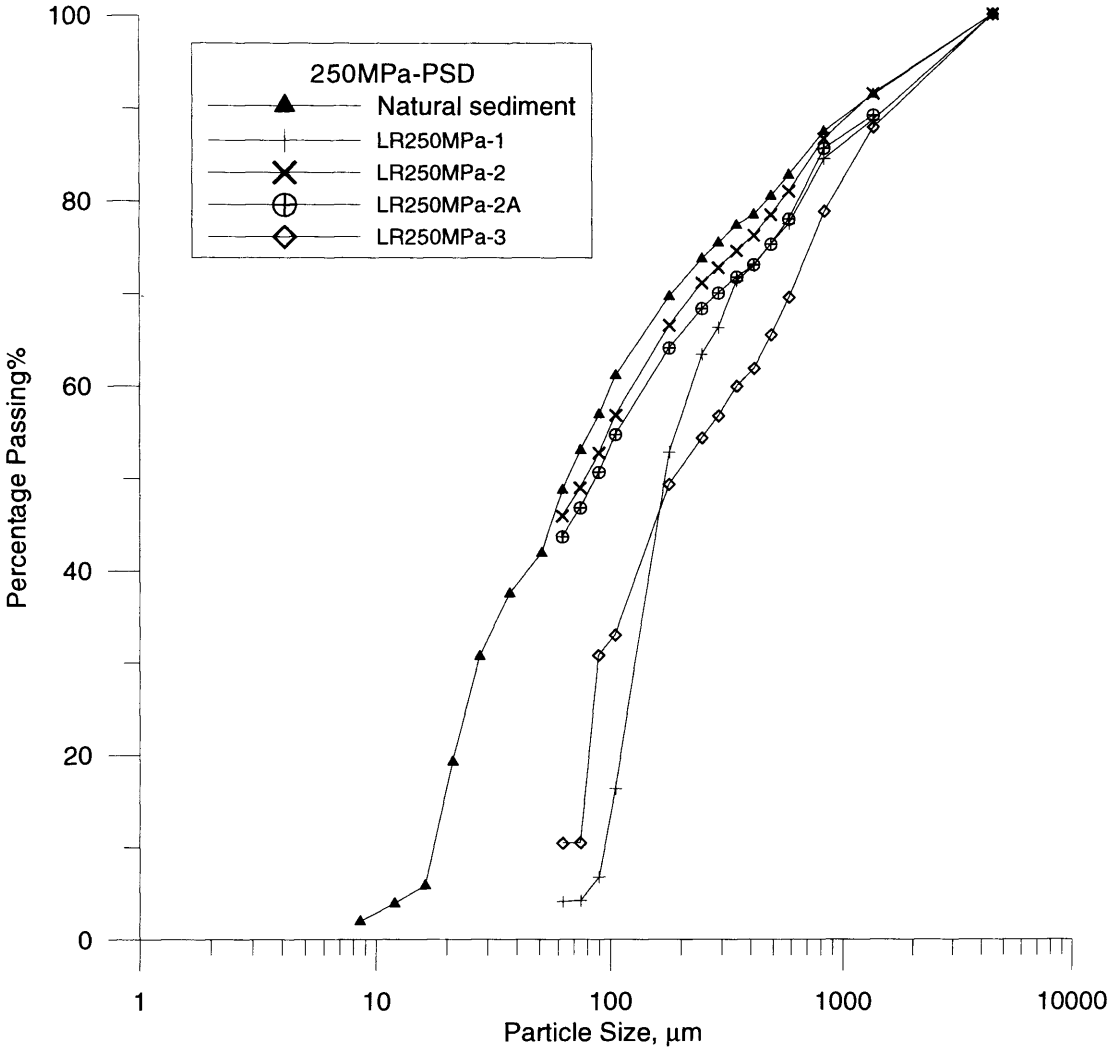

Figure (6-4): Particle size distribution (PSD) after isotropic compression tests by the permeameter and up to 250MPa. The figure also shows the PSD of the natural sediment. Denser samples LR250MPa-1 and LR250MPa-3 showed a reduction in percentage of fines after test due to cold sintering.

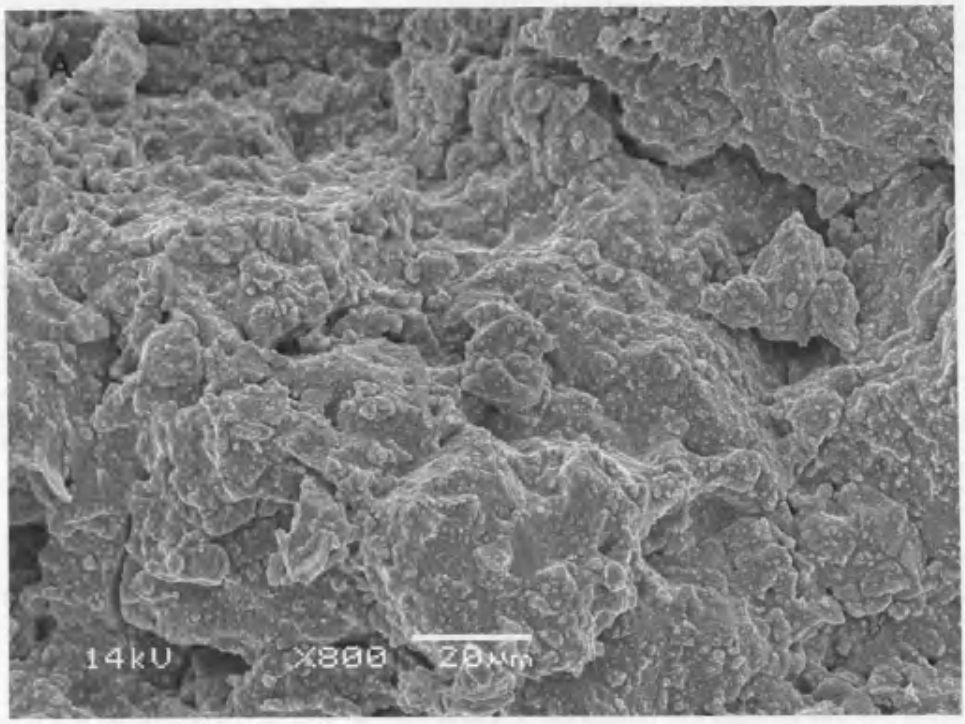
A
14kU X800 20µm

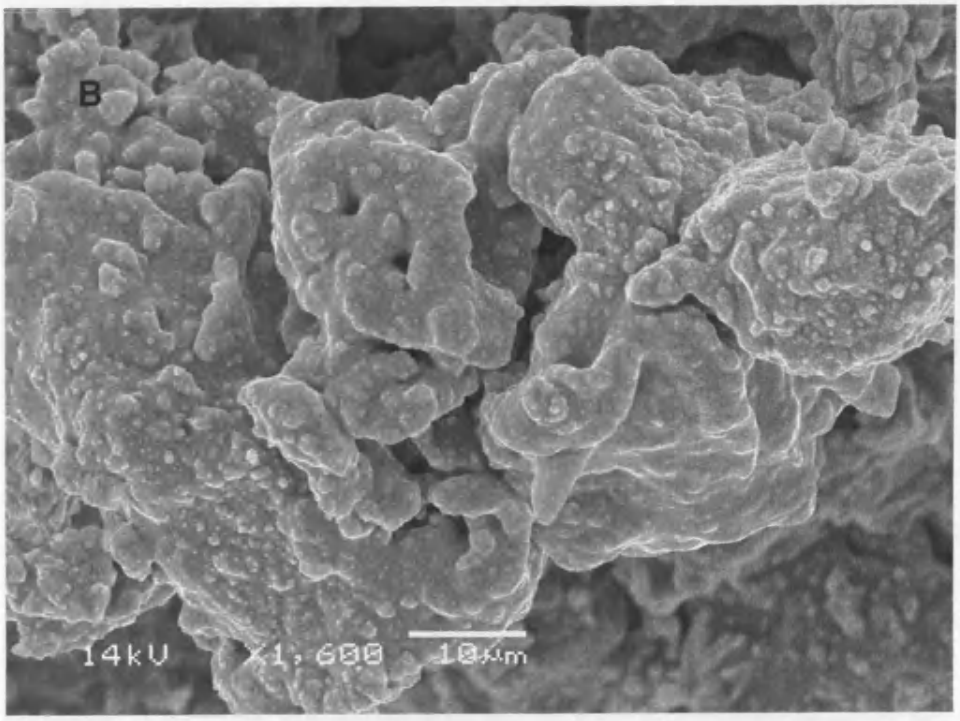
B
14kU X1,600 10µm

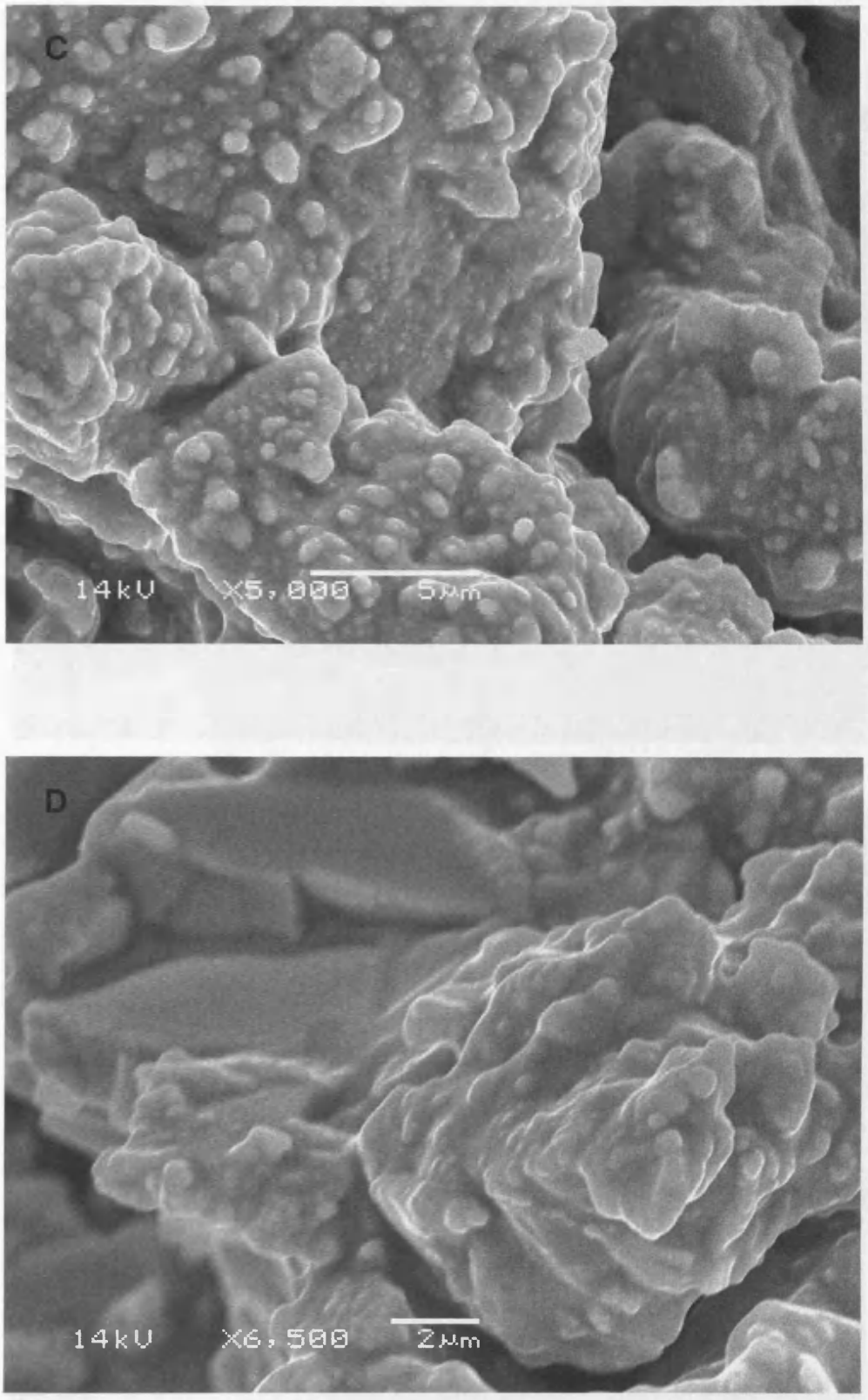

Figure (6-5): Scanning electron microscope images from a sample which was subjected to isotropic compression and up to 250MPa. The sample (LR250-1) showed a reduction in percentage of fines after test due to cold sintering. Increasing magnification from A to D.

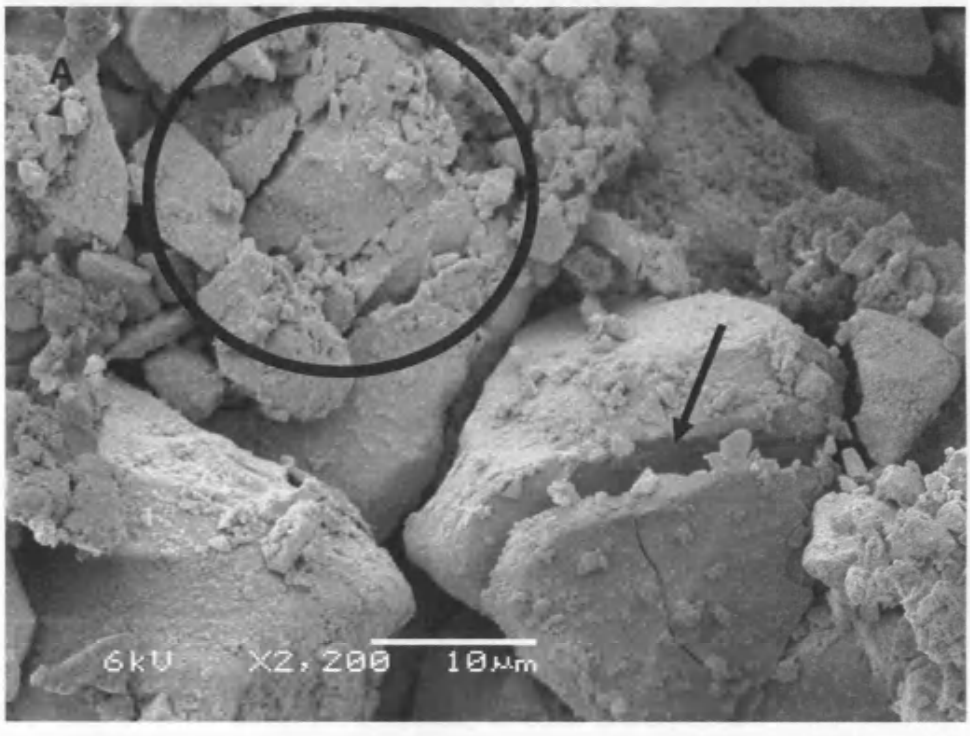
A
6kV X2,200 10µm

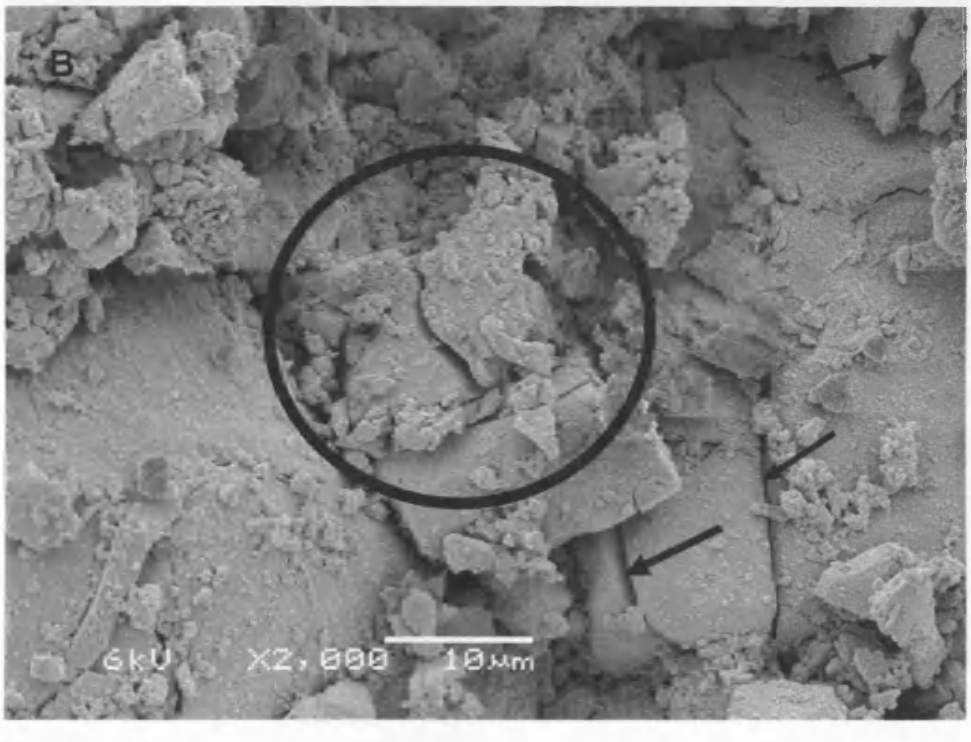
B
6kV X2,000 10µm

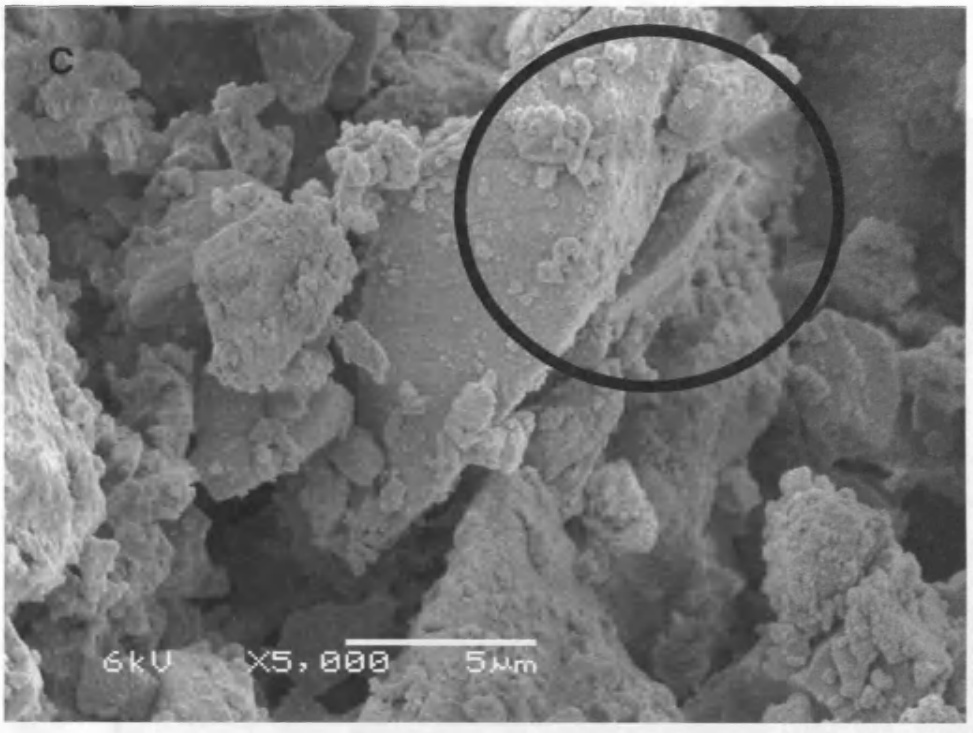

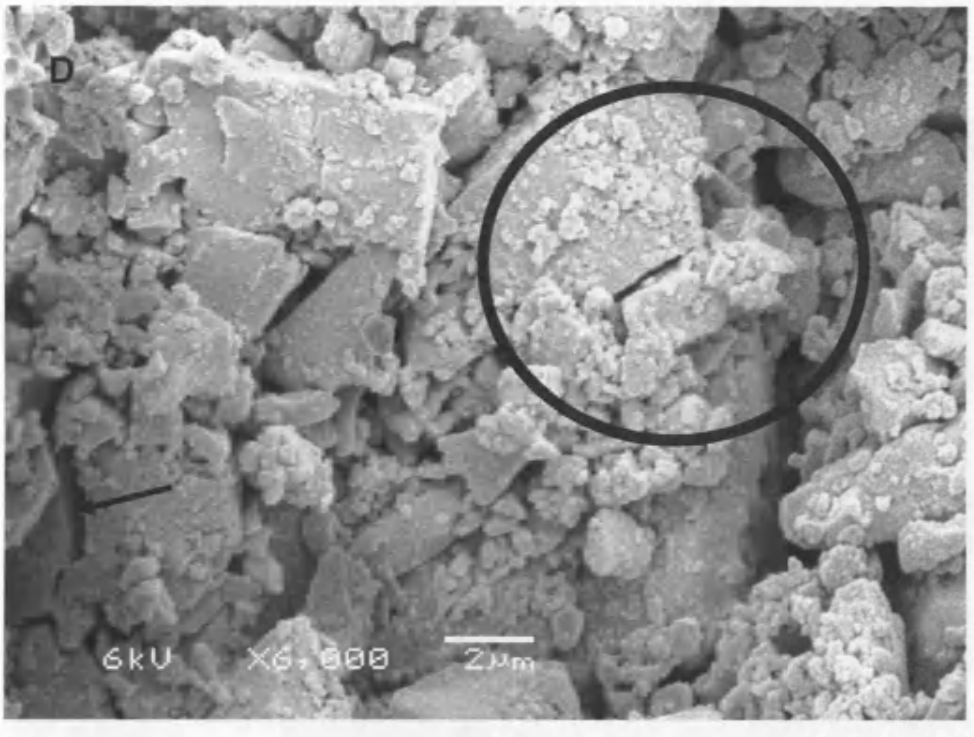

Figure (6-6): Scanning electron microscope images from a sample which was subjected to isotropic compression and up to 250MPa. The sample (LR250-2) showed insignificant particle breakage which did not change its particle size distribution. Magnification increased from A to D.

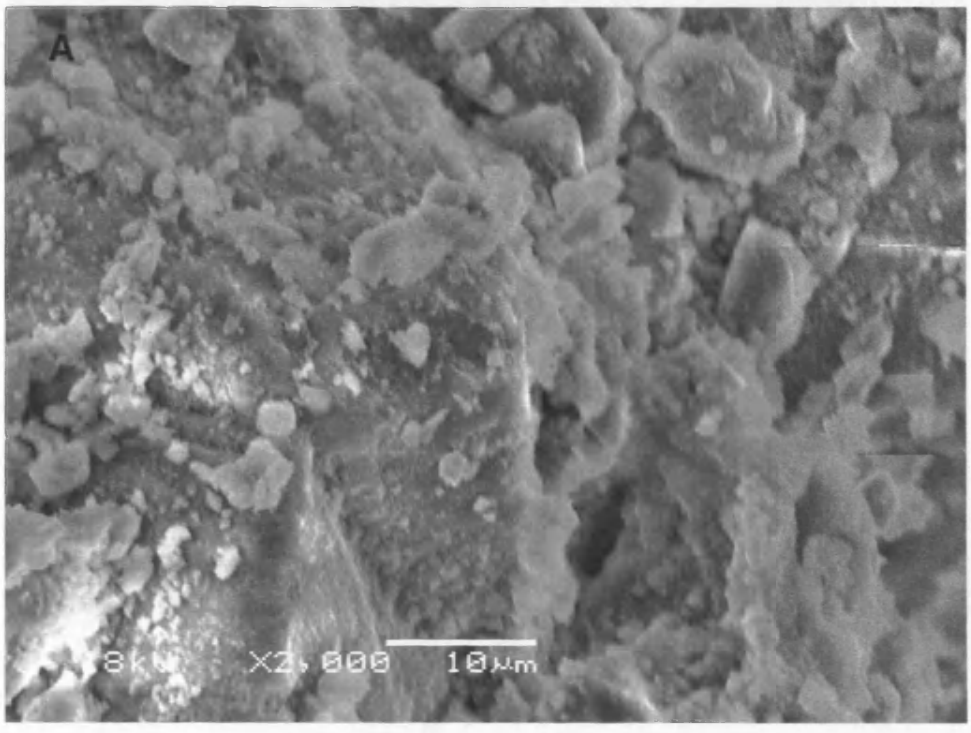
A
8kV X2,000 10µm

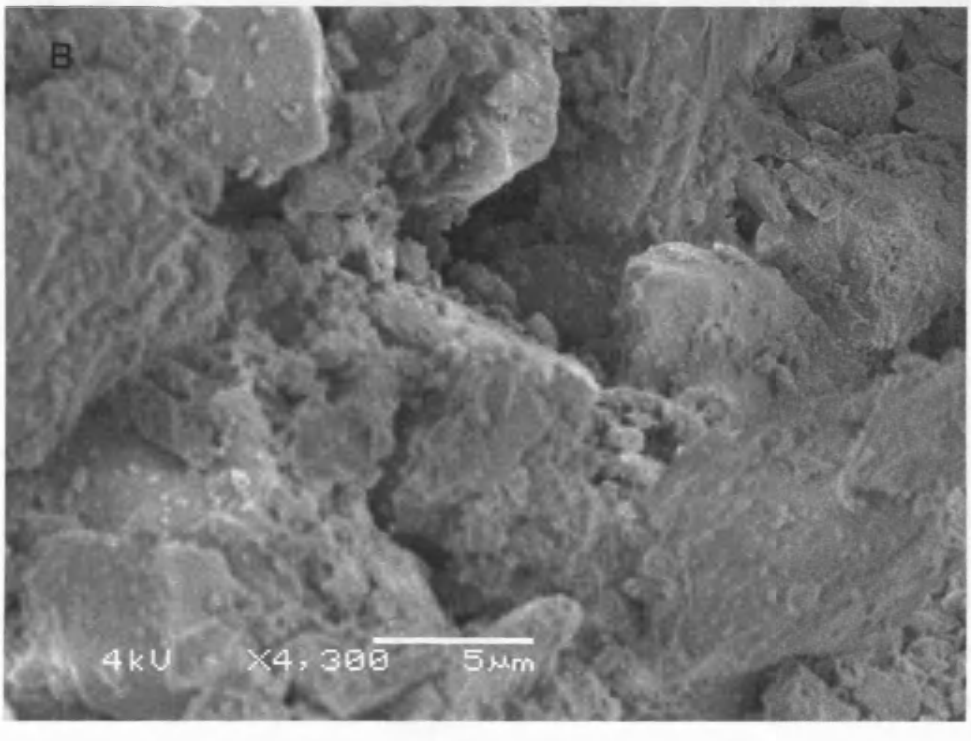
B
4kV X4,300 5µm

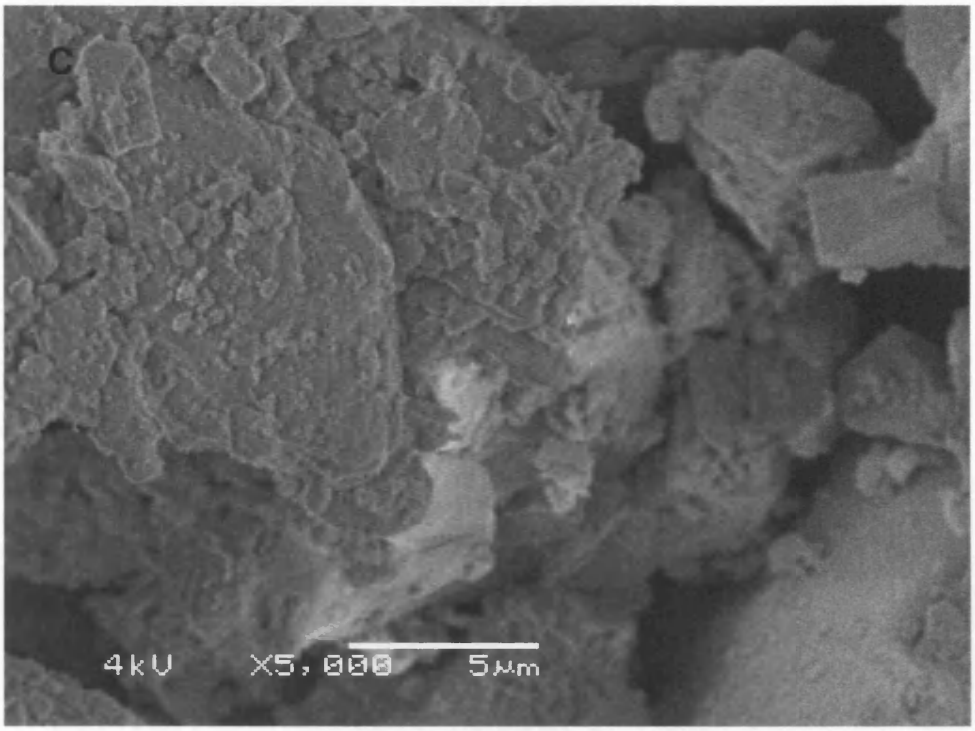

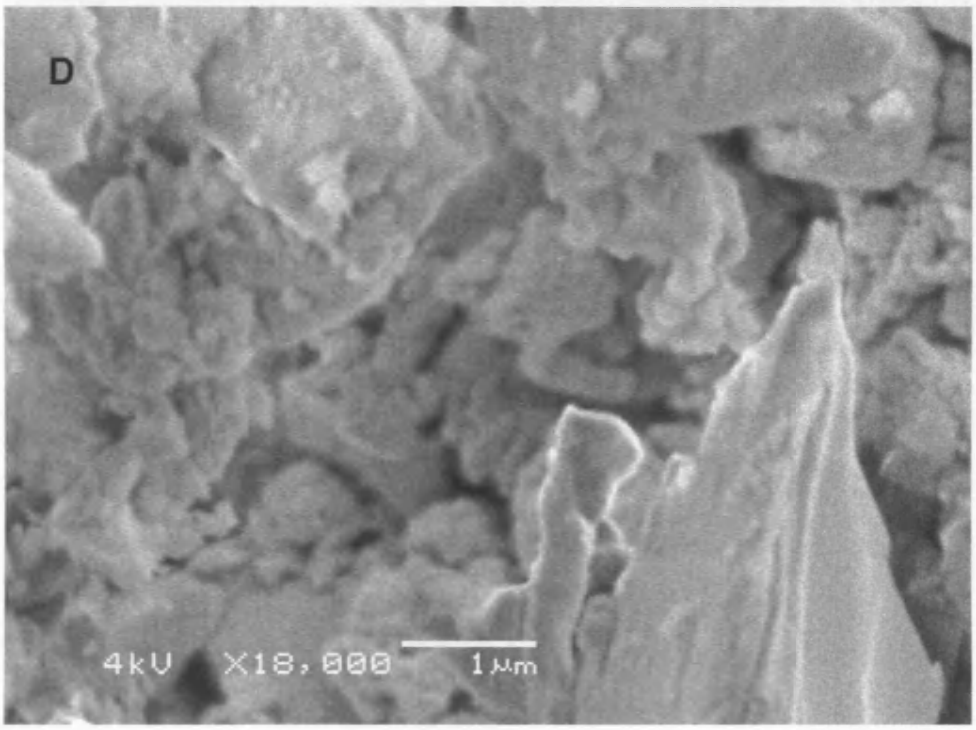

Figure (6-7): Scanning electron microscope images from a sample which was subjected to isotropic compression and up to 250MPa. The sample (LR250-2A) showed insignificant particle breakage which did not change its particle size distribution.

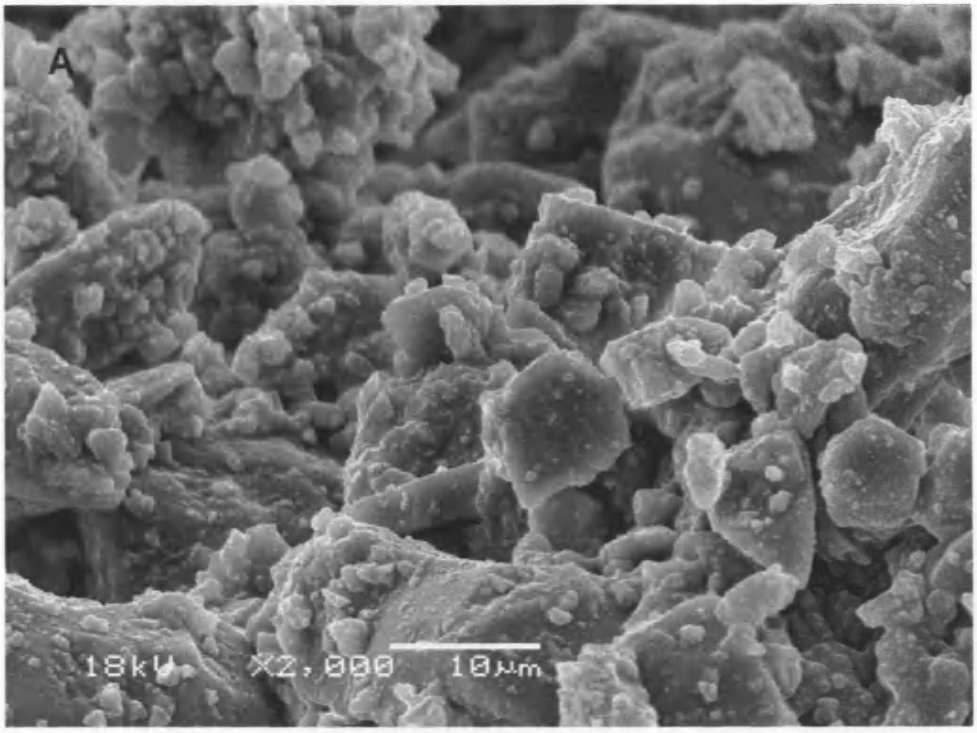
A
18kV X2,000 10µm

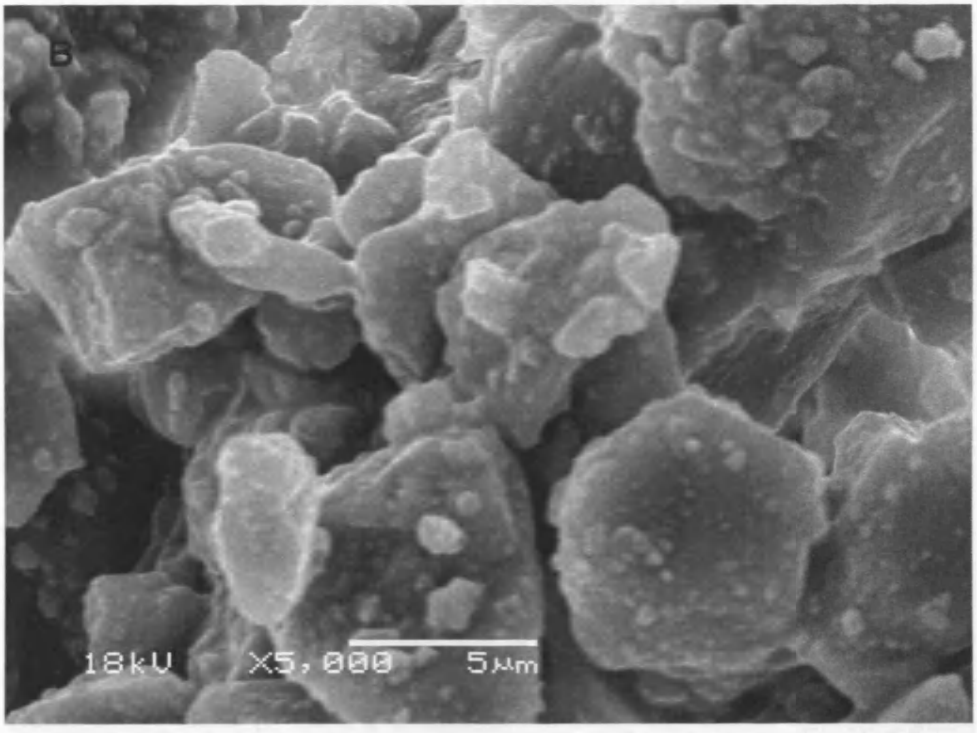
B
18kV X5,000 5µm

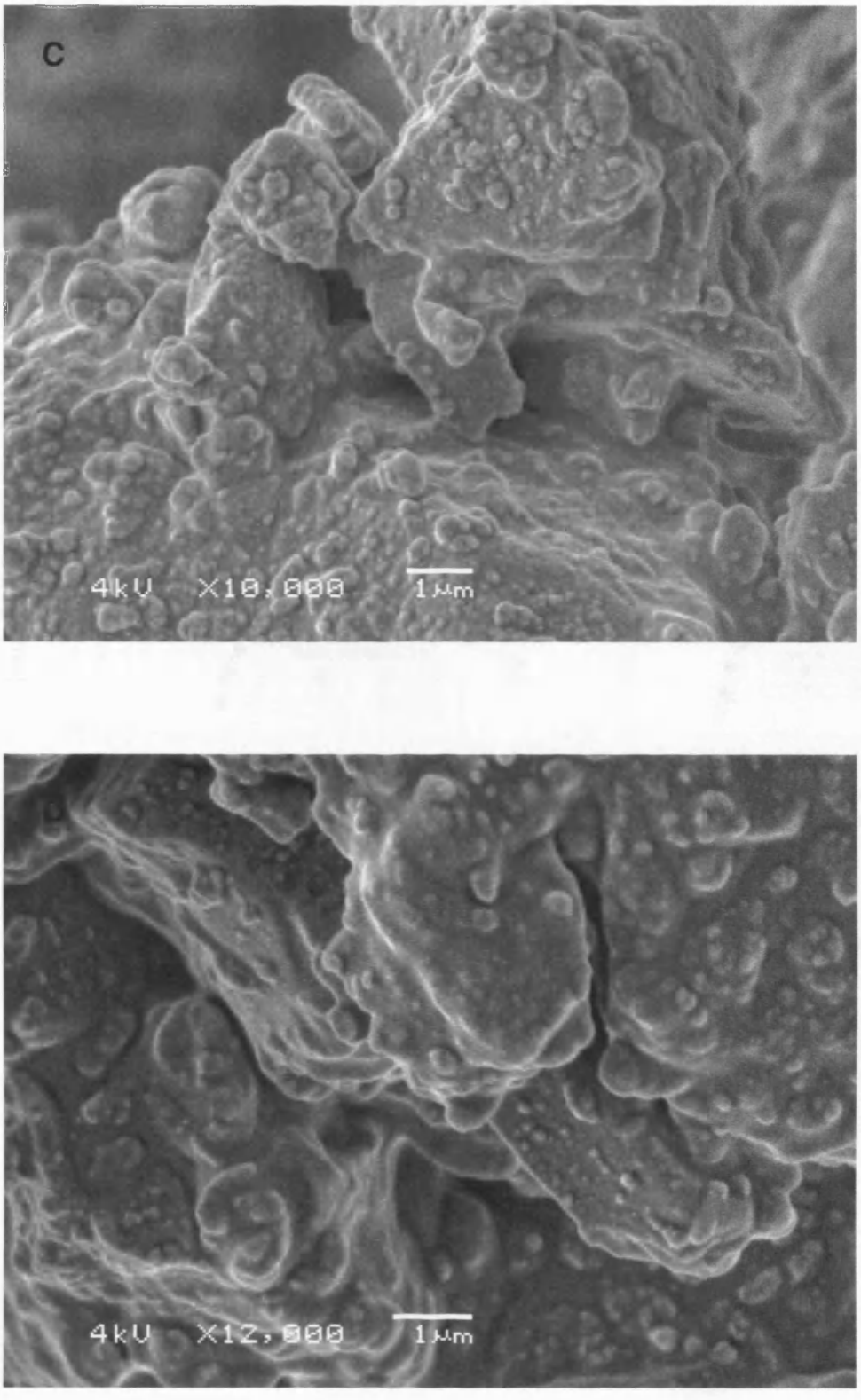

Figure (6-8): Scanning electron microscope images from a sample which was subjected to isotropic compression and up to 250MPa. The sample (LR250-3) showed a reduction in percentage of fines after test due to cold sintering. Magnification increased from A to D.

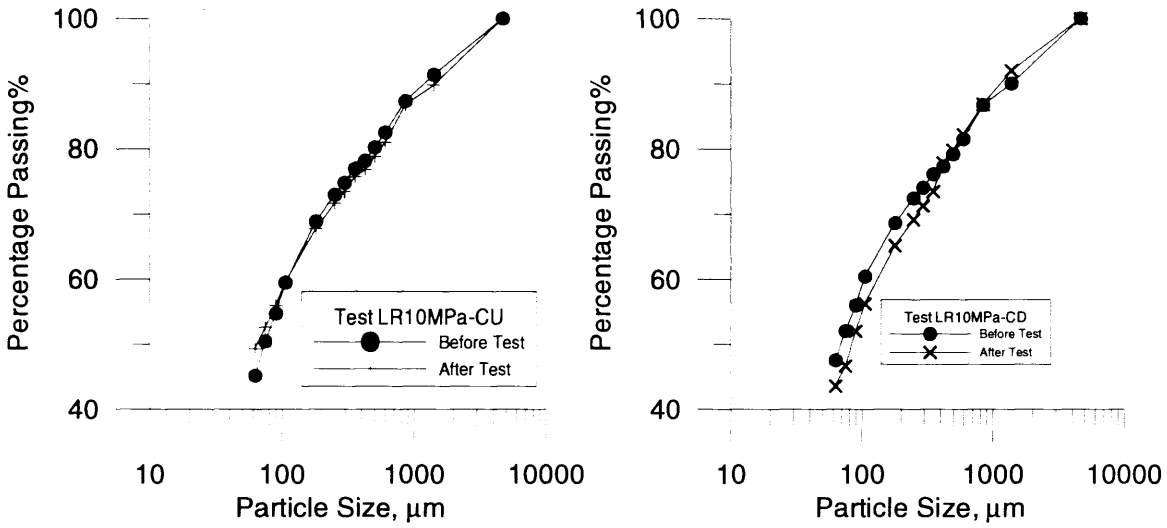

Figure (6-9): PSD curves before and after undrained and drained shearing under confining pressure of 10MPa. The figure shows no change in PSD curves due to shearing.

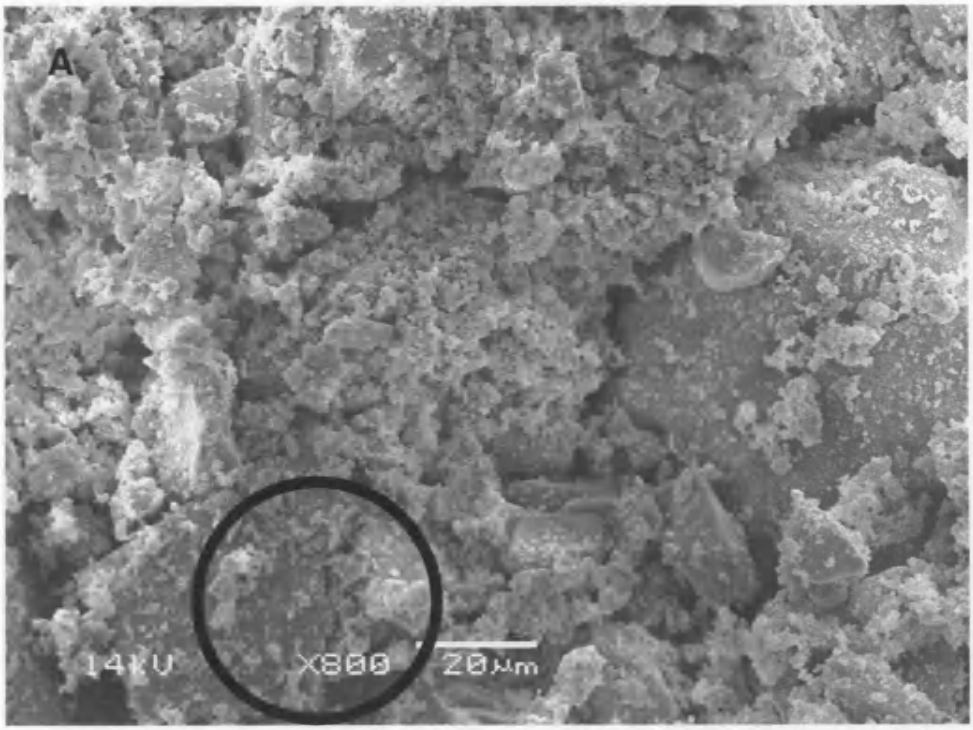
A
14kV X800 20µm

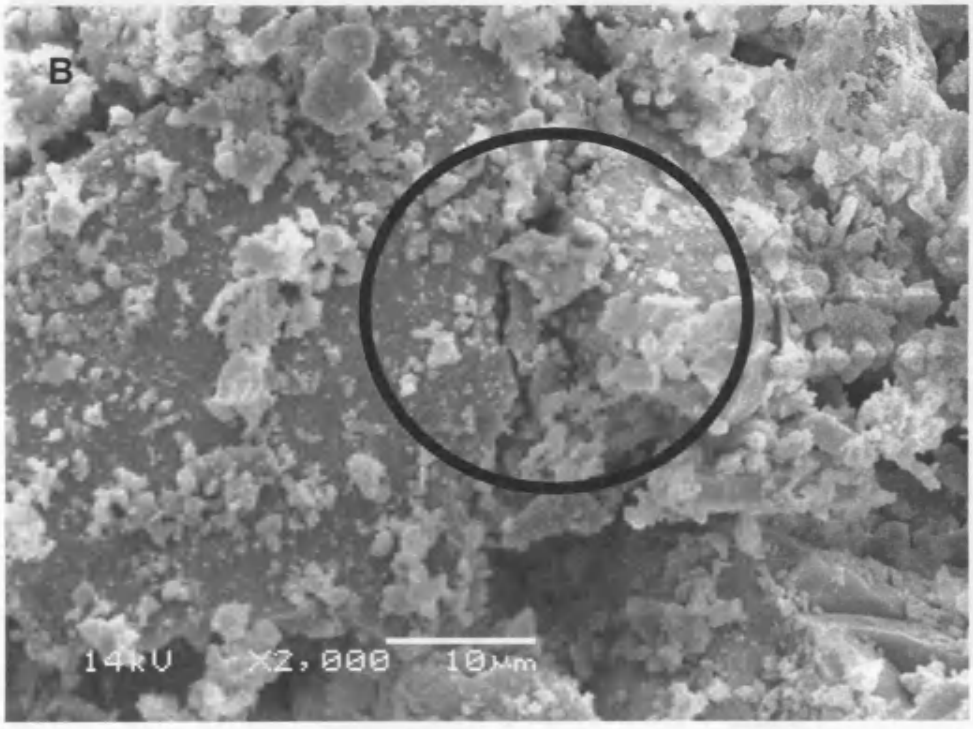
B
14kV X2,000 10µm

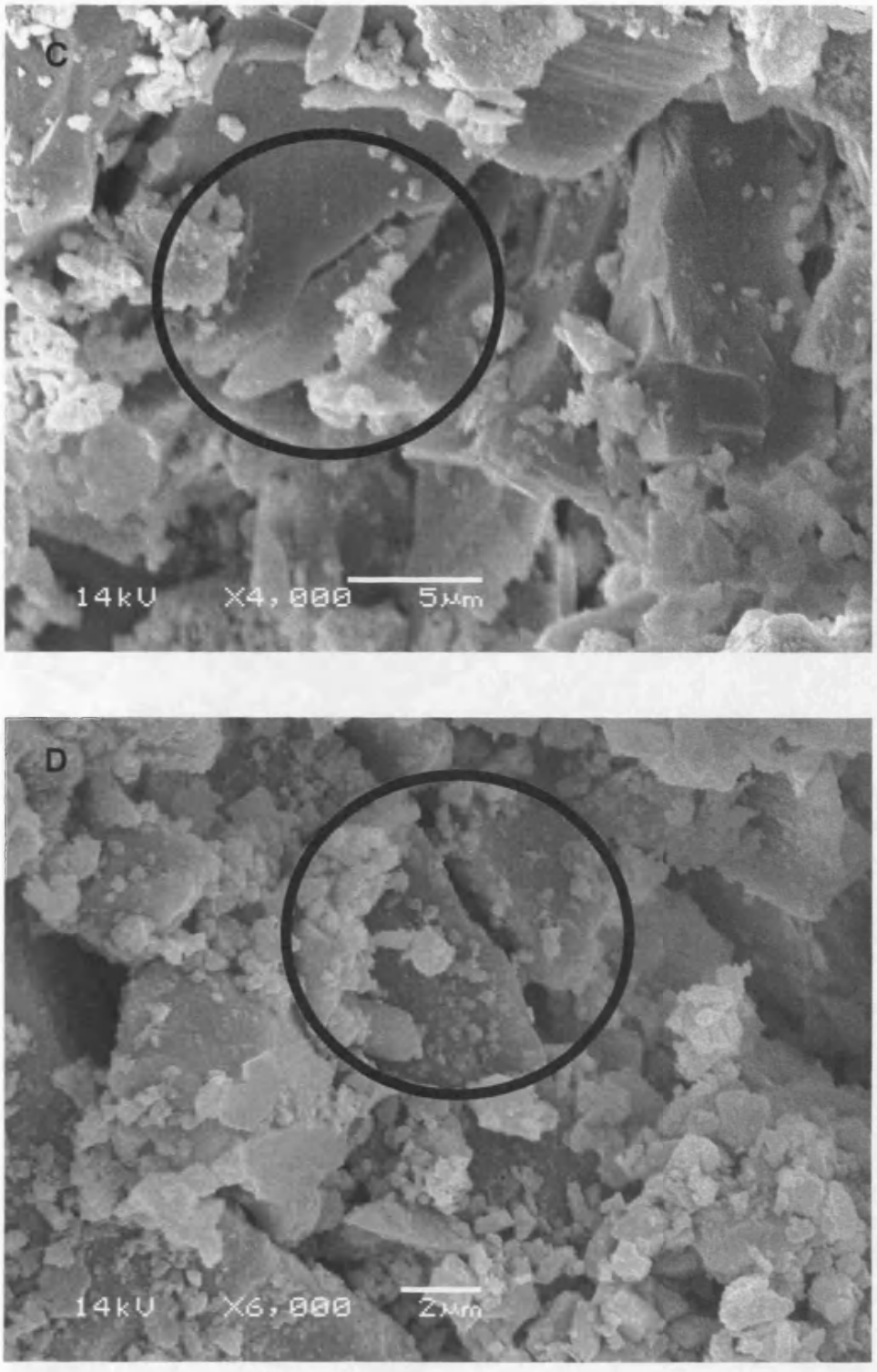

Figure (6-10): Scanning electron microscope images showing particle breakage in a remoulded sample which was sheared in undrained conditions under 10MPa confining pressure.

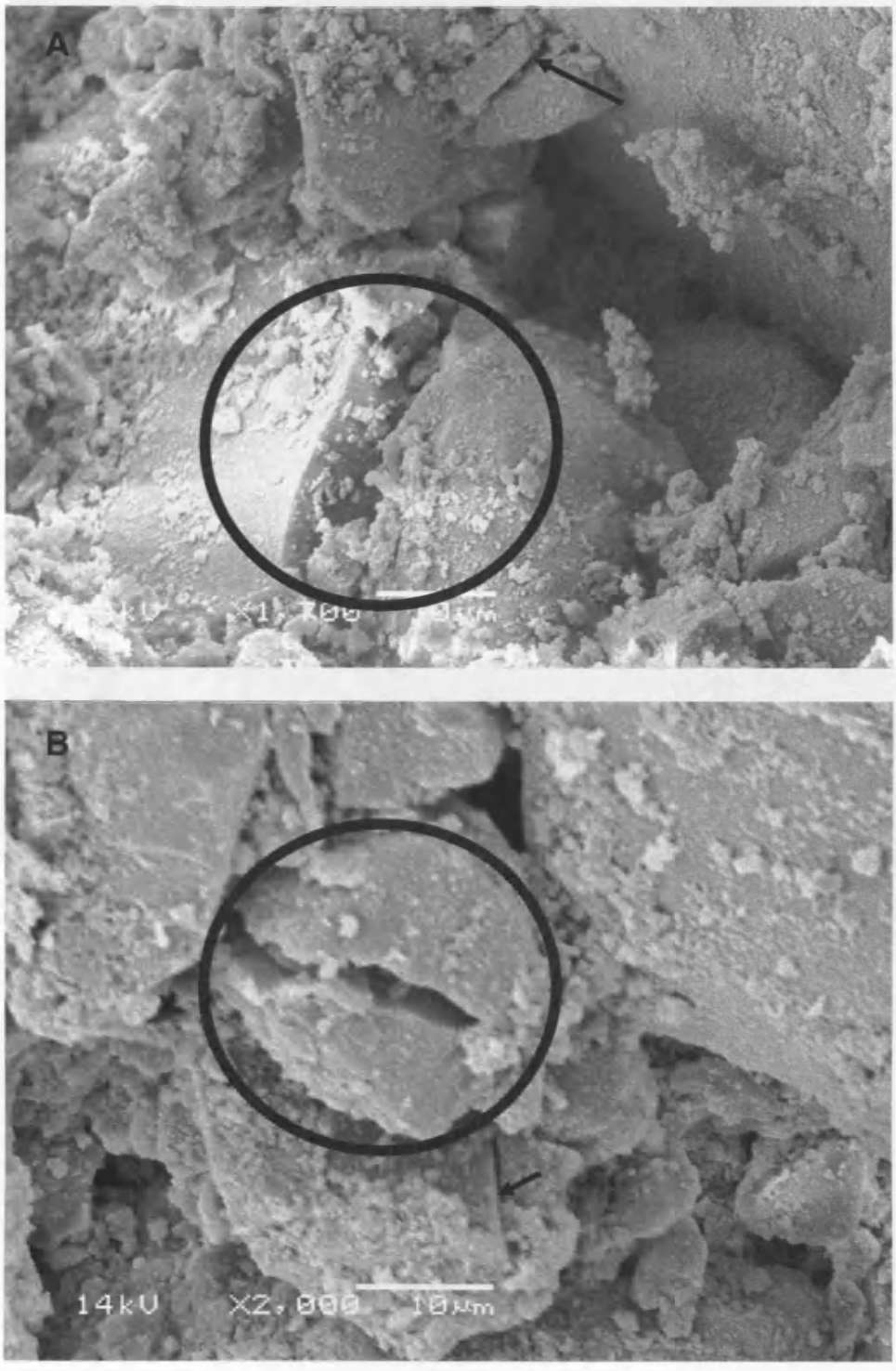
A
B
14kU X2,000 10μm

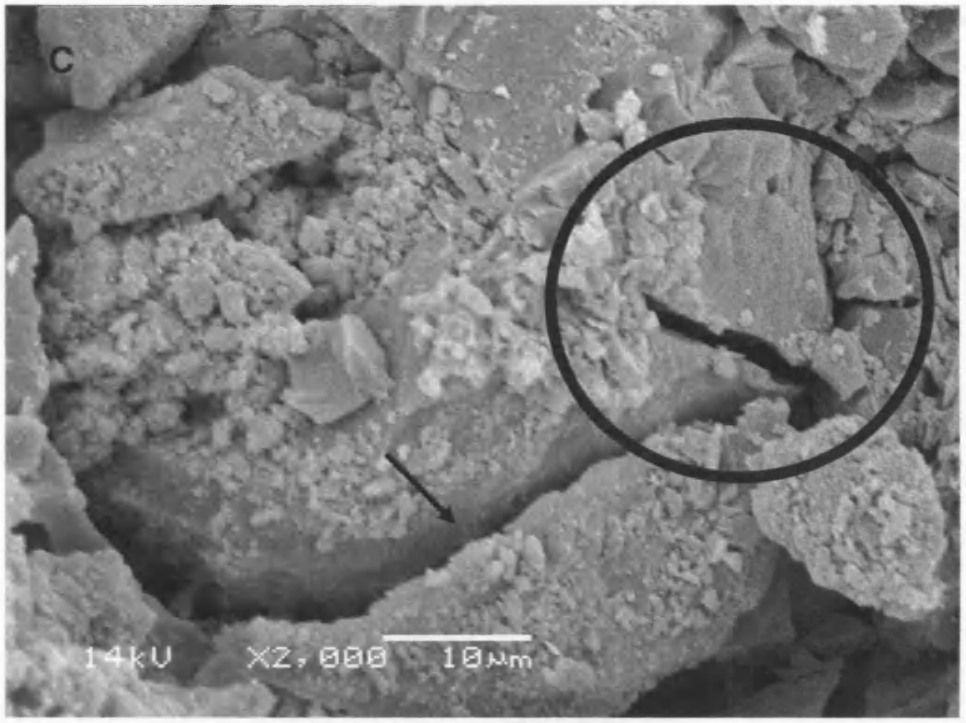

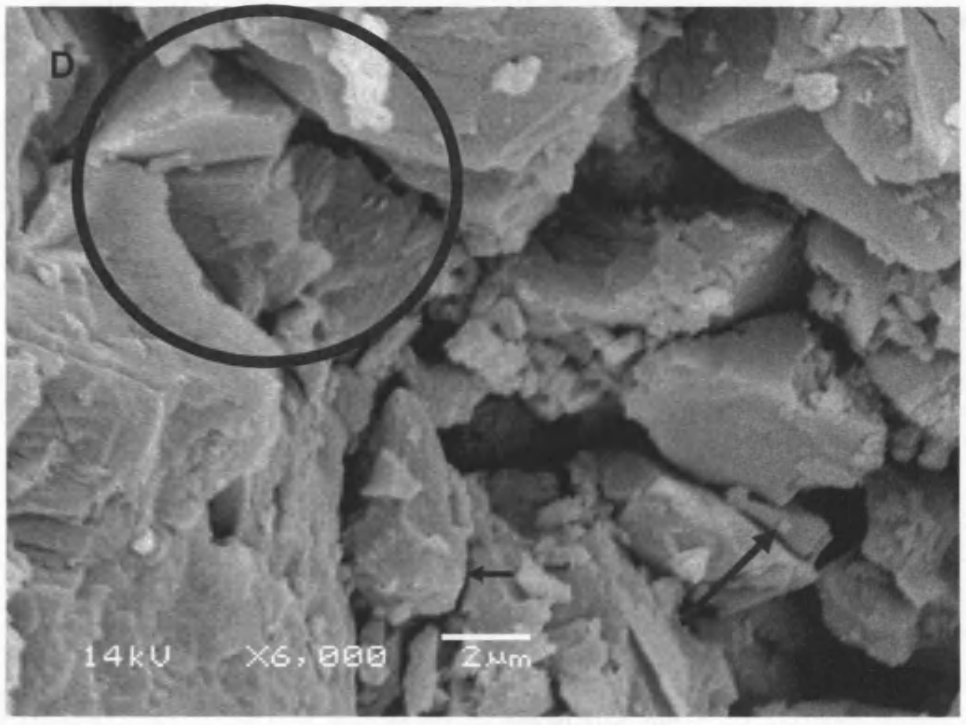

Figure (6-11): Scanning electron microscope images showing breakage in undisturbed sample which was sheared in drained condition under confining pressure of 10MPa.

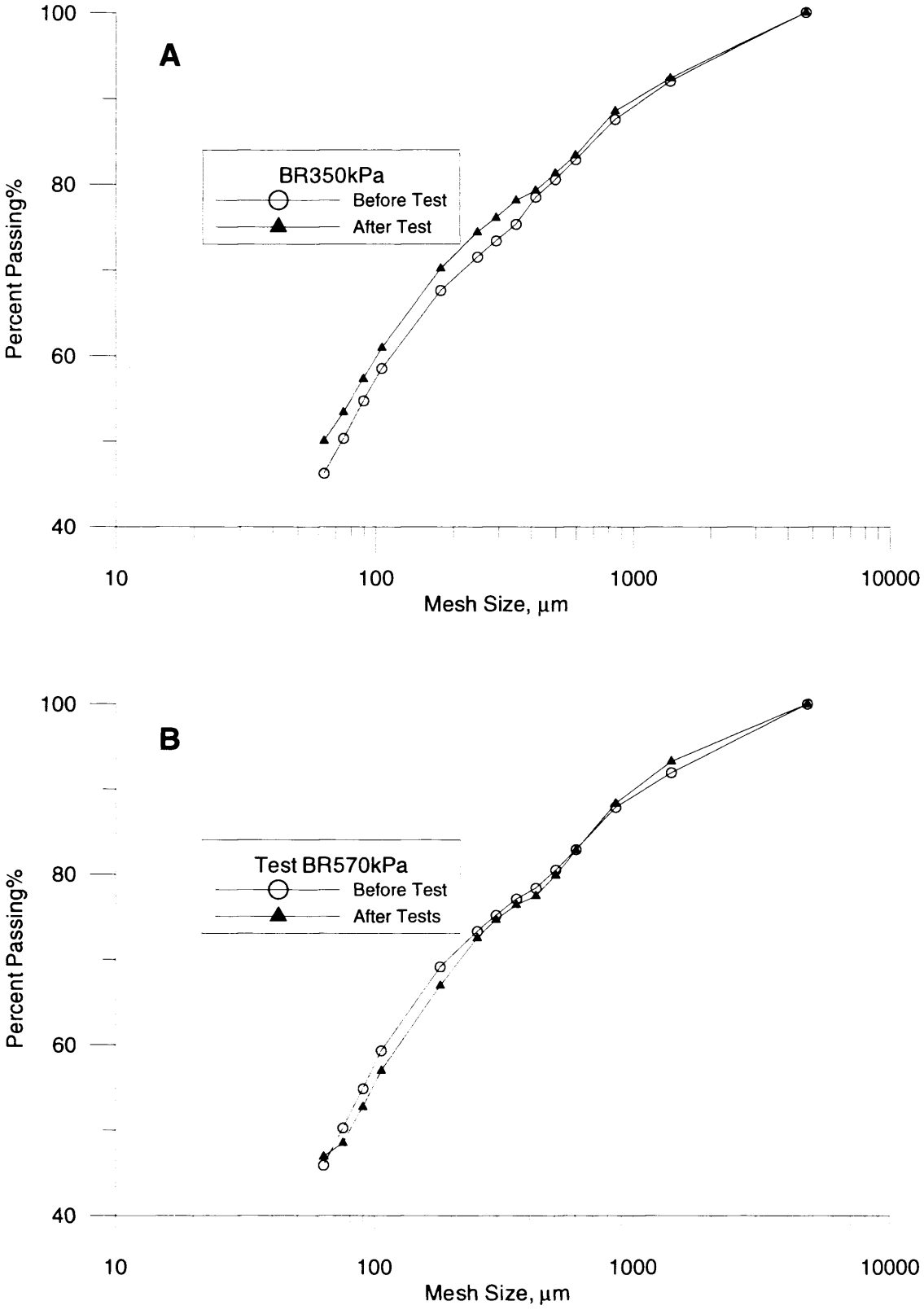

Figure (6-12): Particle size distribution before and after shearing to 50,000% strain in the ring shear apparatus A) For test BR350kPa B) For test BR570kPa.

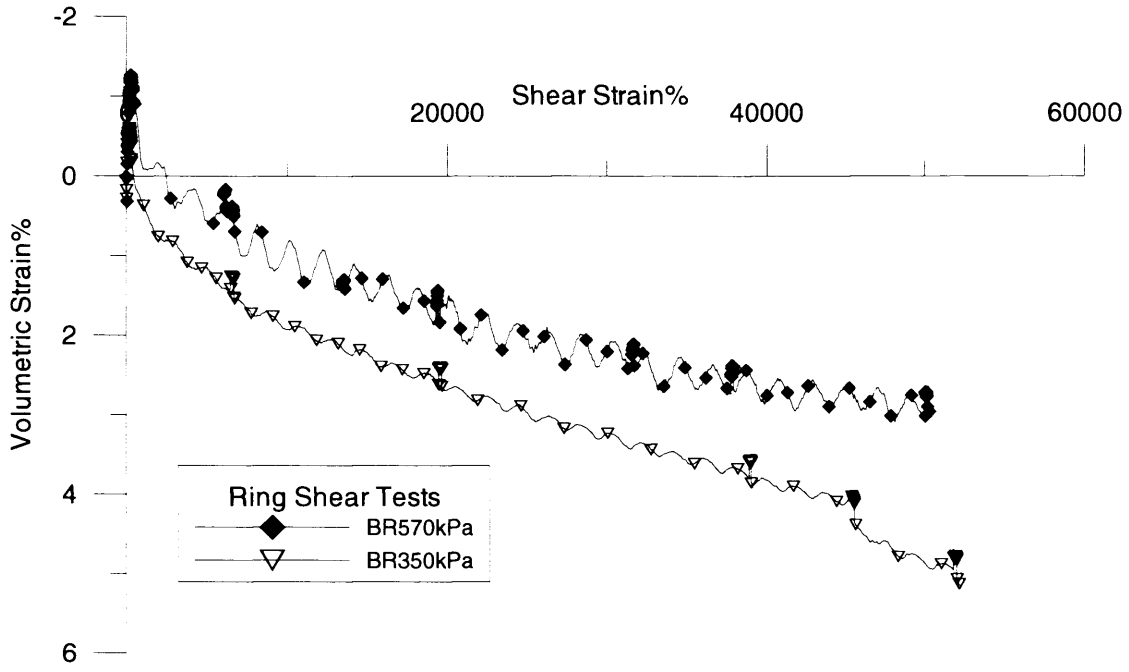

Figure (6-13): Volumetric strain versus shearing strain during tests BR570kPa and BR350kPa.

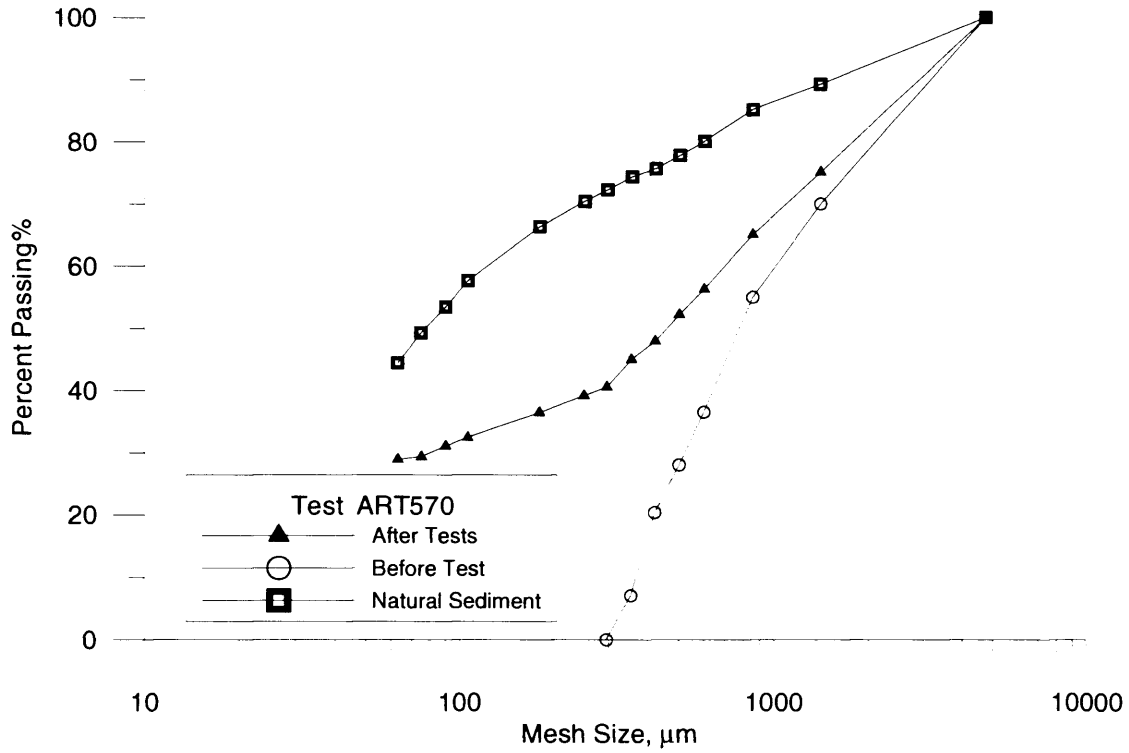

Figure (6-14): Particle size distribution of sample before and after test ART570, the figure also shows the PSD curve for the natural sediment for comparison.

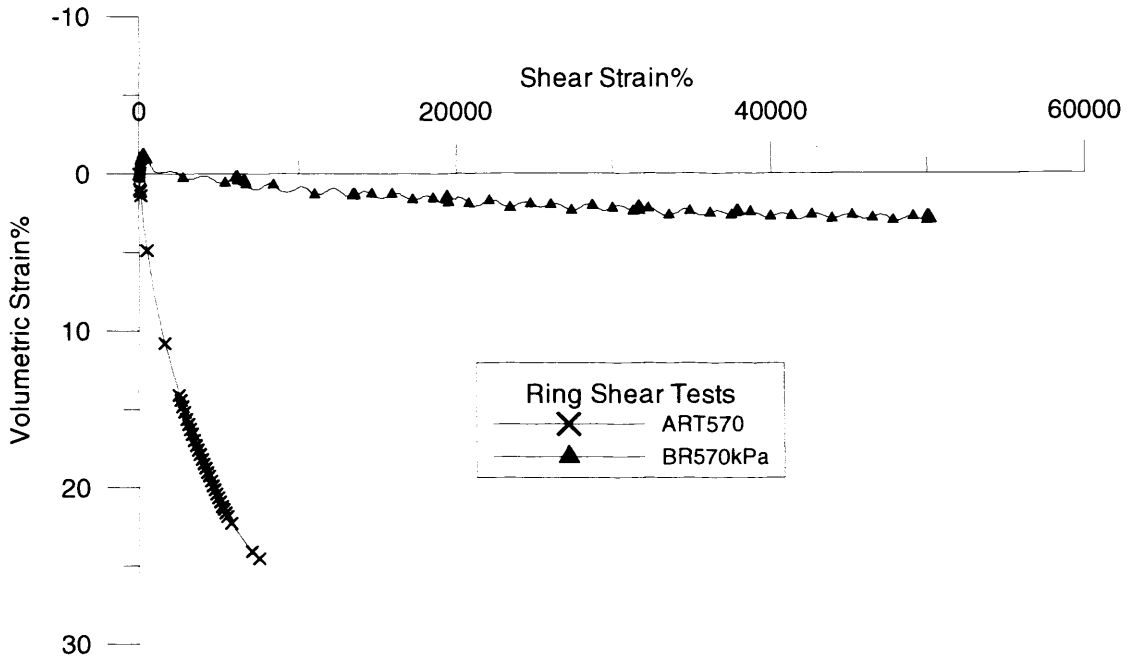

Figure (6-15): A comparison between volumetric strains obtained during shearing tests on natural and artificially graded sediment in the ring shear apparatus.

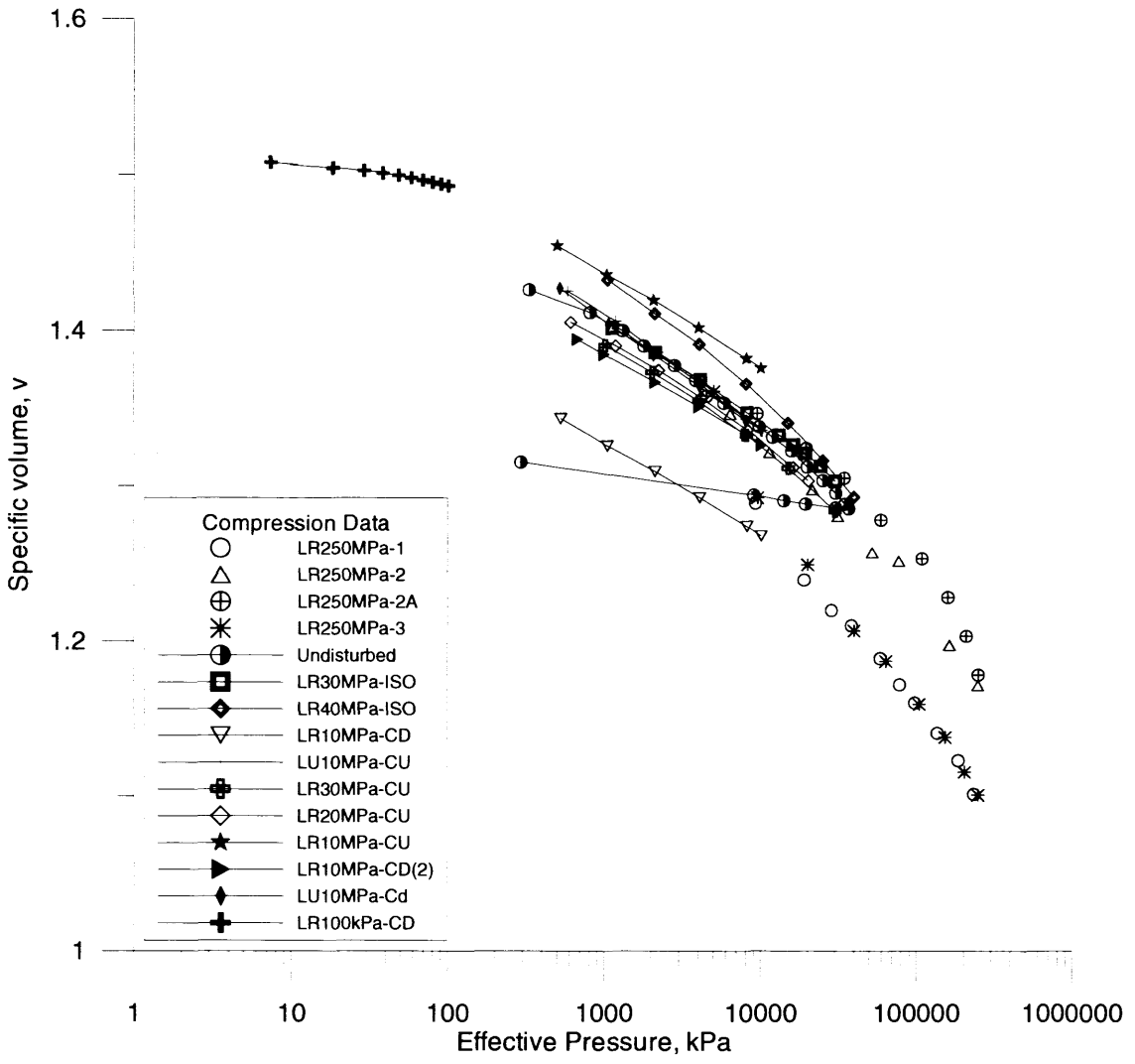

Figure (6-16): Isotropic compression curves of natural sediment of Langjökull. No unique Normal Compression Line was detected for the natural sediment. The compression curves seem to be parallel and they do not seem to converge at any pressure level up to 250MPa.

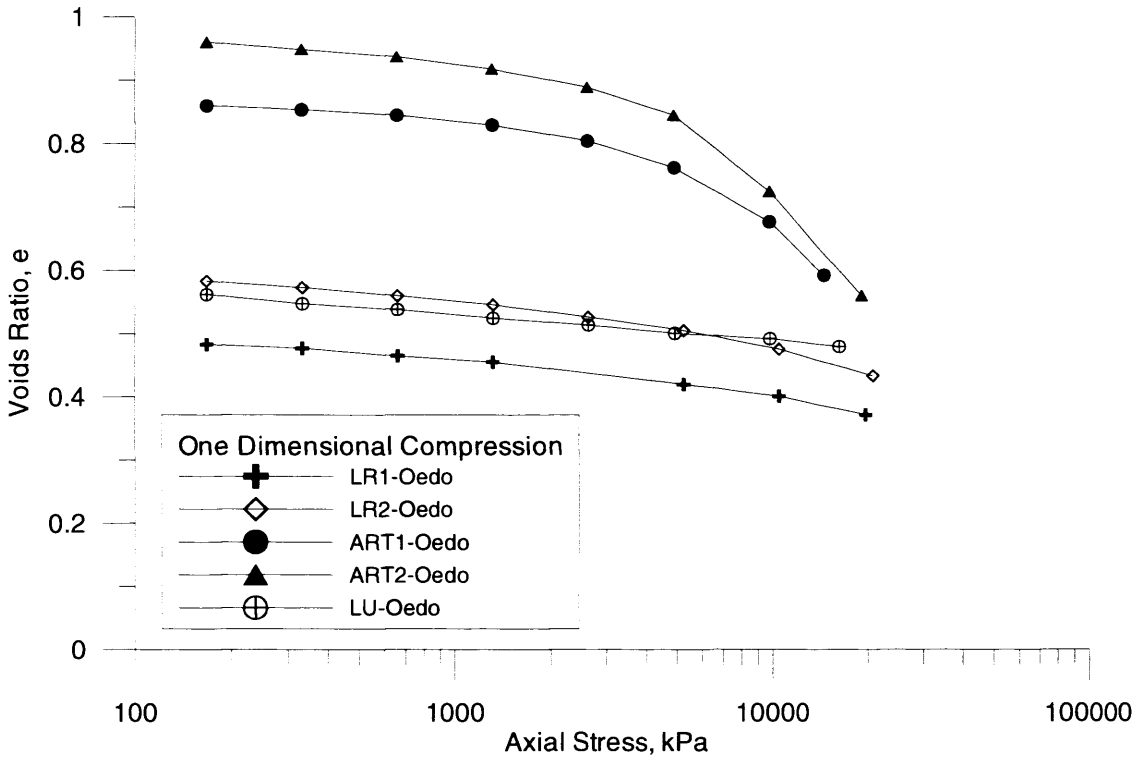

Figure (6-17): One-dimensional compression data of natural sediment of Langjökull (undisturbed and remoulded) and compression curves of artificially graded samples. The artificially graded samples show a clear yielding point with a tendency to form a unique Normal Compression Line.

Chapter Seven

Sediment behaviour during shearing

7.1 Introduction

The behaviour of the Langjökull sediment during shearing needs investigating for a better understanding of the sediment's effect on glacial deformations. The fact that the subglacial sediment of Langjökull has no unique Normal Compression Line, as was shown from compression tests in Chapter Six, questions the validity of the Critical State framework for this sediment, and whether a clear boundary surface (e.g. Roscoe surface (Roscoe et al., 1958) & Hvorslev surface (Hvorslev, 1937)) can be defined for this sediment. In this chapter, the uniqueness of the Critical State Line is examined, and its implication for the validity of the Critical State framework for the sediment.

In addition, the sediment's dilatancy is addressed in terms of the effect of the sample density and pressure on the behaviour of samples during shearing. This will give another insight into the behaviour of the Langjökull sediment, which might help interpret some of the phenomena observed in subglacial deformations such as ploughing and some large particles' (clasts) arrangements, associated with the deformable beds (Hart, 1995).

Most geophysical research which studied the shear strength of subglacial sediments (e.g. Kamb, 1991; Tulaczyk et al., 2000; Tulaczyk, 1999; Iverson et al., 1994; Iverson et al., 1998) did not address the issue of the Critical State Line and all the related parameters which need to be considered when studying the behaviour of the sediment during shearing. On the other hand, geotechnical research on granular soils has associated the Normal Compression Line and the Critical State Line with particle breakage in the sediment. It was shown in Chapter Six that Langjökull sediment has reached its terminal grading, and that it cannot experience further significant

breakage, even when sheared to high strains. This implies that reaching a Critical State for this sediment is not associated with any particle breakage (Altuhafi et al., 2006). Additional results from shearing tests are presented in this chapter to clarify the issue of the Critical State Line.

The stress-strain behaviour during drained and undrained compression tests is presented in the next section (7.2). The Critical State Line in the mean effective pressure- deviator stress plane and the stress paths of undrained shearing tests are discussed in Section 7.3. The sediment's Critical State Line in the specific volume (v) – logarithm of the mean effective pressure (ln p') is presented in Section 7.4, with a special reference to the behaviour of the sediment in drained shearing. The change in shearing modulus and Young's modulus during drained shearing is analysed, as well as the stress-dilatancy behaviour during these drained tests. Normalisation of the tests' stress paths (drained and undrained) and the basis of the normalisation adopted are presented in Section 7.5, with a view to defining a state boundary surface for the sediment. The residual strength, which is an important issue in studying deformation in subglacial sediment, is addressed in Section 7.6. Finally, the uniqueness of the Critical State Line of the Langjökull sediment is discussed referring to the implications and consequences in interpreting the overall behaviour of the sediment.

7.2 Stress-strain behaviour during shearing

Triaxial shearing tests were carried out on the Langjökull sediment by using the conventional cell, the high pressure cell and the fully computer controlled cell described in Section 5.4, in which the behaviour of the sediment during both drained and undrained shearing was investigated. In this section the stress-strain behaviour of the sediment during each test is presented.

7.2.1 Drained triaxial compression tests

Figure (7-1) shows the deviator stress-axial strain relation for the tests conducted on the Langjökull sediment (see Table 5-5). The general trend of these data indicates that the higher the effective confining pressure in the test the higher the position of deviator stress curve in the chart, as would be

expected for granular materials. Some differences are observed between the behaviour of the undisturbed sample (LU10MPa-CD) and the remoulded sample, sheared under a similar confining pressure (LR10MPa-CD), at the early stages of tests. However it is quite clear that the deviatoric stresses developed at high strains is tending to reach similar values for both tests, complying with what was found by Verdugo & Ishihara (1996) on drained tests on Toyoura sand. The figure also shows that it is hard to distinguish the curves of tests carried out under the same effective confining pressure of 2MPa (LU2MPa-CD, LR2MPa-CD and LR2MPa-CD), showing good repeatability of the tests. In general all the drained tests exhibited an increase in the deviatoric stress until they reached an ultimate and maximum value at around 10% axial strain, with the tests under lower confining pressure reaching their ultimate value earlier.

Although the general development of the deviatoric stress during these tests appears to be similar, the volumetric strain change during each test (Figure 7-2) indicates that during the tests on the remoulded samples, the samples compressed during the early stages of shearing until the ultimate deviator stress value was reached, then a dilative behaviour is clearly observed afterward. The start of the dilative behaviour is observed when the ultimate deviator stress is reached at around 10% axial strain. Again the slight increase in volume in the tests carried out under 2MPa confining pressure took place earlier at about 8% of axial strain. In other words, the phase transformation points after which the tendency for dilation becomes dominant (Ishihara et al., 1975), is encountered earlier in those tests performed under lower confining pressure. Purely compressive behaviour is observed during the shearing of undisturbed samples (LU10MPa-CD) and (LU2MPa-CD). The lack of the late dilative behaviour in the shearing of undisturbed samples might be due to the effect of undisturbed fabric of these samples.

The test (LR100kPa-CD) is the only drained test conducted under low pressure shown in this thesis, as some problems in measuring accurate volume changes in all other drained tests carried out in the conventional cell were encountered, which resulted in inaccuracy of the data obtained. This

test, which had a void ratio of 0.49 at the start of shearing, showed again a pure compressive behaviour during shearing (Figures 7-3, 7-4). This was indicated by the increase in volumetric strain with the development of deviatoric stress.

Some of the differences and similarities in the behaviour of the samples during shearing can be interpreted by considering the void ratio of each sample at the beginning of the shearing stage. For tests (LR2MPa-CD) and (LR2MPa-CD(Dense)), two samples both sheared under 2MPa confining pressure, it was observed that the denser sample would exhibit less contraction before starting to dilate. However the phase transformation point during the shearing of the loose sample is encountered earlier (at about 7% of axial strain), than in the dense sample (at about 9% of axial strain).

7.2.2 Undrained triaxial compression tests

The deviatoric stress-axial strain relations for undrained shearing tests at high pressures are shown in Figure (7-5). Although the general trend for these relations looks similar to those observed in drained tests, and the higher confining pressures during the tests, the higher ultimate deviatoric stress values, it is clear that in those tests, the ultimate deviator stress did not develop until high strains were reached. And for the tests under high confining pressures of 20MPa and 30MPa, the values of deviator stress were still increasing when the tests were terminated at 20% and 28% axial strain respectively, due to the limited capacity of the apparatus. When the development of pore water pressure is considered for each test (Figure 7-6), it can be observed that the samples started their dilative behaviour before reaching their ultimate deviator stress. Similar to what was observed in the drained shearing tests, the phase transformation points (Ishihara et al., 1975) are encountered earlier when shearing under lower confining pressure. The dilative behaviour, as indicated by the reduction of the developed pore water pressure, is also found to be higher in tests performed under high confining pressure. The behaviour of the undisturbed sample (LU10MPa-CU) seems to be similar to the remoulded sample (LR10MPa-CU), which was sheared

under similar confining pressure, in terms of both developing deviatoric stress and pore water pressure.

Figures (7-7) and (7-8) show results from three undrained shearing tests on remoulded samples of Langjökull sediment under low confining pressures. Sample (LR4-CU), which had the highest void ratio of the three remoulded samples, was sheared under 100KPa of confining pressure. The sample showed a compressive behaviour all through out the test, but after exhibiting a peak value in deviator stress, it strain-softened to a minimum strength. Although the test was terminated before reaching the ultimate deviator stress value in this test, it is still clear that this sample is behaving in a similar way to the loose samples of Toyoura sand (Verdugo & Ishihara, 1996), see Section (2.3.1). Samples (LR3-CU) and (LR2-CU) which were sheared under 450kPa and 215kPa respectively, exhibited a clear dilative behaviour (from about 2.5% axial strain), before developing their maximum strength. The dilative behaviour in the denser sample (LR3-CU) was found to be more severe than in the looser sample (LR2-CU).

The undisturbed samples (LU1-CU) and (LU2-CU) developed their maximum strength during undrained shearing at about 9% and 5% of axial strain respectively, as shown in Figures (7-9) & (7-10). Similarly to what was observed in the behaviour of the remoulded samples, the denser sample at the start of shearing (LU1-CU), with a void ratio at the beginning of shearing e= 0.43, exhibited a clear dilative behaviour when compared with the behaviour of sample (LU2-CU) (e= 0.50).

The stress ratio (q'/p') development during all tests is shown in Figure (7-11). It is fairly clear that all tests ultimately tend toward a unique value of stress ratio, which corresponds to the M value that defines the slope of the Critical State Line in the p'-q' plane, and is about 1.4 for this sediment. The figure also shows the development of a peak value of stress ratio for those samples which exhibited dilatancy during shearing, before the M value stress ratio was reached, as for example in test (LR3-CU).

7.3 Critical State Line (CSL) in the p′-q′ plane and stress paths during undrained shearing

The stress paths of the drained and undrained triaxial compression tests carried out under high confining pressure, which were discussed above, are shown in Figure (7-12). The stress paths of undrained shearing tests could be characterised by a predominating compressive behaviour during the early stages of shearing which is indicated by the stress path movement to the left, until it reaches the phase transformation point. As was mentioned above the phase transformation points for tests performed at higher initial confining pressures are encountered at relatively higher strains, which reflect the increase in compressive phase magnitude with the increase of initial confining pressure (Figure 7-12). After the phase transformation point, the behaviour is characterised by an increase of the dilative behaviour after which the stress path moves toward a final steady state point. The undisturbed sample (LU10MPa-CU) showed a similar behaviour to the remoulded sample sheared under the same confining pressure (LR10MPa-CU). The behaviour exhibited by these samples, a compressive followed by a dilative behaviour, might give an indication that the initial state of these samples at the commencement of the shearing stage, is in the vicinity of the CSL of this sediment (Thevanayagam & Mohan, 2000).

As for the samples which were sheared under low confining pressure (Figure 7-13), a different trend to that observed in high pressure shearing can be seen. While the loose remoulded sample (LR4-CU) (void ratio at shearing stage = 0.49) and the undisturbed sample (LU2-CU) (with void ratio of 0.50 at the shearing stage), exhibited pure compressive behaviour, with their stress path heading towards the left, a dilation phase was more clearly observed in tests (LR2-CU), (LR3-CU) and (LU1-CU). This can be attributed to the effect of void ratio of the sample at the start of shearing. The remoulded sample (LR2-CU) and the undisturbed sample (LU2-CU), which were sheared under the same initial confining pressure of 215kPa, had different responses. The undisturbed sample started the shearing with a higher void ratio (e=0.5) and exhibited a compressive behaviour while for the remoulded sample, which has a lower void ratio (e=0.4) at the shearing stage, dilatancy was the

dominant characteristic of the behaviour after exhibiting an initial compressive behaviour. A similar behaviour was found for the remoulded dense sample (LR3-CU).

The undisturbed sample (LU1-CU), which was sheared under relatively higher pressures (495kPa), exhibited a compressive behaviour at the early stage of shearing before the phase transformation point. The initial compressive behaviour in (LU1-CU) is indicated by the initial stress path shift to the left in Figure (7-13) and the increase in the developed pore water pressure shown in Figure (7-10). The initial compressive behaviour exhibited by the samples (LR2-CU) and (LR3-CU) is less clearly shown in its stress path which is shown in Figure (7-13). However, the initial compressive behaviour of these samples can be identified from the initial increase in pore water pressure as shown in (Figure 7-8), before the early encountered phase transformation point, after which the sample was dominated by a dilative behaviour.

In spite of all the differences in behaviour which can be observed in these tests, they all seem to join the unique Critical State Line in the p′-q′ plane, regardless of the initial state of the sample, or the confining pressure at which the samples are sheared. This is an important finding as the Langjökull sediment showed transitional behaviour during compression (see Chapter Six), indicated by the lack of a unique NCL. The significance of this finding stems from the fact that other soils which exhibited a transitional behaviour did not seem to have a unique CSL (Ferreira & Bica, 2006; Nocilla et al., 2006). However, the uniqueness of the CSL projection in the p′-q′ plane does not mean that the CSL is unique in the specific volume v-ln p′ plane, and this issue is discussed below.

7.4 Critical State Line in the v–*ln* p′ plane

Data of the shearing tests performed on the Langjökull sediment (discussed in the previous section) are presented in the specific volume (v) –logarithm of mean effective stress (ln p′) plane in Figure (7-14). The figure indicates

clearly the existence of a unique Critical State Line (CSL) in this plane. The CSL can be defined by the equation (1-7):

$$v = \Gamma - \lambda \ln p' \quad \ldots\ldots\ldots \quad [1\text{-}7]$$

Where the gradient λ=0.037 and Γ=1.664, in the intercept at p'=1kPa.

The figure also shows the changes in sample state during the drained and undrained shearing tests, as highlighted by the marked initial and the final sample state for the undrained tests.

The soil's constant value λ, obtained for the Langjökull sediment is much lower than the values of for example London clay, which has a λ value of 0.161 (Atkinson & Bransby, 1978), indicating a much stiffer behaviour for this sediment, with a Critical State Line in almost a horizontal position in the v-ln p' plane.

7.4.1 Behaviour of samples during drained shearing tests

For all the tests performed under drained conditions of loading, Figure (7-14) shows the stress paths in terms of specific volume (v) - logarithmic scale of the mean effective pressure (p'). It can be observed that there is a very good agreement between the steady state conditions obtained from both undrained and drained tests. The behaviour of samples adjacent to the CSL during drained shearing can be described by two phases: at the early stages a compressive behaviour, indicated by the reduction in specific volume with an increase of the mean effective pressure, until a phase transformation point is encountered when the behaviour of the sample changes from compressive to dilative behaviour by experiencing an increase in the specific volume associated with a reduction in p' until a steady state is reached. This behaviour can be seen in the shearing of the remoulded samples (LR2MPa-CD), (LR2MPa-CD (Dense)) and (LR10MPa-CD) which had a sample state adjacent to the CSL at the commencement of shearing (7-14A). The behaviour of the undisturbed samples (LU2MPa-CD) and (LU10MPa-CD), on the other hand, was dominated by a clear compression throughout the tests.

The samples which started the shearing stage from a location above the CSL, by having their specific volume value higher than the specific volume at the Critical State v_{csl} at a certain mean effective pressure ($v>v_{csl}$), as in the case of the remoulded samples (LR20MPa-CD) and (LR30MPa-CD), experienced a compressive behaviour throughout the tests as indicated by the reduction in specific volume with an increase in p' until it ultimately reached the Critical State Line (Figure 7-14A).

To compare the behaviour and sample state of all samples during drained shearing, it is useful to normalise the state paths by correcting the position of states in v-ln p' space so that they lie on a reference section. A similar method to this illustrated in Figure (7-15) was suggested by Atkinson & Bransby (1978). The reference section is chosen to be at p'=1MPa. Thus, a point such as (A) can be mapped on the reference section by drawing a line through (A) at slope λ, parallel to CSL, and the intersection of that line with the reference section, point (A') is used to represent point (A). Similarly, all other points can be represented on the reference section. The value of void ratio on the reference section can be determined from the equation:

$$e_{ref} = e + \lambda \, . \, ln \, p' \ldots\ldots\ldots [7\text{-}1]$$

where:

e_{ref} is the void ratio of the sample on the reference section.

This is equivalent to using a state parameter as was later proposed by Been & Jefferies (1985) or Klotz & Coop (2001) and previously discussed in Section (2.4).

By applying the above mentioned method, the drained shearing tests on remoulded samples can all be drawn in the plane of void ratio on the reference section (which was chosen at p'=1MPa here)- stress ratio (q'/p') as shown in Figure (7-16), which might be a more representative way in describing the state of each samples during test.

The Critical State Line on this plane is represented by the point of e=0.41, which is the value of void ratio at the intersection of the CSL with the reference section p'=1 MPa, and the stress value equals to M=1.4, where all

the tests terminate, which again confirms the uniqueness of the Critical State Line. In this figure (7-16), the samples (LR20MPa-CD) and (LR30MPa-CD), which started their shearing stage from a void ratio higher than the void ratio of the Critical State (0.41), experienced a reduction in void ratio during shearing, indicated by the movement of the sample states to the left until ultimately reaching a Critical State.

Sample (LR10MPa-CD) exhibited a compressive behaviour at the early stage of the test, as shown in Figure (7-16), then the sample behaviour changed to dilative before reaching the Critical State Line. Samples (LR2MPa-CD) & (LR2MPa-CD(Dense)), showed a more or less upward movement with a constant position on the e_{ref} axis, and experienced a compressive behaviour coincide parallel to the CSL as shown more clearly in Figure (7-14)A. Again, as in sample (LR10MPa-CD), the compressive behaviour is followed by a dilation to reach the Critical State.

The drained test which was carried out under low pressure (LR100kPa-CD), exhibited a compressive behaviour as indicated by its stress path which was coincidental with the Critical State Line, in the v-ln p′ plane, as shown in Figure (7-14).

7.4.2 Stress-dilatancy during drained shearing

In this section, the behaviour during drained shearing is examined in terms of the change of volumetric strain to the axial strain ($d\varepsilon_v/d\varepsilon_a$) or what is termed dilatancy, during the test. This gives important information on the soil behaviour and allows comparison with other granular soils' behaviour, for example those discussed in previous literature (Ferreira & Bica, 2006; Desimone & Tamagnini, 2004; Coop & Lee, 1993).

Figure (7-17) shows the dilatancy ($d\varepsilon_v/d\varepsilon_a$) versus stress ratio ($q'/p'$) change for remoulded samples during drained shearing. The Critical State corresponds to zero dilation (steady state), and a value of stress ratio $q'/p'=M=1.4$ was found for this soil. It can be observed that the dilatancy rate tends to be similar for all tests towards Critical State. The figure shows that

the samples tend to exhibit lower dilatancy rate at the early stages of the test, before joining the general trend of dilatancy. The stage where each sample dilatancy rate tends to increase and join the general trend is more dependent on the effective confining pressure during the test. The higher the effective confining pressure the earlier the sample joins the general trend of dilatancy.

Figure (7-18) shows the change in dilatancy rate during the tests carried out under 2MPa. These test showed a low dilatancy trend at the early stages of shearing before joining the general trend (observed above) in Figure (7-17) to reach the steady state. The negative dilatancy values indicate the dilation preceding Critical State. This behaviour was observed during the shearing of the two remoulded samples (LR2MPa-CD) and (LR2MPa-CD (Dense)). The undisturbed sample (LU2MPa-CD) exhibited a low dilatany rate (low dilatancy/stress ratio) during most of the test, and showed no dilation during the test.

The dilatancy behaviour for the drained tests carried out at 10MPa confining pressure is shown in Figure (7-19). Both the remoulded and undisturbed samples showed a low rate of dilatancy at the early stage of shearing before joining the general dilatancy trend (the higher rate of dilatancy/ stress ratio). The remoulded sample seems to join the general dilatancy trend earlier than the undisturbed sample (LU10MPa-CD). The undisturbed sample does not show any dilation, as it approaches the Critical State from the right side of the graph as was also observed for sample (LU2MPa-CD) earlier, while some dilation is observed in the case of the remoulded samples (LR2MPa-CD, LR2MPa-CD(Dense)) and (LR10MPa-CD) which approached the Critical State form the left side of graph. This seems to be a key difference between the behaviour of the remoulded and undisturbed samples.

The remoulded samples which were sheared under higher confining pressures; (LR20MPa-CD) & (LR30MPa-CD) joined the general dilatancy trend earlier than those conducted under lower confining pressure (Figure 7-17), exhibiting a higher dilatancy rate (change of $d\varepsilon_v/d\varepsilon_s$ to change in

stress ratio q′/p′) during most of the shearing with some dilation near the end of the test, thus, approaching the Critical State from the left.

In Summary, there is a general trend of the dilatancy behaviour exhibited by the sediment. The higher the confining pressure during the test, the earlier this behaviour is exhibited, and those tests conducted under lower confining pressure, exhibited lower rate of (dilatancy/ stress ratio) at their early stages of shearing, before joining the general dilatancy trend. The remoulded samples showed some dilation (as indicated by the negative value of dilatancy before reaching the Critical State), a behaviour which was not observed in the shearing of the undisturbed samples which exhibited a lower rate of dilatancy and showed a compressive behaviour throughout all the shearing stage. The undisturbed samples joined the same general trend, as the other remoulded samples, but a bit later than the remoulded samples which were sheared under the same confining pressure.

7.4.3 Shear modulus and Young's modulus

The accurate prediction of deformations depends on the correct definition of the stiffness- strain curve of the soil, and in particular on the elastic stiffness at small strains. For sands, the principal factors controlling soil stiffness are the confining stress and volumetric state relative to the Normal Compression Line, as they would be for clays (Jovičić & Coop, 1997). However, the means of arriving at the initial volume-stress state is also of a great significance in the case of sands, in particular whether the current volumetric state is achieved by geological over-consolidation, or by compaction during the depositional process (Jovičić & Coop, 1997).

For the work presented here, the use of local strain transducers provided an accurate method for determining the soil stiffness in the small strain range (<1%). The shear modulus or shear stiffness (G), and Young's modulus were calculated from the tangent to the stress-strain curve for a monotonic loading path at any particular strain. The change in Young's modulus and in the shear modulus with axial strain (drawn to logarithmic scale), during the

drained tests are shown in Figures (7-20) & (7-21) respectively. The data range starts at strains of about 0.01% and covers the range up to 1% of axial strain. A decrease in the Young's modulus value can be observed with the progress of shearing (Figure 7-20). The data also indicate that the higher the confining stress the higher the values obtained for Young's modulus, which is the usual behaviour observed for both sands and clays (Jovičić & Coop, 1997; Viggiani & Atkinson, 1995).

The change in shear modulus with strain curves (Figure 7-21), shows again the expected characteristics for the soil stiffness change during shearing. The general trend follows a decrease in shear stiffness with strain development, however by observing the shear modulus values at each confining pressure, it is clear that the sample (LR10MPa-CD) is exhibiting higher shear modulus values than sample (LR20MPa-CD), for which the test was conducted under a higher confining stress. This might be the effect of the position of the sample volumetric state relative to the Critical State Line (Jovičić & Coop, 1997). While the samples that were tested under confining pressures of 20MPa and 30MPa, which started their shearing with a volumetric state to the right of the Critical State Line, experienced a severe compressive behaviour (see Section 7.4.2), sample (LR10MPa-CD), which started shearing from a volumetric state that was closer to the Critical State, exhibited a stiffer behaviour than expected at this confining stress.

Figure (7-22), shows a comparison of the shear stiffness values obtained from the three shearing tests conducted under a confining pressure of 2MPa. The values obtained from the remoulded samples show a close trend of shear modulus development at low strains, however, the undisturbed sample exhibited lower values of shear modulus in the same strain range.

7.5 Normalisation of stress paths- boundary surface hypothesis

The Roscoe and Hvorslev surfaces, as described in (Section 1.3.4), represent state boundary surfaces which can be defined as the surfaces which separate states that samples can achieve from states which samples can never achieve (Atkinson & Bransby 1978). Typically, the geometry of the

Roscoe surface is defined by the constant specific volume sections of the surface, which have the same shape but are of different size. The sections can be scaled to a single normalised curve if the stresses are divided by an equivalent pressure on a reference line, for example the Critical State Line (see Section 2.3.2). While the Roscoe surface represents the limit of the normally consolidated samples, the Hvorslev surface limits the states of over-consolidated samples in the q′:p′:v space.

The normalisation method used for scaling all test paths to define the boundary surface for a specific type of soil depends on the soil type itself. The method usually used for normalising clays is based on using the equivalent pressure on the Normal Compression Line, p'_e. However, for those soils where a difficulty is encountered in defining the Normal Compression Line, normalisation of stress paths can be achieved by a scaling method based on using an equivalent pressure on the Critical State Line, p'_{cs} (e.g. Klotz & Coop, 2001;Ferreira & Bica, 2006). The equivalent pressure on the CSL can be determined using the equation.

$$p'_{cs}= \exp [(\Gamma-v)/\lambda] \text{ .....[7-2]}$$

The values of Γ and λ for Langjökull sediment were found to be 1.664 and -0.037 respectively, in Section 7.4. The normalised stress paths for both drained and undrained tests are shown in Figure (7-23), and define the Critical State at a p'/p'_{cs} value of 1.0, and at a q'/p'_{cs} value equal to M=1.4.

The most important feature in the behaviour of the Langjökull sediment is that no definite boundary surface, equivalent to the Roscoe surface, can be defined from normalised test paths, as there is no unique Normal Compression Line for this sediment to define the position from where this boundary surface starts on the p'/p'_{cs} axis. The position where the sample starts shearing is defined by the sample state itself, and its state position is relative to the Critical State Line. Regarding the Hvorslev surface, a better definition of this surface can be obtained from the samples which experienced dilation during shearing. It is expected that a better definition for

this surface would be obtained from shearing paths of very dense samples of the sediment.

7.6 Residual strength of the Langjökull sediment

Once failure of the sediment has taken place, the sediment deformation due to stresses exerted on the subglacial sediment by the moving glacier will be controlled by the residual strength of the sediment. Due to high strains underneath glaciers, it is critical to investigate the residual strength of the subglacial sediment.

The residual strength of the Langjökull sediment was investigated by conducting shear tests in the Bishop-type ring shear apparatus (see Section 5.5). The results obtained from shearing the sediment under 350kPa and 570kPa normal stresses are shown in Figures (7-24) and (7-25). Figure (7-24) shows the volumetric strain during shearing of both samples. The figure indicates that an initial expansion was experienced by both samples which was followed by a compressive behaviour which dominated the sample behaviour for most of the shearing test. The sediment's residual angle of internal friction obtained from these test is shown in Figure (7-25). The value obtained for the residual angle of internal friction for Langjökull sediment is about 35°. This value can be compared with the value of the angle of internal friction of the sediment before failure, which can be determined by using the equation (1-5):

$$M = \frac{q'}{p'} = \frac{6 \sin \Phi'}{3\text{-}\sin \Phi'} \quad \ldots\ldots \quad [1\text{-}5]$$

with M =1.4, a value of 34.6° is obtained for Φ' which is close to the value of residual angle of internal friction found from the ring shear tests.

7.7 The uniqueness of the Critical State Line of the Langjökull sediment

The hypothesis of a unique CSL, presented by Roscoe et al. (1958) has been applied successfully to different types of soils in addition to clays, for example

carbonate sand and decomposed granite (Coop & Lee, 1993), as it was discussed in Chapter Two. However, this hypothesis was not verified in some soils, where no unique Normal Compression Line was observed, for example gap-graded soil (Martins et al., 2001; Ferreira & Bica, 2006) and some silts (Nocilla et al., 2006).

The subglacial sediment of Langjökull has proven through tests conducted under high pressures, and shearing tests to very high shearing strains, that this sediment, in its current grading, has reached a terminal grading where no further pressure or strains can cause a significant breakage to its particles, so that its particle size distribution cannot evolve any more (see Chapter Six). From previous literature on granular soils (see Chapter Two), it was shown that for these soils, the mechanism by which both the Normal Compression Line and Critical State Line are identified is the particle breakage associated with compression and shearing (Coop & Lee, 1993; Hyodo et al., 2004). Since there is no particle breakage associated with compression or shearing for the Langjökull sediment, all deformations which take place as a result of subjecting external stresses to the sediment should be mainly controlled by a particle rearrangement process.

In compression, the test data discussed in Chapter Six, show that the behaviour of Langjökull sediment during compression seems to be governed mainly by the sample density, with no unique Normal Compression Line observed for this sediment, even when very high pressures are reached. In addition, a clear yielding point observed during compression of granular soils, like carbonate sands and some crushable granular soils (Coop & Lee, 1993; Hyodo et al., 2004), usually associated with the start of particle breakage can not be found for Langjökull sediment, which can suffer no further particle breakage.

In shearing, a sample may exhibit a compressive behaviour, if the sample state at the start of shearing is located above the position of the Critical State Line, or exhibit dilative behaviour if the sample state at the start of shearing is located below the Critical State Line. The position of the sample state relative

to the Critical State Line is controlled by the sample's initial density and the consolidation pressure. Therefore, a severe contractive behaviour can be observed from the loose samples which were compressed to high pressures for example (LR20MPa-CD) and (LR30MPa-CD), while dilative behaviour was observed in tests conducted on dense samples which were consolidated to relatively low pressures, or pressures which were not enough to position the sample state on the right of the CSL. So, deformations which take place as a result of subjecting the sediment to external stresses, are mainly due to particle rearrangement of this sediment, which is totally dependant on the sample state itself.

The importance of the uniqueness of the Critical State Line for Langjökull sediment stems from the fact that this sediment, although it exhibited a transitional behaviour during compression, showing no unique Normal Compression Line in the v- ln p' plane, yet, it seems to have a unique Critical State Line as found from the shearing tests presented . The uniqueness of the CSL for this sediment contradicts the findings of Nocilla et al. (2006) and Ferreira & Bica (2006) in their investigation of the Critical State for soils which exhibited transitional behaviour. In both cases investigated, a gap-graded residual soil (Ferreira & Bica, 2006) and an Italian well graded silt (Nocilla et al., 2006), there was no indication of the existence of a unique CSL during shearing. In the case of Langjökull sediment, the test data showed a sediment which exhibits a transitional behaviour during compression, with no unique Normal Compression Line, but still defines a unique CSL during shearing.

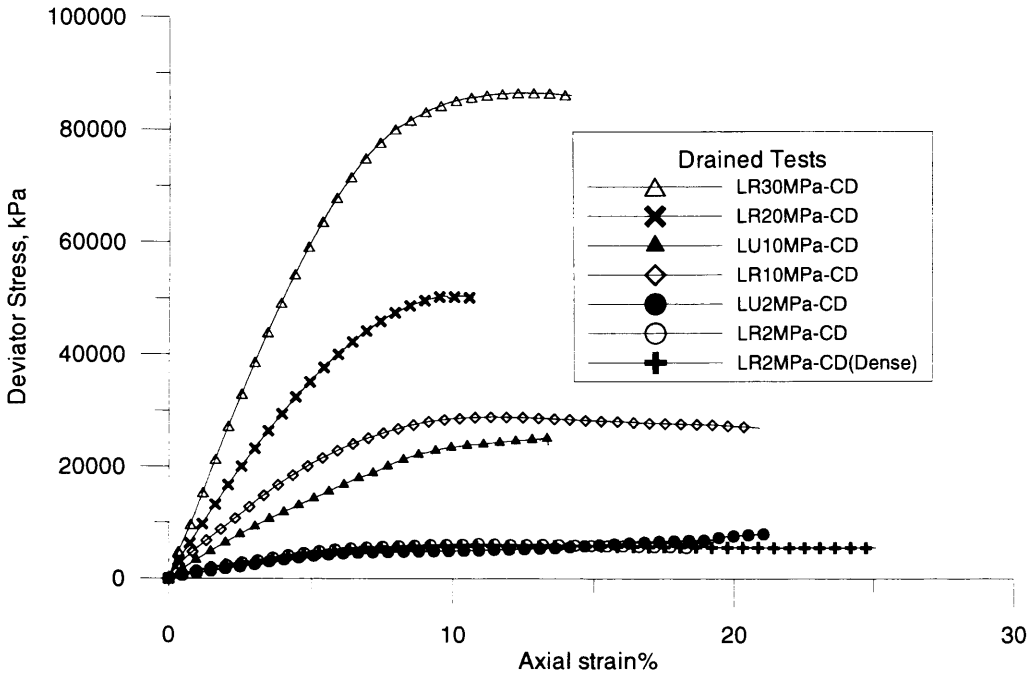

Figure (7-1): The development of deviator stress during drained triaxial compression tests conducted under high confining pressure.

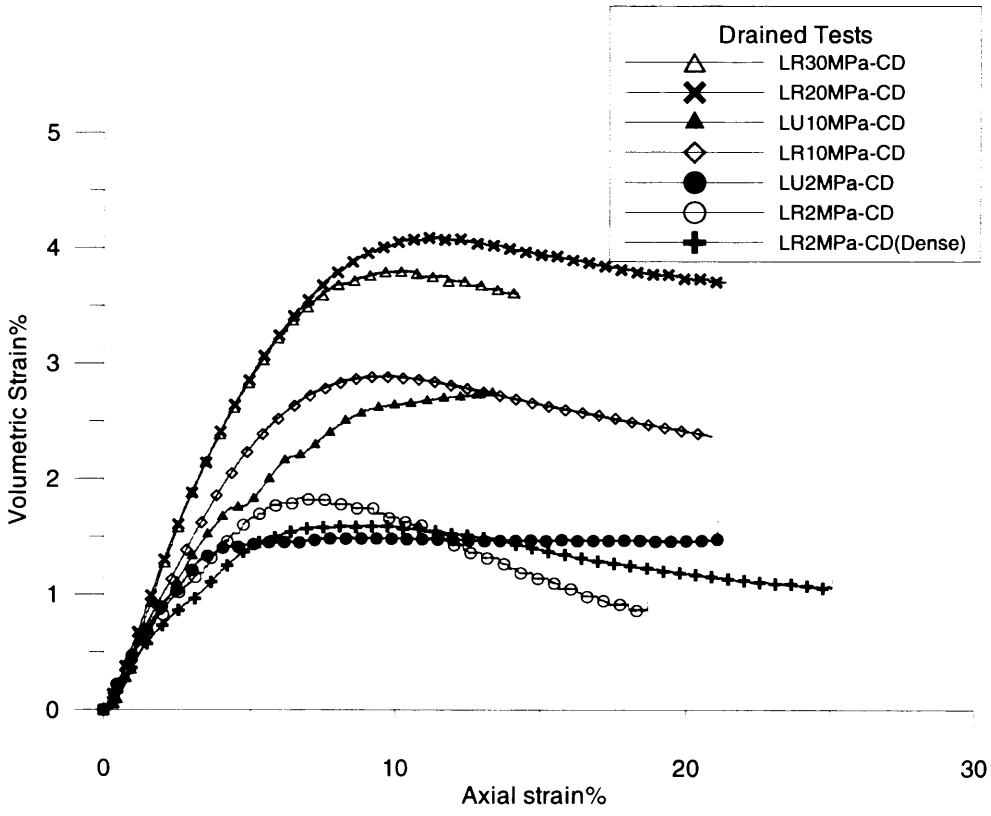

Figure (7-2): Volumetric strain versus axial strain during drained triaxial compression tests conducted under high confining pressure.

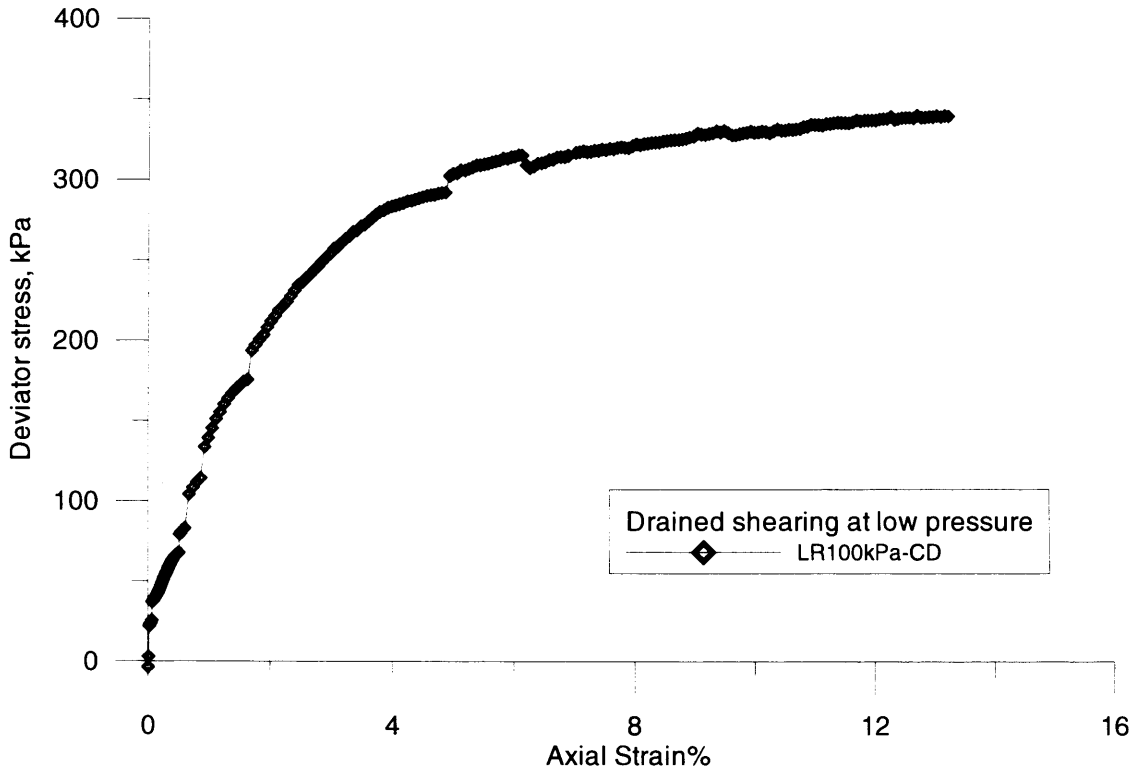

Figure (7-3): Deviator stress development during triaxial compression test conducted under 100kPa.

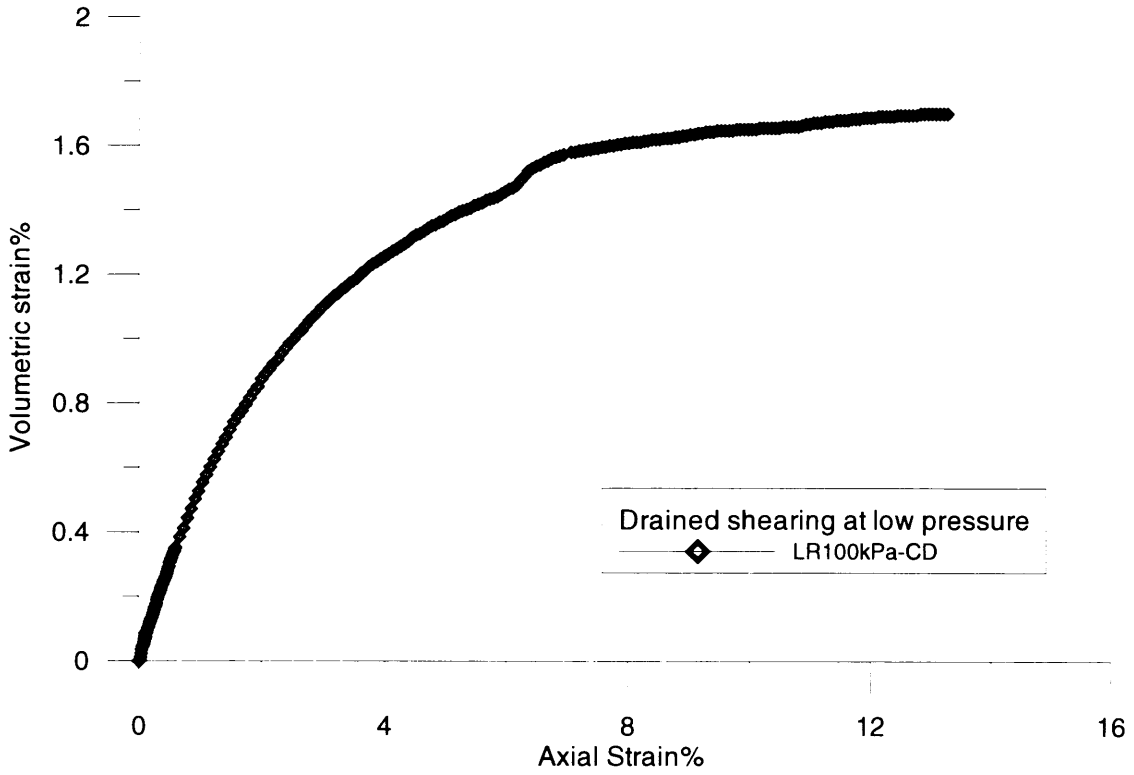

Figure (7-4): Volumetric strain versus axial strain during drained test conducted under 100kPa confining pressure LR100kPa-CD.

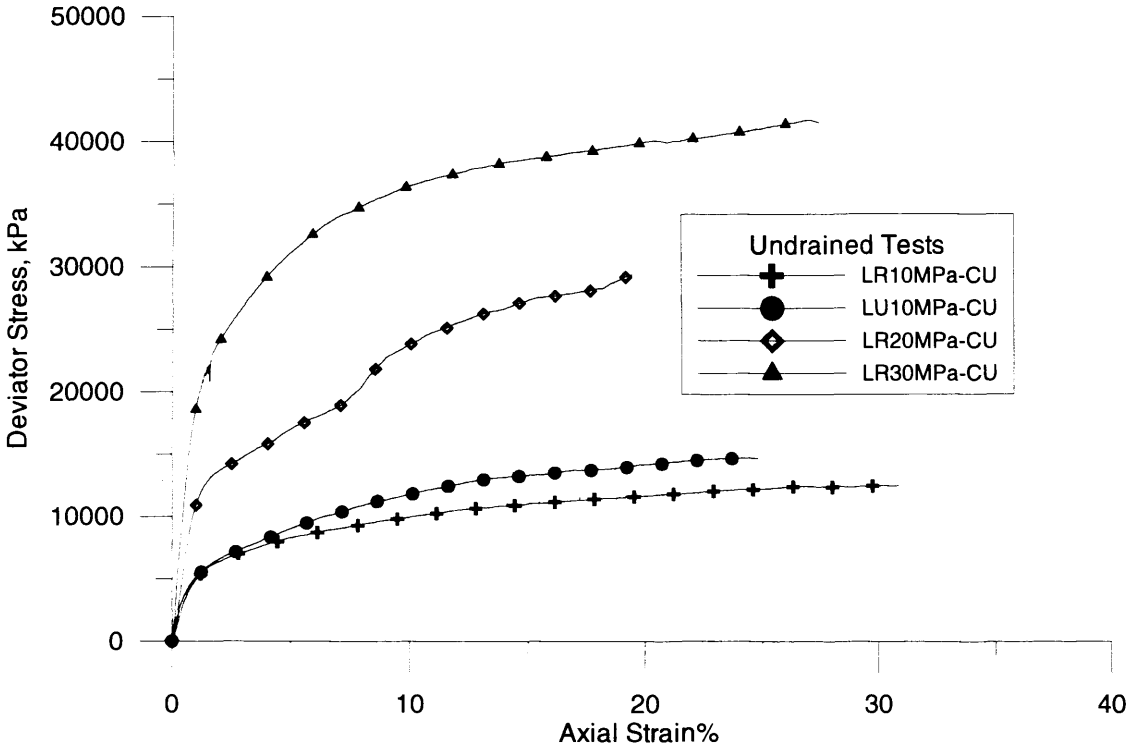

Figure (7-5): Deviator stress development during undrained triaxial compression tests under high confining pressure

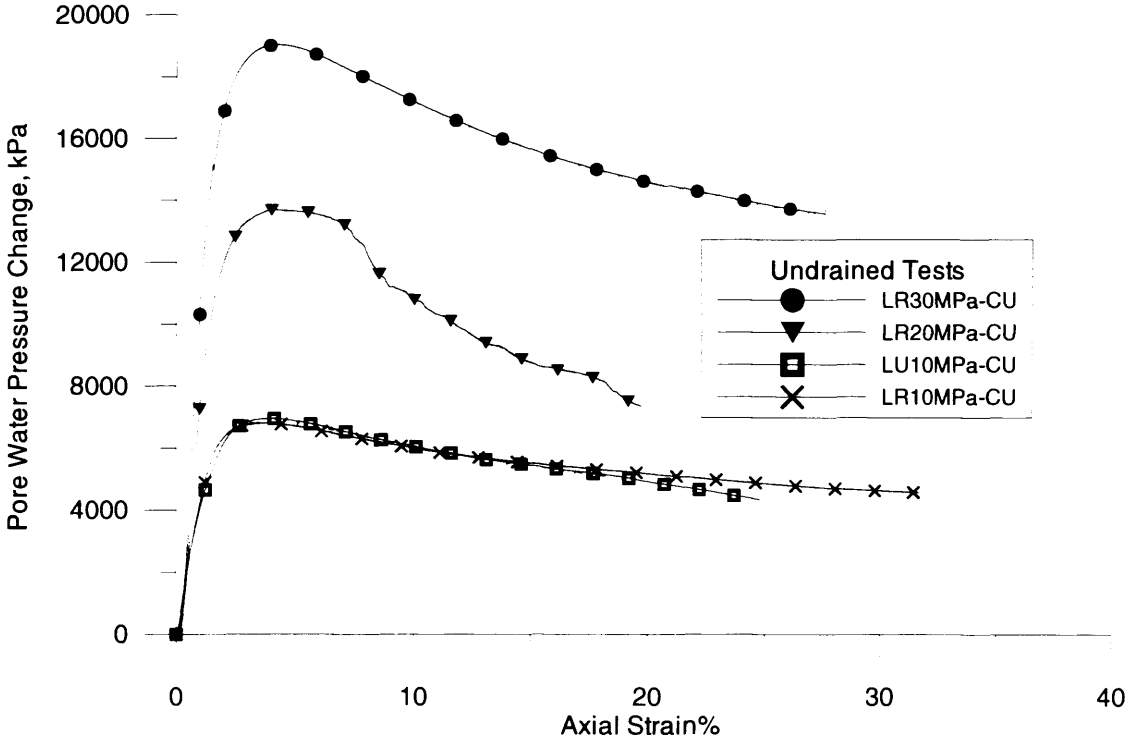

Figure (7-6): Pore water pressure development in undrained triaxial compression tests under high confining pressure.

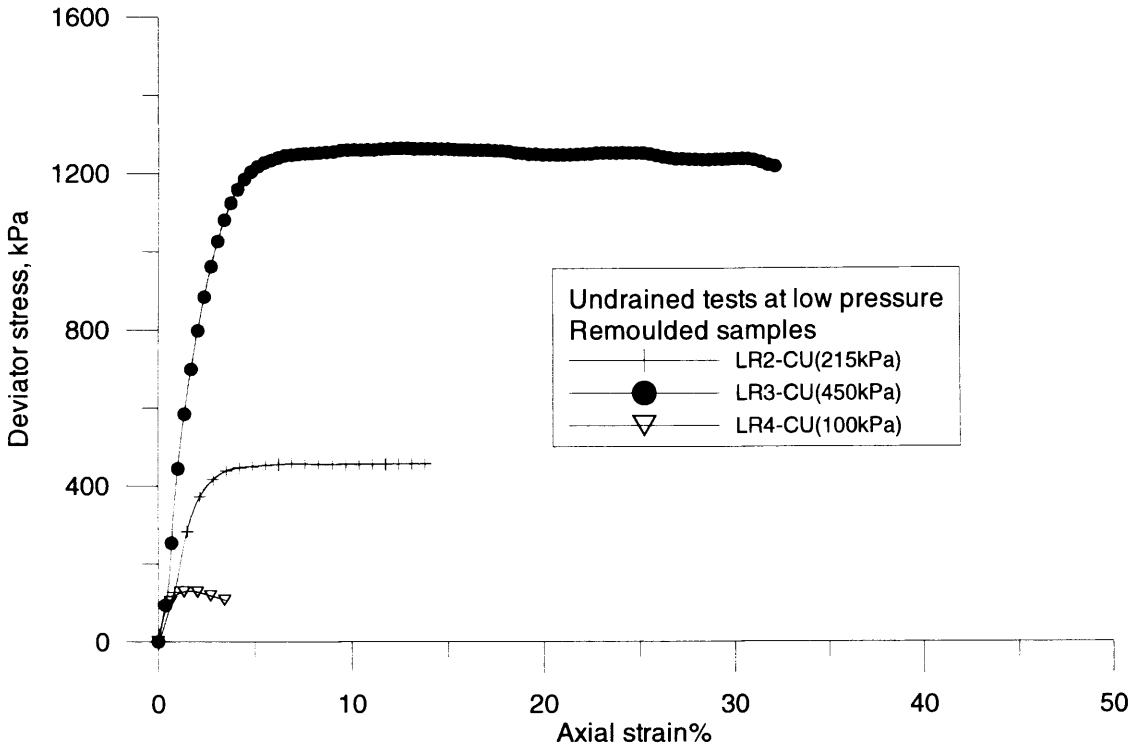

Figure (7-7): Deviator stress development in undrained tests on remoulded samples under low confining pressure.

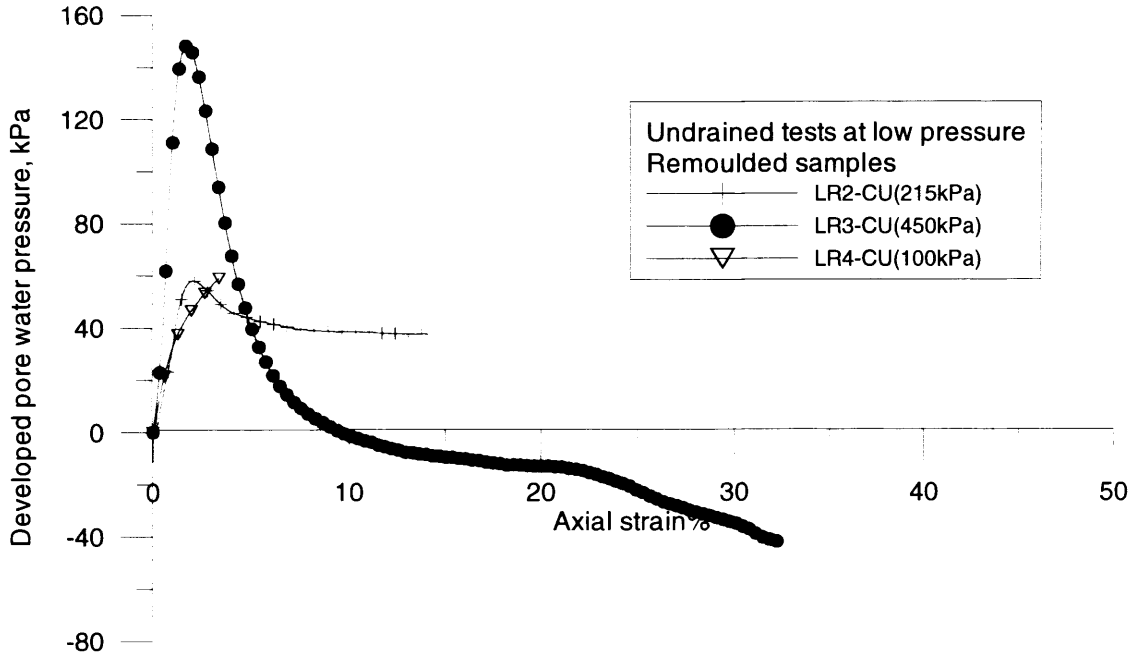

Figure (7-8): Pore water pressure development in undrained tests on remoulded samples under low confining pressure.

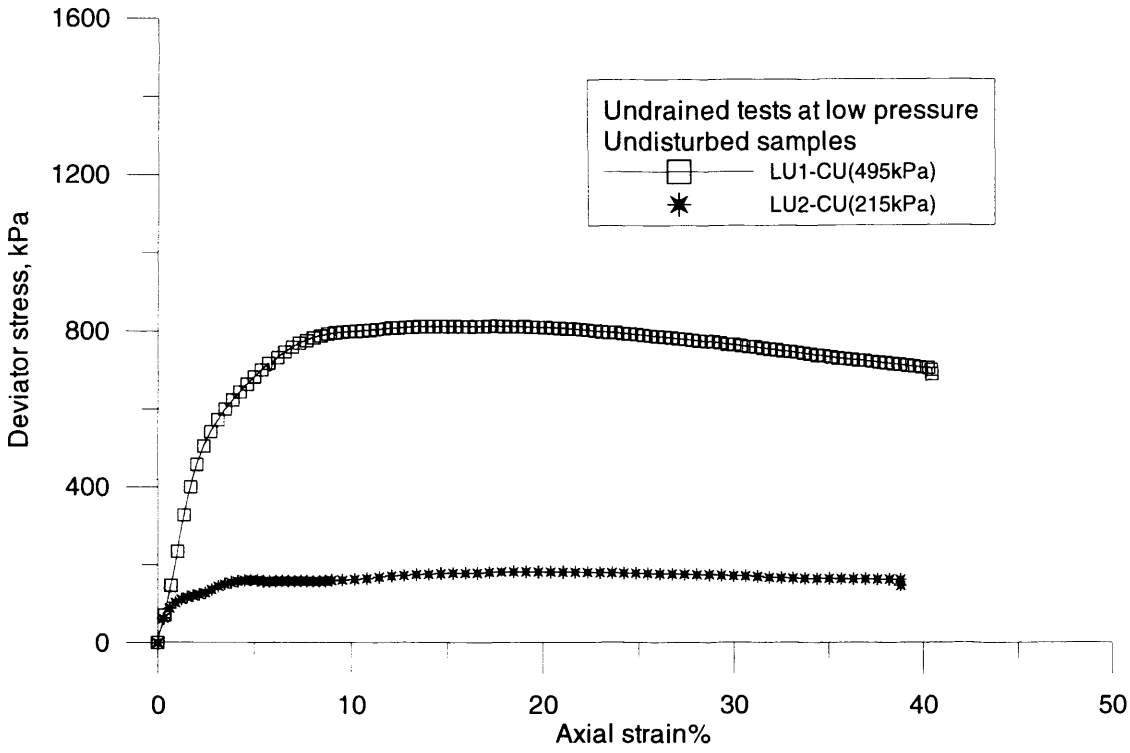

Figure (7-9): Deviator stress development in undrained tests on undisturbed samples under low confining pressure.

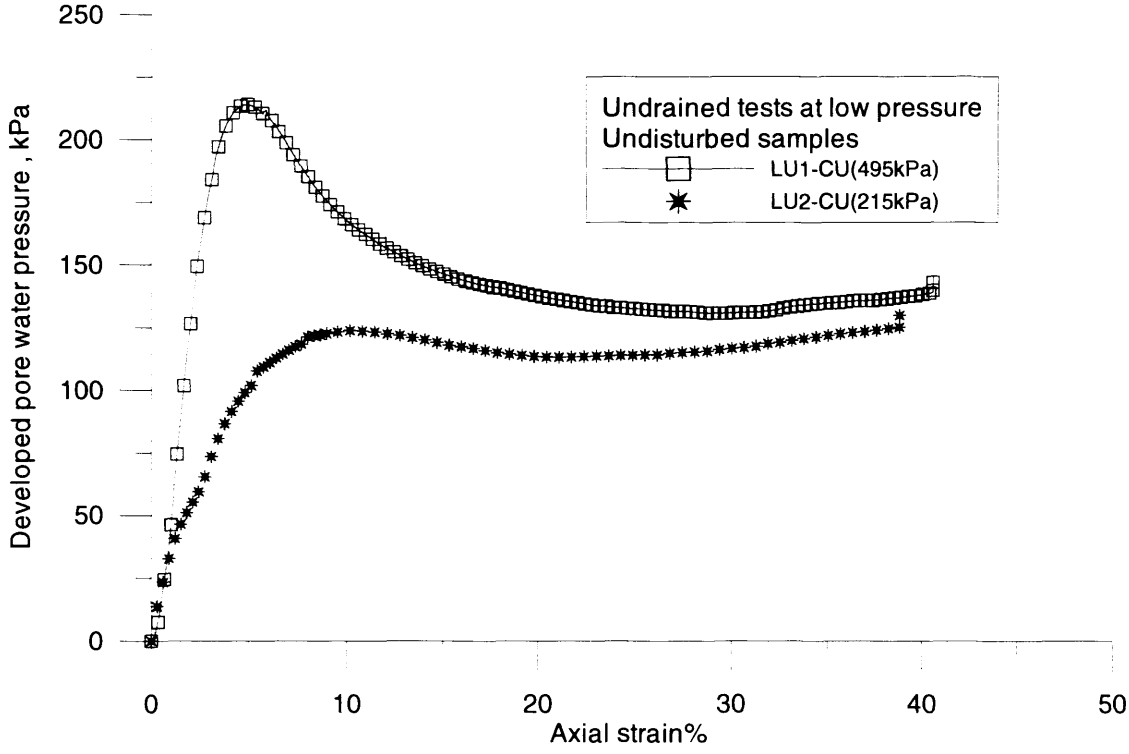

Figure (7-10): Pore water pressure development in undrained tests on undisturbed samples under low confining pressure.

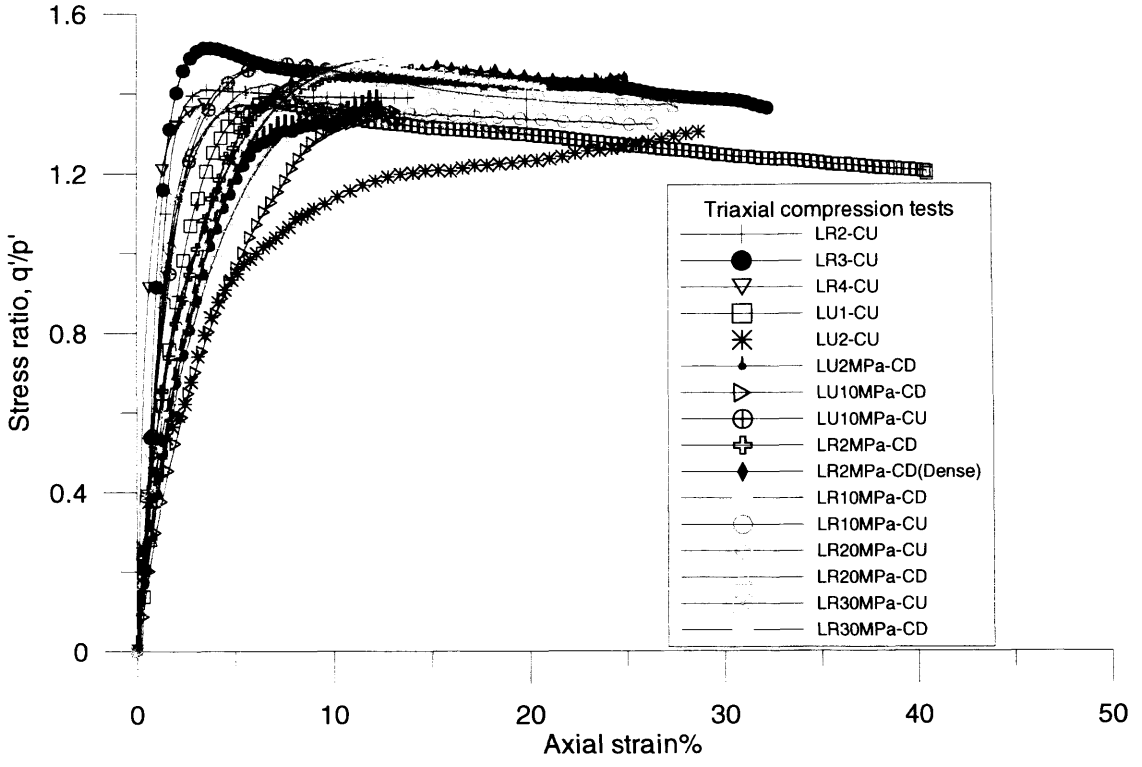

Figure (7-11): Stress ratio versus axial strain for triaxial compression tests on Langjökull sediment.

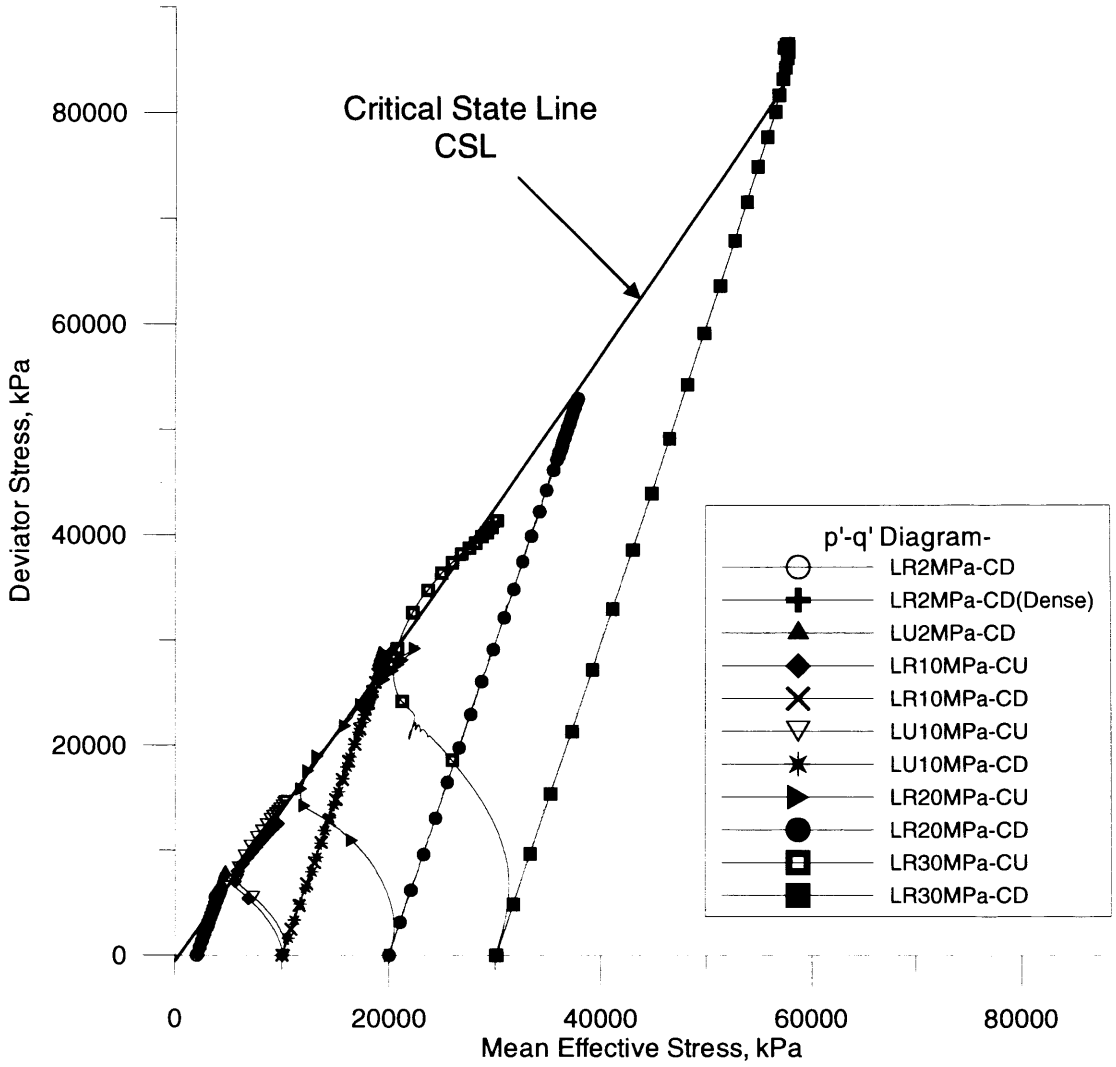

Figure (7-12): Stress paths of tests under high confining pressure, in the deviator stress-mean effective stress plane, showing the critical state line.

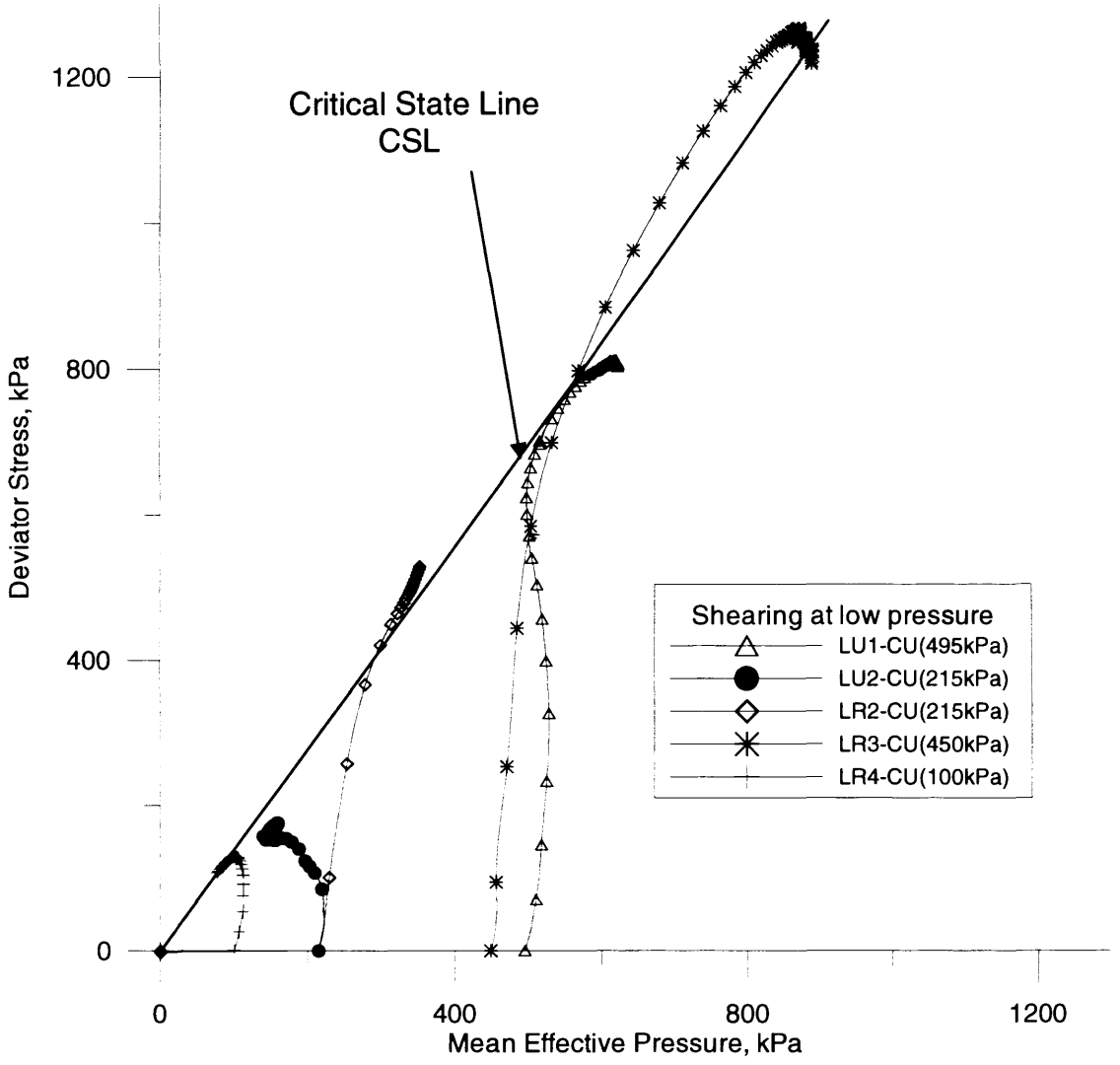

Figure (7-13): Stress paths of tests conducted under low confining pressure, in the deviator stress-mean effective stress plane, showing the Critical State Line.

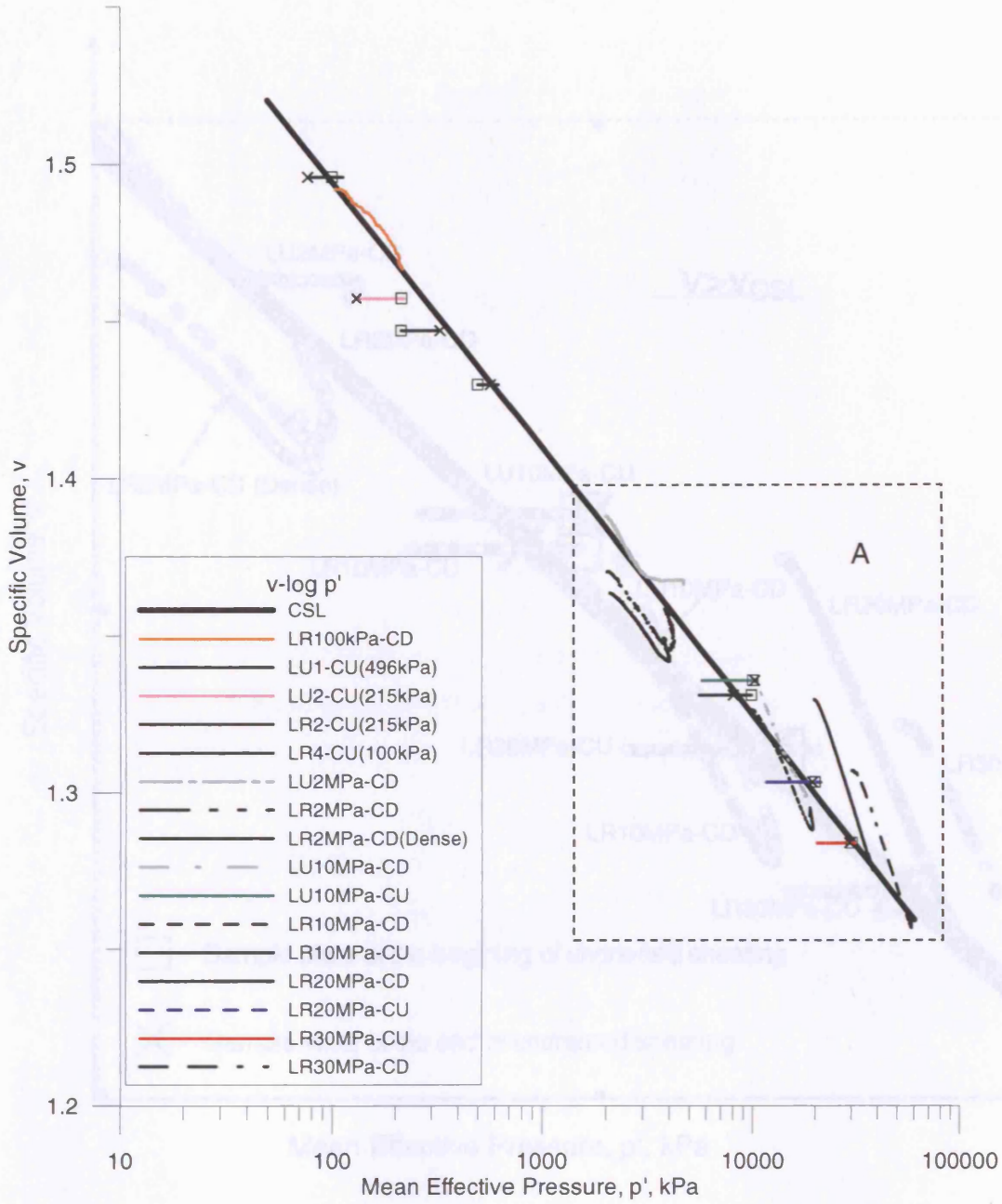

Figure (7-14): Stress paths during tests and the Critical State Line in the specific volume- mean effective pressure (logarithmic scale) plane.

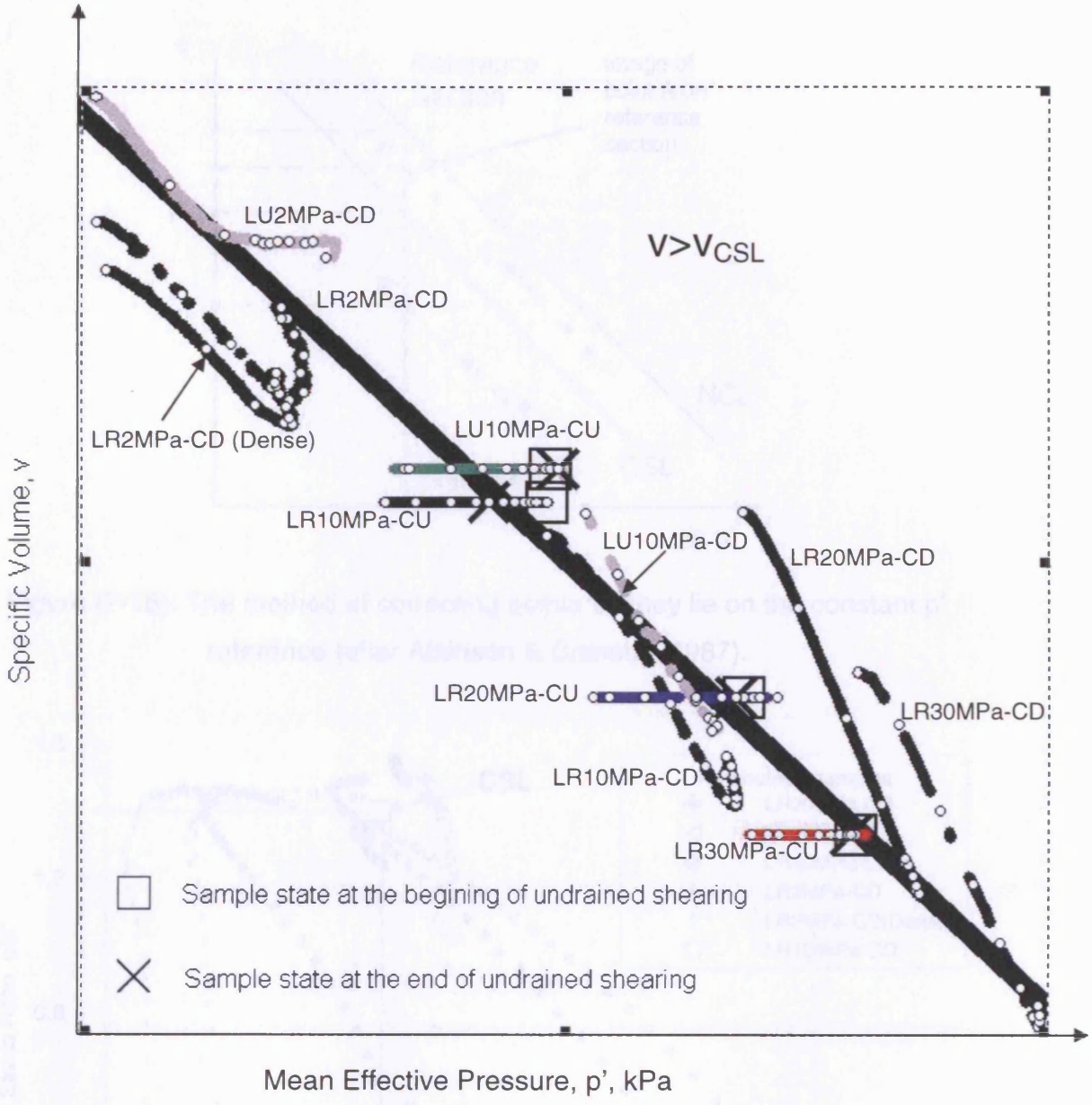

Figure (7-14)A : Detailed graph showing stress paths during tests and the Critical State Line in the specific volume- logarithmic scale of mean effective pressure, in the framed area (A) in Figure (7-14).

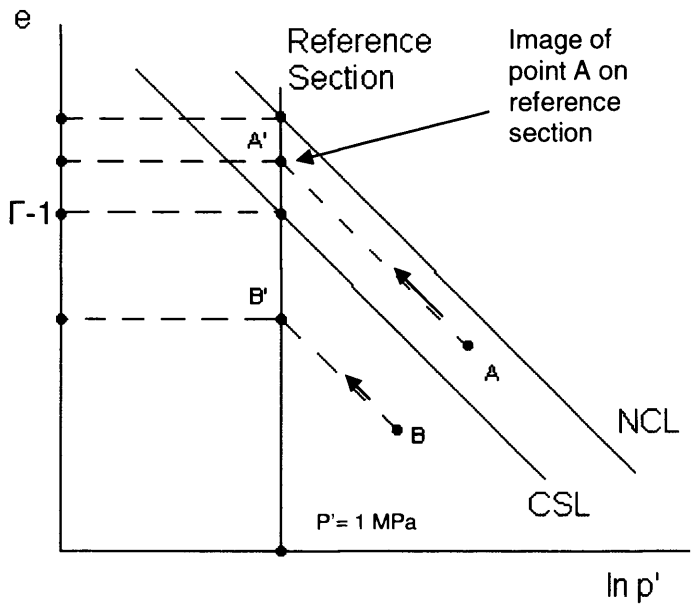

Figure (7-15): The method of correcting points so they lie on the constant p' reference (after Atkinson & Bransby, 1987).

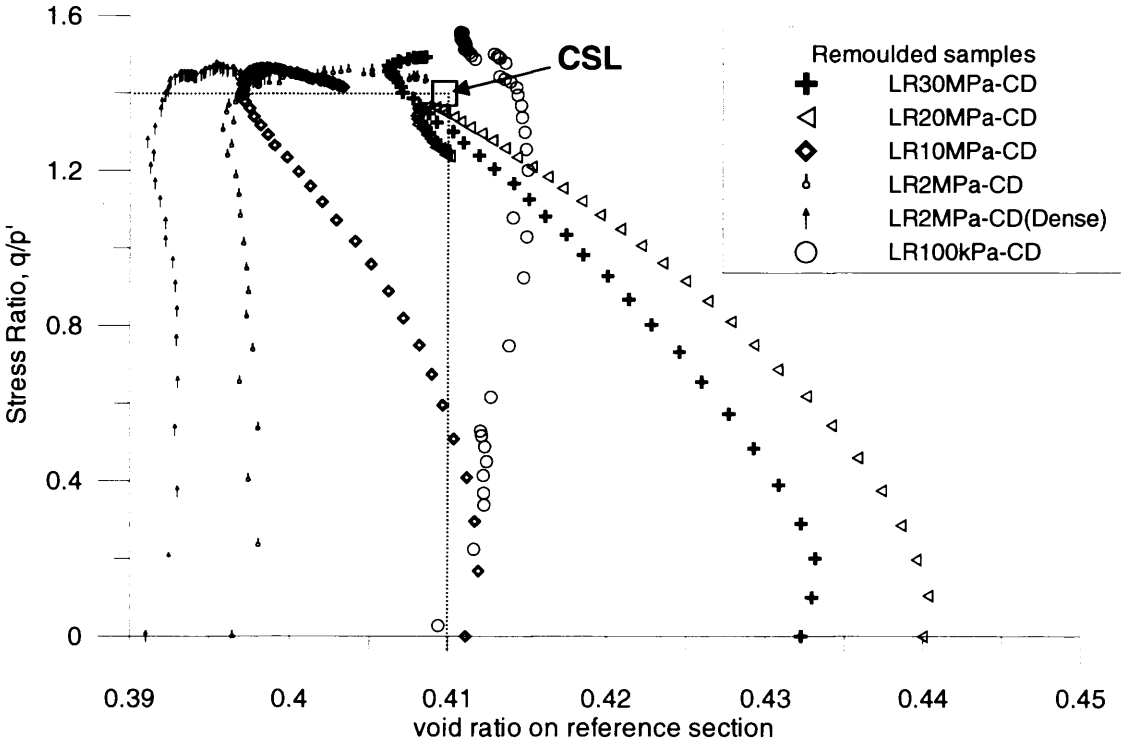

Figure (7-16): Change in void ratio on reference section during drained shearing.

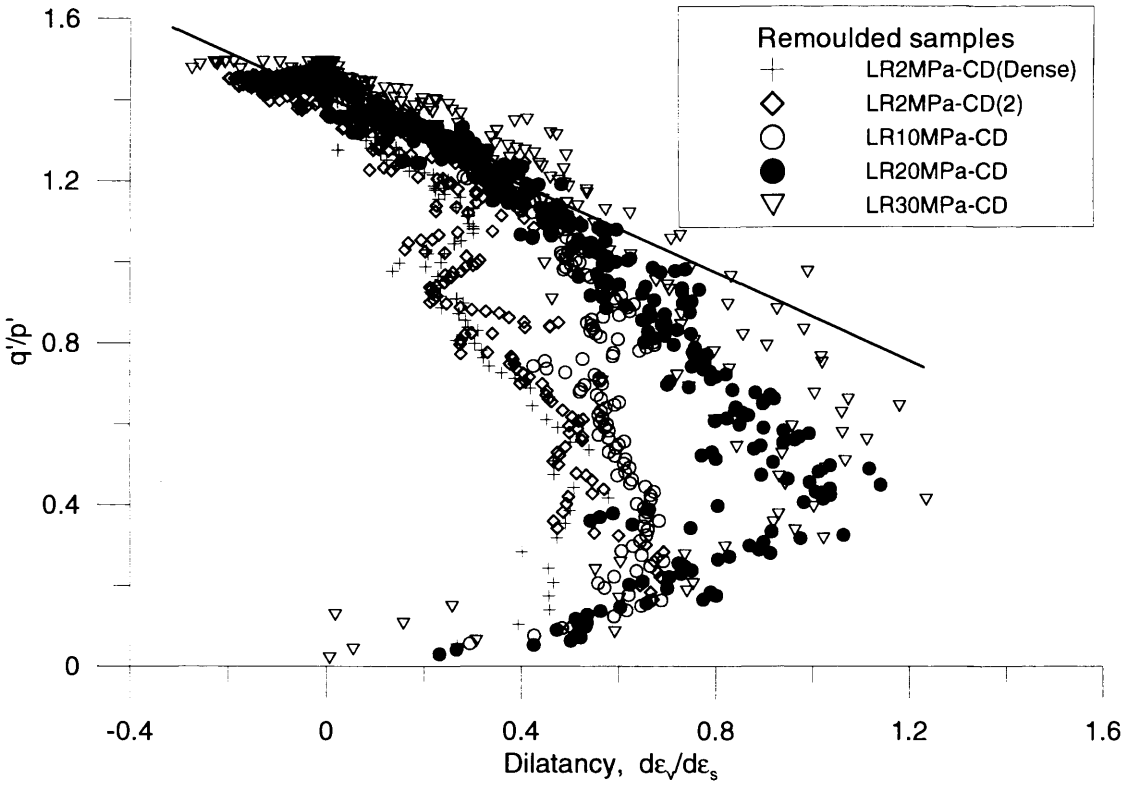

Figure (7-17): Dilatancy during shearing tests on remoulded samples.

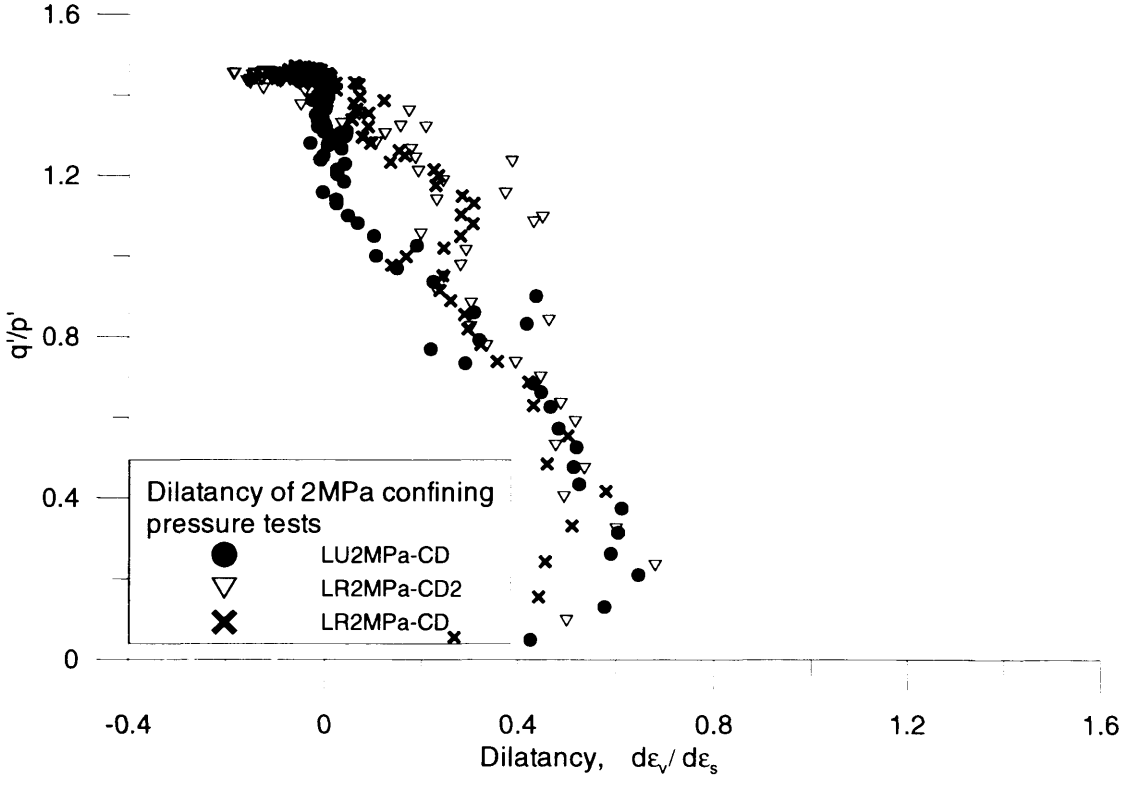

Figure (7-18): Dilatancy during shearing tests carried out under 2MPa confining pressure.

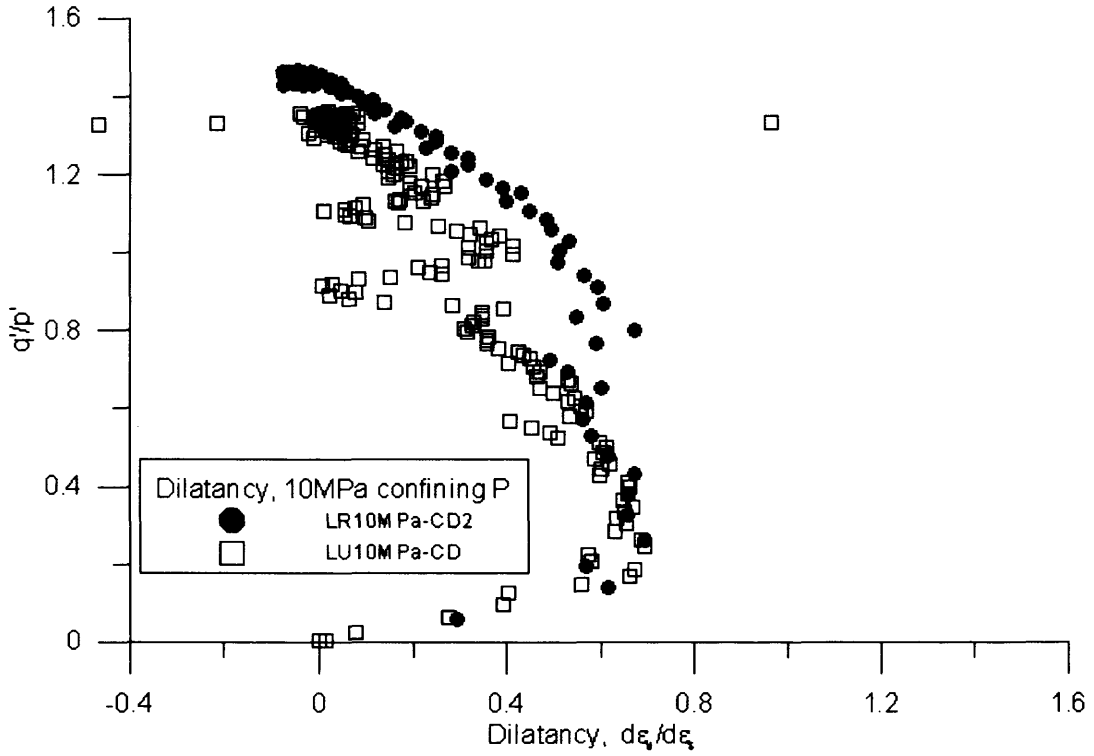

Figure (7-19): Dilatancy during shearing tests carried out under 10MPa confining pressure.

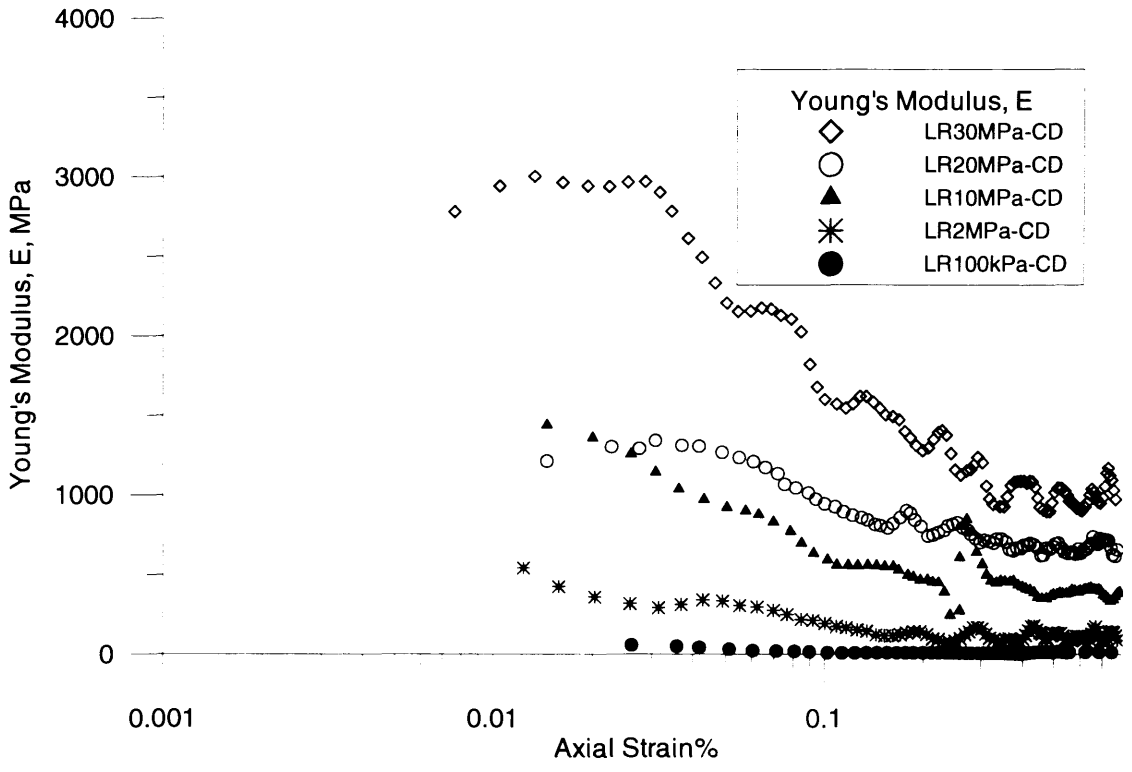

Figure (7-20): Young's modulus change in the low strain range in drained shearing tests.

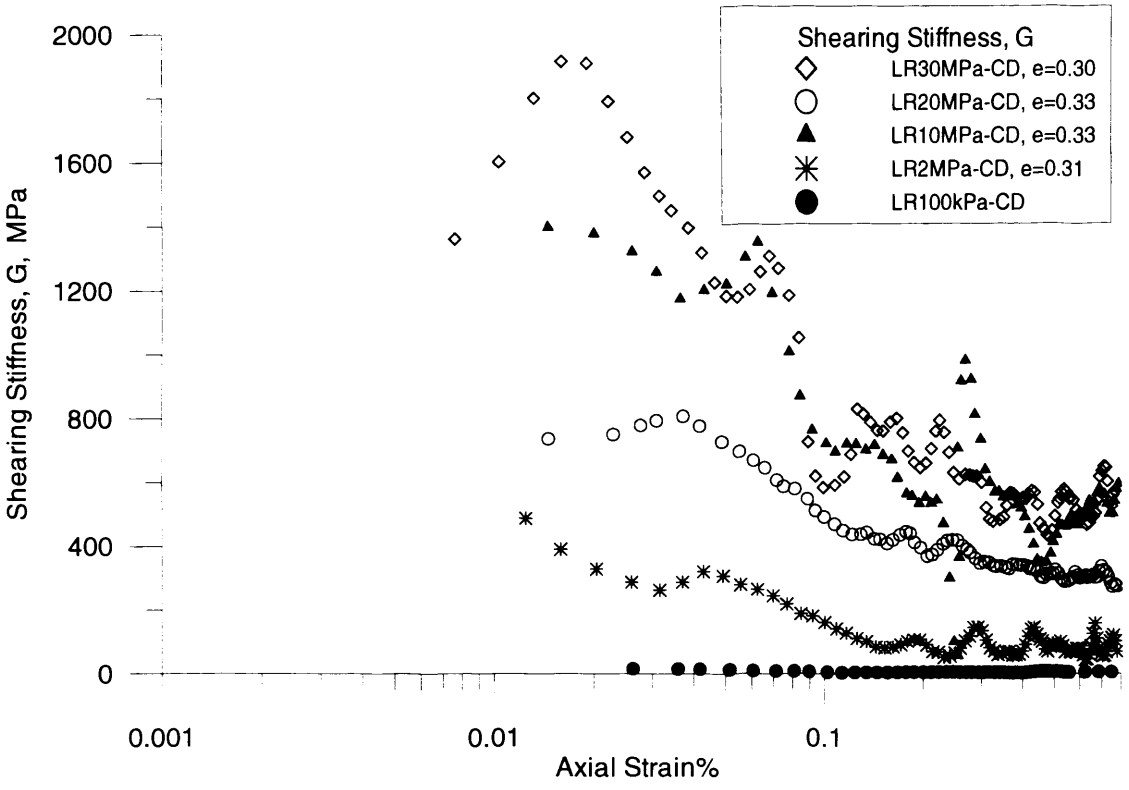

Figure (7-21): Shear stiffness change in the low strain range in drained shearing tests.

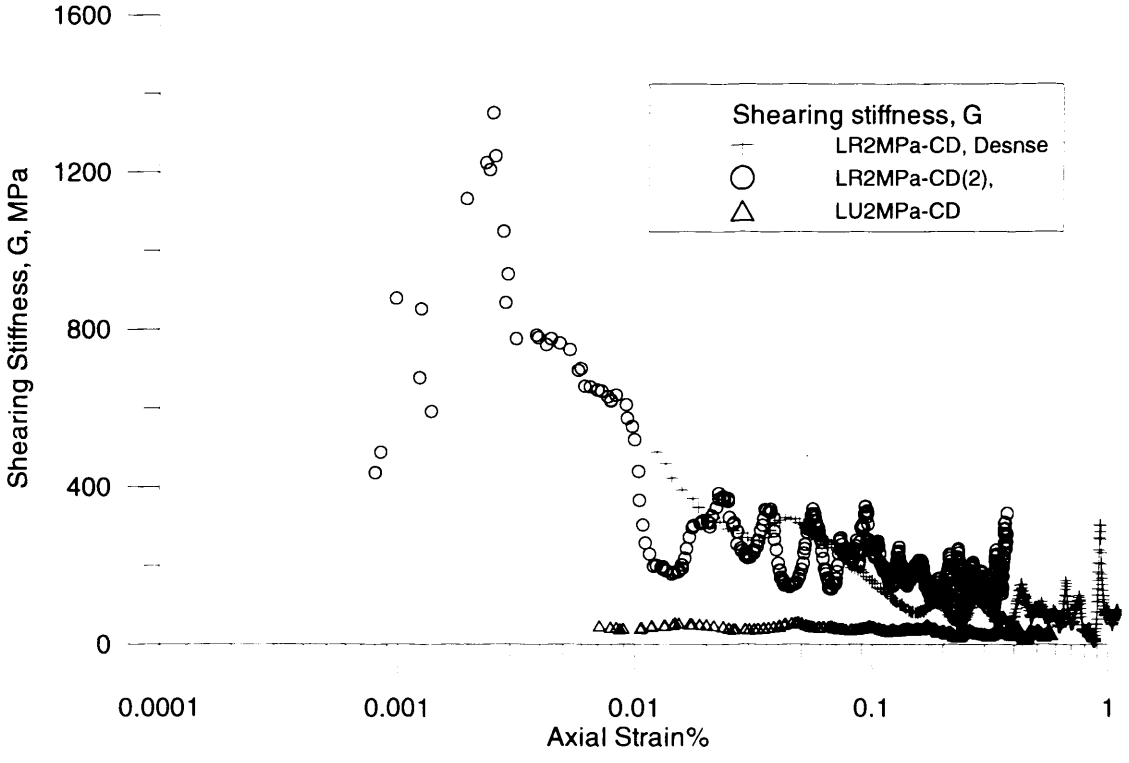

Figure (7-22): Shear stiffness change in the low strain range in drained shearing tests under 2MPa confining pressure.

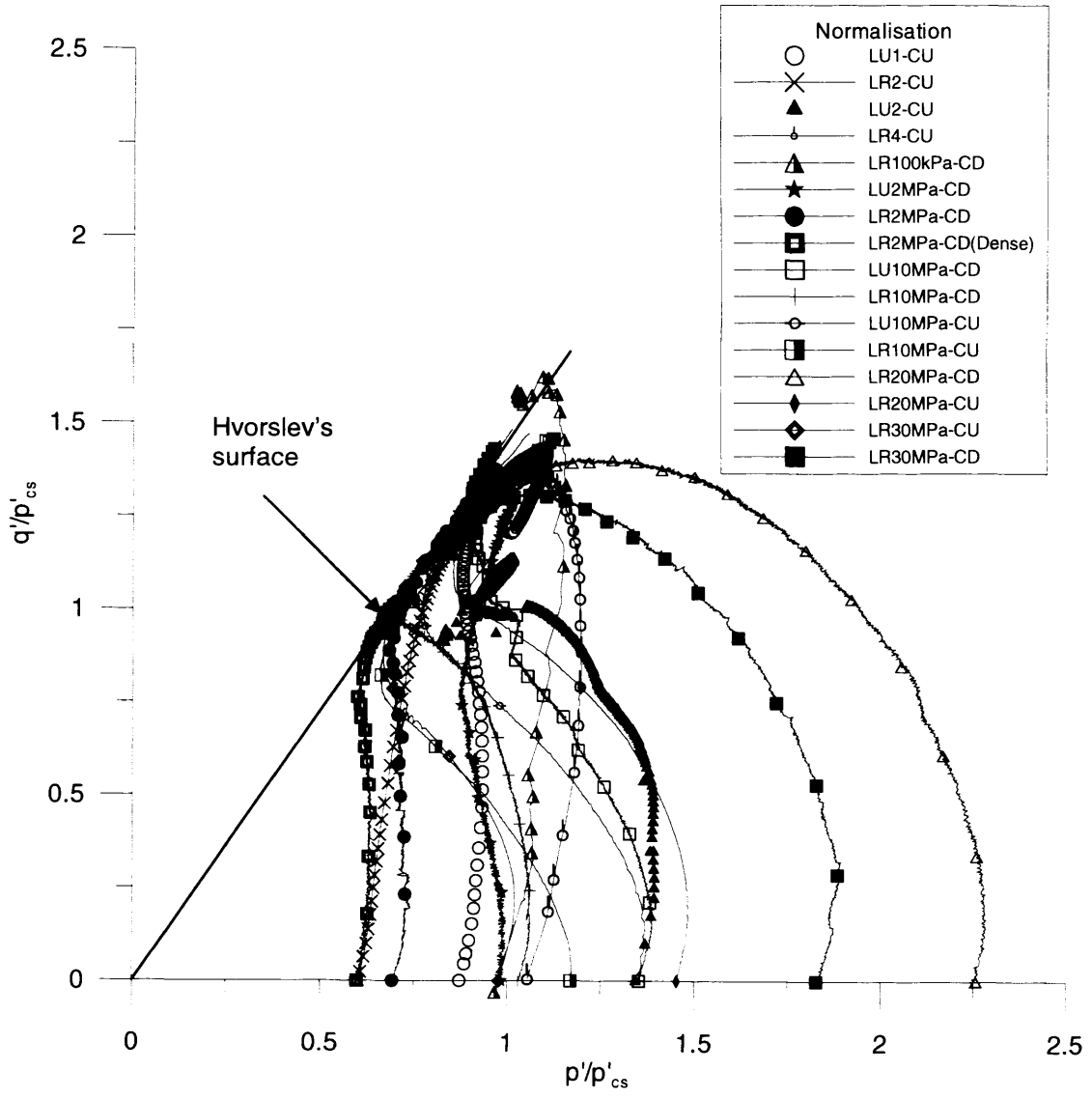

Figure (7-23): Normalisation of stress paths using the equivalent pressure on the Critical State Line p'_{cs}.

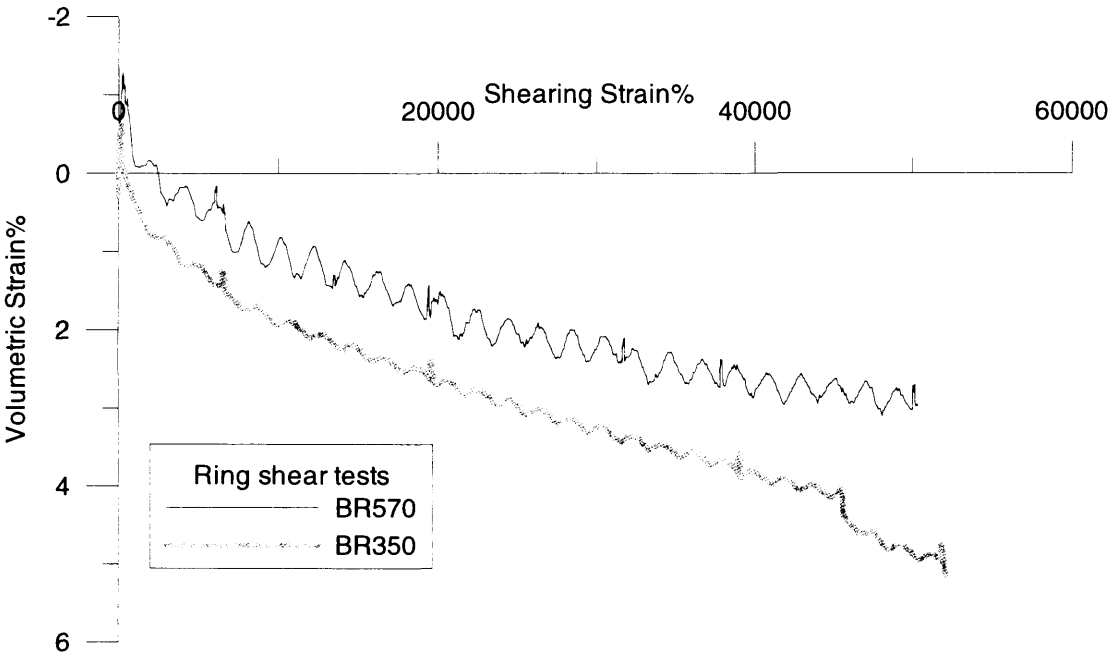

Figure (7-24): Volumetric strain during tests BR570 and BR350.

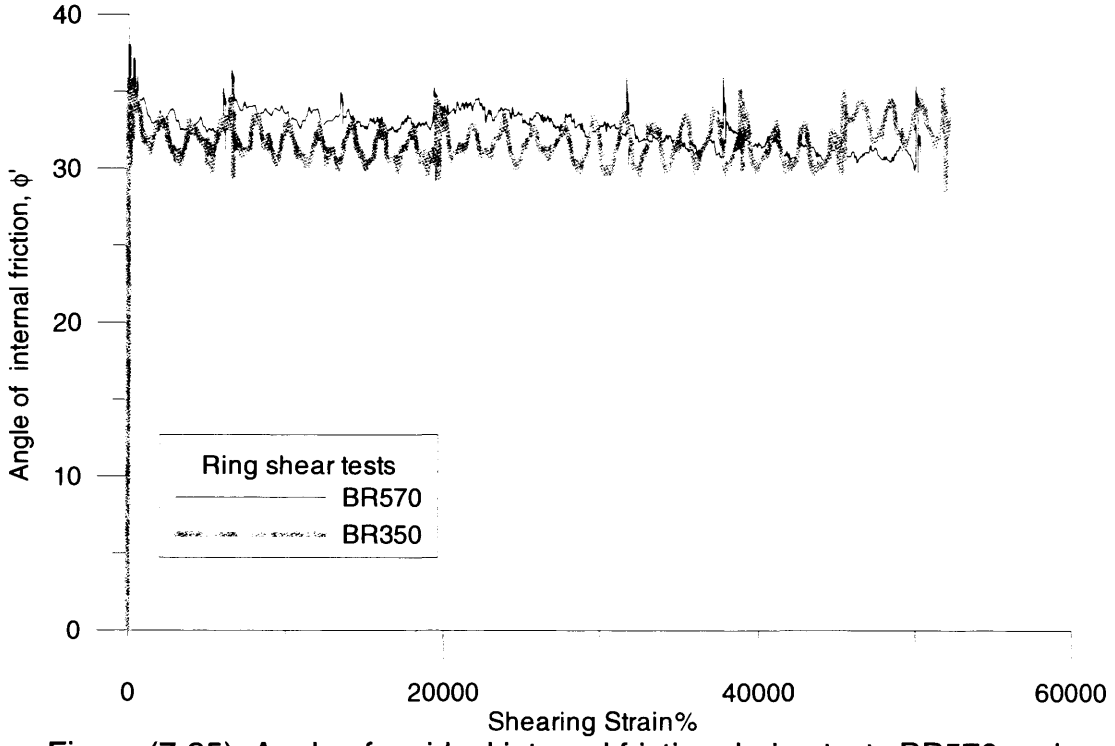

Figure (7-25): Angle of residual internal friction during tests BR570 and BR350.

Chapter Eight

Viscous behaviour of subglacial sediments

8.1 Introduction

Since the study which investigated the shearing deformation under the Breiðamerkurjökull glacier by Boulton & Hindmarsh (1987), subglacial sediment deformation has typically been linked to strain rate changes under glaciers in the literature (e.g. Boulton & Jones, 1979; Boulton & Hindmarsh, 1987; Boulton et al., 2001). The study under Breiðamérkurjökull, which was based on field collected data, emphasised the role of shearing rate in defining the subglacial deformation. Boulton & Hindmarsh (1987) stated that below glaciers where the pore water pressure is almost equal to the overburden pressure, the dominating factor in defining subglacial deformation is the strain rate. They suggested that a sediment subjected to shearing under very low effective stress, would exhibit a viscous behaviour similar to that of the Bingham model (as discussed in Chapter Two).

The importance of strain rate effects on subglacial deformations stems from the wide range of shearing rates underneath glaciers which are imposed by the velocity of the ice basal movement. The shearing rate underneath glaciers can range from a very low rate which might be less than a few millimetres per annum, to extremely high values (See Section 2.8). The suggestion of a viscously deformed sediment by Boulton and Hindmarsh (1987) provoked more geophysical researchers to investigate the validity of their viscous model for defining subglacial behaviour. Subsequently, the viscous behaviour of some subglacial sediments was investigated by field collected data or by geotechnical testing programs (Kamb, 1991; Iverson et al., 1998; Boulton & Dobbie, 1993; Tulaczyk et al., 2000) (see Section 2.8). These studies, although they yielded interesting results, still have not been analysed in a conventional geotechnical manner to clarify the effect of strain rate on subglacial sediment behaviour (Tulaczyk, 1999) (see Section 2.8.2).

In geotechnical engineering, the time effect and viscous behaviour of soils cannot be separated from the plastic model which defines the overall behaviour of soils. Typically, time effects are considered within the framework of the plastic model (Section 2.7), that is a soil which behaves in a plastic manner could still exhibit some viscous behaviour. The time-dependent behaviour of soils such as creep, stress relaxation, and strain rate effects, are all linked and can be grouped into what can be called viscous effects. However, when dealing with subglacial deformations the viscous behaviour is mostly linked to strain rate effects on the shearing behaviour of the subglacial sediment. In this chapter, shearing rate effects on the shearing behaviour of Langjökull sediment are investigated. The chapter also includes a re-analysis of existing data of shearing tests at variable speeds of other subglacial sediment which was collected from Ice stream B- West Antarctica (Tulaczyk et al., 2000).

8.2 Strain rate effect on shearing behaviour of the Langjökull sediment

When investigating subglacial sediment deformation, it is important that all related factors of subglacial environment should be considered. Subglacial sediments usually deform to very high shearing strains, in undrained conditions and with continuously changing shearing rate, depending on the glacier movement velocity on its bed (see Section 2.8). Therefore, to evaluate the shearing rate effect on the behaviour of Langjökull subglacial sediment during shearing, a shearing test by fully computer controlled triaxial cell (described in Section 4.3.7.2) was conducted in undrained conditions, using step-wise changes in strain rate (discussed in Section 2.7.2). However, the strains reached in the triaxial cell are limited, which can not satisfy all simulation factors in subglacial deformation definition. A Bishop-type ring shear apparatus (Section 4.4) was used to reach very high shearing strains. Again shearing rate was changed step-wise to investigate shearing rate effects on the residual strength of this sediment. In this section the results obtained from both triaxial shearing and ring shear tests are presented and the strain rate effects on the shearing behaviour of Langjökull sediment are discussed.

8.2.1 Shearing rate effect on Langjökull sediment shearing behaviour in triaxial cell

A drained triaxial compression test was carried out to investigate the effect of step-wise change of shearing rate on the shearing behaviour of a remoulded sample of Langjökull sediment (V3-60kPa). The sample was sheared from an isotropic state at p'=60kPa. The test was carried out with step changes in the axial strain rate to characterise the viscous behaviour of the sample; more specifically to investigate the influence of strain rate on the stress-strain shearing path, stress path, and change of pore water pressure of the sample. The results obtained from this test will be presented in this section.

a. Effect of step-wise change in strain rate on the stress-strain shearing path and the development of pore water pressure

Figure (8-1) shows the stress-strain path for test V3-60kPa, where the nominal axial strain rate was changed step-wise between two different levels, $9yr^{-1}$ and $67yr^{-1}$ (0.1%/hr- 0.76%/hr). The plot generally shows that when the strain rate is increased the sample builds up additional shearing resistance, initially showing a stiff response before a gradual yielding for the sample to end up re-joining the original strain path. When the strain rate is decreased the sample shows a temporary drop in its shearing resistance, dropping to a lower strain path before gradually rejoining the original stress path before the strain rate was changed. This temporary overshooting in the stress path is the main characteristic of a viscous feature which is only observed upon strain rate changes or what is termed TESRA (Temporary Effect of Strain Rate and strain Acceleration) (Tatsuoka et al., 2000), during shearing of clean sands.

Looking at the effect of strain rate change on the pore water pressure development, it seems that the increase of strain rate is associated with a temporary drop in pore water pressure, while a temporary overshooting in the pore water pressure was observed with the decrease of axial strain rate. Again the temporary undershooting or overshooting of pore water pressure due to the change in axial strain rate is followed by gradual return to the original curve before the axial strain rate change. Although TESRA viscous

behaviour is a characteristic of common clean sands (Tatusuoka et al., 2000; Tatusuoka et al., 2002), it seems that this basaltic sediment is exhibiting a similar behaviour by the temporary overshooting or undershooting associated with strain rate changes.

The same behaviour was observed on the sample when the strain rate was changed step-wise just before the sample stepped towards its steady state. The temporary overshoot in deviator stress gradually experienced yielding to re-join the original path before the strain rate change was imposed.

b. The effect of step-wise changes in axial strain rate on the shearing stress path of Langjökull sediment

The stress path shown by the sample V3-60R, which was sheared with step-wise changes in axial strain rate, fits very well with the data obtained from the shearing tests on Langjökull sediment under low pressure (Figure 8-2), which were presented in the previous chapter. The change in axial strain rate does not seem to impose any change on the location or the inclination of the Critical State Line. This finding complies with what was reported in Soil Mechanics literature (Leroueil & Marques, 1996; Vaid & Campanella, 1977; Soga & Mitchell, 1996). However, a careful examination of the graph shows a temporary change in stress path upon changes in strain rate (Figure 8-3), in which the mean effective stress experienced an increase upon the increase in strain rate, shifting the stress path to the right. Similarly, the stress path would temporally shift to the left due to the undershooting of the mean effective pressure associated with strain rate. With stress increase, the stress path shift which is experienced upon strain rate changes is seen to approach more or less the original stress path, indicating a pure TESRA viscous behaviour. The same behaviour was observed when the strain rate was increased when the sample was approaching its steady state, a temporary shift of the stress path associated with the mean effective pressure increase is observed followed by a yielding indicated by a return to the original stress path.

The viscous behaviour exhibited by Langjökull sediment, which can be described as pure TESRA behaviour, although it imposes immediate and temporary changes on the undrained strength of the sediment, does not affect the rest of soil parameters, like the angle of internal friction of the sediment, the position or the slope of the Critical State Line (Leroueil & Marques, 1996; Vaid & Campanella, 1977; Soga & Mitchell, 1996), which remained unchanged during strain rate changes.

The section above investigated the effect of strain rate on the undrained strength of the sediment up to sample failure. Taking into consideration the subglacial deformation characteristic, deformation of subglacial sediment might go further beyond the failure stage, due to the high displacement expected underneath a glacier which is imposed on this sediment by the moving glacier. The stage where the sediment is deforming beyond failure stage is totally governed by the residual strength of the sediment, a characteristic which will be investigated in the next section.

8.2.2 Strain rate effect on the residual strength of Langjökull sediment

The effect of shearing rate change on the residual strength of Langjökull sediment was investigated using a Bishop-type ring shear apparatus (Section 4.4), in which a remoulded sample of the sediment was sheared with variable shearing displacement rate. The aim of the test was to investigate shearing rate effects on the residual strength of the sediment, at high shearing displacements similar to these expected under glaciers. Figure (8-4) shows the variation in shear stress during an open gap period in the ring shear apparatus during which the shearing velocity was varied as shown in the same figure. From the results shown, it seems that the change in shearing rate did not affect the strength of the sediment represented by the shear stress monitored in the sediment. Although some divergence in the shearing stress value was observed over the shown strain range, this can be attributed to apparatus imprecision more than to a viscous behaviour of the sediment.

This was confirmed by comparing the results obtained from this test which was carried out using variable shearing rates, with ring shear tests which

were carried out with constant shearing rates, as shown in Figure (8-5). The figure shows the angle of internal friction measured from all tests carried out by the ring shear apparatus: BR570, BR350 and BR350-var. The results obtained from each test (during open gap periods only), showed a consistency of the obtained results, indicating a value of about 36° for the residual angle of internal friction for this sediment.

Plotting the data of these tests as normal stress versus shear stress, the trend indicates a linear relation, from which the angle of shearing resistance is defined (Figure 8-6). Again, the data obtained from the variable strain rate test is consistent with the general trend which defines the soil residual shearing parameters. The consistency of these data indicates that practically, there is no clear influence of strain rate on the residual drained strength of Langjökull sediment.

The viscous behaviour exhibited by Langjökull sediment during undrained shearing in the triaxial cell, which was characterised by a pure TESRA behaviour, is the kind of viscous behaviour which is usually observed in time dependent behaviour of granular soils, a category of soils under which Langjökull sediment is included. However, a totally different behaviour might be expected from clayey sediments, such as the clayey subglacial sediment which was collected from Ice Stream B-West Antarctica which will be re-analysed and discussed in the next section.

8.3 Existing data (Results from Ice Stream B- Antarctica) new analysis

Tulaczyk (1999), in his study on the mechanical behaviour of Ice Stream B sediment, conducted three undrained triaxial tests in which he imposed variable axial displacement rates. The tests R1, R2 and R3 were done on remoulded samples which were subjected to isotropic consolidation pressure of 281.3, 35.2 and 204.8 kPa respectively before shearing stage in which the strain rate was varied from $1yr^{-1}$ up to 80,000 yr^{-1}.

The results were compared with results of undrained triaxial tests on undisturbed samples which were carried out on the same sediment with

constant strain rate. Based on the results which exhibited no change in the value of the shearing parameters, Tulaczyk (1999), suggested that the sediment behaviour can be described as plastic with no clear viscous behaviour, attributing the slight changes in the sediment strength with strain rate to strain rate induced variations in pore pressure and effective stress rather than representing a true viscous behaviour (Tulaczyk, 1999) (Figure 8-7).

A more in-depth analysis of the data (*done by the author*) shows the occurrence of temporary over-and under-shooting in deviator stress associated with the strain rate change. This change in deviator stress is an indication of viscous behaviour of the sediment. The development of a high-stiffness zone is followed by clear yielding as shown in Figures (8-8 & 8-10). The subsequent yielding after the initial overshooting will result in another band of shearing stiffness, rather than joining the reference curve. This behaviour is an intermediate behaviour between the temporary effect of strain rate (TESRA) and the Isotach behaviour, a viscous behaviour termed as (General TESRA) (see Section 2.7), which is similar to what was observed for undrained triaxial compression of reconstituted normally consolidated stiff Fujinomori clay (Tatsuoka et al., 2000) or reconstituted normally consolidated London Clay (Sorensen et al., 2007).

The general TESRA property is demonstrated clearly in these tests conducted under higher confining pressures (Figures 8-8 and 8-10). The figures generally show that when the strain rate is increased the sample builds up additional shearing resistance, initially showing very stiff nearly elastic response. Then the soil gradually yields and follows a path above and similar to the lower strain path. A similar behaviour is observed when a decrease of strain rate is imposed during the test, the immediate undershooting of strength after strain rate reduction is followed by a gradual sample strength increase to follow a path under and similar to the upper strain path. Over the tested strain interval the effect of strain rate changes appears to be persistent, and a unique stress-strain curve can be obtained for different constant axial strain rates, as shown by the stippled lines. The

CRS (Constant Rate of Strain) curves moreover appear to be parallel, which is the characteristics of so-called Isotach viscous behaviour, as it was explained previously in Chapter Two.

It should be noted that the behaviour of the sediment under low effective pressure is more relevant in simulating the subglacial conditions, since the pore water pressure underneath glaciers is almost equal to the overburden ice pressure. The shearing behaviour at low effective pressures is established in the data obtained from test R2, which was conducted under 35.2kPa of confining pressure (Figure 8-9). By examining the stress-strain path during the test, it can be observed that the TESRA property in the behaviour of this sample is not as clear as it was observed in samples which were sheared under higher pressures. The change in sample strength due to the shearing rate change is persistent and it does not fade over the tested strain interval. The change in strain rate would result in the stress-strain path to define a new stiffness band which is correspondent to the new shearing rate. This persistent change in stiffness band after each change in strain rate indicates an (Isotach) viscous behaviour, similar to the behaviour typically observed for soft clays (Tatsuoka et al., 2002).

From what was discussed above, it is clear that the sediment exhibits a viscous behaviour during shearing, which is more or less dependent on the stress level. At low confining pressures, the Isotach property is more persistent while a General TESRA viscous behaviour is observed in the samples tested under higher confining pressures.

The influence of strain rate changes on the shearing stress path is illustrated in Figures (8-11) & (8-12), which show the undrained stress path for tests R2 and R3 respectively. It is quite clear that when the axial strain rate is changed step-wise, the stress path jumps between CRS paths for the corresponding strain rates. Similar to what was observed from the effect of strain rate on the deviator stress, the viscous behaviour here seems to be affected by the confining stress level. The sample which was sheared under low confining pressure, R2, exhibited clear viscous behaviour which is similar to what is

called Isotach viscous behaviour. The jump of the stress path due to strain rate change seems to be persistent and did not fade, with different CRS curves for different each specific strain rates, all more or less parallel to each other. The increase in strain rate would result in a shift to the right for the stress path, as indicated by the curves corresponding to strain velocities of (8.467 & 42.33microns/sec), while a shift to the left side is observed when an increase in axial strain rate is imposed during shearing.

The undrained stress path for the sample which was tested under 204.3kPa (R3) confining pressure showed a similar trend to that observed in test R2, although the CRS contours are less clearly defined, which might be due to some immediate overshooting or undershooting associated with the strain rate changes, which was observed in the deviator stress development during the test.

8.4 Viscous behaviour of subglacial sediment

The deformation of subglacial sediment is a critical issue in the analysis of glacier movements, since this deformation accounted for most of this movement (Boulton & Jones, 1979). It was suggested that one of the factors controlling the subglacial sediment deformation under Breðmérkurjökull-Iceland is the strain rate effect (Boulton & Hindmarsh, 1987). This suggestion was built on field collected data of shear strain rate, shear stress and effective pressure. The model which was proposed to simulate till deformation underneath glaciers, based on these data, reflects clearly a change of the sediment shearing failure envelope position, in the normal effective stress versus the shear stress plane, depending on the shearing rate value. This suggested model (Boulton & Hindmarsh, 1987) represented an extreme model, which was too far dependent on strain rate in defining the sediment shearing behaviour. That study emphasised the role of subglacial shearing rate effect on the deformation of subglacial sediment, and encouraged more researchers to question the viscous behaviour of this sediment, for example (Kamb, 1991; Boulton & Dobbie, 1993; Tulaczyk, 1999; Tulakzyk et al., 2000; Iverson et al., 1998; Dobbie, 1992). Dobbie (1992) proposed a model to simulate the behaviour of clayey glacial till from

the Netherlands (discussed in Chapter Two). This model, which was based on ring shear test data, also indicated a change of shearing failure envelope of the sediment. Despite that, still some of these researches favoured the plastic model in defining the subglacial sediment behaviour (Kamb, 1991; Iverson et al., 1998).

In geotechnical engineering the viscous and the plastic behaviour cannot be considered separately. A soil might behave viscously but it still follows the plastic model as proposed by the Mohr-Coulomb yield criterion (discussed in Chapter One). The investigation which was carried out on Langjökull sediment to define the viscous behaviour of the sediment, indicated a temporary effect of strain rate and strain acceleration (TESRA) on the sediment strength, which, although it imposes immediate changes to the sample strength, this change will not be reflected on the sediment mechanical parameters like the slope, position of the Critical State Line of the sediment or the angle of internal friction.

The viscous behaviour which was exhibited by Langjökull sediment, which is a granular sediment with no clay minerals (see Chapter Three), is a typical behaviour exhibited by pure sands. On the other hand, the effect of strain rate changes on a more clayey subglacial sediment like the subglacial sediment which was collected from Ice Stream B-West Antarctica, was more persistent (Isotach), indicating that the viscous property of the subglacial sediment is dependent to a certain extent on its mineralogical composition. The relation between mineralogy, grain shape and viscous response is a very topical complex subject still being researched (Sorensen et al., 2007; Tatsuoka, 2007).

The two cases presented in this chapter; the Langjökull sediment and the Ice Stream B- West Antarctica sediment, which have two different mineralogies, yielded an interesting result: the viscous behaviour exhibited by these sediments, did not impose any changes to soil sediment shearing parameters. This fact although complying with previous soil mechanics literature (Leroueil & Marques, 1996; Vaid & Campanella, 1977; Soga &

Mitchell, 1996), contradicts geo-physical models which favoured the viscous model (Boulton & Hindmarsh, 1987; Dobbie, 1992), where soil parameters are affected by strain rate.

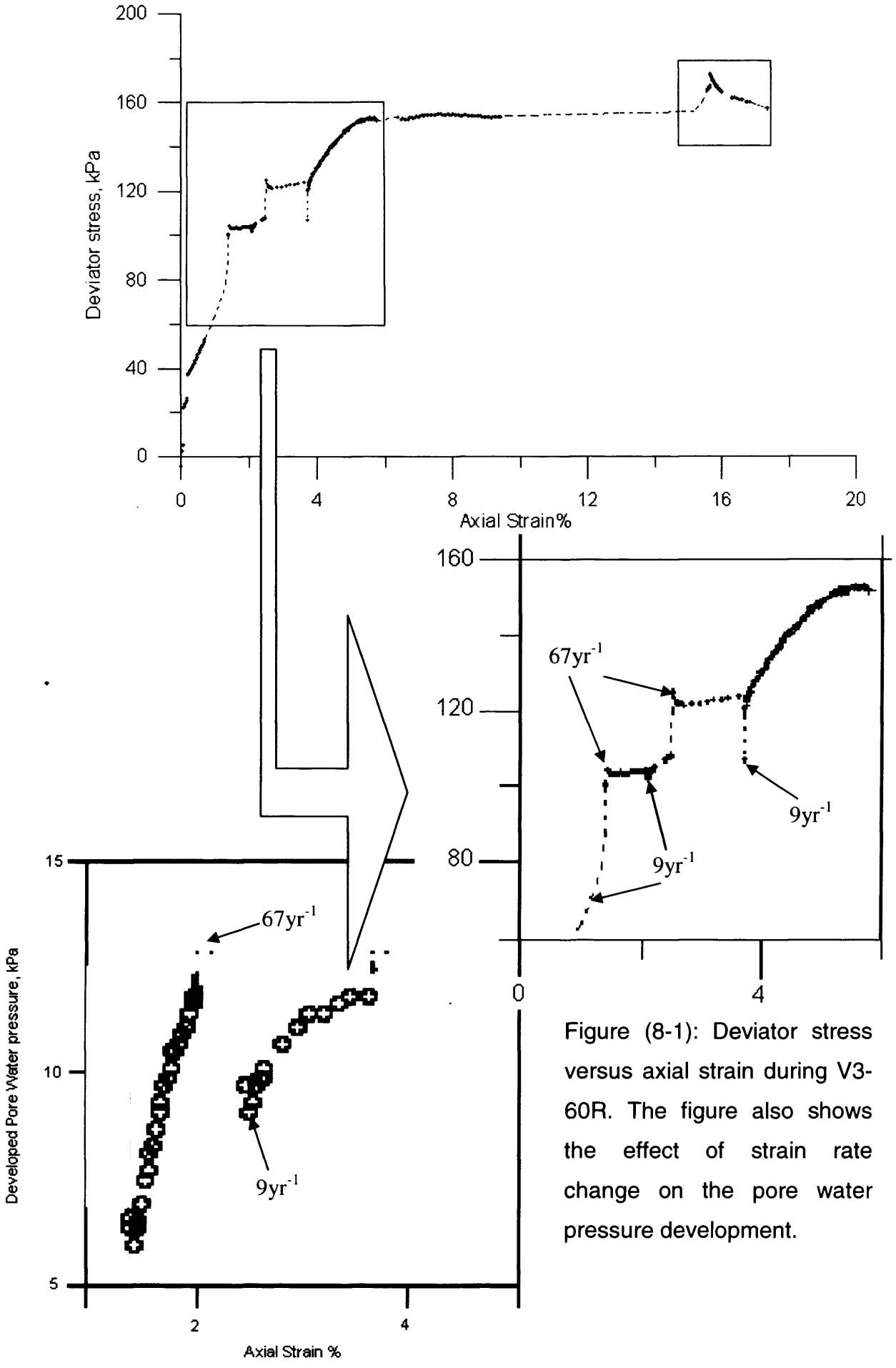

Figure (8-1): Deviator stress versus axial strain during V3-60R. The figure also shows the effect of strain rate change on the pore water pressure development.

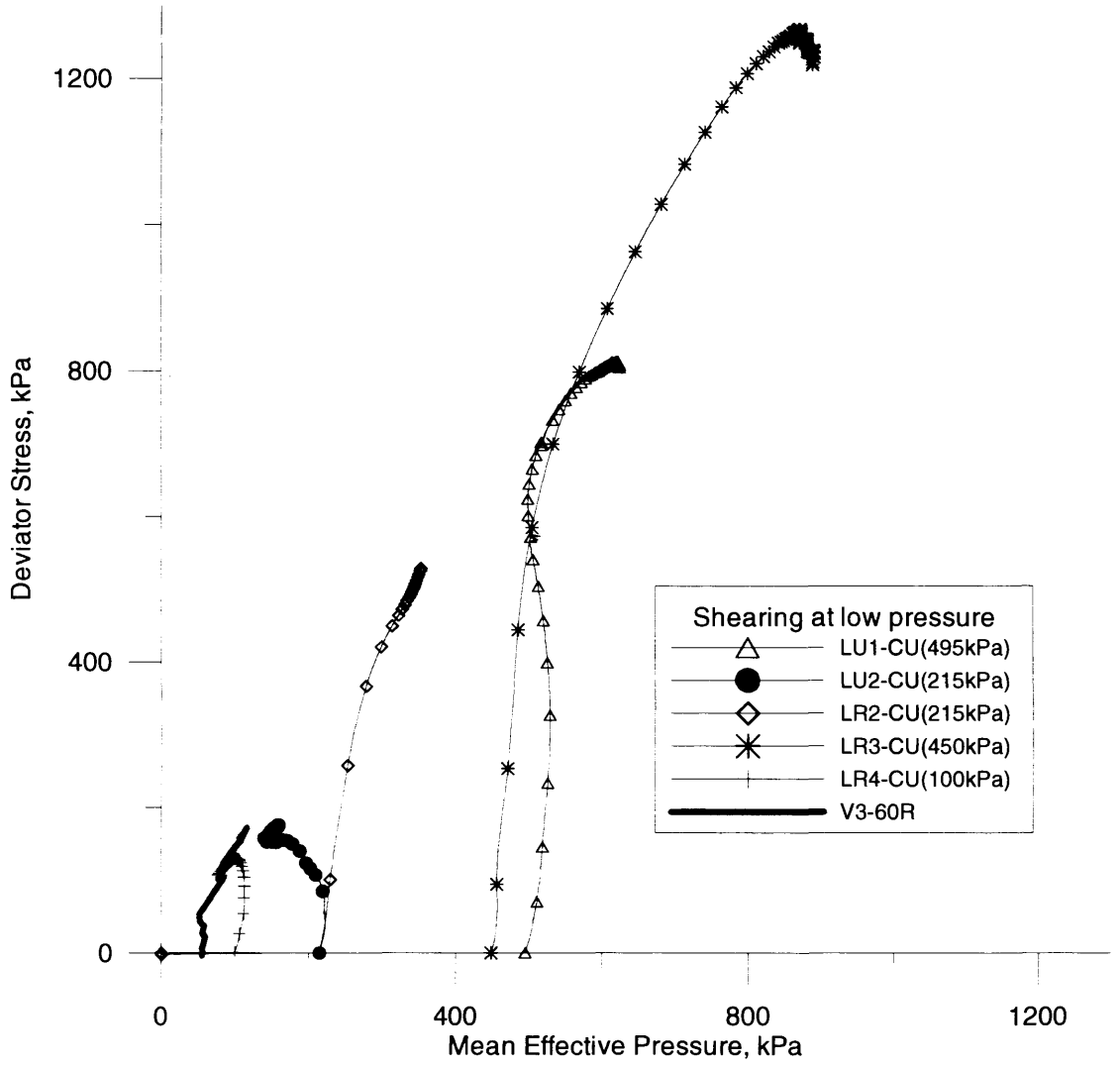

Figure (8-2): Stress paths of triaxial compression tests conducted at low pressures. The figure also shows the stress path of variable strain rate test V3-60R.

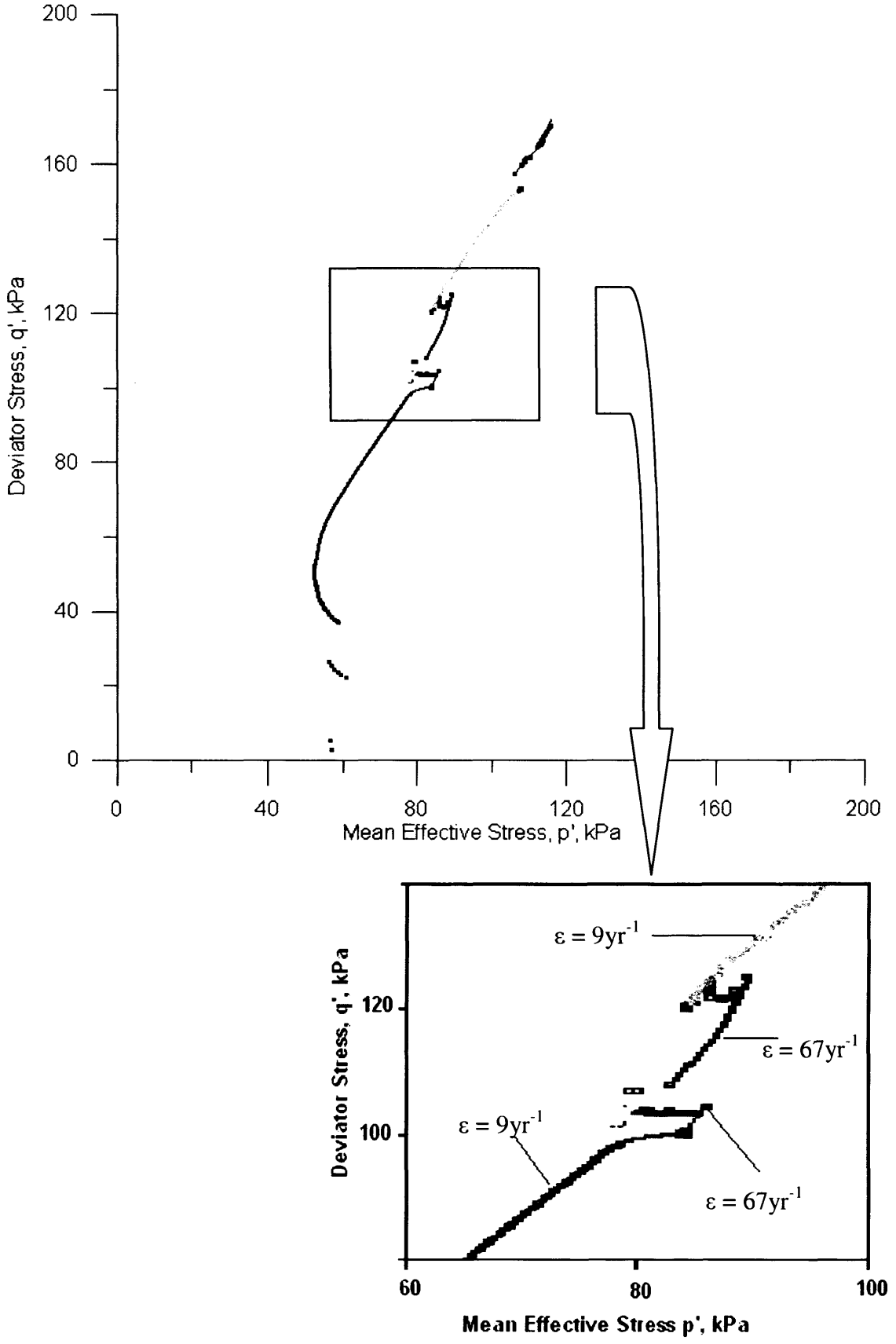

Figure (8-3): Stress path of variable strain rate test V3-60R. The figure shows the effect of step-wise strain rate change on the shearing stress path.

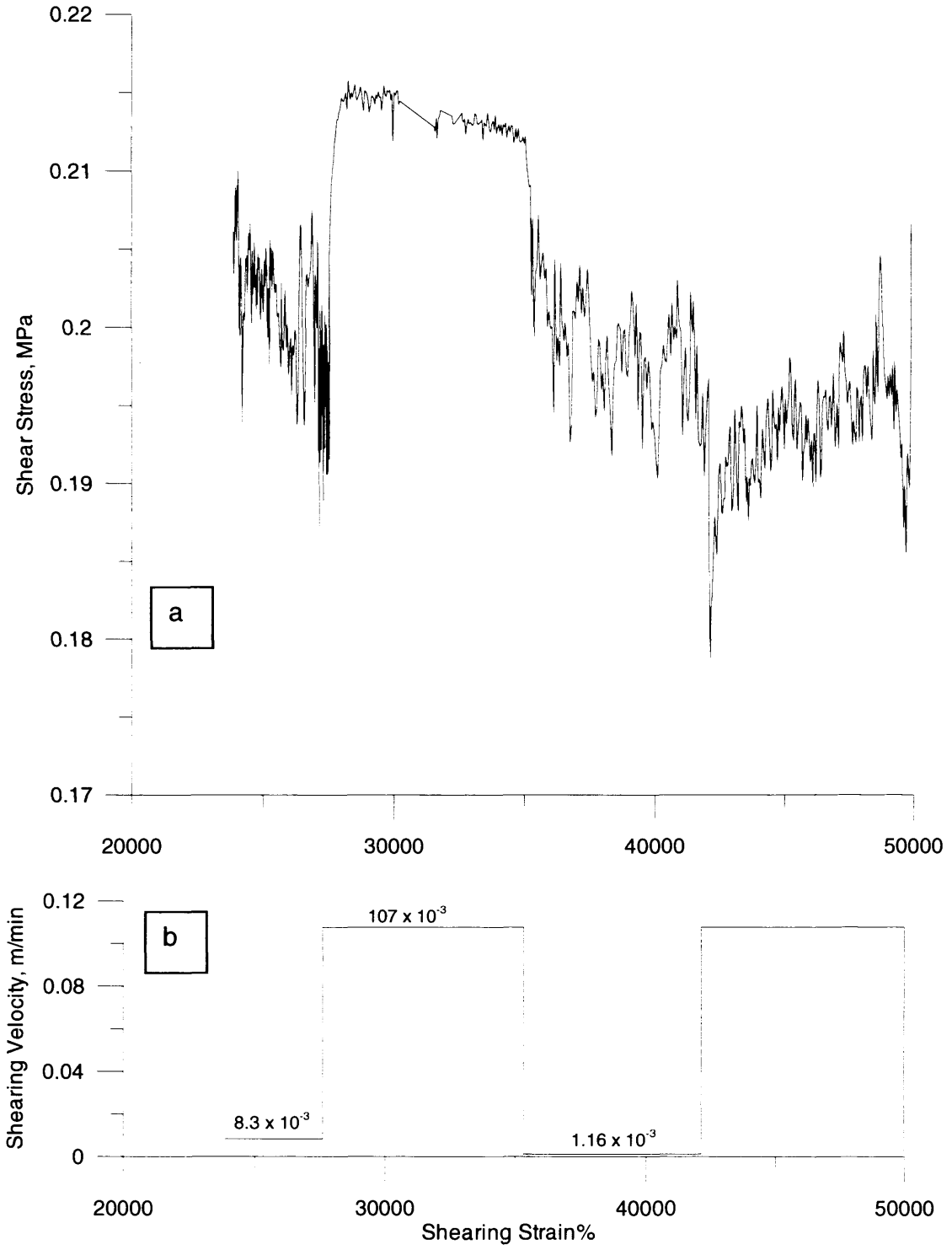

Figure (8-4): Shear stress change with shear strain for test BR350-var (a) during open gap period, where the shearing velocity was step-wise changed (b) to investigate the sediment viscous behaviour.

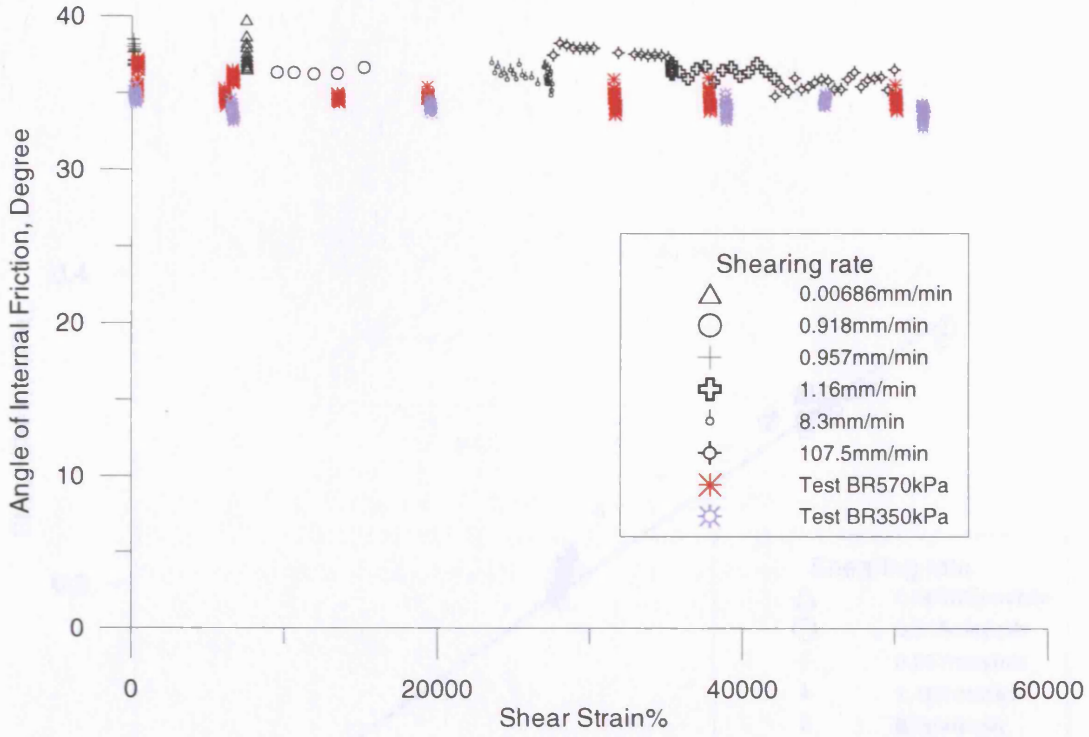

Figure (8-5): Angle of internal friction obtained from ring shear tests at constant shearing rate (BR570 & BR350) and variable shearing rate (BR350-var).

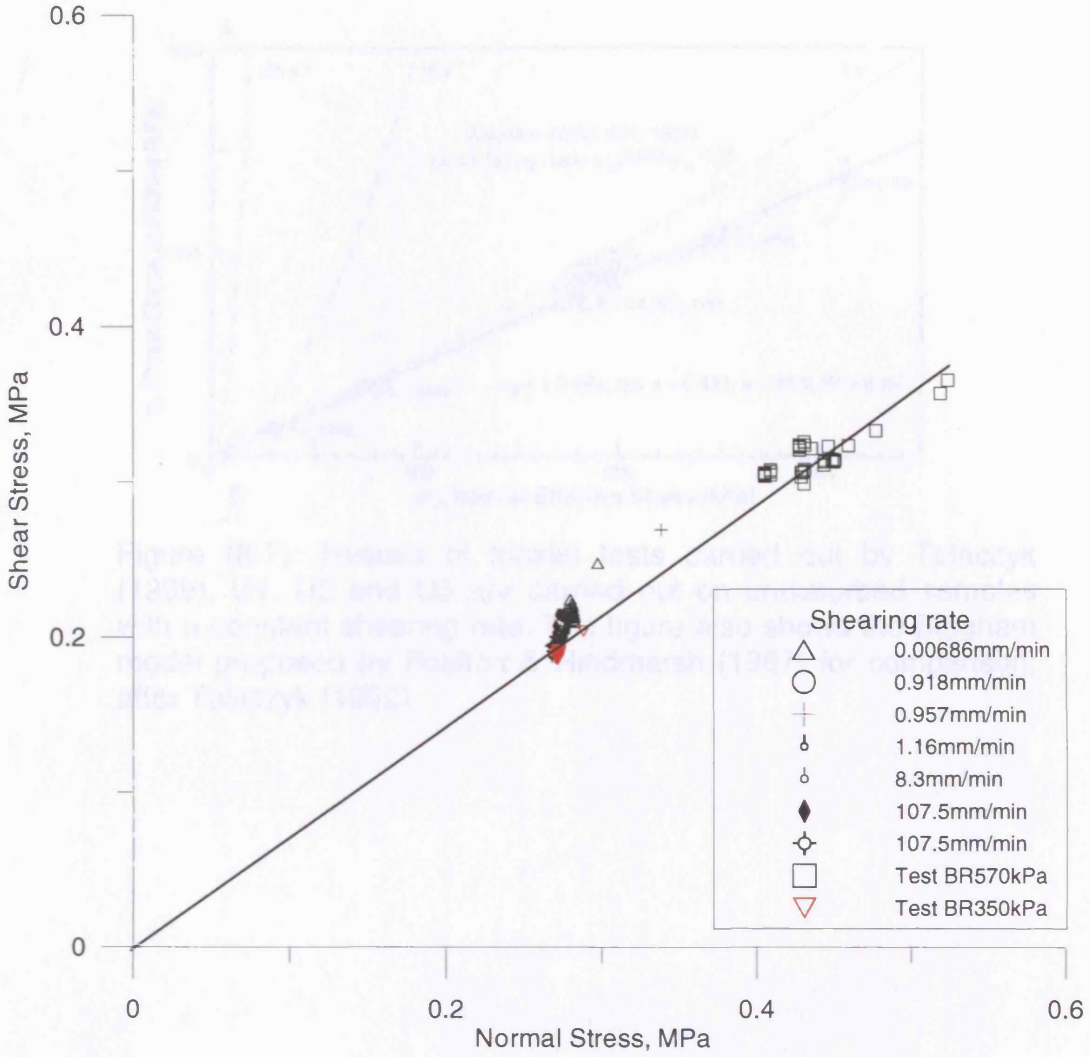

Figure (8-6): Normal stress versus shear stress for open gap periods for tests conducted on Langjökull sediment using the ring shear apparatus.

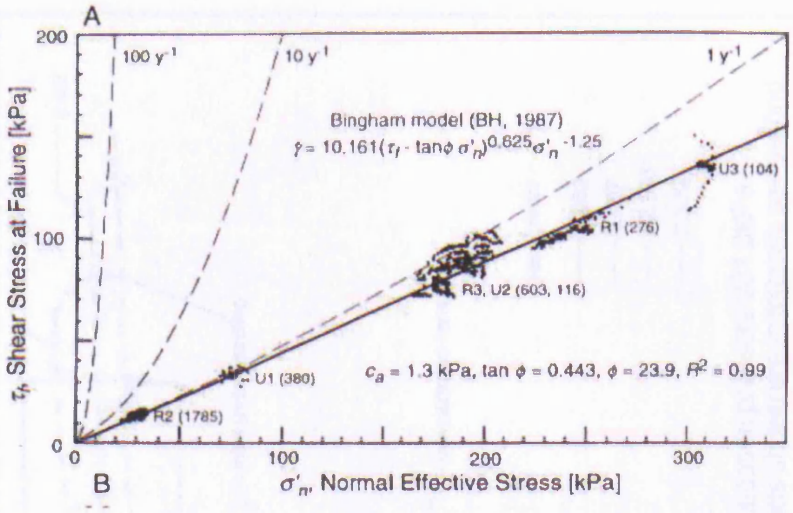

Figure (8-7): Results of triaxial tests carried out by Tulaczyk (1999). U1, U2 and U3 are carried out on undisturbed samples with a constant shearing rate. The figure also shows the Bingham model proposed by Boulton & Hindmarsh (1987) for comparison, after Tulaczyk (1999).

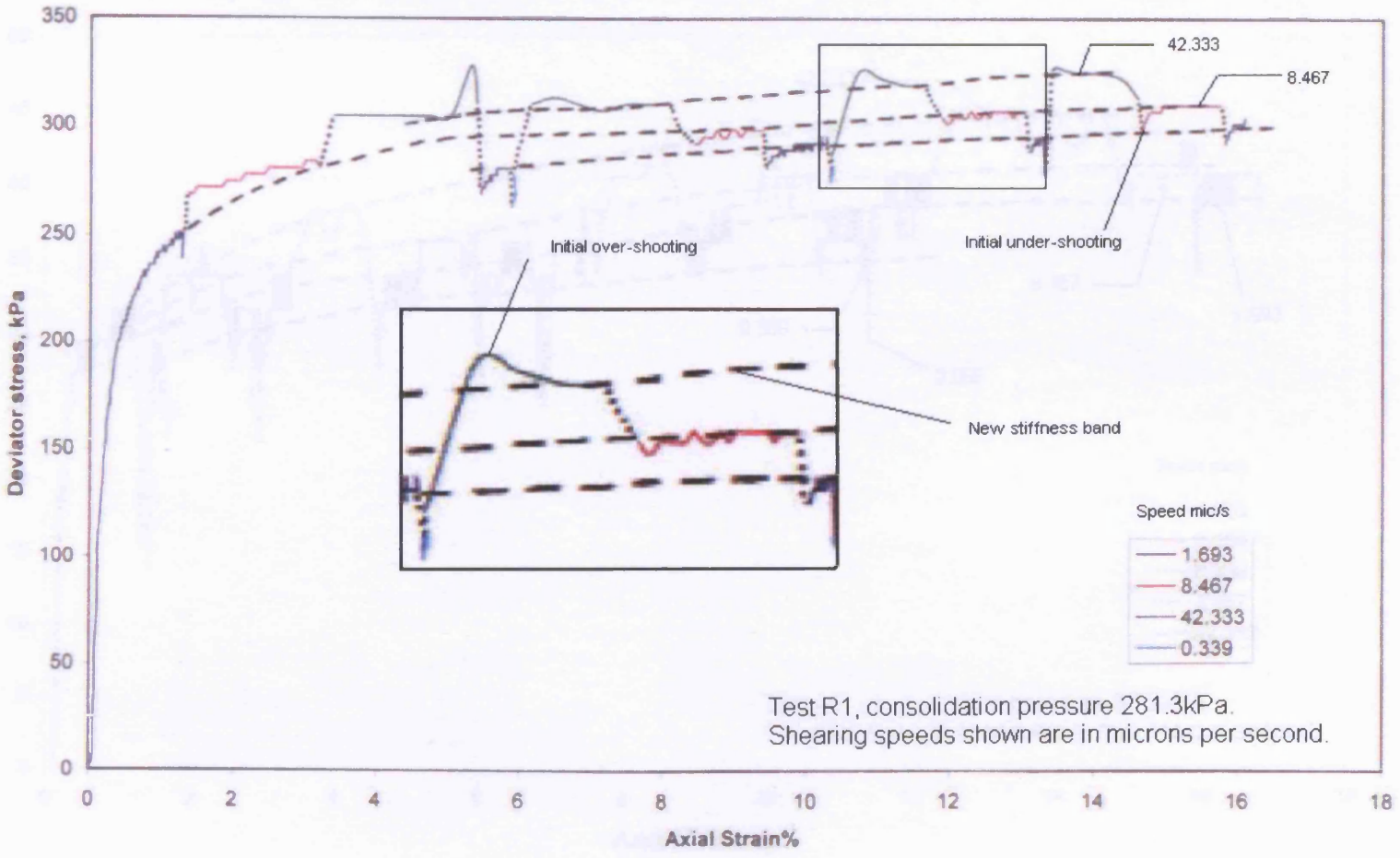

Figure (8-8): Replotted test R1 data (data from Tulaczyk, 1999).
Variable shearing rates were used.

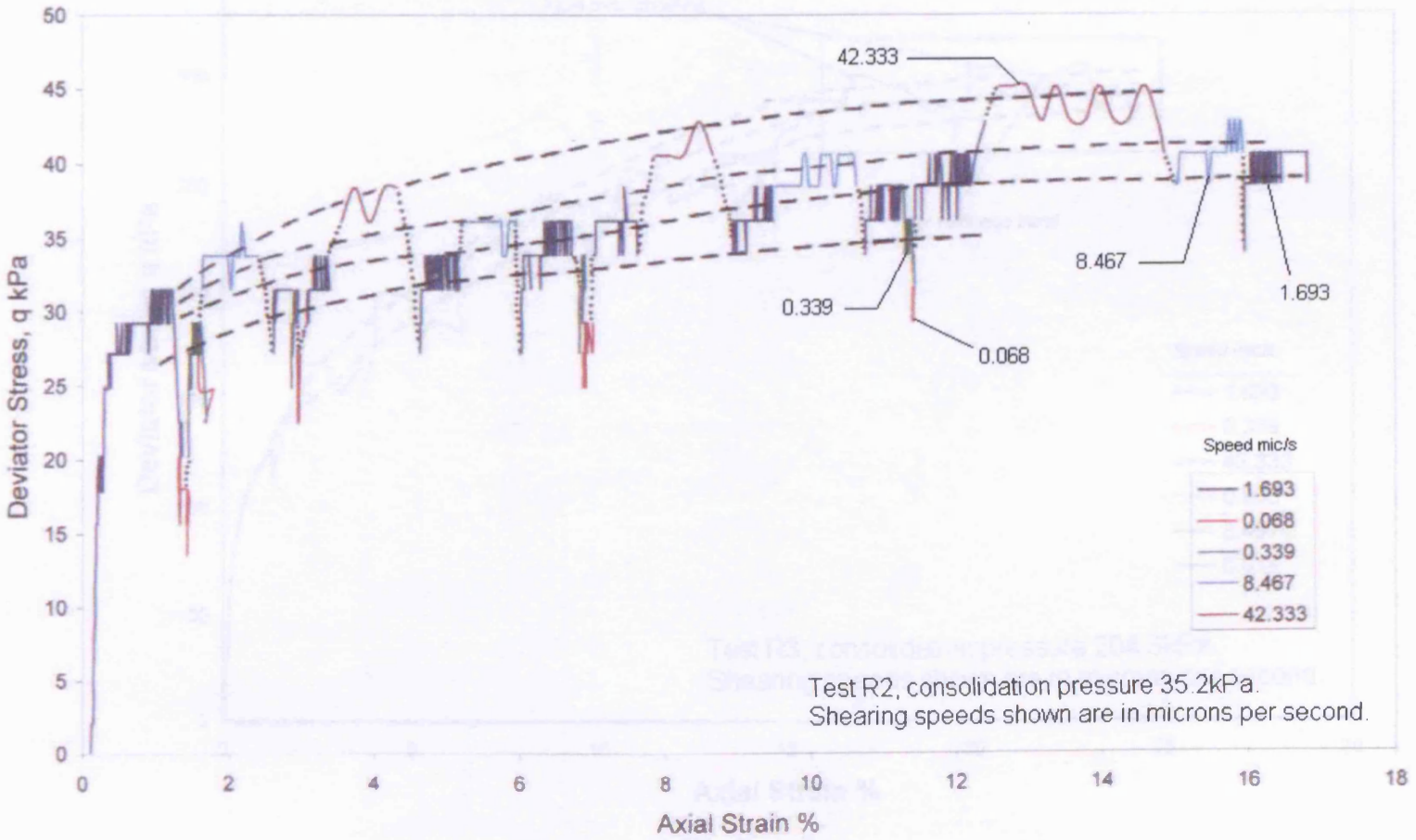

Figure (8-9): Replotted test R2 data (data from Tulaczyk, 1999).
Variable shearing rates were used.

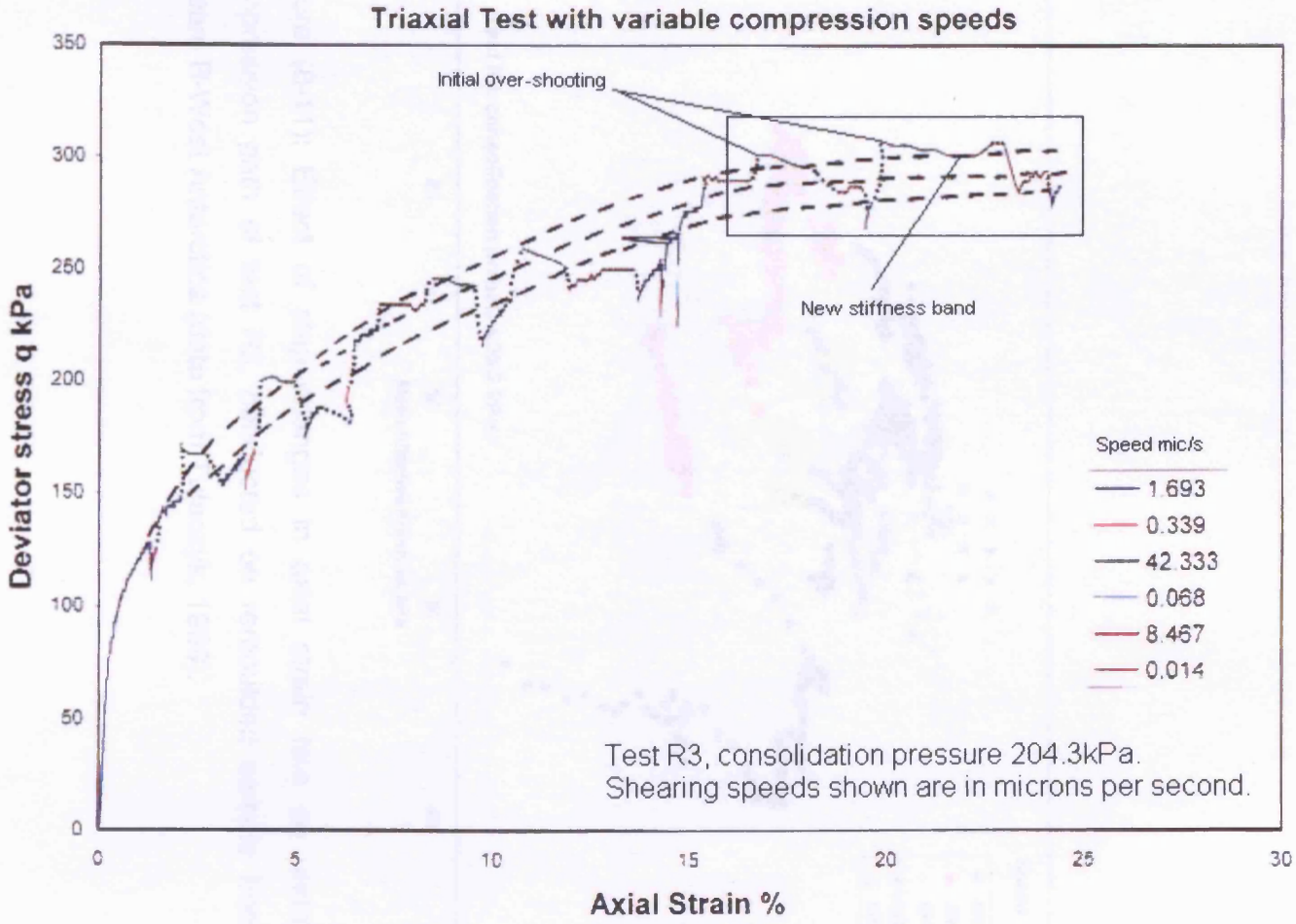

Figure (8-10): Replotted test R3 data (data from Tulaczyk, 1999).
Variable shearing rates were used.

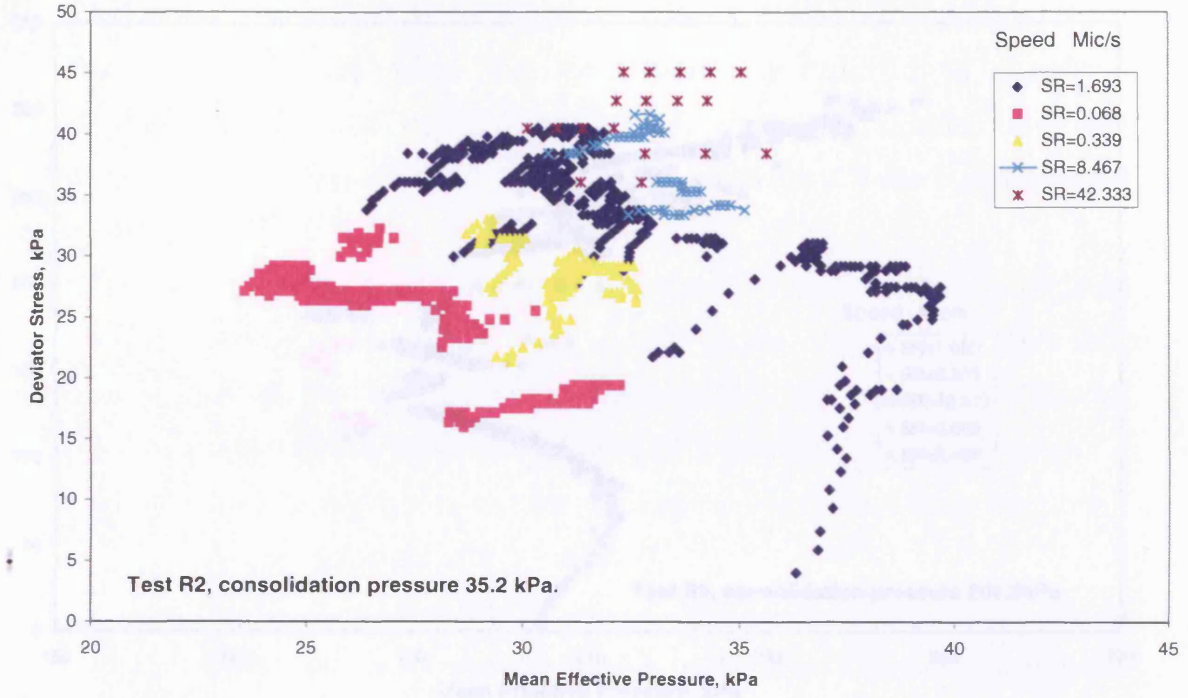

Figure (8-11): Effect of step changes in axial strain rate on undrained compression path of test R2, conducted on remoulded sample from Ice Stream B-West Antarctica (data from Tulaczyk, 1999).

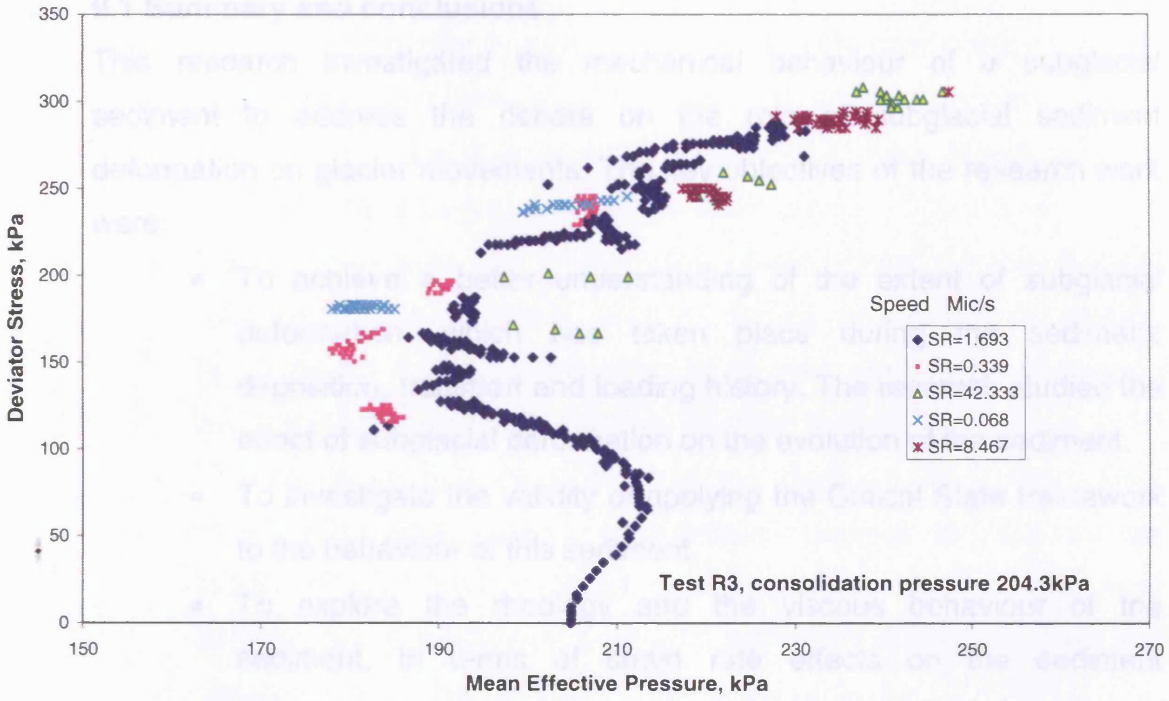

Figure (8-12): Effect of step changes in axial strain rate on undrained compression path of test R3, conducted on remoulded sample from Ice Stream B-West Antarctica (data from Tulaczyk, 1999).

Chapter Nine

Conclusions and recommendations for further studies

9.1 Summary and conclusions

This research investigated the mechanical behaviour of a subglacial sediment to address the debate on the role of subglacial sediment deformation on glacier movements. The key objectives of the research work were:

- To achieve a better understanding of the extent of subglacial deformation, which has taken place during the sediment; deposition, transport and loading history. The research studied the effect of subglacial deformation on the evolution of the sediment.
- To investigate the validity of applying the Critical State framework to the behaviour of this sediment.
- To explore the rheology and the viscous behaviour of the sediment, in terms of strain rate effects on the sediment deformation.

To address the key objectives a series of triaxial, oedometer and ring shear tests were conducted in this research project. In these tests, different ranges of pressures and shearing strains were applied to the sediment. On the basis of the literature review and the findings from these tests, the subglacial sediment deformation and particle breakage was evaluated. This was achieved by evaluating the particle size distribution of the sediment, and the effect of the stresses and strains applied on the sediment grading.

The results of these tests were also analysed in terms of stresses and volumetric deformation, to explore the validity of applying the Critical State framework on the behaviour of the subglacial sediment. The research also investigated the rheology of the sediment by exploring the shearing strain

rate effect on the sediment behaviour. The findings and conclusions from the literature review and experimental work are summarised below.

9.1.1 The Langjökull subglacial sediment

The subglacial sediment which was retrieved from a pro-glacial area of Langjökull, is:

- A well graded (poorly sorted) sediment, with sub-rounded to sub-angular shaped particles. The sediment which comprises mainly feldspar and pyroxenes contains about 45% of fines. However, there was no trace of clay minerals in the sediment.
- The mineralogical test result also gives a hint on the type of weathering this sediment was subjected to during its history, favouring the mechanical weathering as the main type of weathering which this sediment was subjected to under the glacier.
- The mineralogy test results also indicate that the mineral composition of different particle sizes of the sediment particles is the same -an indication of a homogeneous parent rock, and/or that the finer particles are actually an outcome of extreme erosion, abrasion and grinding of the larger particles of the same sediment.
- The sediment specific gravity was found to be 3.10, which is high compared to most granular soils.
- The sediment particles have a great ability for packing, an ability which was imposed by the well-graded nature of the sediment. This is reflected in the low values of both the minimum and the maximum void ratios (specific volume) of this sediment, with a maximum void ratio observed in the field (undisturbed samples).

9.1.2 The effect of subglacial deformations on the sediment particle size distribution evolution

The study, presented in Chapter Six, comprises a series of high pressure triaxial compression tests (isotropic and shearing) and ring shear tests which were carried out to investigate the influence of high stresses and high strains

on the evolution of the sediment's particle size distribution (PSD). In addition to the sieving method which was used to monitor the change in PSD of the sediment during tests, scanning electron microscope images were used to identify particle breakage in some of the tested samples. Artificially graded samples were also tested for further understanding of the breakage potential of the soil. One-dimensional compression tests were conducted using the oedometer to investigate the effect of particle size distribution of the sediment on its compressibility. The results of these tests which were conducted on both, naturally graded samples and artificially graded samples indicated that:

- The Langjökull sediment, which is a well-graded sediment, had been subjected to extreme deformation during its depositional and loading history, which resulted in the current grading of the sediment.
- The sediment, in its current grading has reached a terminal grading where no further significant particle breakage can be expected by applying any pressures or strains to the sediment. This reflects the large depositional distance this sediment has travelled from its source (parent rock) under the glacier during the sediment depositional history.
- The volumetric strains during shearing of naturally graded sediment are limited to those volumetric strains associated with particle rearrangements during shearing rather than the high volumetric compressive strains which are usually linked to particle breakage during compression and shearing of granular soils.
- The effect of the sediment grading on its compressibility behaviour was reflected by multiple parallel compression curves in the v-ln p′ plane, obtained from compression tests conducted on the naturally graded sediment. The sediment showed no clear yielding point, as there was no breakage expected during compression, exhibiting no unique Normal Compression Line, even when extremely high isotropic compression pressures were applied to the sediment.

- A more uniformly graded sample of this sediment showed different compressive behaviour than the naturally graded sample, exhibiting a clear yielding point with a tendency to form a unique Normal Compression Line, indicating that the sediment grading is a key factor in defining the sediment's compressive behaviour.

9.1.3 The sediment behaviour within the Critical State framework

The study, presented in Chapter Seven, comprised of a series of isotropic and shearing triaxial tests, conducted in a wide range of cell pressures on both undisturbed and reconstituted samples. These tests were carried out to investigate the validity of the Critical State framework in defining the sediment behaviour during shearing. The most important findings and conclusions drawn from previous literature and the results were:

- The sediment behaviour during compression indicated that the sediment exhibited a transitional behaviour, showing no unique Normal Compression Line, a behaviour which was previously noted in some gap-graded residual sediment and some well graded silts. The position of the compression curves in the v-ln p' plane is dependent on the sample initial density, or specific volume. However, compression of more uniformly graded samples of the same sediment exhibited a clear tendency to form a unique Normal Compression Line.
- In contrast to the transitional behaviour exhibited by some soils as was noted in previous literature, the sediment behaviour during shearing defined a unique Critical State Line, with a low value of λ, indicating very stiff behaviour of this sediment.
- By normalising the stress paths for all tests conducted, the dominating factors in defining the position of boundary surfaces were found to be the maximum and minimum void ratio, or density of the sample. Samples which started their shearing stage from a state which lies to the right of the Critical State Line (wet of critical) in the v-ln p' plane, tend to compress and harden during shearing till the sample reaches its Critical State. The denser samples or

samples for which their state lies to the left and down the Critical State Line (dry of critical), exhibit a dilative behaviour during shearing and tend to soften, following a stress path on the Hvorslev surface to reach their Critical States.

- The behaviour of those remoulded samples which started their shearing stage from a state positioned close to the Critical State Line was mainly dominated by an initial compressive behaviour before it showed a dilative behaviour untill it reached failure. The state of the undisturbed samples was noted to be very close to the Critical State Line. However, the behaviour of the undisturbed samples was dominated by compressive behaviour all through the test.
- Generally, the shear modulus of the sediment showed a decrease with strain development. Although the results showed a general increase with confining pressure, there was an indication of the sample state influencing the shearing stiffness values. The intact sample exhibited very low stiffness during shearing compared to the values exhibited by the reconstituted samples.

9.1.4 The viscous behaviour of the sediment and the effect of strain rate on the sediment behaviour

The influence of strain rate, as presented in Chapter Eight, was studied by imposing variable axial strain rates during undrained triaxial shearing of the sediment. The strain rate effect on the sediment residual strength was also investigated by conducting variable strain rate ring shear tests. The results were compared with the results obtained from shearing tests on another subglacial sediment (Ice Stream B-West Antarctica). The study conducted on the sediment along with the re-analysis of the existing data showed that:

- Langjökull sediment exhibited a temporary over or under shooting associated with the increase or decrease of the shearing strain rate. However, with the development of strain the stress strain curve gradually yields to join a Constant strain Rate (CSR) curve before the change of

the shearing strain rate was imposed. This kind of behaviour is what so-called in previous literature by the TESRA behaviour. This temporary effect was also observed on the sample stress path and the development of pore water pressure.

- The viscous behaviour exhibited by Langjökull sediment, although it imposes immediate temporary changes on the undrained strength of the sediment, did not enforce any change on the failure envelope or parameters such as the angle of friction of the sediment and the position or the slope of the Critical State Line.
- The sediment's drained residual strength was not seen to be affected by the shearing rate changes. This was concluded from the results obtained by shearing the sediment to very high strains using a Bishop-type ring shear apparatus.
- The sediment mineralogy has great effect in defining its rheology. The Temporary Effect of Strain Rate and Acceleration (TESRA) behaviour exhibited by Langjökull sediment, which is mainly composed of basalt and with no clay minerals, is a property which is typically exhibited by pure sands. However, for a clay-rich sediment, such as the one from Ice Stream B-West Antarctica, the behaviour was more persistent. The clayey sediment showed behaviour between the (Isotach) and the (TESRA) property. This behaviour as it was termed in previous literature is (General TESRA).
- A moderate viscous behaviour was observed for both cases discussed in this study, Langjökull sediment and Ice Stream B- West Antarctica. This moderate viscous behaviour, which does not influence the soil parameters, contradicts the viscous model proposed by Boulton & Hindmarsh (1987), which represent an extreme of the

viscous model by suggesting a change of all soil parameters due to strain rate changes.

9.2 Recommendations for further studies

The experimental work in this study has concentrated on studying the mechanical behaviour of the glacial sediment. The analysis made of these data showed that a subglacial sediment like the Langjökull sediment, which has already reached a terminal grading due to substantial shearing deformation under the glacier, exhibits a transitional mechanical behaviour. In the view of findings and discussion therefore, the following recommendations for further research on the mechanical behaviour of subglacial sediments, are made:

- **Studying the mechanical behaviour of different gradings of the sediment:** In studying Langjökull sediment's mechanical behaviour, tests showed that particle breakage was not the key factor in defining its mechanical behaviour. This conclusion was derived from a series of tests which proved that this sediment has already reached its terminal grading. However, a different grading exhibited significant particle breakage in shearing and thus different behaviour during compression, which was fully controlled by particle breakage. This would require a further investigation of the validity of the hypothesis that a transitional behaviour may be a property of sediments which have reached their terminal grading.
- **Investigating the PSD evolution effect on the mechanical behaviour of subglacial sediments:** further investigation needs to be carried out on subglacial sediments which still have the ability for their particles to break (preferably with a similar mineralogy to Langjökull sediment). This will provide a good source of comparison of the behaviour of two sediments with different levels of travelling distances from their parent source and thus different grading.

- **Computer simulation** of crushable subglacial sediment might give an insight into the evolution of particle size distribution with the development of shearing strains and compression stresses. Some distinct element models have been shown to be capable of replicating the complex behaviour of sands in relation to their strength, dilatancy and Critical State. Estimating the sediment's single particle strength might be used for interpreting the evolution of the PSD, however, the hypothesis of the existence of a terminal or critical grading of the sediment should be taken into consideration when simulating particle breakage of the sediment.
- **Influence of the sedimentation structure on the viscous behaviour of subglacial sediment:** The effect of sedimentation structure on the viscous behaviour of the sediment might be studied by comparing the behaviour of undisturbed samples with that of reconstituted ones.
- **Influence of strain rate change on the sediment residual strength in undrained condition:** In this study, the effect of strain rate change on the sediment residual strength was investigated by using the Bishop-type ring shear apparatus which imposes a drained condition while shearing. However, it is worthwhile to investigate the sediment behaviour at high strains in undrained condition which is more relevant to the condition underneath glaciers.
- **Influence of creep and stress relaxation on the behaviour of the sediment:** In this study, the sediment's viscous and time-dependent behaviour was studied by concentrating on studying strain rate effects. However, the time-dependent behaviour of the sediment would include a wider range of influencing factors such as creep and stress relaxation, which are also relevant to the conditions of subglacial environment.

References

Alley, R.B. (1989). "Water-pressure coupling of sliding and bed deformation: II. Velocity-depth profiles". *Journal of Glaciology,* 35, pp.119-129.

Alley,R. B., Blankenship, D. D., Bentley, C.R., & Rooney, S.T. (1986). "Deformation of till beneath Ice Stream B, west Antarctica.", *Nature*, vol. 322, No. 6974, pp. 57-59.

Alley, R. B., Blakenship, D. D., Rooney, S. T., & Bentley, C. R. (1987). "Till beneath ice stream-B.", *Journal of Geophysical Research- Solid Earth and planets*, vol. 92, pp. 8921-8940.

Alley, R.B., Blakenship, D.D., Rooney, S.T. & Bentley, C.R. (1989)."Sedimentation beneath ice shelves-the view from Ice stream B". *Marine Geology,* 85, pp.101-120.

Altuhafi, F., Baudet, B.A., & Sammonds, P. (2006). "Particle breakage in glacial sediments", in *Geomechanics and Geotechnics of Particulate Media*, Hyodo & Nakata, eds., pp. 21-24

Andres, A., Morten, L. & Poul V. L. (2004). "Evaluation of Time-Dependent behaviour of soils", *Int. J. of Geomechanics*, ASCE, September 2004, pp.137-155.

Atkinson, J. & Bransby, P.L. (1978). *The Mechanics of Soils; An introduction to critical state soil mechanics*, McGraw -Hill, London .

Been, K. & Jefferies, M. 1985, "A state parameter for sands", *Geotechnique*, vol. 35, no. 2, pp. 99-112.

Benn, D. I. (1995). "Fabric signiture of subglacial till deformation, Breidamerkurjokull, Iceland", *Sedimentology*, No. 42, pp. 735-747.

Benn, D. I. & Evans, D. J. A. (1998). *Glaciers & Glaciation*, Arnold.

Bennett, M. R., & Glasser, N. F. (1996). *Glacial Geology- Ice sheets and landforms,* John Wiley&Sons Ltd.

Bindschadler, R.A., King, M.A., Alley, R.B., Anandakrishnan, s. & Padman, L. (2003). " Tidally controlled stick-slip discharge of a west Antarctic ice stream", *Science,* 301, (5636), pp. 1087-1089.

Bishop, A.W., Green, G.E., Andersen, A., Brown, J.D. & Garaga, V.K. (1971). " a new ring shear apparatus and its application to the measurment of the residual strength", *Geotechnique*, Vol. 21, issue 4, pp 273-328.

Bjornsson, H. (1998)." Hydrological characteristics of the drainage system beneath a surging glacier". *Nature,* 395, pp. 771-774.

Blake, E. W. (1994). "Direct measurment of sliding at the glacier bed", *Journal of Glaciology*, vol. 40, pp. 595-599.

Blake, E. W., Clarke, G. K. C., & Gerin, M. C. (1992). "Tools for examining subglacial bed deformation.", *Journal-of-Glaciology*, vol. 38, No. 130, pp. 388-396.

Boulton, G.S. (2006). "Glaciers and their coupling with hydraulic and sedimentary processes", in *Glacier Science and Environment Change*, First edn, P. G. Knight, ed., Blackwell Science Ltd., pp. 3-22.

Boulton, G.S. (1996). "Theory of glacial erosion, transport and deposition as a consequence of subglacial sediment deformation", *Journal of Glaciology*, vol. 42, No. 140, pp. 43-62.

Boulton, G.S., & Dobbie, K.E. (1993). "Consolidation of sediments by glaciers; relations between sediment geotechnics, soft-bed gloacier dynamics and subglacial grownd water flow", *Journal of Glaciology*, vol. 39, No. 131, p. 26.

Boulton, G.S., & Hindmarsh, R.C.A. (1987). "Sediment deformation beneath glaciers : Rheology and geological consequences", *Journal of Geophysical Research*, vol. 92, No. B9, pp. 9059-9082.

Boulton, G.S. & Jones, A.S. (1979). "Stability of temperate ice caps and ice sheets resting on beds of deformable sediment". *Journal of Glaciology,* 24 (90), pp. 29-43.

Boulton G.S. (1976). "The development of geotechnical properties in glacial till", in *Glacial till*, Lagget R.F., ed., The Royal Society of Canada, pp. 292-303.

Boulton, G.S., Dent, D.L., & Morris, E.M. (1974). "Subglacial Shearing and crushing, and the role of water pressures in tills from south-east Iceland", *Geografiska Annaler*, vol. 56A, No. 3-4, pp. 135-145.

Boulton, G. S., Dobbie, K. E., & Zatsepin, S. (2001). "Sediment deformation beneath glaciers and its coupling to the subglacial hydraulic system", *Quaternary international*, vol. 86, No. 1, pp. 3-28.

Brodzikowski, K. & van Loon, A. J. (1991). *Glacigenic Sediments*, Elsevier Science Publishers BV, Netherlands.

Casagrande, A. (1936). "The determination of the preconsolidation load and its practical significance", Proc. 1st Int. Conf. on Soil Mechanics & Foundation Engng., 3, pp.60-64.

Cazacliu, B., Yasin, S.J.M.&Matasushita, M. (1998), Internal report. Geotechnical Laboratory, University of Tokyo.

Chu, J. & Leong, W.K. (2002). "Effect of fines on instability behaviour of loose sand", *Geotechnique*, 52, No. 10, pp. 751-755.

Coop, M.R. & Airey, D.W. (2003). "Carbonate sands", *characterisation and engineering properties of natural soils* pp. 1049-1085.

Coop, M.R. & Atkinson, J.H. (1993), "The mechanics of cemented carbonate sands", *Geotechnique*, vol. 43, No. 1, pp. 53-67.

Coop, M. R. & Lee, I. K. 1993, "The Behaviour of Granular Soils at elevated Stresses.", *Predictive soil Mechanics* pp. 186-198.

Coop, M.R., Sorensen, K., Bodas Freitas, & Georgoutsos, G. 2004, "Particle breakage during shearing of a carbonate sand", *Geotechnique*, vol. 54, No. 3, pp. 157-163.

Craig, R. F. (1974). *Soil Mechanics*, Fifth edn, Chapman & Hall.

Cuccovillo, T. & Coop, M.R. (1997). " The measurment of local axial strainsvin triaxial tests using LVDTs", *Geotechnique,*47, No.1, pp.167-171.

Daouadji, A. & Hicher, P. Y. (2006). "Modeling influence of grain breakage", in *Geomechanics and Geotechnics of Particulate Media*, Hyodo & Nakata, eds., pp. 319-325.

Dobbie, K.E. (1992)."Till geotechnic and ice sheets dynamics", PhD thesis, University of Edinburgh.

Dreimanis, A. (1976). "Tills: Their origin and properties," in *Glacial till*, R. F. Legget, ed., The Royal Society of Canada Special Publications, No.12, pp. 11-49.

Dreimanis, A & Vagners, U.J. (1971). "Bimodal distribution of rock and mineral fragments in basal tills", In: Goldthwait, R.P. (Ed). Till: A symposium, Ohio State University Press-Ohio, pp.237-250.

Engelhardt, H. & Kamb, B. (1997). "Basal hydraulic system of a west Antarctic ice stream: constraints from borehole observations.", *Journal of Glaciology*, vol. 43, pp. 207-230.

Eyre, N. (2003). *The role of subglacial processes in glacial dynamics,* PhD, University of Bristol.

Ferreira P.M. & Bica A.V.D. (2006). "Problems in identifying the effects of structure and critcal state in a soil with transitional behaviour", *Geotechnique*, vol. 56, 7, pp. 445-454.

Flint, R. F. (1971). *Glacial and Quaternary Geology*, John Wiley & Sons, Inc.

Fischer, U.H. & Clarke, G.K.C. (1997). "Stick slip sliding behaviour at the base of glacier", *Journal of Glaciology* , No. 24, pp. 390-396.

Fountain, A.G. (1994). "Borehole water level variations and implications for the subglacial hydraulics of south Cascade glacier, washington state USA", *Journal of Glaciology*, vol. 40, No. 135, pp. 293-304.

Fowler, A.C. (2002). "Correspondence Rheology of subglacial till", *Journal of Glaciology,* 48,163, pp.631-632.

Fowler, A.C. (2003)."On the rheology of till", *Ann. Glaciol.,*37, pp.55-59.

Fuller, S. & Murray, T. (2000). "Evidence against pervasive bed deformation during the surge of an Icelandic glacier", *Deformation of Glacial Materials*, Editors: Maltman, A. J., Hubbard, B., and Hambrey, M. J. [176], pp. 203-216. Geological Society Special Publication.

Gasparre, A., Coop, M. R., & Cotecchia, F. (2003). "An experimental investigation of creep processes in a crushable sand", in *Deformation Characteristics of Geomaterials*, Benedetto et al., ed., Swets & Zetinger, Lisse, pp. 773-778.

Georgiannou, V.N., Burland, J.B. & Hight, D.W. (1990). "The undrained behaviour of clayey sands in triaxial compression and extention", *Geotechnique*, 40, No.3, pp.431-449.

Georgoutsos, G. D. (2002). *An investigation into the critical state of sands with particular reference to particle breakage,* MSc., Imperial College of Science Technology and Medicin/ Dept. of Civil & Environmental Eng.

Goldthwait, R. P. (1960), *Formation of ice cliffs. In "Study of ice cliffs in Nunatarssuaq, Greenland".* 39.

Graham, J., Crooks, J. H. A., & Bell, A. L. (1983). "Time effects on the stress-strain behaviour of natural soft clays", *Geothechnique*, vol. 33, No. 3, pp. 327-340.

Hambrey, M. (1994). "Glacier Dynamics," in *Glacier Environments*, UCL press Ltd.

Hamilton, J. J. & Crawford, C. B. (1959). "Improved determination of preconsolidation pressure of a sensitive clay", in *Papers on soils, ASTM*, pp. 254-271.

Hardin, B.O. (1985), "Crushing of soil particles", *Journal of Geotechnical Engineering*, vol. 111, No. 10, pp. 1177-1192.

Hart, J.K. (1995). " Subglacial errosion, deposition and deformation associated with deformable beds", *Progress in Physical Geography,* 19, 2, pp.173-191.

Hart, J.K. , Khatwa, A. & Sammonds, P. (2004). "The effect of grain texture on the occurrence of microstructural properties in subglacial till", *Quaternary Science Reviews*, vol. 2004, No. 23, pp. 2501-2512.

Hart, J. K. & Smith, B. (1997). "Subglacial deformation associated with fast ice flow, from columbia glacier, Alaska.", *Sedimentary Geology*, vol. 111, pp.177-197.

Hindmarsh, R. (1997). "Deforming beds: viscous and plastic scales of deformation", *Quaternary Science Reviews,*16, 9, pp. 1039-1056.

Hooke, R.LeB. & Iverson, N.R. (1995), "Grain size distribution in deforming subglacial tills: Role of grain fracture", *Geology*, pp. 57-60.

Humphrey, N., Kamb, B., Fahnestock, M. & Engelhardt, H. (1993). "Characteristics of the bed of the lower Columbia Glacier, Alaska", *Journal of Geophysical Research*, vol. 98, No. B1, pp. 837-846.

Hvorslev, M. J. (1937). "Uber die Festigkeitseirgenschaften Gestorter Bindigere Boden", *Ingeniorvidenskabelige Skrifter,* A, No.45

Hyodo, M., Hyde,A.F.L., Aramaki, N. & Nakata, Y. (2002). "Undrained montonic and cyclic shear behaviour of sand under low and high confining stresses", *Soils and Foundation*, vol.42, No.3, pp. 63-76, June 2002, Japanese Geotechnical Society.

Ishihara, K., Tatsuoka, F., & Yasuda, S. (1975). "Undrained deformation and liquifaction of sand under syclic stresses". *Soil and foundations,* 15,No.1, pp.29-44.

Ishihara, K. (1993). "Liquifaction and flow failure during earthquakes", *Geotechnique*, 43, No. 3, pp. 351-415.

Iverson, N.R., Baker, R.W., Hooke, R.LeB., Hanson, B. & Jansson, P. (1999). "Coupling between a glacier and a soft bed: Arelation between effective pressure and local shear stress determined from till elasticity", *Journal of Glaciology*, vol. 45, No. 149.

Iverson, N.R., Hanson, B., Hooke, R. LeB. & Jansson, P. (1995). "Flow mechanisims of glaciers on soft beds", *Science*, vol. 267, No. 5194, pp. 80-81.

Iverson, N.R., Jansson, P. & Hooke, R. LeB. (1994). "In-situe measurements of the strength of deforming subglacial till", *Journal of Glaciology*, vol. 40, No. 136, pp. 497-503.

Iverson, N.R., Hooyer, T.S. & Baker, R.W. (1998). "Ring shear studies of till deformation; Coulomb plasic behaviour and distributed strain in glacier beds", *Journal of Glaciology*, vol. 44, No. 148, pp. 634-641.

Janbu, N., Tokheim, O. & Senneset, K. (1981). "Consolidation tests with continous loading", Proc. 10th ICSMFE, 1, pp.645-654.

Jovicic, V.T. & Coop, M.R. (1997). "The stiffness of coarse grained soils at small strains", *Geotechnique*, 47, No.3, pp. 545-561

Kamb, B. (1991). "Rheological nonlinearity and flow instability in the deforming bed mechanisim of ice stream mothion", *Journal of Geophysical Research*, vol. 96, No. B10, pp. 16585-16595.

Karrow, P. F. 1976, "Texture, mineralogy, petrography of North American till," in *Glacial till*, Robert F Legget, ed., p. 95.

Kenny, T.C. (1977). "Residual strengths of mineral mixtures", Proc. 9th Int. Conf. Soil Mechanics, Tokyo 1, pp. 155-160

Klotz, E.U. & Coop, M.R. (2001). "An investigation of the effect of soil state on the capacity of driven piles in sands", *Geotechnique*, 51, No.9, pp.733-751.

Lefebvre, G. & Leboeuf, D. (1987). "Rate effect and cyclic loading of sensetive clays", *J. Geotech. Eng.*, 113 (5), pp.476-489.

Leroueil, S. & Marques, M. E. S. (1996). "Importance of strain rate and temperature eects in geotechnical engineering," in *ASCE Geotechnical Special Publication 61*, pp. 1-60.

Leroueil, S., Kabbaj, M., Tavenas, F., & Bouchard, R. (1985). "Stress-strain-strain-rate relation for the compressibility of sensetive natural clay", *Geotechnique*, vol. 35, No. 2, pp. 159-180.

Leung, C. F., Lee, F. H., & Yet, N. S. (1996). "The role of particle breakage in pile creep on sand", *Canadian Geotechnical Journal*, vol. 33, pp. 888-898.

Li, X. S. & Dafalias, Y. F. (2000). "Dilatancy for cohesionless soils", *Geotechnique*, vol. 50, No. 4, pp. 449-460.

Luzzani, L. & Coop, M.R. (2002). "On the relationship between particle breakage and the critical state of sands", *Soils & Foundations*, 42,No.2, pp.71-82.

MacAyeal, D.R. (1989). " Large -scale ice flow over a viscous basal sediment: Theory and application to Ice Stream B, Antarctica.", *J. Geophysical Res.*, 94,pp. 4071-4087.

Martins, F. B., Bressani, L. A., Coop, M. R., & Bica, A. V. D. (2001), "Some aspects of the compressibility behaviour of a clayey sand", *Can.Geotech.J.*, vol. 38, pp. 1177-1186.

Matsushita, M., Yasin, S. J. M., Cazazliu, B., Tatsouka, F., & Koseki, J. (1998)a. "Strain acceleration- dependency of sand deformation in plain strain compression", *Proc 33rd Japan National Conf. on Geotechnical Eng., JGS,* Yamaguchi (in Japanese), pp. 515-516.

Matsushita, M., Yasin, S. J. M., Cazazliu, B., Tatsouka, F., & Koseki, J. (1998)b. "Effects of strain acceleration on deformation-strength characteristics of sand", *Proc. 53th Annual Conf. of Japanese Society of Civil Engs,* III A, Kobe- Japan, pp. 62-63 (in Japanese).

McDowell, G.R. (2003). "Micromechanics of creep of granular material", *Geotechnique*, 53, 10, pp. 915-916.

McDowell, G. & Bolton, M. (1998). "On the micromechanics of crushable aggregates", *Geotechnique*, vol. 48, No. 5, pp. 667-679.

Menzies, J. (1995). *Modern Glacial Environments, Processes , dynamics and sediments*, 1st edn, Butterworth-Heinemann Ltd.

Milligan, V. (1976). "Geotechnical aspects of glacial till," in *Glacial till,* R.F.Legget, ed., The Royal Society of Canada, pp. 269-291.

Mimura, M. (2003). "Chracterisitics of some Japanese natural sands- data from undisturbed frozen samples", *Characterisation and Engineering Properties of Natural Soils*- Tan et al. (eds.), Swets & Zetlinger, Lisse. pp. 1149-1168.

Mitchell, J.K. (1976). "Fundemantals of soil behaviour", New York : Wiley.

Miura, S. & Yagi, K. (2003). "Mechanical behaviour and particle crushing of volcanic coarse -grained soils in Japan", *characterisation and engineering properties of natural soils*.

Murray, T. (1994). "Glacial Deformation," in *The Geological Deformation of Sediments*, first edition edn, A. J. Maltman, ed., Chapman and Hall, pp. 73-93.

Nakata,Y., Hyde, A.F.L., Hyodo, M. & Murata, H. (1999). "A probablistic approach to sand particle crushing in the triaxial test", *Geotechnique*, vol. 49, No. 5, pp. 567-583.

Nakata, Y., Hyde, A.F.L., Hyodo, M., Kato, Y. & Murata, H. (2001). "Microscopic particle crushing of sand subject to high pressure one-dimensional compression", *Soils & Foundations*, Vol. 41, No.1, pp.69-82.

Ni, Q., Tan, T.S., Dasari, G.R. & Hight, D.W. (2004). "Contribution of fines to the compressive strength of mixed soils", *Geotechnique*, 54, No. 9, pp561-569.

Nocilla, A., Colleselli, F., & Coop, M. R. (2006). "The mechanics of an Italian silt: an example of "transitional" behaviour.", *Geotechnique*, vol. 56, No. 4, pp. 261-271.

Oka, F., Kodaka, T., Kimoto, S. Ishigaki, S. & Tsuji, C. (2003). "Step-changed strain rate effect on the stress strain relations of clays and a constitutive modelling", *Soils & Foundations*, 43, No. 4, pp.189-202.

Paterson, W. S. B. (1969). *The Physics of Glaciers*, Third Edition edn, Elsevier Science Ltd.

Pitman, T.D., Robertson, P.K. & Sego, D.C. (1994). "Influence of fines on the collapse of loose sands", *Can. Geotechnich. J.*, 31, pp. 728-739.

Porter, S. C., Murray, T., & Dowdeswell, J. A. (1997). "Sediment deformation and basal dynamics beneath a glacier surge from: Bakaninbreen, Svalbard.", *Annals of Glaciology*, vol. 24, pp. 21-26.

Roscoe, K. H., Schofield, A. N., & Worth, C. P. (1958). "On the yielding of soils.", *Geotechnique*, vol. 8, pp. 22-53.

Santucci de Magistris, F. (1998). Internal report, Geotechnical Engineering Laboratory, University of Tokyo.

Santucci de Magistris, F., Sato, T., Koseki, J. & Tatsuoka, F. (1998). "Effect of strain rate and ageing on small strain behaviour of compacted silty sand", *The Geotechnics of Hard Soils-Soft Rocks, Proc. of Second Int. Conf. on Hard Soils and Soft Rocks,* Evamgelista & Picarelli eds, Balkema, 1, pp. 843-851.

Shilts W.W.(1976). "Till and mineral prospecting," in *Glacial till*, Robert F Legget, ed..

Shreve, R. L. (1972). "Movement of water in glaciers", *Journal-of-Glaciology*, vol. 30, pp. 341-347.

Sigurdsson, O., (1998). "Glacier Variations in Iceland, 1930-1995", *Jokull*, 45, pp. 3-26.

Skempton, A.W. (1954). " The pore pressure coefficients A and B". *Geotechnique*, vol 4, No. 4.

Smith, R. E. & Wahls, H. E. (1969). "Consolidation under constant rates of strain", *Journal Soil mechanics and foundations Div*, vol. 95(SM2), pp. 519-539.

Soga, k. & Mitchell, J.K. (1996). "Rate dependent deformation of structured natural clays", *ASCE Geotechnical special publication*, No.61, pp.243-257.

Sorensen, K. (2001), *Investigation into the particle breakage of a carbonate sand,* MSc. thesis, Imperial College.

Sorensen, K. (2006), "Influence of viscosity and aging on the behaviour of clays", PhD thesis, UCL.

Sorensen, K., Baudet, B., & Simpson, B. (2007). "Influence of structure on the time dependent behaviour of a stiff sedimentary clay", *Geotechnique,* vol. 57, 1, pp. 113-124.

Takei, M., Kusakabe, O. & Hayashi, T. (2001). "Time dependent behaviour of crushable materials in one-dimensional compression tests", *Soil & Foundations*, 41, pp. 97-121.

Tatsuoka, F. (2006). "Keynote lecture: Inelastic deformation characteristics of geomaterials and their simulation", *Soil stress-strain behaviour; measurment, modelling and analysis. Geotechnical symposium*, Roma.**

Tatsuoka, F., Ishihara, M., Di Benedetto, H., & Kuwano, R. (2002). "Time-dependant shear deformation characteristics of geomaterials and their simulation", *Soils and Foundations*, vol. 42, No. 2, pp. 103-129.

Tatsuoka, F., Santucci de Magistris, F., Hayano, K., Koseki, J., & Momoya, Y. (2000). "Some new aspects of time effects on the stress-strain behaviour of stiff geomaterials.", Keynote Lecture, *The Geotechnics of Hard soils-Soft Rocks, Proc. of Second Int. Conf. on Hard Soils and soft Rocks,* Napoli, Evamgelista and Picarelli eds., Balkema, 2, pp. 1285-1371.

Tavenas, F., Leroueil, S., La Rochelle, P., & Roy, M. (1978). "Creep behaviour o an undisturbed lightly overconsolidated clay.", *Canadian Geotechnical journal*, vol. 15, no. 3, pp. 402-423.

Tavenas, F. & Leroueil, S. (1977). "Effect of stresses and time on yielding of clays", 9th Int. Conf. Soil Mech. Found. Engng., Tokyo1, pp. 319-326.

Terzaghi, K. (1936). "The shearing resistance of saturated soils and the angle between the planes of shear.", *Proc. 1st Int. Conf. soil Mechanics and Foundation Engng.,* vol. 1, Harvard, Mass., pp. 54-56.

Thevanayagam, S. & Mohan, S. (2000). "Intergranular state variables and stress-strain behaviour of silty sands", G*eotechnique,* vol.50, 1, pp.1-23.

Truffer M., Harrison W.D., & Echelmeyr K.A. (2000). "Glacier motion dominated by processes deep in underlying till", *Journal-of-Glaciology*, vol. 46, No. 153, pp. 213-221.

Tulaczyk S.M. (1999). *Basal mechanics and geologic record of ice streaming, West Antarctica,* PhD, California Institute of Technology, Pasadena-California.

Tulaczyk S.M. (2006)A. "Fast glacier flow and ice streaming", in *Glacier Science and Environment Change*, First edn, P. G. Knight, ed., Blackwell Science Ltd., pp. 353-359.

Tulaczyk, S. (2006)B. "Scale independance of till rheology", *Journal of Glaciology*, vol. 52, No. 178, pp. 377-380.

Tulaczyk, S., Kamb, B. & Engelhardt, H.F. (2000). "Basal mechanics of Ice Stream B, West Antarctica", *Journal of Geophysical Research*, vol. 105, No. B1, pp. 463-481.

Vaid, Y. P. & Campanella, R. G. (1977). "Time dependent behaviour of undisturbed clay", *J.Geotech.Div.ASCE*, vol. 103, No. No. GT 7, pp. 693-709.

Vaid, Y. P., Robertson, P. K., & Campanella, R. G. (1979). "Strain rate behaviour of Saint-Jean Vianney clay", *Canadian Geotechnical journal*, vol. 16, pp. 34-42.

Verdugo, R. & Ishihara, K. (1996). "The steady state of sandy soils", *Soils and Foundations*, vol. 36, No. 2, pp. 81-91.

Vesic, A.S. & Clough, E. W. (1968). "Behaviour of granular materials under high stresses", Proc. ASCE, 94 (SM3), pp.661-688.

Viggiani, G. & Atkinson, J.H. (1995). "Stiffness of fine-grained soil at very small strains", *Geotechnique*, 45, No.2, 249-265.

Weertman, J. (1957). "On the sliding of glaciers", *Journal of Glaciology*, vol. 3, pp. 33-38.

Wood, D. M. (2006). "Geomaterials with chaniging grading: A route towards modelling", in *Geomechanics and Geotechnics of Particulate Media*, Hyodo, M. & Nakata, eds., Taylor & Francis Group, London, pp. 313-325.

Yamamuro, J.A. & Lade, P.V. (1993). "Effect of strain rate on instability of granular soils", *Geotech. Testing J.*, GTJODJ, 16 (3), pp. 304-313.

Zhu, J.G., Yin, J.H. & Luk, S.T. (1999). "Time dependent stress strain behaviour of soft Hong Kong marine deposits", *Geotech. Testing J.*, GTJODT, 22 (2), pp.112-120.

Zlatovic, S. & Ishihara, K. (1995). "On the influence of non-plastic fines on residual strength", *Proc. IS-Tokyo 1995, 1st Int. Conf. on Earthquake Geotech. Eng.*, Tokyo, pp. 239-244.

Appendix 1:
Grain size scale

Phi (Φ) scale	*Size (mm)*	*British sieve sizes*	*US sieve no*	*Wentworth scale*
				boulder
-8	256			
-6	64	63 mm		cobble
-4	16	20 mm		
-2	4	6.3 mm	5	pebble
-1.75	3.36	3.35 mm	6	
-1.5	2.83		7	granule
-1.25	2.38		8	
-1	2	2.00 mm	10	
-0.75	1.68		12	
-0.5	1.41		14	very coarse
-0.25	1.19	1.18 mm	16	sand
0	1		18	
0.25	0.84		20	
0.5	0.71		25	coarse sand
0.75	0.59	600 µm	30	
1	0.50		35	
		425 µm		
1.25	0.42		40	
1.5	0.35		45	medium sand
1.75	0.30	300 µm	50	
2	0.25	212 µm	60	
2.25	0.210		70	
2.5	0.177		80	fine sand
2.75	0.149	150 µm	100	
3	0.125		120	
3.25	0.105		140	
3.5	0.088		170	very fine
3.75	0.074		200	sand
4	0.0625	63 µm	240	
4.25	0.053		270	
4.5	0.044		325	coarse silt
4.75	0.037		400	
5	0.031			
6	0.0156			medium silt
7	0.0078			fine silt
8	0.0039			very fine silt
9	0.0020			
10	0.00098			
11	0.00049			
12	0.00024			clay
13	0.00012			
14	0.00006			

Appendix 2:

Grain size distribution – Laser Granulometry - Royal Holloway

Department of Geology
Royal Holloway and Bedford New College
University of London

Telephone / Fax
Mobile
E-mail

From: Professor

FAO: Dr Catherine Stafford **30 November 2000**

Grain size analysis of Icelandic till samples

Results of the grain size analyses are enclosed.

The till sample was analyzed in a number of different ways:

(a) wet sieving to claculate percentages of gravel, sand and mud which were as follows:

gravel (>2.0 mm)	34.07%
sand (0.063 - 2.0mm)	38.34%
mud (<0 063 mm)	27.59%
sand: mud ratio	1.39
textural classification:	muddy sandy gravel

(b) dry sieving of >0.063 mm fraction by dry sieving

coarse gravel	1.70%
medium gravel	2 60%
fine gravel	5.30%
very fine gravel	9 80%
very coarse sand	12 90%
coarse sand	14 3%
medium sand	14 2%
fine sand	15 7%
very fine sand	23 6%
textural classification:	very poorly sorted gravelly sand

(c) laser granulometry of <1 00 mm fraction

mean size	82 27 um
median	33 45 um
mode	37 96 um
% sand (63um - 1.0mm)	31.50%
% silt (2-63 um)	67 80%
% clay (0.4 - 2 um)	10 70%

The sample is multimodal with a marked primary mode at 38 um and a significant secondary mode at 1 um: other modes occur at 220 um and 450 um.

The other samples were analyzed only by laser granulometry; results on attached printout sheets.

1

Costs involved are as follows:

3 laser granulometry analyses @ £15 per sample	£45.00
1 dry sieving analysis @ £20 per sample	£20.00
1 wet sieving analysis @ £35 per sample	£35.00
Total	£100.00

Please make out a cheque payable to ' Royal Holloway University of London'

If you have any queries please contact me by e-mail.

Yours sincerely,

Professor of Environmental Geology

SAMPLE STATISTICS

SAMPLE IDENTITY: **Till >63 um** ANALYST & DATE: JR, 17/11/00

SAMPLE TYPE: Trimodal, Very Poorly Sorted TEXTURAL GROUP: Gravelly Sand

SEDIMENT NAME: Very Fine Gravelly Very Fine Sand

	µm	ϕ
MODE 1:	76.50	3.731
MODE 2:	302.5	1.747
MODE 3:	605.0	0.747
D_{10}:	82.38	-1.943
MEDIAN or D_{50}:	416.1	1.265
D_{90}:	3846.1	3.602
(D_{90} / D_{10}):	46.69	-1.853
(D_{90} - D_{10}):	3763.7	5.545

GRAIN SIZE DISTRIBUTION

GRAVEL: 19.3%	COARSE SAND: 14.3%
SAND: 80.7%	MEDIUM SAND: 14.2%
MUD: 0.0%	FINE SAND: 15.7%
	V FINE SAND: 23.6%
V COARSE GRAVEL: 0.0%	V COARSE SILT: 0.0%
COARSE GRAVEL: 1.7%	COARSE SILT: 0.0%
MEDIUM GRAVEL: 2.6%	MEDIUM SILT: 0.0%
FINE GRAVEL: 5.2%	FINE SILT: 0.0%
V FINE GRAVEL: 9.8%	V FINE SILT: 0.0%
V COARSE SAND: 12.9%	CLAY: 0.0%

	METHOD OF MOMENTS			FOLK & WARD METHOD		
	Arithmetic µm	Geometric µm	Logarithmic ϕ	Geometric µm	Logarithmic ϕ	Description
MEAN ($\bar{x}$):	1577.2	501.1	1.018	470.6	1.106	Medium Sand
SORTING (σ):	3160.0	4.328	2.114	4.486	2.165	Very Poorly Sorted
SKEWNESS (Sk):	3.847	0.493	-0.493	0.168	-0.169	Coarse Skewed
KURTOSIS (K):	19.41	2.332	2.332	0.784	0.783	Platykurtic

GRAIN SIZE DISTRIBUTION

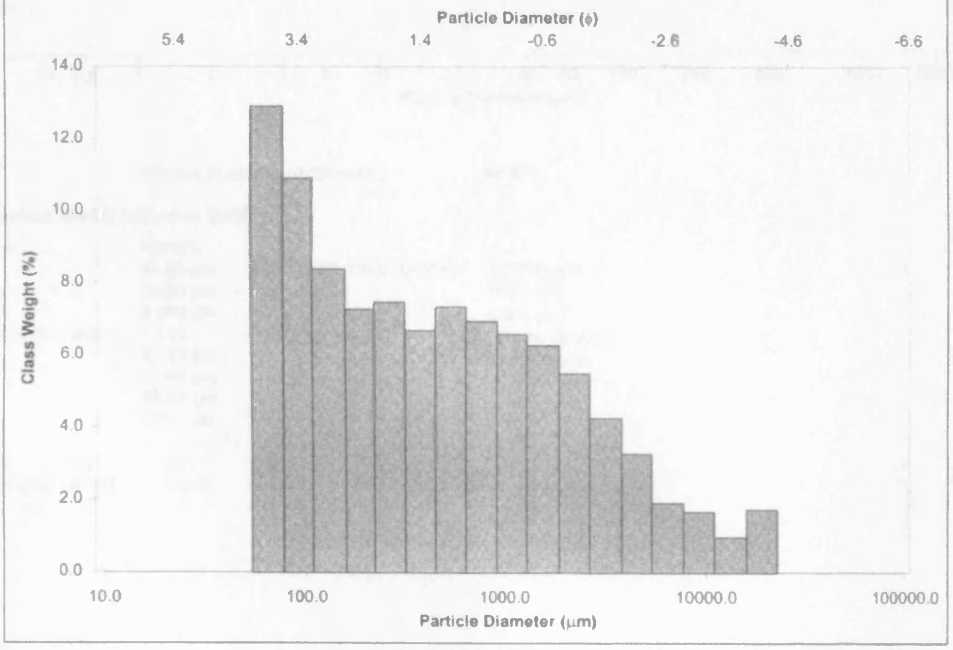

Royal Holloway
University of London

COULTER® LS Particle Size Analyzer

1 Dec 2000

Surface Processes & Modern Environments Research Group

File name:	till.$01	Group ID:	Till
Sample ID:	LPT2		
Operator:	JR	Run number:	1
Comments:	L. Proglacial Till 63 um Sonicated, calgon		
Optical model:	Fraunhofer		
LS 230	Fluid Module		
Start time:	14:03 11 Oct 2000	Run length:	61 Seconds
Pump speed:	100		
Obscuration:	7%		
PIDS Obscur:	43%		
Fluid:	Tap water		
Software:	2.11	Firmware:	2.02 2.02

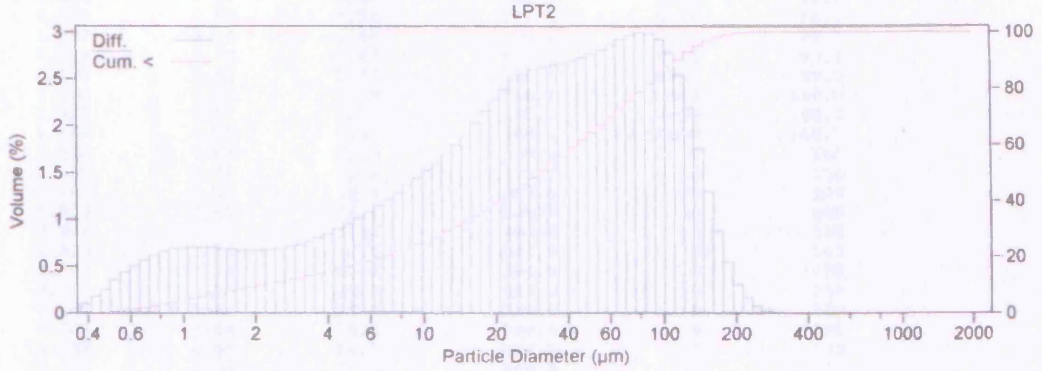

Volume Statistics (Arithmetic) till.$01

Calculations from 0.375 µm to 2.000 µm

Volume	100.0%		
Mean:	44.25 µm	95% Conf. Limits:	0-130.6 µm
Median:	29.05 µm	S.D.:	44.05 µm
D(3,2):	6.089 µm	Variance:	1,941 µm^2
Mean/Median Ratio:	1.523	Skewness:	1.284 Right skewed
Mode:	80.08 µm	Kurtosis:	1.328 Leptokurtic
d_{10}:	2.081 µm		
d_{50}:	29.05 µm		
d_{90}:	110.0 µm		

% <	10	25	50	75	90
Size µm	2.081	9.218	29.05	68.21	110.0

Royal Holloway University of London

COULTER® LS Particle Size Analyzer

1 Dec 2000

Surface Processes & Modern Environments Research Group

till.$01

Channel Diameter (Lower) µm	Diff. Volume %	Cum. < Volume %	Channel Diameter (Lower) µm	Diff. Volume %	Cum. < Volume %
0.375	0.094	0	69.62	2.96	75.7
0.412	0.17	0.094	76.43	2.98	78.6
0.452	0.25	0.26	83.90	2.98	81.6
0.496	0.35	0.51	92.09	2.92	84.6
0.545	0.43	0.85	101.1	2.78	87.5
0.598	0.50	1.28	111.0	2.54	90.3
0.657	0.56	1.78	121.8	2.19	92.8
0.721	0.61	2.34	133.7	1.76	95.0
0.791	0.65	2.95	146.8	1.30	96.7
0.869	0.68	3.60	161.2	0.87	98.0
0.953	0.69	4.28	176.8	0.54	98.9
1.047	0.70	4.98	194.2	0.30	99.5
1.149	0.70	5.67	213.2	0.15	99.8
1.261	0.69	6.37	234.1	0.067	99.9
1.385	0.68	7.07	256.8	0.022	100.0
1.520	0.67	7.75	282.1	0.0039	100.0
1.669	0.67	8.43	309.6	0.00029	100.0
1.832	0.66	9.09	339.8	0	100
2.010	0.67	9.76	373.1	0	100
2.207	0.67	10.4	409.6	0	100
2.423	0.68	11.1	449.7	0	100
2.660	0.70	11.8	493.6	0	100
2.920	0.73	12.5	541.9	0	100
3.206	0.76	13.2	594.9	0	100
3.519	0.80	14.0	653.0	0	100
3.862	0.84	14.8	716.9	0	100
4.241	0.89	15.6	786.9	0	100
4.656	0.95	16.5	863.9	0	100
5.111	1.01	17.5	948.2	0	100
5.611	1.08	18.5	1,041	0	100
6.158	1.14	19.5	1,143	0	100
6.761	1.21	20.7	1,255	0	100
7.421	1.29	21.9	1,377	0	100
8.147	1.36	23.2	1,512	0	100
8.944	1.44	24.5	1,660	0	100
9.819	1.52	26.0	1,822	0	100
10.78	1.61	27.5	2,000		100
11.83	1.69	29.1			
12.99	1.79	30.8			
14.26	1.90	32.6			
15.65	2.02	34.5			
17.18	2.15	36.5			
18.86	2.28	38.7			
20.70	2.39	41.0			
22.73	2.48	43.4			
24.95	2.55	45.8			
27.38	2.59	48.4			
30.07	2.62	51.0			
33.00	2.64	53.6			
36.24	2.66	56.2			
39.77	2.69	58.9			
43.66	2.72	61.6			
47.93	2.76	64.3			
52.63	2.81	67.1			
57.77	2.86	69.9			
63.41	2.92	72.7			

Royal Holloway University of London

COULTER® LS Particle Size Analyzer

1 Dec 2000

Surface Processes & Modern Environments Research Group

till.$01

Size µm	ASTM	Cum. < Volume
0	999	0
38	400	57.6
45	325	62.4
53	270	67.3
63	230	72.5
75	200	78.0
90	170	83.6
106	140	88.9
125	120	93.4
150	100	97.0
180	80	99.0
212	70	99.7
250	60	100.0
300	50	100.0
355	45	100
425	40	100
500	35	100
600	30	100
710	25	100
850	20	100
1,000	18	100
1,180	16	100
1,400	14	100
1,700	12	100
2,000	10	100
		100

Royal Holloway
University of London

COULTER® LS Particle Size Analyzer

1 Dec 2000

Surface Processes & Modern Environments Research Group

File name:	till.$02	Group ID:	Till
Sample ID:	LPT1		
Operator:	JR	Run number:	2
Comments:	L. Proglacial Till <63 um Sonicated, calgon		
Optical model:	Fraunhofer		
LS 230	Fluid Module		
Start time:	14:14 11 Oct 2000	Run length:	60 Seconds
Pump speed:	100		
Obscuration:	7%		
PIDS Obscur:	43%		
Fluid:	Tap water		
Software:	2.11	Firmware:	2.02 2.02

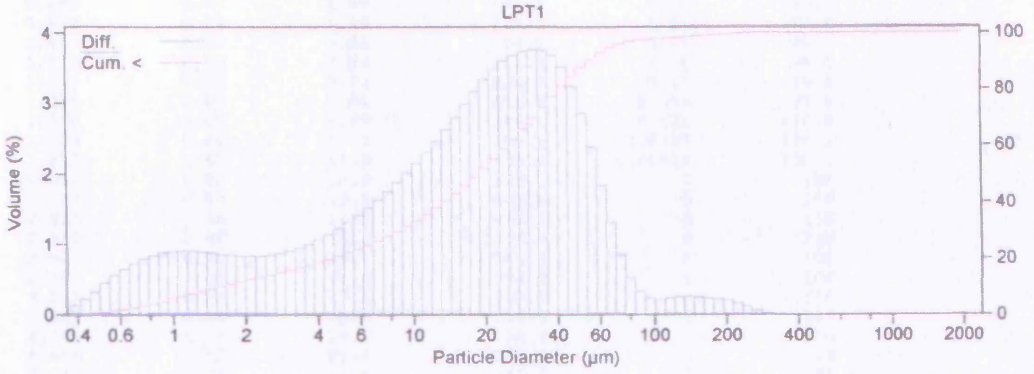

Volume Statistics (Arithmetic) till.$02

Calculations from 0.375 µm to 2.000 µm

Volume	100.0%		
Mean:	24.80 µm	95% Conf. Limits:	0-80.89 µm
Median:	17.84 µm	S.D.:	28.61 µm
D(3,2):	4.804 µm	Variance:	818.7 µm^2
Mean/Median Ratio:	1.390	Skewness:	3.521 Right skewed
Mode:	31.50 µm	Kurtosis:	19.33 Leptokurtic
d_{10}:	1.541 µm		
d_{50}:	17.84 µm		
d_{90}:	51.90 µm		

% <	10	25	50	75	90
Size µm	1.541	6.279	17.84	34.34	51.90

Royal Holloway University of London

COULTER® LS Particle Size Analyzer

1 Dec 2000

Surface Processes & Modern Environments Research Group

till.$02

Channel Diameter (Lower) µm	Diff. Volume %	Cum. < Volume %	Channel Diameter (Lower) µm	Diff. Volume %	Cum. < Volume %
0.375	0.12	0	69.62	0.85	95.9
0.412	0.21	0.12	76.43	0.51	96.8
0.452	0.31	0.33	83.90	0.32	97.3
0.496	0.44	0.64	92.09	0.23	97.6
0.545	0.55	1.09	101.1	0.21	97.8
0.598	0.63	1.63	111.0	0.23	98.1
0.657	0.71	2.27	121.8	0.24	98.3
0.721	0.78	2.98	133.7	0.25	98.5
0.791	0.83	3.76	146.8	0.24	98.8
0.869	0.87	4.59	161.2	0.23	99.0
0.953	0.89	5.46	176.8	0.21	99.2
1.047	0.89	6.35	194.2	0.19	99.5
1.149	0.89	7.24	213.2	0.16	99.6
1.261	0.88	8.13	234.1	0.11	99.8
1.385	0.87	9.01	256.8	0.059	99.9
1.520	0.85	9.88	282.1	0.021	100.0
1.669	0.84	10.7	309.6	0.0037	100.0
1.832	0.83	11.6	339.8	0.00026	100.0
2.010	0.82	12.4	373.1	0	100
2.207	0.83	13.2	409.6	0	100
2.423	0.84	14.0	449.7	0	100
2.660	0.86	14.9	493.6	0	100
2.920	0.90	15.7	541.9	0	100
3.206	0.94	16.6	594.9	0	100
3.519	0.99	17.6	653.0	0	100
3.862	1.06	18.6	716.9	0	100
4.241	1.13	19.6	786.9	0	100
4.656	1.22	20.8	863.9	0	100
5.111	1.31	22.0	948.2	0	100
5.611	1.41	23.3	1,041	0	100
6.158	1.51	24.7	1,143	0	100
6.761	1.63	26.2	1,255	0	100
7.421	1.75	27.8	1,377	0	100
8.147	1.87	29.6	1,512	0	100
8.944	2.01	31.5	1,660	0	100
9.819	2.15	33.5	1,822	0	100
10.78	2.30	35.6	2,000		100
11.83	2.45	37.9			
12.99	2.62	40.4			
14.26	2.79	43.0			
15.65	2.98	45.8			
17.18	3.16	48.8			
18.86	3.33	51.9			
20.70	3.47	55.2			
22.73	3.59	58.7			
24.95	3.67	62.3			
27.38	3.73	66.0			
30.07	3.75	69.7			
33.00	3.74	73.5			
36.24	3.67	77.2			
39.77	3.50	80.9			
43.66	3.23	84.4			
47.93	2.85	87.6			
52.63	2.36	90.4			
57.77	1.83	92.8			
63.41	1.30	94.6			

till.$02

Size µm	ASTM	Cum. < Volume %
0	999	0
38	400	79.0
45	325	85.4
53	270	90.6
63	230	94.5
75	200	96.6
90	170	97.5
106	140	98.0
125	120	98.3
150	100	98.8
180	80	99.3
212	70	99.6
250	60	99.9
300	50	100.0
355	45	100.0
425	40	100
500	35	100
600	30	100
710	25	100
850	20	100
1,000	18	100
1,180	16	100
1,400	14	100
1,700	12	100
2,000	10	100
		100

Royal Holloway University of London

COULTER® LS Particle Size Analyzer

1 Dec 2000

Surface Processes & Modern Environments Research Group

File name:	till.$03	Group ID:	Till
Sample ID:	LPT3-150		
Operator:	JR	Run number:	3
Comments:	L. Proglacial Till 150 um Sonicated, calgon		
Optical model:	Fraunhofer		
LS 230	Fluid Module		
Start time:	14:26 11 Oct 2000	Run length:	60 Seconds
Pump speed:	100		
Obscuration:	8%		
PIDS Obscur:	50%		
Fluid:	Tap water		
Software:	2.11	Firmware:	2.02 2.02

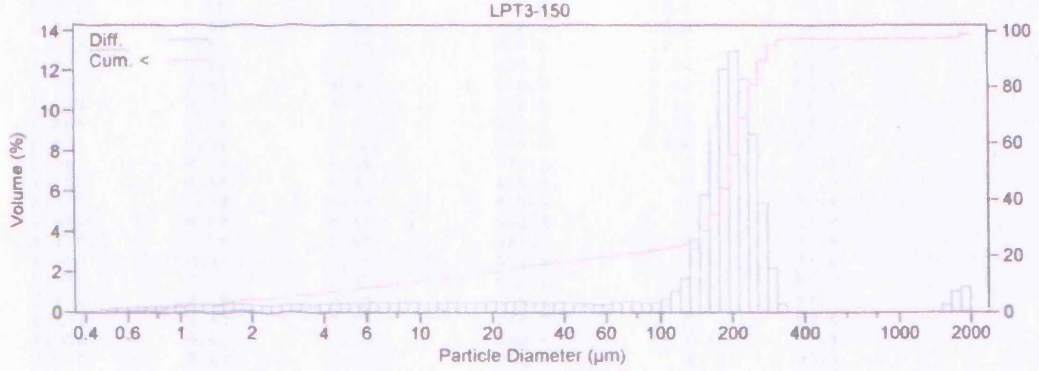

Volume Statistics (Arithmetic) till.$03

Calculations from 0.375 µm to 2.000 µm

Volume	100.0%		
Mean:	203.2 µm	95% Conf. Limits:	0-741.5 µm
Median:	185.5 µm	S.D.:	274.7 µm
D(3,2):	14.27 µm	Variance:	75,453 µm^2
Mean/Median Ratio:	1.095	Skewness:	5.097 Right skewed
Mode:	203.5 µm	Kurtosis:	27.45 Leptokurtic
d_{10}:	7.812 µm		
d_{50}:	185.5 µm		
d_{90}:	259.5 µm		

% <	10	25	50	75	90
Size µm	7.812	128.2	185.5	224.0	259.5

Royal Holloway
University of London

COULTER® LS Particle Size Analyzer

1 Dec 2000

Surface Processes & Modern Environments Research Group

till.$03

Channel Diameter (Lower) µm	Diff. Volume %	Cum. < Volume %	Channel Diameter (Lower) µm	Diff. Volume %	Cum. < Volume %
0.375	0.029	0	69.62	0.51	20.6
0.412	0.055	0.029	76.43	0.48	21.1
0.452	0.093	0.084	83.90	0.43	21.6
0.496	0.13	0.18	92.09	0.46	22.0
0.545	0.16	0.31	101.1	0.64	22.4
0.598	0.20	0.47	111.0	1.00	23.1
0.657	0.23	0.67	121.8	1.68	24.1
0.721	0.26	0.89	133.7	3.14	25.8
0.791	0.28	1.15	146.8	5.80	28.9
0.869	0.30	1.43	161.2	9.25	34.7
0.953	0.32	1.73	176.8	12.1	44.0
1.047	0.33	2.05	194.2	12.9	56.1
1.149	0.34	2.38	213.2	11.6	69.0
1.261	0.35	2.73	234.1	8.83	80.6
1.385	0.35	3.08	256.8	5.41	89.4
1.520	0.35	3.43	282.1	2.16	94.8
1.669	0.35	3.78	309.6	0.39	97.0
1.832	0.34	4.12	339.8	0.016	97.4
2.010	0.34	4.46	373.1	0	97.4
2.207	0.33	4.80	409.6	0	97.4
2.423	0.33	5.13	449.7	0	97.4
2.660	0.33	5.47	493.6	0	97.4
2.920	0.34	5.80	541.9	0	97.4
3.206	0.35	6.14	594.9	0	97.4
3.519	0.36	6.49	653.0	0	97.4
3.862	0.38	6.85	716.9	0	97.4
4.241	0.40	7.23	786.9	0	97.4
4.656	0.41	7.63	863.9	0	97.4
5.111	0.42	8.04	948.2	0	97.4
5.611	0.43	8.46	1,041	0	97.4
6.158	0.43	8.89	1,143	0	97.4
6.761	0.44	9.32	1,255	0	97.4
7.421	0.44	9.76	1,377	0.025	97.4
8.147	0.45	10.2	1,512	0.36	97.4
8.944	0.45	10.7	1,660	1.01	97.8
9.819	0.46	11.1	1,822	1.22	98.8
10.78	0.46	11.6	2,000		100
11.83	0.46	12.0			
12.99	0.45	12.5			
14.26	0.46	12.9			
15.65	0.46	13.4			
17.18	0.47	13.9			
18.86	0.48	14.3			
20.70	0.48	14.8			
22.73	0.49	15.3			
24.95	0.49	15.8			
27.38	0.47	16.3			
30.07	0.44	16.8			
33.00	0.42	17.2			
36.24	0.45	17.6			
39.77	0.47	18.1			
43.66	0.45	18.5			
47.93	0.39	19.0			
52.63	0.36	19.4			
57.77	0.38	19.7			
63.41	0.46	20.1			

till.$03

Size µm	ASTM	Cum. < Volume %
0	999	0
38	400	17.8
45	325	18.7
53	270	19.4
63	230	20.1
75	200	21.0
90	170	21.9
106	140	22.8
125	120	24.5
150	100	30.2
180	80	46.2
212	70	68.2
250	60	86.8
300	50	96.2
355	45	97.4
425	40	97.4
500	35	97.4
600	30	97.4
710	25	97.4
850	20	97.4
1,000	18	97.4
1,180	16	97.4
1,400	14	97.4
1,700	12	98.0
2,000	10	100
		100

Royal Holloway
University of London

COULTER® LS Particle Size Analyzer

1 Dec 2000

Surface Processes & Modern Environments Research Group

File name:	till $04	Group ID:	Till
Sample ID:	T1<2mm		
Operator:	JR	Run number:	1
Comments:	2mm sieve		
Optical model:	Fraunhofer		
LS 230	Fluid Module		
Start time:	8:57 10 Nov 2000	Run length:	60 Seconds
Pump speed:	100		
Obscuration:	7%		
PIDS Obscur:	46%		
Fluid:	Tap water		
Software:	2.11	Firmware:	2.02 2.02

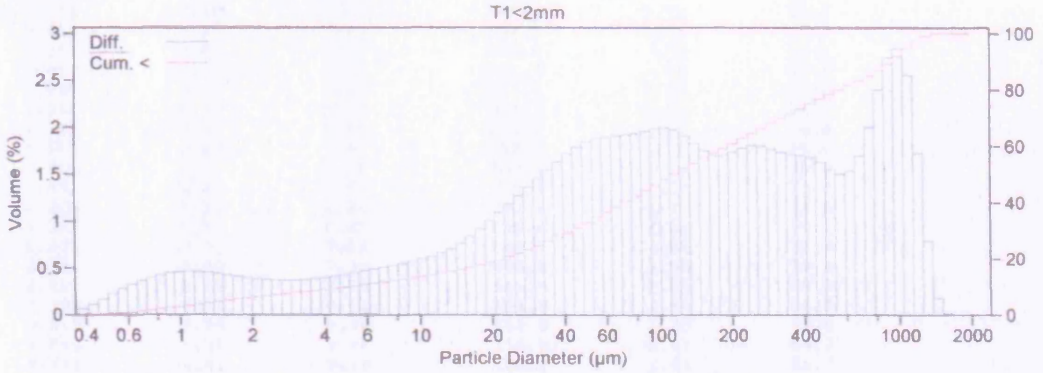

Volume Statistics (Arithmetic) till $04

Calculations from 0.375 µm to 2,000 µm

Volume	100.0%		
Mean:	277.8 µm	95% Conf. Limits:	0-954.9 µm
Median:	110.2 µm	S.D.:	345.5 µm
D(3,2):	10.23 µm	Variance:	119,349 µm^2
Mean/Median Ratio:	2.521	Skewness:	1.390 Right skewed
Mode:	993.5 µm	Kurtosis:	0.786 Leptokurtic
d_{10}:	5.014 µm		
d_{50}:	110.2 µm		
d_{90}:	889.9 µm		

% <	10	25	50	75	90
Size µm	5.014	30.72	110.2	406.8	889.9

Royal Holloway
University of London

COULTER® LS Particle Size Analyzer

1 Dec 2000

Surface Processes & Modern Environments Research Group

till.$04

Channel Diameter (Lower) µm	Diff. Volume %	Cum. < Volume %	Channel Diameter (Lower) µm	Diff. Volume %	Cum. < Volume %
0.375	0.060	0	69.62	1.92	40.4
0.412	0.11	0.060	76.43	1.94	42.3
0.452	0.16	0.17	83.90	1.96	44.2
0.496	0.22	0.32	92.09	1.99	46.2
0.545	0.28	0.54	101.1	2.00	48.2
0.598	0.32	0.82	111.0	1.98	50.2
0.657	0.36	1.14	121.8	1.92	52.1
0.721	0.40	1.50	133.7	1.84	54.1
0.791	0.43	1.90	146.8	1.75	55.9
0.869	0.45	2.32	161.2	1.71	57.7
0.953	0.46	2.77	176.8	1.70	59.4
1.047	0.46	3.23	194.2	1.74	61.1
1.149	0.46	3.69	213.2	1.79	62.8
1.261	0.45	4.14	234.1	1.81	64.6
1.385	0.44	4.60	256.8	1.80	66.4
1.520	0.42	5.03	282.1	1.77	68.2
1.669	0.41	5.46	309.6	1.74	70.0
1.832	0.40	5.87	339.8	1.72	71.7
2.010	0.38	6.26	373.1	1.70	73.4
2.207	0.37	6.65	409.6	1.68	75.1
2.423	0.37	7.02	449.7	1.63	76.8
2.660	0.36	7.38	493.6	1.56	78.4
2.920	0.37	7.75	541.9	1.51	80.0
3.206	0.37	8.11	594.9	1.54	81.5
3.519	0.38	8.48	653.0	1.70	83.0
3.862	0.39	8.86	716.9	2.01	84.7
4.241	0.41	9.26	786.9	2.41	86.7
4.656	0.43	9.66	863.9	2.74	89.2
5.111	0.44	10.1	948.2	2.84	91.9
5.611	0.46	10.5	1,041	2.56	94.7
6.158	0.48	11.0	1,143	1.73	97.3
6.761	0.50	11.5	1,255	0.79	99.0
7.421	0.52	12.0	1,377	0.17	99.8
8.147	0.55	12.5	1,512	0.016	100.0
8.944	0.57	13.1	1,660	0	100
9.819	0.60	13.6	1,822	0	100
10.78	0.63	14.2	2,000		100
11.83	0.66	14.9			
12.99	0.71	15.5			
14.26	0.77	16.2			
15.65	0.84	17.0			
17.18	0.92	17.8			
18.86	1.01	18.8			
20.70	1.10	19.8			
22.73	1.19	20.9			
24.95	1.27	22.0			
27.38	1.36	23.3			
30.07	1.45	24.7			
33.00	1.55	26.1			
36.24	1.64	27.7			
39.77	1.72	29.3			
43.66	1.79	31.0			
47.93	1.84	32.8			
52.63	1.88	34.7			
57.77	1.90	36.5			
63.41	1.91	38.4			

till.$04

Size µm	ASTM	Cum. < Volume %
0	999	0
38	400	28.5
45	325	31.6
53	270	34.8
63	230	38.3
75	200	41.9
90	170	45.7
106	140	49.2
125	120	52.7
150	100	56.3
180	80	59.7
212	70	62.7
250	60	65.9
300	50	69.4
355	45	72.5
425	40	75.8
500	35	78.6
600	30	81.6
710	25	84.6
850	20	88.7
1,000	18	93.5
1,180	16	97.9
1,400	14	99.8
1,700	12	100
2,000	10	100
		100

Royal Holloway University of London

COULTER® LS Particle Size Analyzer

1 Dec 2000

Surface Processes & Modern Environments Research Group

File name:	till.$05	Group ID:	Till
Sample ID:	T1<2mm * < [illegible]		
Operator:	JR	Run number:	2
Comments:	2mm sieve		
Optical model:	Fraunhofer		
LS 230	Fluid Module		
Start time:	9:03 10 Nov 2000	Run length:	60 Seconds
Pump speed:	100		
Obscuration:	9%		
PIDS Obscur:	54%		
Fluid:	Tap water		
Software:	2.11	Firmware:	2.02 2.02

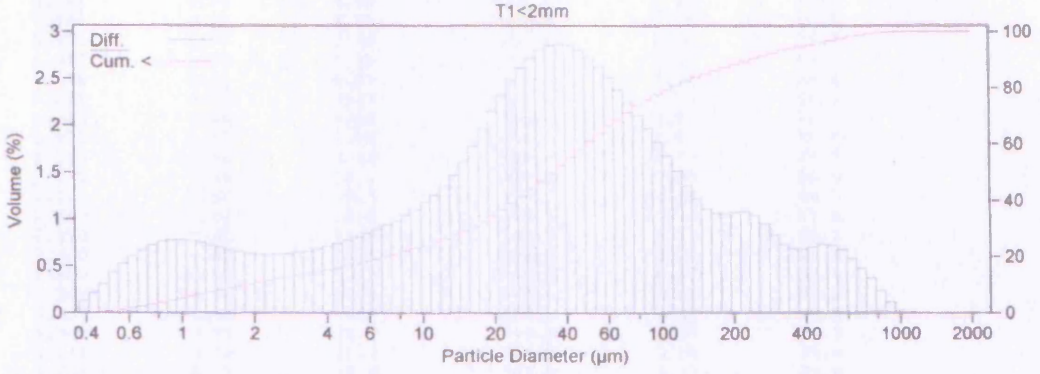

Volume Statistics (Arithmetic) till.$05

Calculations from 0.375 µm to 2,000 µm

Volume	100.0%		
Mean:	82.27 µm	95% Conf. Limits:	0-347.1 µm
Median:	33.45 µm	S.D.:	135.1 µm
D(3,2):	5.858 µm	Variance:	18,260 µm^2
Mean/Median Ratio:	2.459	Skewness:	3.020 Right skewed
Mode:	37.96 µm	Kurtosis:	10.09 Leptokurtic
d_{10}:	1.814 µm		
d_{50}:	33.45 µm		
d_{90}:	224.7 µm		

% <	10	25	50	75	90
Size µm	1.814	10.67	33.45	81.89	224.7

Royal Holloway University of London

COULTER® LS Particle Size Analyzer

1 Dec 2000

Surface Processes & Modern Environments Research Group

till.$05

Channel Diameter (Lower) µm	Diff. Volume %	Cum. < Volume %	Channel Diameter (Lower) µm	Diff. Volume %	Cum. < Volume %
0.375	0.12	0	69.62	2.24	71.2
0.412	0.21	0.12	76.43	2.11	73.5
0.452	0.30	0.32	83.90	1.97	75.6
0.496	0.43	0.63	92.09	1.82	77.5
0.545	0.52	1.05	101.1	1.67	79.4
0.598	0.60	1.57	111.0	1.51	81.0
0.657	0.66	2.17	121.8	1.35	82.5
0.721	0.72	2.84	133.7	1.21	83.9
0.791	0.75	3.55	146.8	1.11	85.1
0.869	0.77	4.31	161.2	1.06	86.2
0.953	0.77	5.08	176.8	1.06	87.3
1.047	0.76	5.85	194.2	1.08	88.3
1.149	0.74	6.61	213.2	1.08	89.4
1.261	0.72	7.35	234.1	1.04	90.5
1.385	0.69	8.07	256.8	0.94	91.5
1.520	0.67	8.76	282.1	0.83	92.5
1.669	0.65	9.43	309.6	0.73	93.3
1.832	0.63	10.1	339.8	0.68	94.0
2.010	0.62	10.7	373.1	0.68	94.7
2.207	0.62	11.3	409.6	0.70	95.4
2.423	0.62	11.9	449.7	0.73	96.1
2.660	0.62	12.6	493.6	0.72	96.8
2.920	0.64	13.2	541.9	0.67	97.5
3.206	0.66	13.8	594.9	0.58	98.2
3.519	0.68	14.5	653.0	0.47	98.8
3.862	0.70	15.2	716.9	0.37	99.3
4.241	0.73	15.9	786.9	0.24	99.6
4.656	0.77	16.6	863.9	0.11	99.9
5.111	0.81	17.4	948.2	0.026	100.0
5.611	0.85	18.2	1,041	0.0027	100.0
6.158	0.89	19.0	1,143	0	100
6.761	0.93	19.9	1,255	0	100
7.421	0.98	20.8	1,377	0	100
8.147	1.04	21.8	1,512	0	100
8.944	1.10	22.9	1,660	0	100
9.819	1.17	24.0	1,822	0	100
10.78	1.25	25.1	2,000		100
11.83	1.35	26.4			
12.99	1.47	27.7			
14.26	1.61	29.2			
15.65	1.77	30.8			
17.18	1.96	32.6			
18.86	2.14	34.5			
20.70	2.32	36.7			
22.73	2.48	39.0			
24.95	2.61	41.5			
27.38	2.72	44.1			
30.07	2.80	46.8			
33.00	2.85	49.6			
36.24	2.87	52.5			
39.77	2.85	55.3			
43.66	2.81	58.2			
47.93	2.73	61.0			
52.63	2.62	63.7			
57.77	2.51	66.3			
63.41	2.38	68.8			

Royal Holloway
University of London

COULTER® LS Particle Size Analyzer

1 Dec 2000

Surface Processes & Modern Environments Research Group

till.$05

Size µm	ASTM	Cum. < Volume %
0	999	0
38	400	53.9
45	325	59.1
53	270	63.9
63	230	68.7
75	200	73.0
90	170	77.0
106	140	80.2
125	120	82.9
150	100	85.4
180	80	87.5
212	70	89.3
250	60	91.2
300	50	93.0
355	45	94.3
425	40	95.6
500	35	96.9
600	30	98.3
710	25	99.2
850	20	99.8
1,000	18	100.0
1,180	16	100
1,400	14	100
1,700	12	100
2,000	10	100
		100

Royal Holloway University of London

COULTER® LS Particle Size Analyzer

10 Nov 2000

Surface Processes & Modern Environments Research Group

File name:	TILL.$05	Group ID:	Till
Sample ID:	T1<[redacted] 1mm		
Operator:	JR	Run number:	2
Comments:	2mm sieve		
Optical model:	Fraunhofer		
LS 230	Fluid Module		
Start time:	9:03 10 Nov 2000	Run length:	60 Seconds
Pump speed:	100		
Obscuration:	9%		
PIDS Obscur:	54%		
Fluid:	Tap water		
Software:	2.11	Firmware:	2.02 2.02

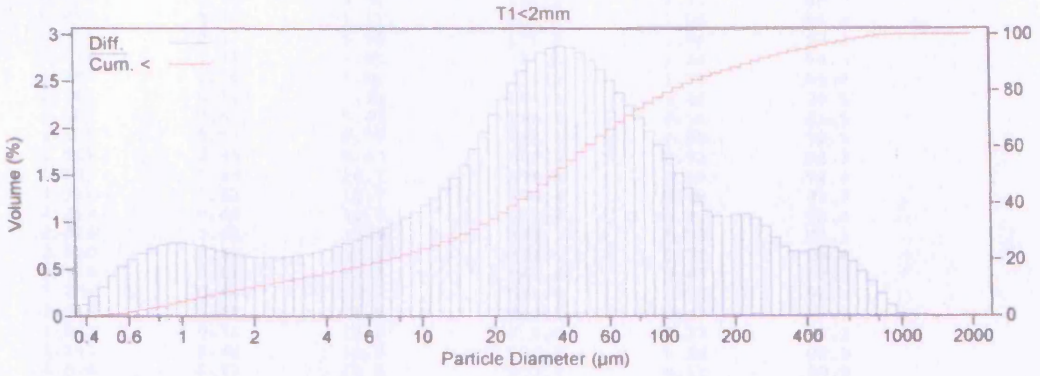

Volume Statistics (Arithmetic) till.$05

Calculations from 0.375 µm to 2,000 µm

Volume	100.0%		
Mean:	82.27 µm	95% Conf. Limits:	0-347.1 µm
Median:	33.45 µm	S.D.:	135.1 µm
D(3,2):	5.858 µm	Variance:	18,260 µm²
Mean/Median Ratio:	2.459	Skewness:	3.020 Right skewed
Mode:	37.96 µm	Kurtosis:	10.09 Leptokurtic
d_{10}:	1.814 µm		
d_{50}:	33.45 µm		
d_{90}:	224.7 µm		

% <	10	25	50	75	90
Size µm	1.814	10.67	33.45	81.89	224.7

Royal Holloway
University of London

COULTER® LS Particle Size Analyzer

10 Nov 2000

Surface Processes & Modern Environments Research Group

till.$05

Channel Diameter (Lower) µm	Diff. Volume %	Cum. < Volume %	Channel Diameter (Lower) µm	Diff. Volume %	Cum. < Volume %
0.375	0.12	0	69.62	2.24	71.2
0.412	0.21	0.12	76.43	2.11	73.5
0.452	0.30	0.32	83.90	1.97	75.6
0.496	0.43	0.63	92.09	1.82	77.5
0.545	0.52	1.05	101.1	1.67	79.4
0.598	0.60	1.57	111.0	1.51	81.0
0.657	0.66	2.17	121.8	1.35	82.5
0.721	0.72	2.84	133.7	1.21	83.9
0.791	0.75	3.55	146.8	1.11	85.1
0.869	0.77	4.31	161.2	1.06	86.2
0.953	0.77	5.08	176.8	1.06	87.3
1.047	0.76	5.85	194.2	1.08	88.3
1.149	0.74	6.61	213.2	1.08	89.4
1.261	0.72	7.35	234.1	1.04	90.5
1.385	0.69	8.07	256.8	0.94	91.5
1.520	0.67	8.76	282.1	0.83	92.5
1.669	0.65	9.43	309.6	0.73	93.3
1.832	0.63	10.1	339.8	0.68	94.0
2.010	0.62	10.7	373.1	0.68	94.7
2.207	0.62	11.3	409.6	0.70	95.4
2.423	0.62	11.9	449.7	0.73	96.1
2.660	0.62	12.6	493.6	0.72	96.8
2.920	0.64	13.2	541.9	0.67	97.5
3.206	0.66	13.8	594.9	0.58	98.2
3.519	0.68	14.5	653.0	0.47	98.8
3.862	0.70	15.2	716.9	0.37	99.3
4.241	0.73	15.9	786.9	0.24	99.6
4.656	0.77	16.6	863.9	0.11	99.9
5.111	0.81	17.4	948.2	0.026	100.0
5.611	0.85	18.2	1,041	0.0027	100.0
6.158	0.89	19.0	1,143	0	100
6.761	0.93	19.9	1,255	0	100
7.421	0.98	20.8	1,377	0	100
8.147	1.04	21.8	1,512	0	100
8.944	1.10	22.9	1,660	0	100
9.819	1.17	24.0	1,822	0	100
10.78	1.25	25.1	2,000		100
11.83	1.35	26.4			
12.99	1.47	27.7			
14.26	1.61	29.2			
15.65	1.77	30.8			
17.18	1.96	32.6			
18.86	2.14	34.5			
20.70	2.32	36.7			
22.73	2.48	39.0			
24.95	2.61	41.5			
27.38	2.72	44.1			
30.07	2.80	46.8			
33.00	2.85	49.6			
36.24	2.87	52.5			
39.77	2.85	55.3			
43.66	2.81	58.2			
47.93	2.73	61.0			
52.63	2.63	63.7			
57.77	2.51	66.3			
63.41	2.38	68.8			

Royal Holloway
University of London

COULTER® LS Particle Size Analyzer

10 Nov 2000

Surface Processes & Modern Environments Research Group

till.$05

Size µm	ASTM	Cum. < Volume %
0	999	0
38	400	53.9
45	325	59.1
53	270	63.9
63	230	68.7
75	200	73.0
90	170	77.0
106	140	80.2
125	120	82.9
150	100	85.4
180	80	87.5
212	70	89.3
250	60	91.2
300	50	93.0
355	45	94.3
425	40	95.6
500	35	96.9
600	30	98.3
710	25	99.2
850	20	99.8
1,000	18	100.0
1,180	16	100
1,400	14	100
1,700	12	100
2,000	10	100
		100

Triangular Diagram

SAMPLE IDENTITY: **Till >63 um, sieved half Phi**
TEXTURAL CLASS: Gravelly Sand
FULL CLASS NAME: Granular Very Fine Sand

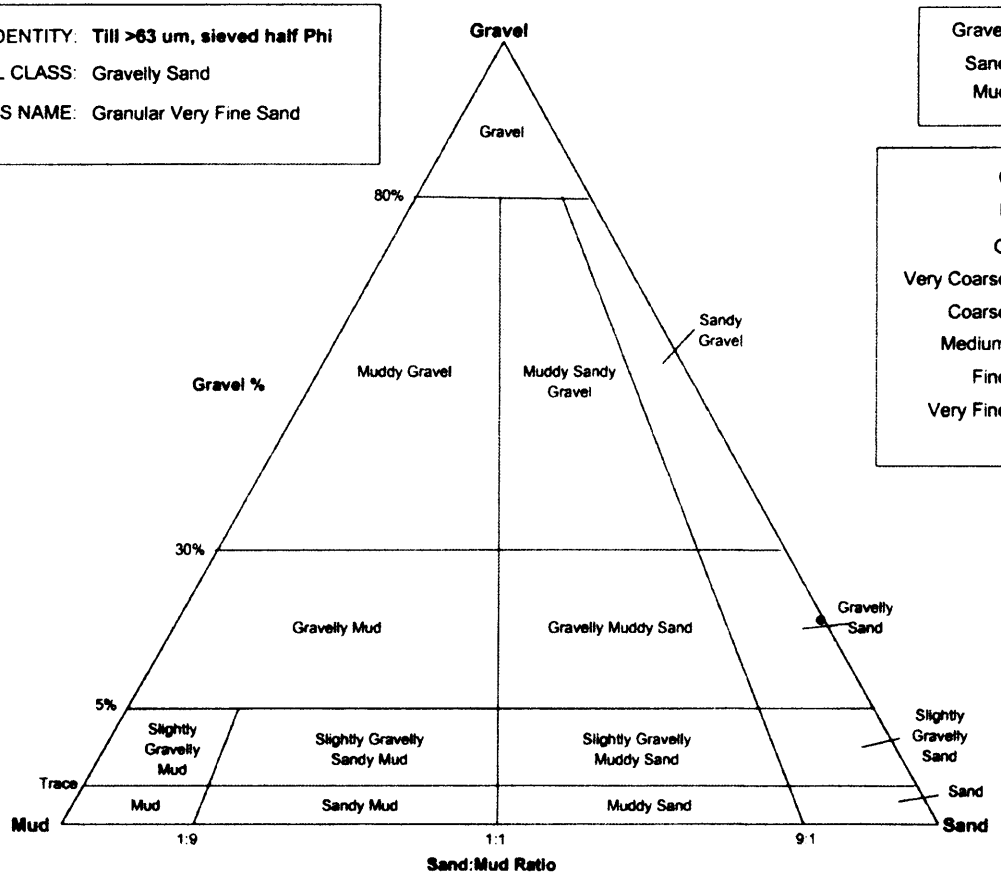

Gravel:	19.3%
Sand:	80.7%
Mud:	0.0%

Cobble:	0.0%
Pebble:	9.5%
Granule:	9.8%
Very Coarse Sand:	12.9%
Coarse Sand:	14.3%
Medium Sand:	14.2%
Fine Sand:	15.7%
Very Fine Sand:	23.6%
Mud:	0.0%